May, 1982 LIDS-TH-1209

LATERAL CONTROL SYSTEM DESIGN FOR VTOL LANDING ON A DD963 IN HIGH SEA STATES

by

Marc Bodson

This report is based on the unaltered thesis of Marc Bodson, submitted in partial fulfillment of the requirements for the degrees of Master of Science in Electrical Engineering and Computer Science and Master of Science in Aeronautics and Astronautics at the Massachusetts Institute of Technology in May, 1982. This research was conducted at the M.I.T. Laboratory for Information and Decision Systems, with partial support provided by the NASA Ames and Langley Research Centers under grant NASA/NGL-22-009-124.

Laboratory for information and Decision Systems
Massachusetts Institute of Technology
Cambridge, MA 02139

LATERAL CONTROL SYSTEM DESIGN FOR VTOL LANDING ON A DD963 IN HIGH SEA STATES

by

MARC BODSON

Ingénieur Civil Mécanicien et Electricien
Université Libre de Bruxelles, Belgium
(1980)

SUBMITTED TO THE DEPARTMENT OF
ELECTRICAL ENGINEERING AND COMPUTER SCIENCE
AND TO THE DEPARTMENT OF
AERONAUTICS AND ASTRONAUTICS
IN PARTIAL FULFILLMENT OF THE
REQUIREMENTS OF THE
DEGREES OF

MASTER OF SCIENCE IN
ELECTRICAL ENGINEERING AND COMPUTER SCIENCE

and

MASTER OF SCIENCE IN
AERONAUTICS AND ASTRONAUTICS

at the

MASSACHUSETTS INSTITUTE OF TECHNOLOGY

May 1982

Signature of Author _____ May 7, 1982
Department of Electrical Engineering and Computer Science
Department of Aeronautics and Astronautics

Certified by _____
Michael Athans
Thesis Supervisor

Certified by _____
William S. Widnall
Thesis Reader

Accepted by _____
Arthur C. Smith
Chairman, Departmental Graduate Committee
Electrical Engineering and Computer Science

Accepted by _____
Harold Y. Wachman
Chairman, Departmental Graduate Committee
Aeronautics and Astronautics

LATERAL CONTROL SYSTEM DESIGN FOR VTOL LANDING

ON A DD963 IN HIGH SEA STATES

by

Marc Bodson

Submitted to the Department of Electrical Engineering and Computer Science, and to the Department of Aeronautics and Astronautics on May 7, 1982, in partial fulfillment of the requirements for the degrees of Master of Science in Electrical Engineering and Computer Science, and of Master of Science in Aeronautics and Astronautics.

ABSTRACT

The problem of designing robust control systems for the safe landing of VTOL aircrafts on small ships is addressed for the lateral motions. A precise ship model is derived, using hydrodynamic data for the DD963 destroyer. The issues of estimation and prediction of ship motions are discussed, using optimal linear estimation techniques. The roll motion is the most important of the lateral motions, and it is found that it can be predicted for up to 10 seconds in perfect conditions.

The automatic landing of the VTOL aircraft is considered, and a lateral controller, defined as a ship motion tracker, is designed, using optimal control techniques. The tradeoffs between the tracking errors and the control authority are obtained. The important couplings between the lateral motions and controls are demonstrated, and it is shown that the adverse couplings between the sway and the roll motion at the landing pad are significant constraints in the tracking of the lateral ship motions.

The robustness of the control system, including the optimal estimator, is studied, using the singular values analysis. Through a robustification procedure, a robust control system is obtained, and the usefulness of the singular values to define stability margins that take into account general types of unstructured modelling errors is demonstrated. The minimal destabilizing perturbations indicated by the singular values analysis are interpreted and related to the multivariable Nyquist diagrams.

Thesis Supervisor: Michael Athans

Title: Professor of Systems Science and Engineering

ACKNOWLEDGEMENT

I would like to express my deep gratitude to Professor Michael Athans for his guidance as my thesis supervisor. His help throughout the course of the research and in the development of this report were greatly appreciated.

I am grateful to Professor William Widnall who agreed to be my thesis reader. His comments and suggestions represent valuable contributions to this report.

Finally, I want to thank Professor Michael Triantafyllou for his considerable help in the part of this thesis related to the ship motions. I am also grateful to him for many stimulating discussions and for his friendly support.

This research was conducted at the M.I.T. Laboratory for Information and Decision Systems, with partial support provided by the NASA Ames and Langley Research Centers under grant NASA/NGL-22-009-124.

To those who, despite time and distance,
have shown me their constant and
sincere affection

TABLE OF CONTENTS

TABLE OF CONTENTS (continued)

TABLE OF CONTENTS (continued)

LIST OF FIGURES

LIST OF FIGURES (continued)

LIST OF FIGURES (continued)

LIST OF FIGURES (continued)

LIST OF TABLES

LIST OF ABBREVIATIONS

A/C	aircraft
LQ	linear quadratic
LQG	linear quadratic gaussian
MIMO	multiple-input multiple-output
MLS/DME	microwave landing system / distance measuring equipment
RTA	research technology aircraft
SISO	sing e-input single-output
VTOL	vertical takeoff and landing (aircraft)
V/STOL	vertical and/or short takeoff and landing (aircraft)

det	determinant
diag	diagonal (matrix)
exp	exponential
rms	root-mean-square

CHAPTER 1

INTRODUCTION

1.1 Introduction and Motivation

The landing of small VTOL aircraft on destroyers is an extremely challenging problem if it is to be realized under high sea state conditions and zero visibility. Without special aids, this task is almost impossible for a human pilot.

There are basically two possible strategies in the solution of this problem. The first is to leave to the pilot the complete control of the aircraft, but help him with advanced displays. These give him information about the aircraft position and attitude, as well as those of the ship (and possibly some prediction of the ship motions). They may also indicate some desirable flight path (flight director). Advanced controls may be provided to partly relieve the pilot from the high load of controlling the VTOL aircraft.

The second strategy is to leave the task of landing the aircraft completely to an automatic controller. The role of the pilot is then to supervise the correct landing of the aircraft. This would allow him to take care of other tasks he might not have been able to carry out otherwise.

Note that both strategies could be mixed. For example, the tracking of the lateral ship motions may be left to an automatic controller/tracker, while the task of vertical tracking and landing would be left to the pilot,

possibly with the help of some display indicating him the present and future ship vertical position.

In this thesis, the emphasis is focused on the design of an automatic controller. A previous study [1] has addressed the problem of the longitudinal motions, i.e. the motions in the vertical plane. The most significant ship motion in this plane is the vertical motion, called heave. The pitch motion is not very significant, except for the heave motion it induces at the landing pad (which is significantly behind the ship center of rotation). The present study addresses the ship motion tracking problem for the lateral case. Then, the most significant motion is the ship roll motion, which can be very large. The lateral translation motion, called sway, is also important, especially due to the large sway component induced by the roll at the landing pad (located above the ship center of rotation).

The challenge of the tracking of the ship motions by the VTOL lies in the strong limitations of the control authority available, in the high level of the perturbations (wind disturbances, ground effects, ship airwake), in the strong couplings present in the system, and in the need for a highly robust control system.

Usually, studies of this problem use loop-by-loop control system designs, using classical control theories [2], [3], [4], [5], [6]. In this case, the controller ignores the internal couplings of the system. Similarly, the issue of robustness is often addressed on a loop-by-loop basis, but almost never in a real multivariable sense (although individual loop stability margins may not represent at all the overall system stability

margins). The design process used in this thesis does not suffer from such limitations.

The limitations on the available control authority justify the use of some optimization criterion, and of related modern control theories (LQ/LQG). These methods have the advantage of naturally handling multivariable systems, and of recognizing the coupling present in such systems. Some recent results in the analysis of the robustness of multivariable systems (and its improvement for LQG based designs) are also important tools in the design of control systems operating under critical conditions.

The purpose of this thesis is not to produce an engineering design. Nor does it provide new theoretical results. It illustrates how modern control theories and related recent results can be used to design a control system for such an advanced application, and evaluate the controller performance and robustness. This work also analyzes the physical constraints of the tracking process of the lateral ship motions. These constraints are independent of the control system design methodology adopted. The requirements and physical limitations related to the VTOL landing problem are studied.

Although this thesis mainly details the design of an automatic controller, the accuracy achievable in the prediction of ship motions is also assessed, as it is a key element in any piloted VTOL landing.

1.2 Contributions of the Research

The main contributions of the research are:

- the derivation of an accurate ship model that retains the stochastic nature of the ship motions, and the couplings amongst them

- the analysis of an optimal predictor of the ship motions for applications in piloted landings, and the assessment of lower bounds on the prediction errors

- the design of an optimal controller/tracker for applications in automatic landings, the indication of the tradeoffs between tracking errors and control authority, and the analysis of the important couplings and physical constraints related to the tracking of the lateral ship motions

- the demonstration of the use of the singular values analysis, and the robustification procedure, to obtain a robust control system.

1.3 Thesis Overview

Chapter 2 indicates the general problems of the landing of VTOL aircraft, and introduces the methodology used to design the control system, as well as some aspects specific to this particular application.

Chapter 3 details the derivation of the ship model from hydrodynamic data, and indicates the important characteristics of the model.

Chapter 4 is an analysis of the issues of estimation and prediction of the ship motion, using the model derived in chapter 3.

Chapter 5 summarizes the aircraft model obtained from [1], and gives a brief description of this model, and of the important couplings present

between the motions and controls.

Chapter 6 details the design of an optimal control system based on LQ theory to track the ship motions. Important characteristics such as root-locus, step responses, and tracking errors versus control authority are analyzed, with their relation to the couplings amongst the motions and controls.

Chapter 7 shows the design of an optimal estimator for the aircraft motions, and indicates the degradation of performance due to the presence of noise in the sensor measurements.

Chapter 8 addresses the important issues of robustness of the control system to modelling errors, and demonstrate the usefulness of the singular values analysis and of the robustification procedure.

Chapter 9 concludes with some general comments and suggestions for further research.

CHAPTER 2

OVERVIEW : OBJECTIVES AND METHODOLOGY

2.1 Introduction

The landing of VTOL aircrafts on small platforms is a delicate operation that interests civilians (oil platforms) as well as military (destroyers). In this research, we consider a moving platform, specifically the landing pad of a destroyer, type DD-963, in sea state 5. Such sea state corresponds to waves of heights around 10ft, and winds around 20 kts. Until now, this is still a goal, and it justifies studies as this to assess the navigation systems, the aircraft performance, and the control system required to perform such an operation.

A previous study by McMuldroch [1] has addressed the VTOL landing problem for longitudinal motions. These are called heave (vertical motion), surge (fore and aft motion), and pitch. The aircraft considered in this work (as in the present work) is the Lift/Fan Cruise Research Technology Aircraft (RTA). More details about this aircraft can be found in [1] and in chapter 4. The specific aircraft studied is not really of great importance, as most VTOL's have the same kind of limitations and possibilities. The main characteristic of an RTA-type of VTOL aircraft - which makes it different from a helicopter for example - is the possibility of deflecting the engine thrusts to produce translation motions without rotating the aircraft. In other words, this kind of VTOL has as many controls as it has degrees of freedom, so that, to the limit,

perfect tracking of the landing pad motion can be acheived.

In the present work, we use the model derived in [1] for the RTA aircraft. Our goal is to complete McMuldroch's work with a study of the controls needed for the lateral motions. The lateral motions are called sway (lateral translation), roll and yaw. The longitudinal and lateral motions can be decoupled to a good approximation for the ship motions. This does not mean that they are independent: in fact, they are strongly correlated because they are generated by the same wave. However, except for this common excitation force the dynamic equations for longitudinal and lateral motions can be decoupled to first order and can be analyzed separately. The decoupling of longitudinal and lateral motions for the aircraft is a little less obvious, due mainly to gyroscopic cross-coupling terms [7] . These terms can be quite important, due to the large size of the engines of a VTOL aircraft. To a first approximation, however, they can be neglected, so that longitudinal and lateral motions can be studied separately.

In fact, the issues for the longitudinal and for the lateral case are quite different. For the longitudinal case, the important motion is heave. Pitch is quite small and surge is negligible. Moreover, they can be controlled easily. Heave is more critical, as it requires an increase in the overall engine power (or thrust to weight ratio). This is a control which is strongly limited in amplitude, and also in its speed of response. The limitations are so strong that one may look for an end-point controller, instead of a tracking controller.

In the lateral case, two of the three motions are about as important: they are the sway and the roll motion. The yaw motion is almost insignificant, and can be controlled very easily. In many situations, the aircraft roll may be left uncontrolled, or, more precisely, stabilized to zero (so that it does not track the ship's roll). In this case, the landing gear will simply damp the shock at the landing. However, ship roll can be as large as 30 degrees peak to peak (even more in the case of decaying seas), so that this strategy is not always satisfactory. Then, both ship roll and sway motions have to be tracked.

The limitations in control authority are less severe than in the longitudinal case. In particular, a lateral side force can be produced by a deflection of the thrusts, and a roll moment by an exchange of power between the engines. These controls can be generated very quickly, so that there is no significant problem with bandwidth in the lateral case. The problem is probably more in the adverse couplings present in the lateral motions and in the robustness of the closed-loop system. These two aspects will be examined in more detail later. The consequence of these remarks is that the problems are slightly different for the longitudinal and lateral cases. The lateral controller can be a tracking controller, while the landing itself occurs at a moment decided by the longitudinal controller. The responsibility of the lateral controller is then to minimize the tracking errors at impact.

As the research on the longitudinal motions had shown that precise ship modelling was essential to obtain meaningful results, a large part

of this thesis is devoted to accurate ship motion modelling, estimation and prediction. The prediction part of the study is irrelevant to the automatic controller design part, but has applications in piloted landings, when some indication has to be given to the pilot about where the ship deck is now and will be in the near future.

2.2 Control System Design Methodology

2.2.1 Introduction

Different methodologies have been proposed recently for the design of multivariable control systems. Whether applied in the time domain or in the frequency domain, each method has its own advantages and limitations.

For aerospace applications, the linear-quadratic-gaussian (LQ-LQG) methodology has shown successful, especially because:

- the limited control authority available makes the optimization imperative
- the number of states is small (with a good approximation)
- the equations of motion (and of the system in general) are quite well known, and the state-space description is natural
- the systems are often unstable, and strongly coupled.

2.2.2 LQ Methodology

We summarize in this section the LQ methodology to specify the notation used subsequently. More detailed descriptions can be found in [8]

and [9].

Given the system:

$$\dot{\underline{x}} = A\underline{x} + B\underline{u} + \underline{\xi} \tag{2.1}$$

$$\underline{x}(0) = \underline{x}_o \tag{2.2}$$

where :

$\underline{x}$ is the state vector (nxl)

$\underline{x}_o$ is the initial state vector (nxl)

$\underline{u}$ is the control vector (mxl)

$\underline{\xi}$ is a white Gaussian noise vector (nxl) (driving noise) of spectral intensity matrix (nxn) Ξ

A is a matrix (nxn)

B is a matrix (mxm)

One wants to minimize the quadratic optimization criterion:

$$J = \lim_{T\to\infty} E\left\{ \frac{1}{T} \int_0^T (\underline{x}^T Q \underline{x} + \underline{u}^T R \underline{u})\, dt \right\} \tag{2.3}$$

where:

Q is the positive semi-definite matrix (nxn) of the state weights

R is the positive definite matrix (mxm) of the control weights

The pair (A,B) is assumed to be stabilizeable and the pair $(A,Q^{\frac{1}{2}})$ detectible (two conditions easily satisfied).

The solution is a time-varying control law $\underline{u}(t)$ which, for large t (far from the origin of time), becomes a linear, time-invariant,

state feedback:

$$\underline{u} = - G \underline{x} \tag{2.4}$$

where G is an (mxn) matrix given by:

$$G = R^{-1} B^T K \tag{2.5}$$

and K is the (nxn) positive matrix solution of the matrix algebraic Riccatti equation:

$$KA + A^T K - KBR^{-1} B^T K + Q = 0 \tag{2.6}$$

2.2.3 LQG Methodology

The LQG methodology is the extension of the LQ methodology when the state $\underline{x}$ is not available for measurement but, instead, we have a measurement vector $\underline{y}$, which is a noisy linear combination of the state $\underline{x}$:

$$\underline{y} = C\underline{x} + \underline{\theta} \tag{2.7}$$

where:

$\underline{y}$ is a measurement vector (pxl)

C is a matrix (pxn)

$\underline{\theta}$ is a white Gaussian noise vector (pxl) (measurement noise) of spectral intensity matrix (pxp) Θ

The optimization problem is the same and, from the separation principle, it is known that the solution is the cascade of an optimal estimator (Kalman filter) providing an estimate $\underline{\hat{x}}$ of the state vector $\underline{x}$, and of

the same control law as before, acting on $\hat{\underline{x}}$ instead of $\underline{x}$:

$$\underline{u} = - G \hat{\underline{x}} \tag{2.8}$$

The Kalman filter structure is:

$$\dot{\hat{\underline{x}}} = A\hat{\underline{x}} + B\underline{u} + H(\underline{y}-C\hat{\underline{x}}) \tag{2.9}$$

where H is an (nxp) matrix given by:

$$H = P\, C^T \Theta^{-1} \tag{2.10}$$

and P is an (nxn) matrix, positive solution of the matrix algebraic Riccatti equation:

$$PA^T + AP + \Xi - PC^T\Theta^{-1}CP = 0 \tag{2.11}$$

The solution of Riccatti equations is now done routinely by the use of a modern control system design package [10].

2.2.4 LQ Controller and Ship Tracking

In the VTOL landing problem, we are interested in the tracking, by the aircraft, of certain ship states (ship motions and velocities). We have a situation in which we want to track an uncontrollable system (the ship deck) by a controllable system (the VTOL).

For the ship, we have the following state-space description:

$$\dot{\underline{x}}_S = A_S\underline{x}_S + \underline{\xi}_S \tag{2.12}$$

$$\underline{w}_S = W_S \underline{x}_S \tag{2.13}$$

where $\underline{w}_S$ are the ship states that we want to track.

For the aircraft:

$$\dot{\underline{x}}_A = A_A \underline{x}_A + B_A \underline{u} + \underline{\xi}_A \tag{2.14}$$

$$\underline{w}_A = W_A \underline{x}_A \tag{2.15}$$

where $\underline{w}_A$ are the aircraft states corresponding to $\underline{w}_S$.

The general system equations are:

$$\dot{\underline{x}} = A\underline{x} + B\underline{u} + \underline{\xi} \tag{2.16}$$

where:

$$\underline{x} = \begin{bmatrix} \underline{x}_S \\ \underline{x}_A \end{bmatrix} \tag{2.17}$$

$$A = \begin{bmatrix} A_S & 0 \\ 0 & A_A \end{bmatrix} \tag{2.18}$$

$$B = \begin{bmatrix} 0 \\ B_A \end{bmatrix} \tag{2.19}$$

$$\underline{\xi} = \begin{bmatrix} \underline{\xi}_S \\ \underline{\xi}_A \end{bmatrix} \tag{2.20}$$

We want to minimize the tracking errors and the control authority, i.e.:

$$J = E\left(\int_0^\infty \left((\underline{w}_S - \underline{w}_A)^T Q_w (\underline{w}_S - \underline{w}_A) + \underline{u}^T R \underline{u}\right) dt\right) \tag{2.21}$$

$$= E\left(\int_0^\infty \left(\underline{x}^T Q \underline{x} + \underline{u}^T R \underline{u}\right) dt\right) \tag{2.22}$$

where:

$$Q = \begin{bmatrix} W_S^T Q_w W_S & -W_S^T Q_w W_A \\ -W_A^T Q_w W_S & W_A^T Q_w W_A \end{bmatrix} \tag{2.23}$$

The optimal LQG controller is:

$$\underline{u} = -G\,\hat{\underline{x}} = -(G_S\ ,\ G_A)\begin{pmatrix} \hat{\underline{x}}_S \\ \hat{\underline{x}}_A \end{pmatrix} = -G_S \hat{\underline{x}}_S - G_A\,\hat{\underline{x}}_A \tag{2.24}$$

Since the ship is uncontrollable, the ship states and the gain matrix G_S appear as a feedforward path, while the feedback path is coming from the aircraft states only, through the gain matrix G_A. As indicated in the next paragraph, the estimation problems are also decoupled, so that the controller structure is that of Fig. 2.1.

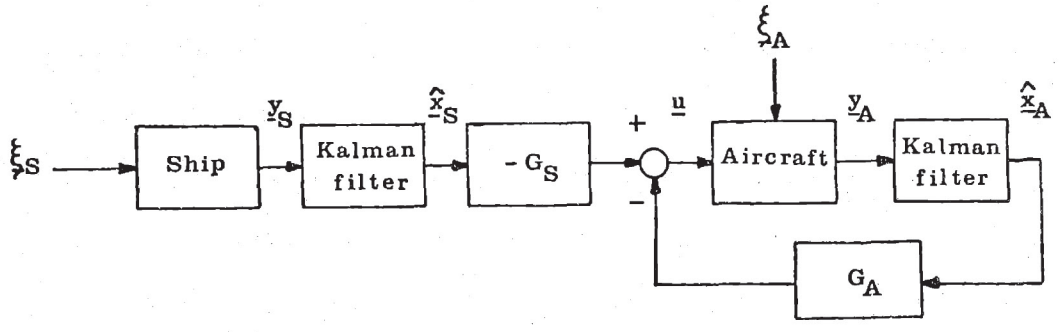

Figure 2.1: VTOL Controller Structure

An important remark is that the gain matrix G_A is the same than the matrix obtained by solving the optimization problem:

$$J = E\left(\int_o^\infty (\underline{w}_A^T Q_w \underline{w}_A + \underline{u}^T R \underline{u})\, dt\right) \tag{2.25}$$

The gain matrix G_A is then independent of the ship model.

To see this, we assume that the solution of the Riccatti equation corresponding to (2.21) is :

$$K = \begin{bmatrix} K_{11} & K_{12} \\ K_{12}^T & K_{22} \end{bmatrix} \tag{2.26}$$

Then:

$$G = R^{-1} B^T K \tag{2.27}$$

$$= (R^{-1} B_A^T K_{12} \ , \ R^{-1} B_A^T K_{22}) \tag{2.28}$$

and:

$$G_A = R^{-1} B_A^T K_{22} \tag{2.29}$$

depends only on K_{22}.

The Riccatti equation is (2.6), and can be partitioned in terms of the ship and the aircraft parts:

$$K_{11} A_S + A_S^T K_{11} - K_{12} B_A R^{-1} B_A^T K_{12}^T + W_S^T Q_w W_S = 0 \tag{2.30}$$

$$K_{12} A_A + A_S^T K_{12} - K_{12} B_A R^{-1} B_A^T K_{22} - W_S^T Q_w W_A = 0 \tag{2.31}$$

$$K_{22}A_A + A_A^T K_{22} - K_{22}B_A R^{-1} B_A^T K_{22} - W_A^T Q_w W_A = 0 \qquad (2.32)$$

The equation giving K_{22} is independent of the others and is actually the same as the one corresponding to the quadratic criterion (2.25). The same is true for the gain matrix G_A. This means that the feedback gain matrix G_A is independent of the dynamics of the signal that is tracked, namely the ship in this case. The ship only influences the feedforward gain matrix. In other words, the closed-loop dynamic behavior of the system is only dependent on the Q and R matrices, and is the same whether we want to track the ship or simply to stabilize the aircraft (track a zero reference signal). For this reason, the closed-loop behavior fo the system can be studied independently from the ship model (in this, we include the optimal root-locus, the step responses, and the robustness characteristics of the system). Note however that the ship model influences the system performance (tracking errors) which, in turn, may influence the specific choice of the Q and R matrices.

2.3 State Estimation and Implementation Issues

The accuracy of the measurements of the ship and aircraft motions will be a determining factor of the performance attainable in the landing of VTOL aircraft in high sea states and poor visibility conditions. It is expected that, in a practical realization, the measurement process will involve:

- accelerometers and gyroscopes aboard the aircraft
- a combined microwave landing system / distance measuring equipment (MLS/DME) giving measurements of the relative position of the ship and the

the aircraft.

Theoretically, the estimation of the aircraft and of the ship motions are coupled, in the sense that the relative position measurement would influence the estimation of the ship motions if a Kalman filter is used for the overall system. In practice, the estimation of the ship motion, and the estimation of the aircraft motion can be reasonably decoupled. A justification for this is that the instruments aboard the ship will be of somewhat greater precision than those aboard the aircraft, and the estimation errors obtained will be smaller than the errors on the aircraft motion. The estimation part of the LQG algorithm can then be separated in an estimation of the ship states by a Kalman filter, and a similar but independent estimation process for the aircraft.

Practically, the estimation of the ship states is done aboard the ship, and the results are data-linked to the aircraft. With the combined use of the accelerometers, gyroscopes, and MLS/DME measurements, a computer aboard the aircraft estimates the aircraft-ship relative positions and velocities, and through the use of a Kalman filter, obtains optimal estimates of the aircraft states. The control law is then easily obtained aboard the aircraft.

As the computing capabilities aboard the ship can be more powerful, a high order model can be used. In our case, it is a 16 states model (see chapter 3). On the aircraft, the computing capabilities are more limited, so that a low order model is desirable. The aircraft model used here is a 6 states model (see chapter 5). The importance of robustness becomes

critical, however. While the approximations on the ship model have consequences only on the performance of the controller, those on the aircraft model come in the feedback structure, and influence the robustness as well as the performance of the controller.

2.4 Summary

In this chapter, we discussed the general aspects of the VTOL landing problem. The decoupling between the longitudinal and lateral motions was explained, and it was indicated that the controller for the lateral motions can be conceived as a ship motion tracker.

The LQ/LQG control system design methodology was introduced, and its use for this application was justified in view of the limited control authority available. It was demonstrated that the application of this methodology to the VTOL landing problem leads to a decoupling of the ship and of the aircraft effects, so that the ship motion and the ship dynamics only influence the feedforward structure of the control system, while those of the VTOL impact the feedback structure.

Finally, the issues of estimating the ship and aircraft states were briefly addressed, and it was shown that the problems of estimation of ship and aircraft motions could be reasonably decoupled.

CHAPTER 3

SHIP MODEL DERIVATION

3.1 Introduction

The importance of accurate ship modelling in VTOL landing has been indicated by McMuldroch in [1]. Ship motions have relatively narrow band power spectra (between 0.2 and 2 rad/s) that require high order models to be represented accurately. A good ship model, that is often used in studies of VTOL landings, is available in [11]. The motions are modelled as sums of 6 to 32 sinusoïds, with random phases. For simulations (especially for flight simulators), such a representation is adequate. However, it fails to represent the random nature of ship motions for longer periods of time, and it is not appropriate for estimation of ship motions from noisy measurements, and for ship motion prediction.

In this chapter, we derive a ship model that retains the stochastic nature of the ship motions and the important couplings among the various motions. The model is derived in state-space form, so that the powerful techniques of linear estimation in the time domain can be applied. The equations are obtained from hydrodynamic considerations, that lead to linear differential equations with frequency dependent coefficients, and infinite dimensional transfer functions. Finite dimensional approximations are considered, and the model finally includes 16 states for the lateral motions. The following sections indicate the structure of the model and the approximations made. More details can be found in [12], [13] and [14].

3.2 Ship Model Structure

The lateral ship motions, and the sign conventions used here, are shown on Fig. 3.1. The origin of the reference system is located in the plane of symmetry of the ship, at the level of the waterline, and at the middle of the ship. This point is close to the center of gravity and has the advantage of being independent of the ship load conditions.

The ship motions are assumed to be small, in order to derive linear equations of motion. This assumption is justified by the fact that waves have limited wave to length ratio (at most 1/7, and usually much smaller), since waves having higher heights break and loose their energy. As a result, the major part of the force is linear and can be obtained by a first order perturbation expansion of the non-linear fluid equation. The wave spectrum is typically contained in the 0.2-2 rad/s range. Given the large mass of the vessel, the resulting motions, within this frequency range, are of the order of a few feet and a few degrees, so that the linearity assumption can be justified. Roll motion requires more attention however. Due to the slender form of the ship, the roll motion may become large and then, the non-linear damping is predominant.

The ship model is basically divided into three parts. The first part represents the incoming waves (sea model) which are described by the wave elevation at a reference point located amidships. The wave elevation is known to be a stochastic process, defined by a relatively narrow band power spectrum to which various approximations have been proposed.

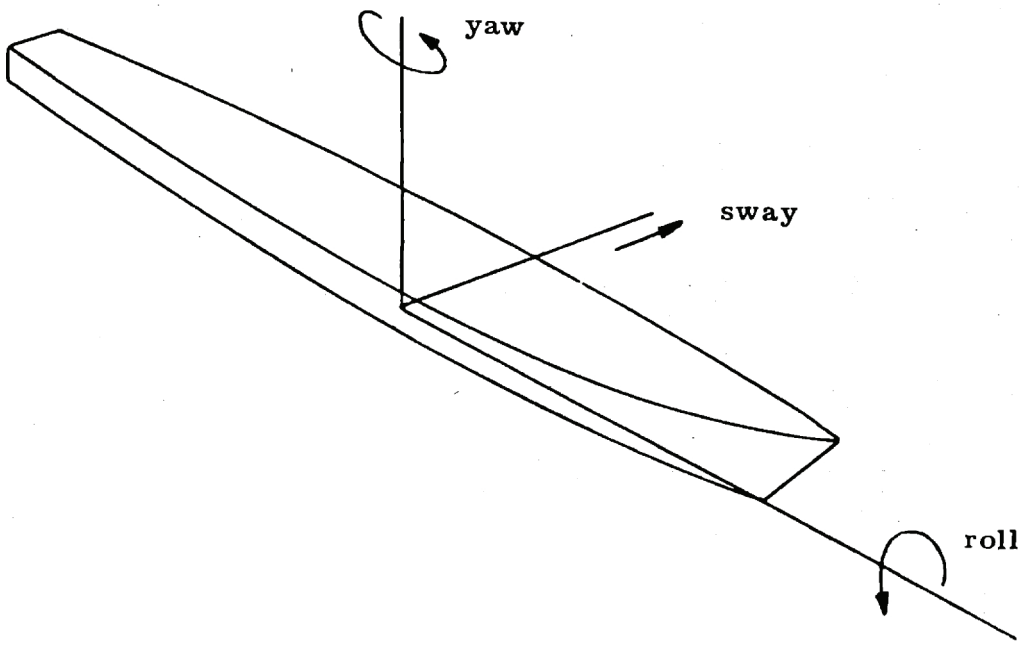

Figure 3.1 : Lateral Ship Motions

The second and third parts of the model put together, represent the response of the ship to the waves. Using the hypothesis of linearity, this response can be represented by a transfer matrix from the wave height to the ship motions. The second part of the model represents the dynamics of the forces generated by the incoming waves, while the third part of the model represent the rigid body dynamics as well as the dynamics induced by the ship motions on the water motion resulting in additional fluid forces. These forces are :

- the inertia force caused by the acceleration of the fluid particles displaced by the ship (added mass)

- the damping force caused by the loss of energy carried away by waves generated by the ship motions

- the hydrostatic force (spring constant).

For a purely sinusoïdal wave, the equations of motion lead to the following differential equation :

$$(M+A_h)\ddot{\underline{x}}_h + B_h\dot{\underline{x}}_h + C_h\underline{x}_h = \underline{F} \qquad (3.1)$$

where :

- M is the mass matrix of the ship, including mass terms, products of inertia and coupling terms due to the difference between the center of the axes and the center of gravity

- A_h is the added mass

- $\underline{x}_h$ is the vector of the ship motions (sway, roll and yaw)

- B_h is the damping term

- C_h is the hydrostatic term
- $\underline{F}$ is the vector of the forces and moments generated by the incoming wave

The terms $\underline{F}$, A_h, and B_h depend on the frequency of the incoming wave, so that the equation of motion is strictly valid for monochromatic waves. For an irregular sea elevation, equation (3.1) becomes an integro-differential equation. An additional difficulty is due to the fact that wave forces and moments are obtained by integrating over the ship hull the space-varying pressure forces, so that their magnitude and phase constitute the transfer function of an infinite dimensional system. Obtaining a finite dimensional model of reasonable size and complexity definitely requires several simplifying approximations that will be indicated in the subsequent paragraphs.

The geometric and mass properties of the DD-963 were analyzed by the M.I.T. Ocean Engineering Department Seakeeping Program [15] . The hydrodynamic coefficients (M, A_h, B_h and C_h) and forces were first obtained, and subsequently the overall ship model was derived.

The parameters of the model are : the speed of the vessel, the direction of the waves, the significant wave height, and the modal frequency of the wave spectrum.

3.3 Sea Modelling

The sea waves are generated by the wind, except for very rare cases (seismic waves). The high frequencies of the wind gusts create wavelets on the surface of the sea, while the steady-state condition of the sea develops

slowly through a nonlinear interaction mechanism creating waves whose phase velocity is close to the wind speed. Since the process starts with high frequencies, a young storm will contain a peak at high frequency. As soon as the wind stops blowing, the water viscosity dissipates the high frequency waves so that the so-called "swell" forms, which consists of long waves (low frequency) which travel away from the storm that originates them. For this reason, swell can be found together with another local storm, in which case the wave height spectrum contains two peaks.

The intensity of the storm can be described in various ways, of which the best is probably the significant wave height H, defined as the statistical average of the 1/3 highest waveheights. At any point, the wave elevation is a stochastic process described by its power spectrum. This power spectrum (if it is single-peaked) is a function primarily of two parameters, H and ω_m. The Bretschneider spectrum is defined as :

$$S(\omega) = \frac{1.25}{4} H^2 \frac{\omega_m^4}{\omega^5} \exp\left(-1.25 \left(\omega_m/\omega\right)^4\right) \qquad (3.2)$$

It was found to fit reasonably well in any sea location, and is strictly valid for unidirectional seas, with unlimited fetch, infinite depth, and no swell.

As the ship moves toward the waves, the apparent frequency of the wave is modified, and the frequency of encounter ω_e is :

$$\omega_e = \omega + k\, U \cos\phi \qquad (3.3)$$

where :

- U is the ship speed
- ϕ is the angle between the x axis of the ship and the direction of the wave propagation
- k is the wave number.

In deep water, the dispersion relation for the waves is :

$$\omega^2 = kg \tag{3.4}$$

so that :

$$\omega_e = \omega + \frac{\omega^2}{g} U \cos\phi \tag{3.5}$$

The spectrum seen from ship coordinates is then :

$$S(\omega_e) = \left(\frac{S(\omega)}{d\omega_e/d\omega} \right)_{\omega=f(\omega_e)} \tag{3.6}$$

where :

$$\omega = f(\omega_e) = \frac{-1 + \sqrt{1 + 4\,\omega_e \frac{U\cos\phi}{g}}}{2\,\frac{U}{g}\cos\phi} \tag{3.7}$$

To obtain a state-space representation, the wave height is represented as the output of a filter with rational transfer function, driven by white noise.

The transfer function is selected to be :

$$H_a(s) = \sqrt{\pi S_o} \; \frac{(\frac{s}{\omega_o})^2}{(1 + 2J(\frac{s}{\omega_o}) + (\frac{s}{\omega_o})^2)^3} \qquad (3.8)$$

where the values of S_o, ω_o, and J are dependent on the sea state and are given in Appendix A.

The coefficient π was introduced to match the differences in definition for the power spectrum. Here, we use :

$$S(\omega) = \int_{-\infty}^{\infty} R(\tau)\, e^{-i\omega\tau}\, d\tau \qquad (3.9)$$

A one-sided (positive frequency) power spectrum is used in wave theory (and for the Bretschneider spectrum):

$$S(\omega) = \frac{1}{\pi} \int_{-\infty}^{\infty} R(\tau)\, e^{-i\omega\tau}\, d\tau \qquad \omega>0 \qquad (3.10)$$

The Bretschneider spectrum and the approximation are illustrated in Fig.3.2.

3.4 Ship Transfer Matrices

The ship transfer matrix from the wave height to the sway, roll and yaw motions can be separated in:

- a transfer matrix from the wave height to the force and moments

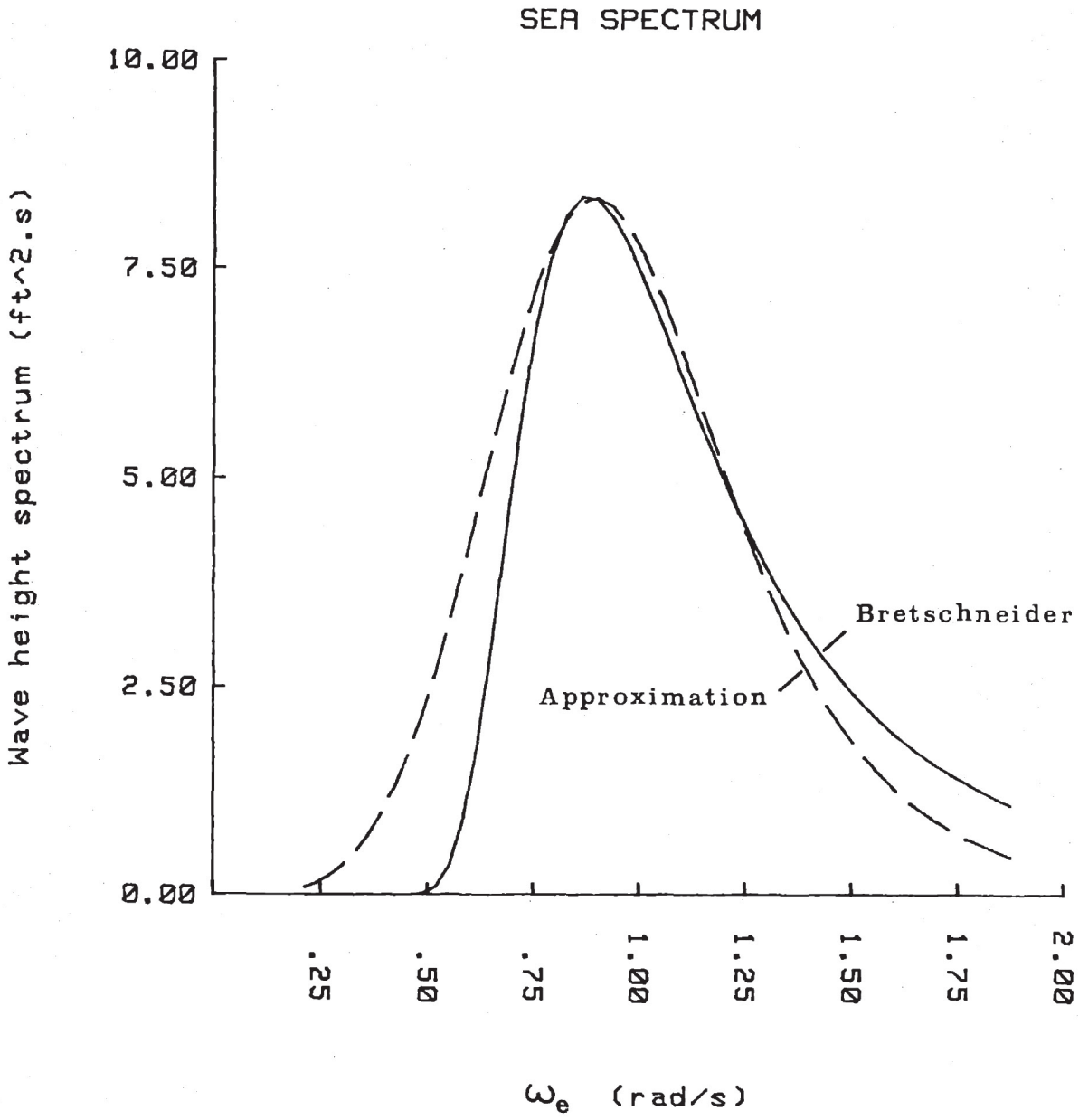

Figure 3.2: Bretschneider Spectrum and Approximation
(H=10ft, ω_m=0.72rad/s)

generated by the incoming wave

- a transfer matrix from the force and moments to the actual motions. These transfer matrices are obtained from the values of the forces, added mass, damping, mass, and hydrostatic forces, using equation (3.1). For monochromatic waves, these were obtained by the M.I.T. Ocean Engineering Seakeeping program from the geometry of the DD-963 hull. Rational approximations were made in order to obtain a standard state-space representation.

An important fact is that whatever approximations are made, they do not influence the stability margins of the aircraft control system. The ship model only comes in the ship Kalman filter design and in the computation of the feedforward gain matrix. The only effect of the approximations on the control system is on the performance attained in the ship motion tracking, not on the system robustness.

3.4.1 Force Dynamics

The transfer functions between a unit amplitude regular wave (1ft) and the sway force (tons) and the roll and yaw moments (tons-feet) as functions of the frequency of encounter are shown in logarithmic scale in Figs 3.3,3.4,3.5 for the case U=0,ϕ=90 degrees and in Figs 3.6,3.7,3.8 for the case U=15.5ft/s and ϕ=45 degrees.

The forces were approximated by simple second-order systems, for example:

$$\underline{F}_i = \frac{F_i\, s^2}{1 + 2\, J_i/\omega_i + (s/\omega_i)^2} \qquad \begin{matrix} i=s,r,y \\ \text{for sway,roll and yaw} \end{matrix} \qquad (3.11)$$

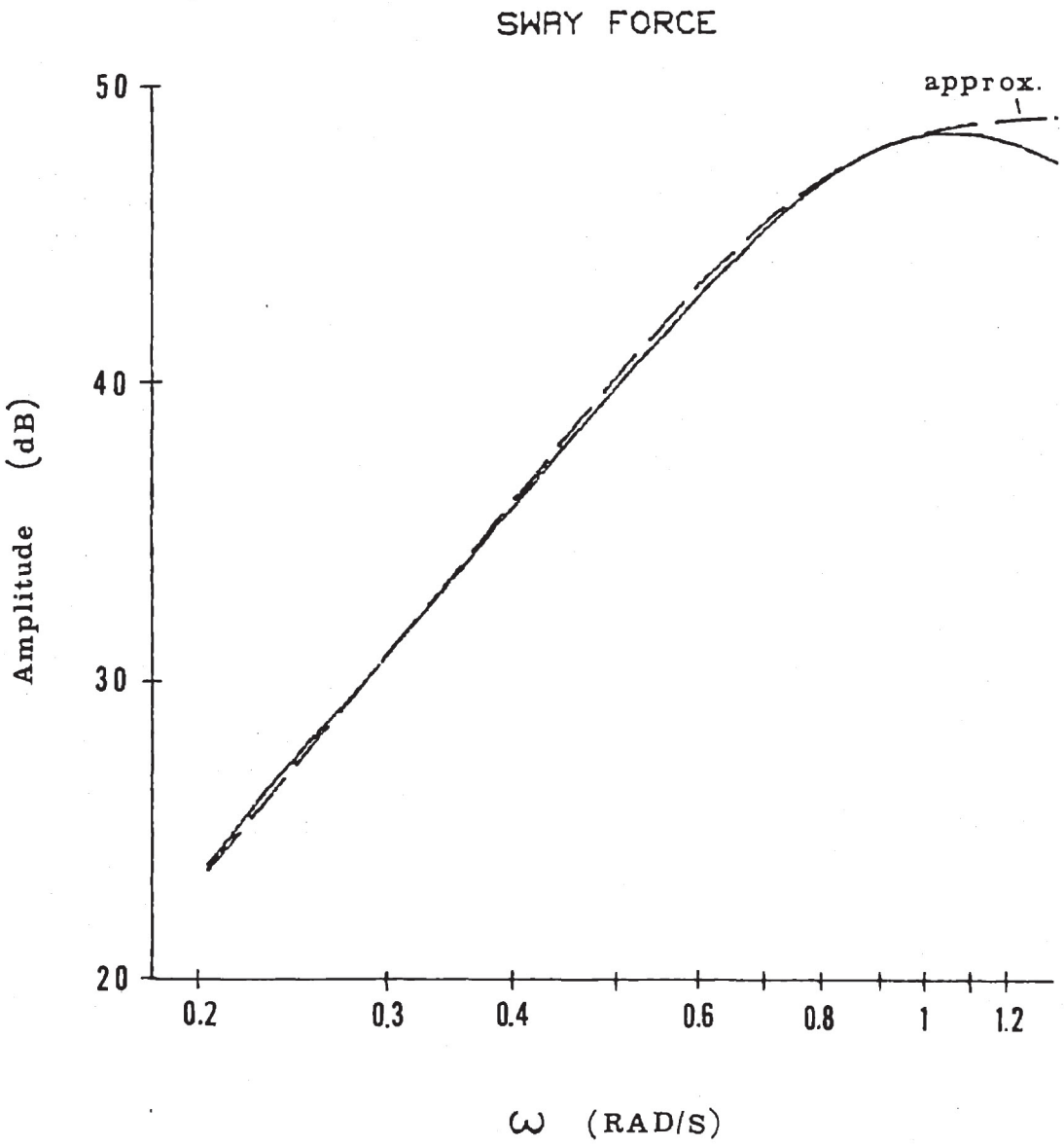

Figure 3.3: Sway Force and its Approximation (U=0, ϕ=90deg)

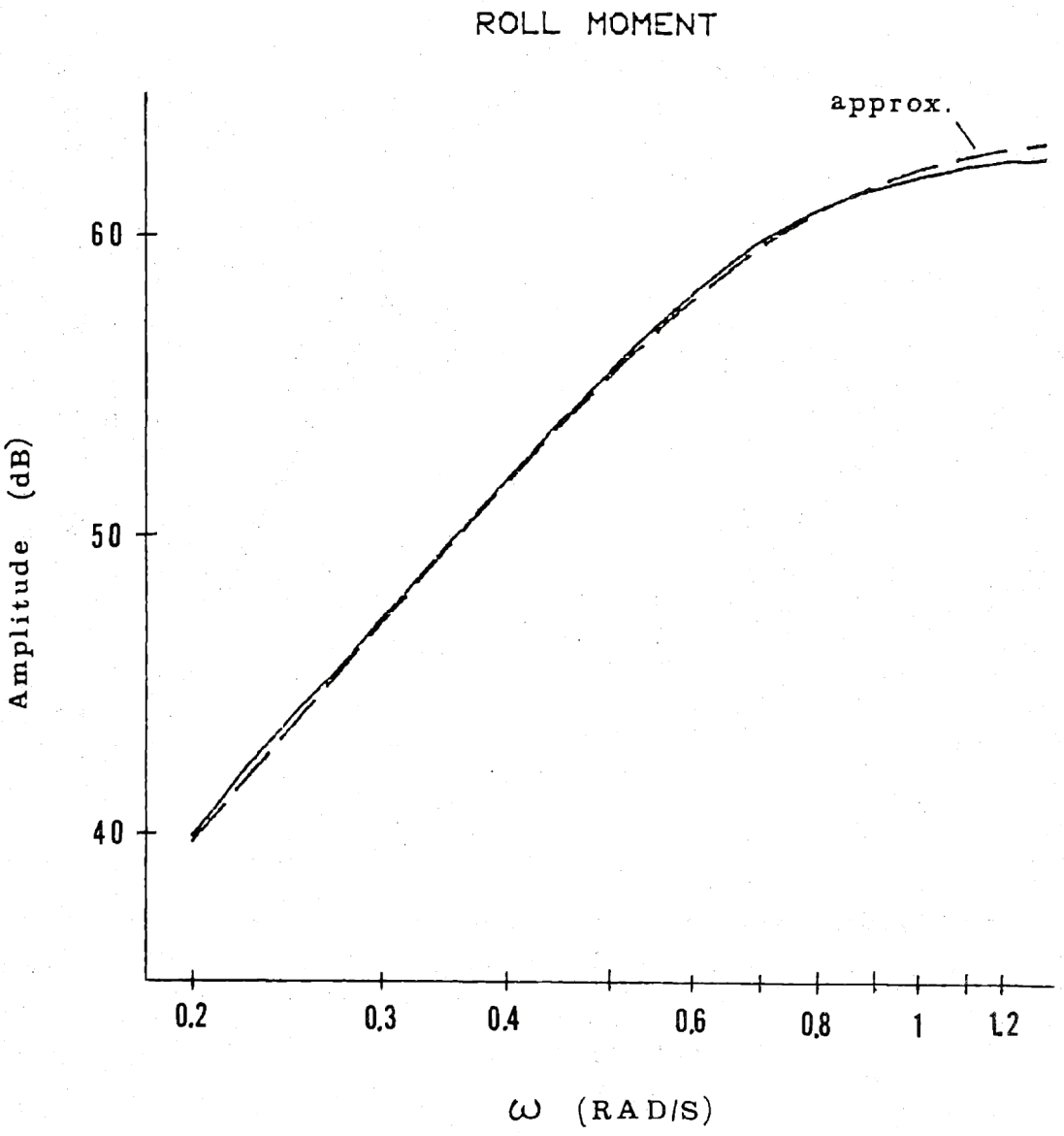

Figure 3.4: Roll Moment and its Approximation (U=0, ϕ=90deg)

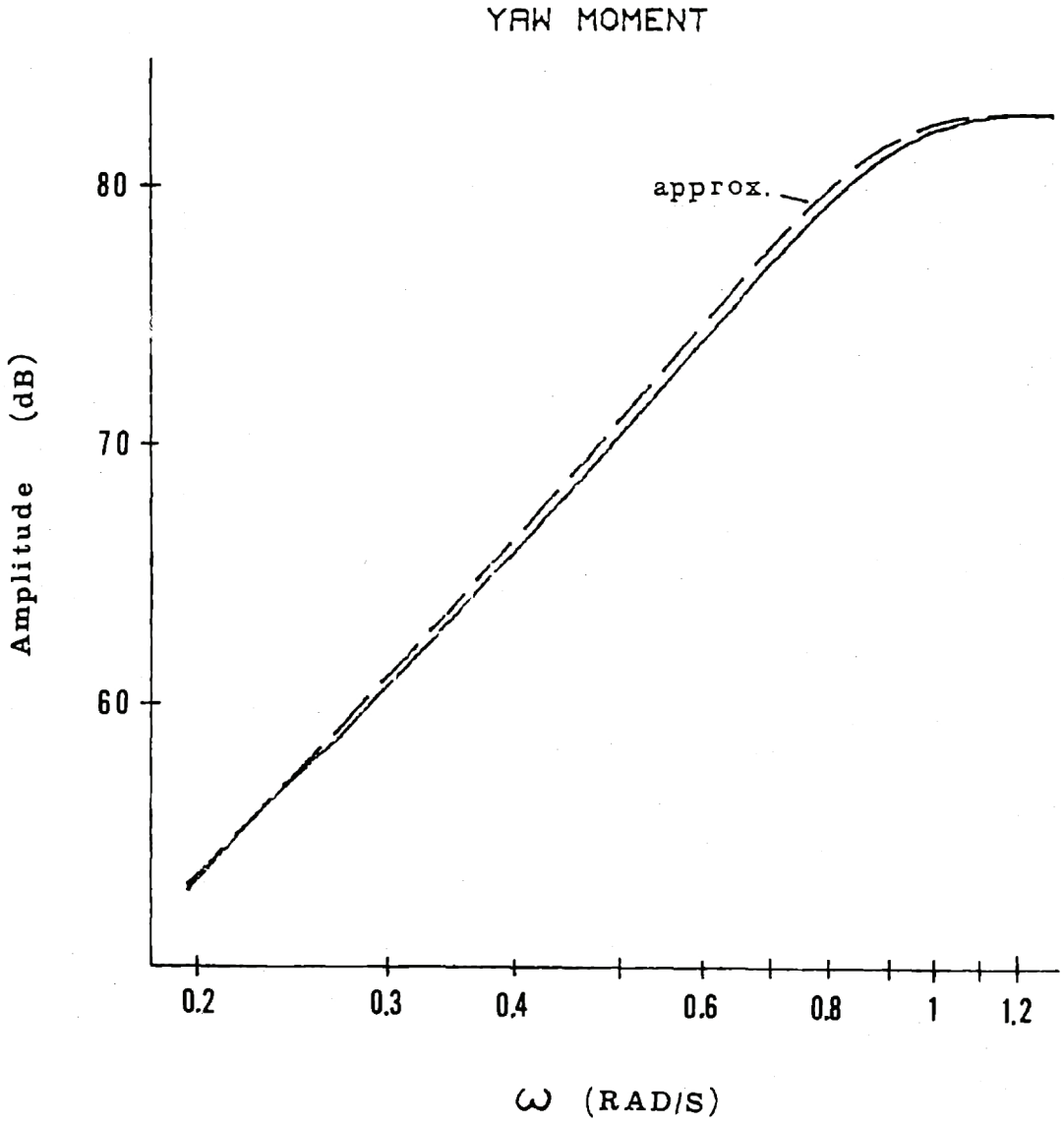

Figure 3.5: Yaw Moment and its Approximation (U=0, ϕ=90deg)

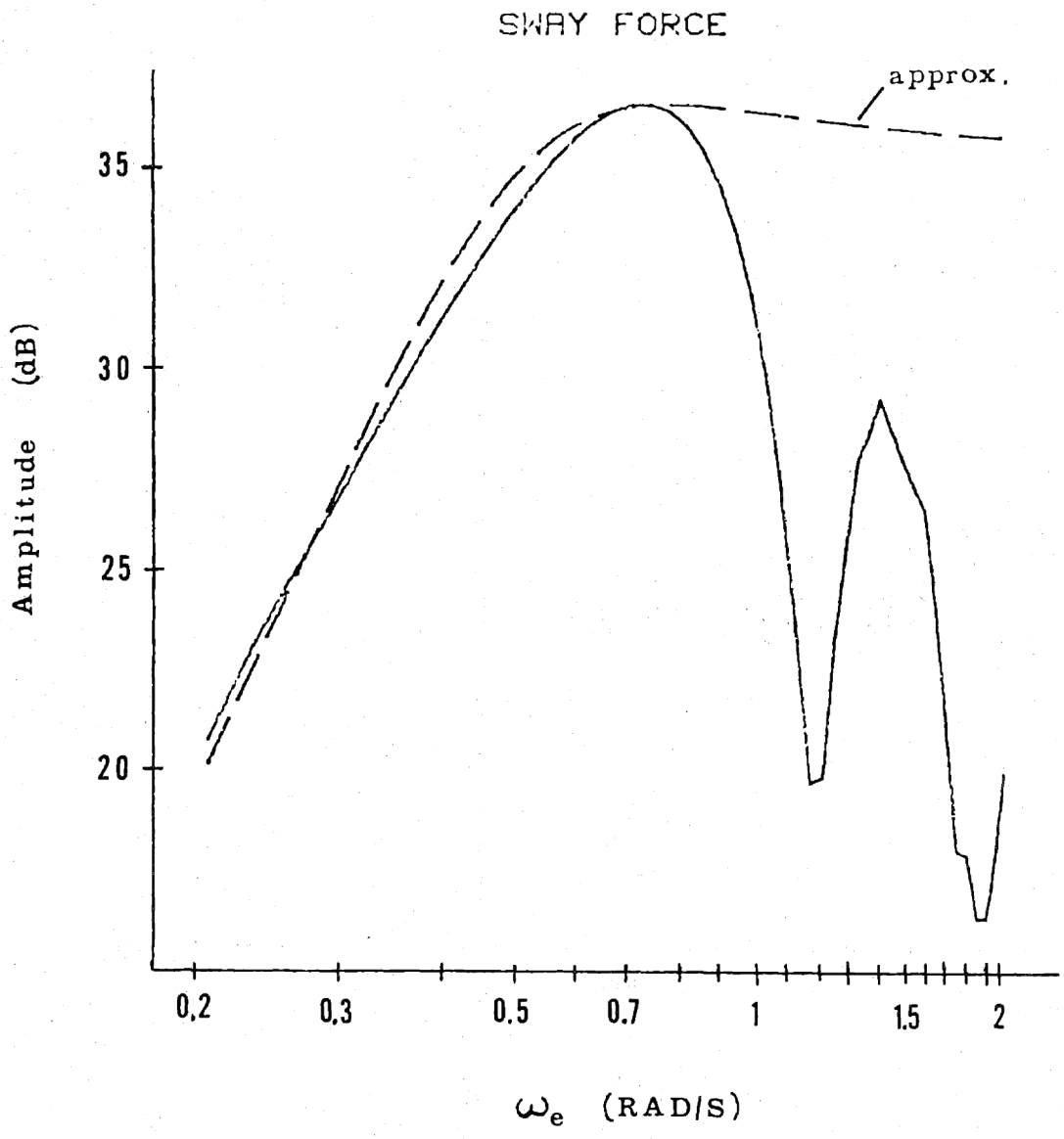

Figure 3.6: Sway Force and its Approximation (U=15.5ft/s, ϕ=45deg)

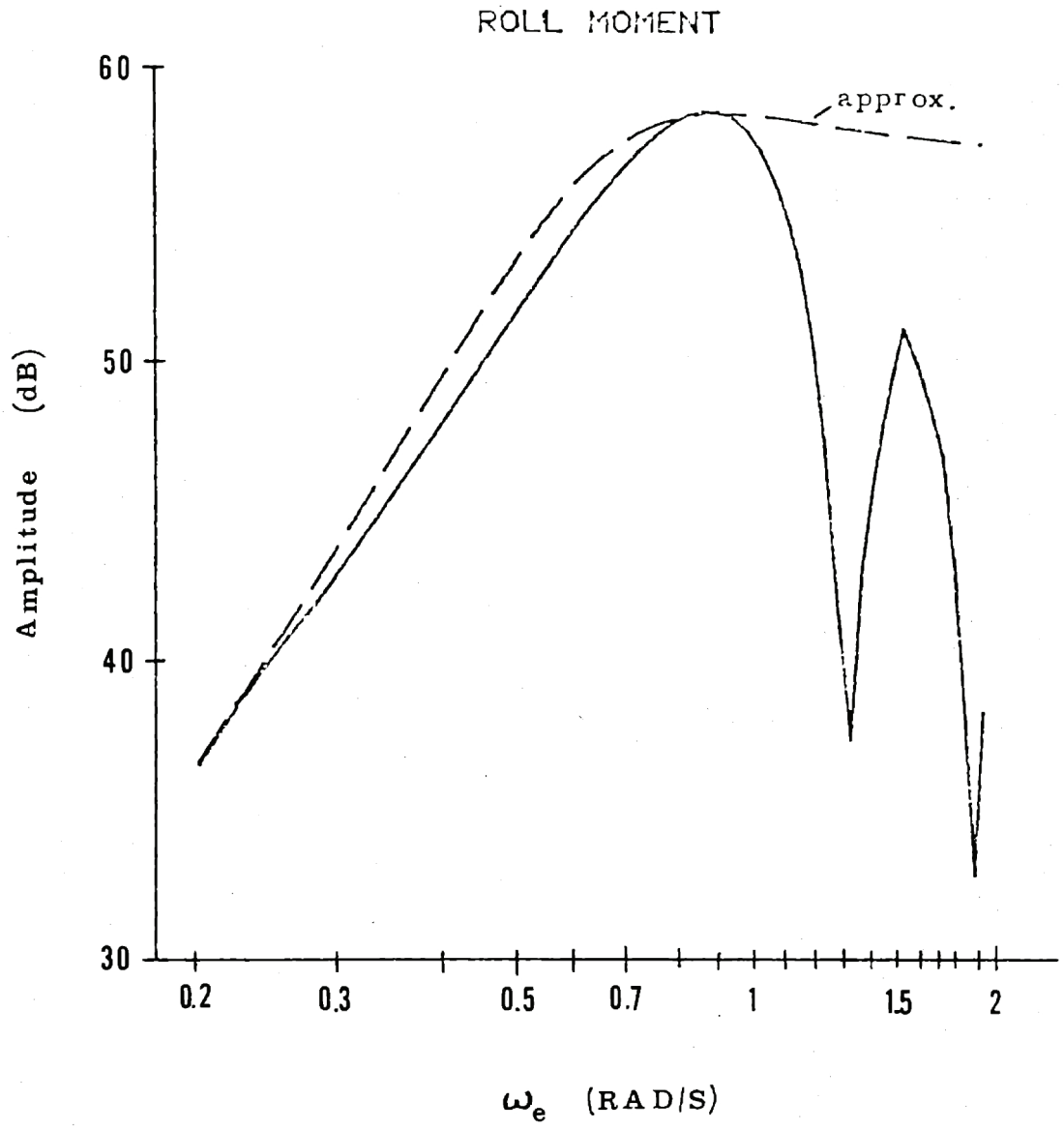

Figure 3.7: Roll Moment and its Approximation (U=15.5ft/s, ϕ=45deg)

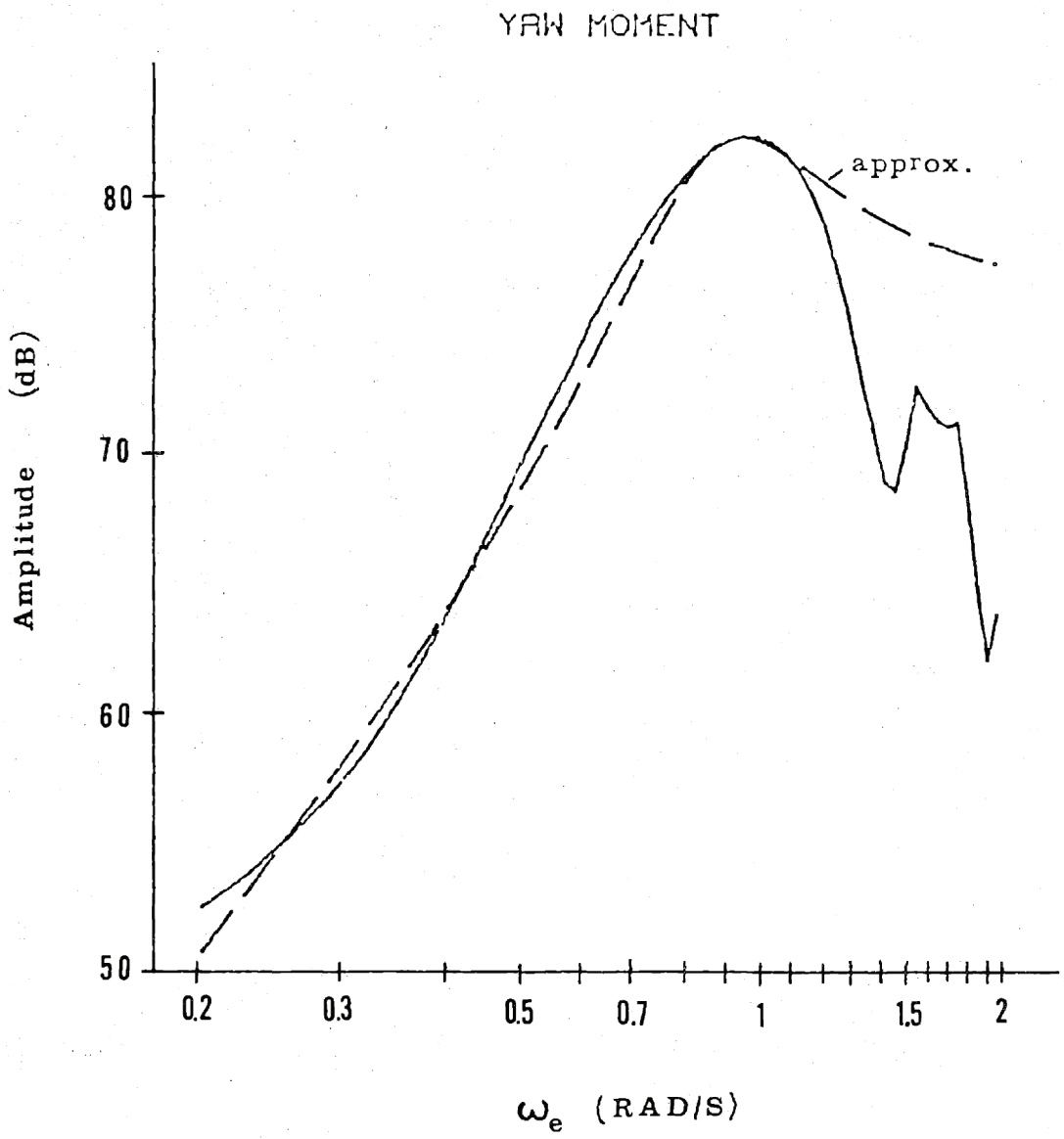

Figure 3.8: Yaw Moment and its Approximation (U=15.5ft/s, ϕ=45deg)

In the case when U=15.5ft/s, ϕ=45degrees, the higher frequency behavior shows the infinite dimensional characteristic of the force dynamics. For simplicity, this effect is not represented in the model, because it is beyond the area of significant wave power.

The values of the coefficients in the transfer function, and their dependence upon ship speed and wave heading angle, are summarized in Appendix A.

3.4.2 Ship Dynamics

The other ship dynamics are related to the matrices A_h, B_h, and C_h. As indicated earlier, the matrices A_h and B_h are dependent on the frequency of the incoming wave, so that the order of the differential equation:

$$(M+A_h)\ddot{\underline{x}}_h + B_h\dot{\underline{x}}_h + C_h\underline{x}_h = \underline{F} \qquad (3.12)$$

is higher than 2 times the three motions.

However, the roll motion turns out to be highly concentrated around the roll peak frequency. The sway and yaw power spectra are more widely dispersed, but, due to the concentration of the sea spectrum in frequency, the motions are all concentrated within a narrow frequency band. Consequently, the added mass and damping matrices variations with frequency are neglected, and the values of these matrices at the roll peak frequency are used here.

Another important variation of the A_h and B_h matrices is due to the ship speed and heading angle. These produce coupling terms between the

motions that, again, are frequency dependent. These couplings are accounted for but, consistently with the previous discusssion, their influence is assumed to be constant with frequency, and their value is taken equal to their actual value at the roll peak frequency. With these approximations, the values of the added mass, damping, and hydrostatic terms, as well as their variations with speed and heading angle, are contained in Appendix A.

Figures 3.9, 3.10, and 3.11 show the overall result of the approximations on the ship dynamics. The highly-tuned second-order behavior of the roll transfer function is obvious, and the approximations appear to be very good. The higher frequency dynamics are neglected, but the approximations are in a sense conservative.

The derivation of a state-space model from the rational transfer functions obtained for the sea and the forces is straightforward. For the ship dynamics, some care has to be taken.

Taking the matrices A_h and B_h constant, the differential equation:

$$(M+A_h)\ddot{\underline{x}}_h + B_h\dot{\underline{x}}_h + C_h\underline{x}_h = \underline{F} \tag{3.13}$$

is of order 6. By selecting $R = (M+A_h)^{-1}$, $P = (M+A_h)^{-1}B_h$, and $Q = (M+A_h)^{-1}C_h$, the following state-space representation can be obtained:

$$\begin{bmatrix} \dot{\underline{x}}_h \\ \underline{x}_h \end{bmatrix} = \begin{bmatrix} -P & -Q \\ I & 0 \end{bmatrix} \begin{bmatrix} \dot{\underline{x}}_h \\ \underline{x}_h \end{bmatrix} + \begin{bmatrix} R \\ 0 \end{bmatrix} \underline{F} \tag{3.14}$$

The state-space representation includes 6 states (3 motions and their

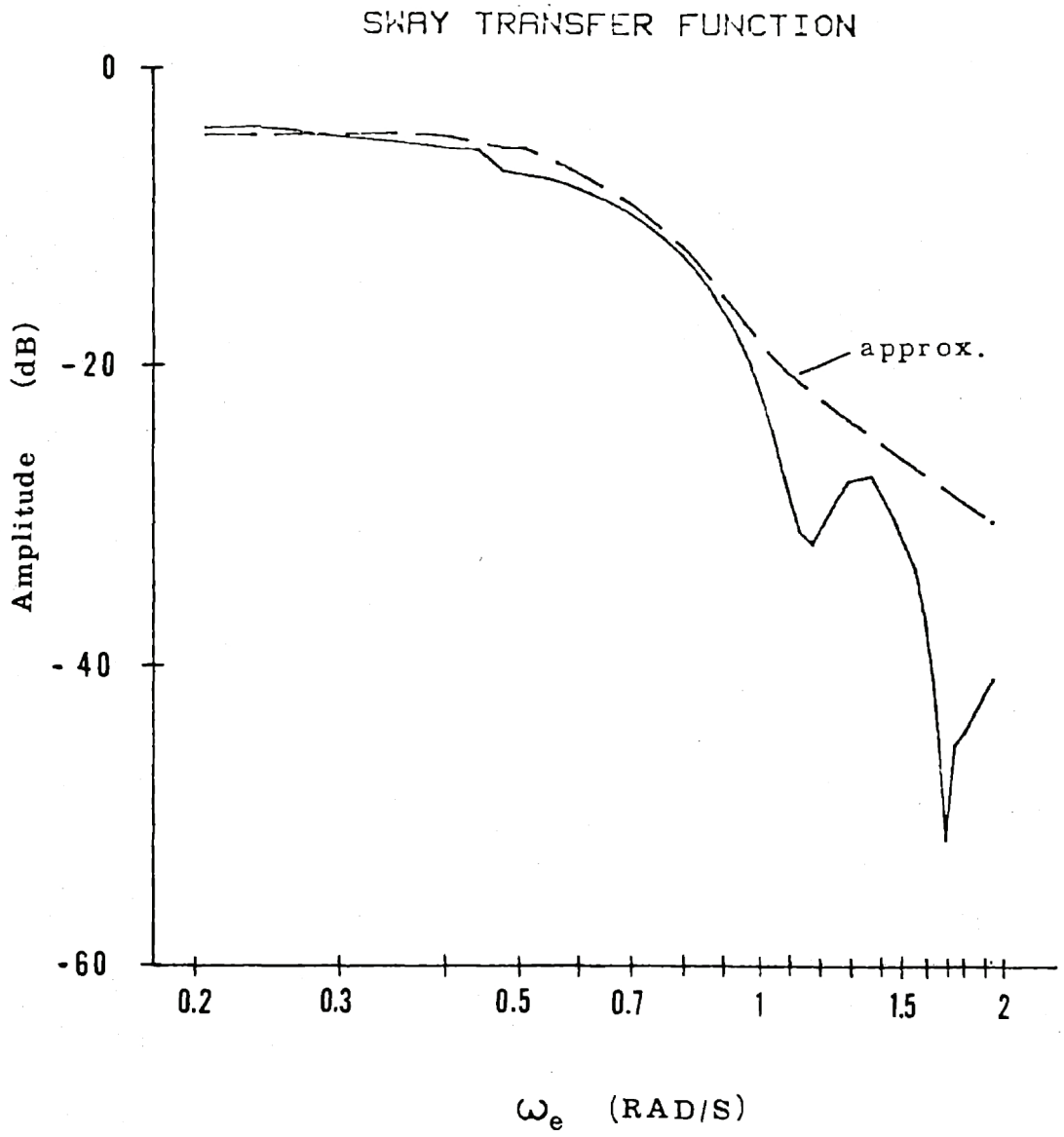

Figure 3.9: Sway Transfer Function and its Approximation
(U=15.5ft/s, ϕ=45deg)

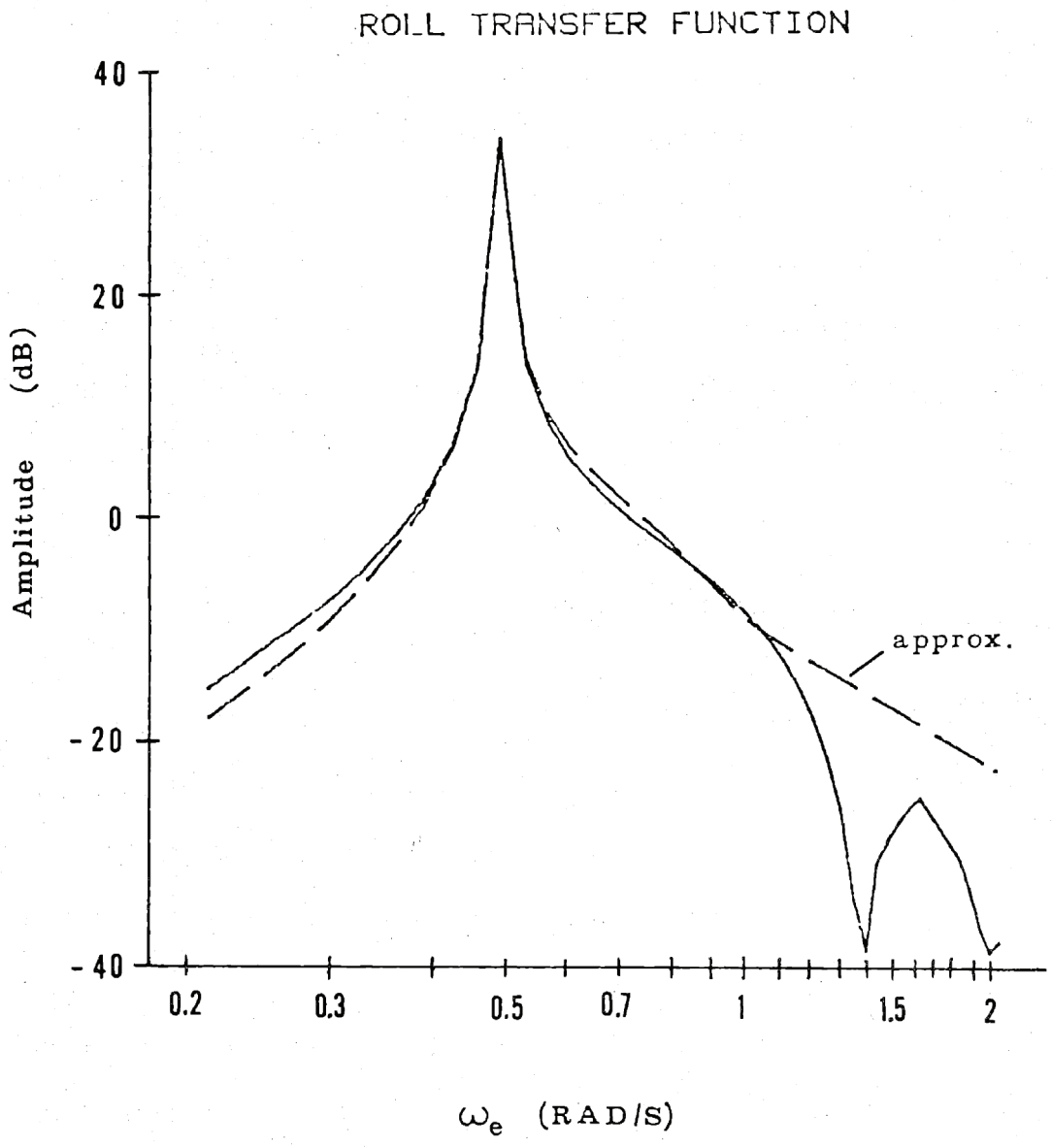

Figure 3.10: Roll Transfer Function and its Approximation (U=15.5ft/s, ϕ=45deg)

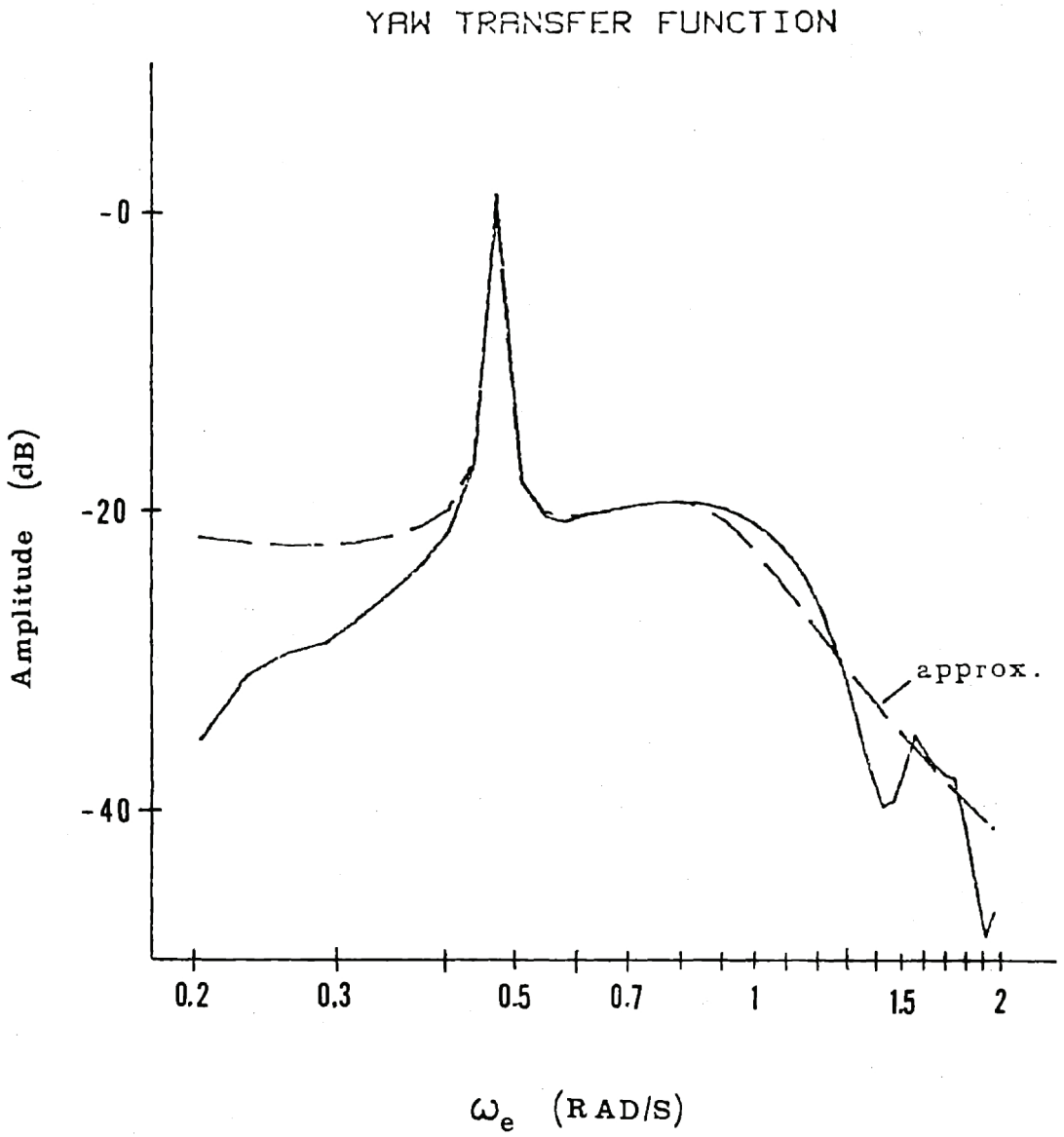

Figure 3.11: Yaw Transfer Function and its Approximation (U=15.5ft/s, ϕ=45deg)

derivatives).

When combining this model with the model for the forces, two pole-zero cancellations occur. The ship dynamics include two poles at the origin, which are due to the zero spring constant for sway and yaw, while the forces dynamics have each two zeros at the origin, as previously mentionned. These pole-zero cancellations lead to a non-minimal order system, and to instabilities in numerical simulations. By simple algebraic manipulations, detailed in Appendix A, this problem can be resolved, and a 4th order model of the ship dynamics is obtained, including the sway, roll, yaw motions, and only the roll derivative.

3.5 Overall Ship Model

The overall ship model is written in state-space form :

$$\dot{\underline{x}}_S = A_S \underline{x}_S + \underline{\xi}_S \tag{3.15}$$

The state vector contains 16 states :

x_1 : wave elevation (ft)

x_2 : wave elevation derivative (ft/s)

x_3 to x_6 : states related to the sea dynamics

x_7 : $\int$ sway force (tons.s)

x_8 : sway force (tons)

x_9 : $\int$ roll moment (tons.ft.s)

x_{10} : roll moment (tons.ft)

x_{11} : $\int$ yaw moment (tons.ft.s)

x_{12} : yaw moment (tons.ft)

x_{13} : sway displacement (ft)

x_{14} : roll rate (rad/s)

x_{15} : roll angle (rad)

x_{16} : yaw angle (rad)

The structure of the matrix A_S is defined on Table 3.1, and the numerical values for the condition : H=10ft, ω_m=0.72rad/s, U=15.5ft/s, and ϕ=45degrees are given in Table 3.2 and Table 3.3 (for any condition, see Appendix A).

The vector $\underline{\xi}_S$ is a white noise vector whose only non-zero element is the 6th row element. Its spectral intensity is πS_o.

3.6 Additional Comments

Weather conditions of zero visibility and sea state 5 are considered in this study. Sea state 5 corresponds to a significant wave height of 10ft and a modal frequency of 0.72rad/s, for fully developed seas. The ship speed will be assumed to be 15.5ft/s (about 10kts) and the wave heading angle 45 degrees. A second sea condition will be sometimes used. It corresponds to the condition numbered condition 4 in [11], with significant wave height 12ft and modal frequency 0.4807rad/s (this is the less common case of decaying seas).

The ship model poles and the rms motions values (at the reference point) are given in Table 3.4. The model poles are also shown on Fig.3.12, for the case H=10ft, ω_m=0.72rad/s. Six poles correspond to the sea spectrum.

$$
A_S =
\left[\begin{array}{cccc|cccc|cccc|cccc}
0 & 1 & 0 & 0 & 0 & 0 & 0 & 0 & 0 & 0 & 0 & 0 & 0 & 0 & 0 & 0 \\
-\omega_o^2 & -2J\omega_o & \omega_o^2 & 0 & 0 & 0 & 0 & 0 & 0 & 0 & 0 & 0 & 0 & 0 & 0 & 0 \\
0 & 0 & 0 & 1 & 0 & 0 & 0 & 0 & 0 & 0 & 0 & 0 & 0 & 0 & 0 & 0 \\
0 & 0 & -\omega_o^2 & -2J\omega_o & \omega_o^2 & 0 & 0 & 0 & 0 & 0 & 0 & 0 & 0 & 0 & 0 & 0 \\
0 & 0 & 0 & 0 & 0 & 1 & 0 & 0 & 0 & 0 & 0 & 0 & 0 & 0 & 0 & 0 \\
0 & 0 & 0 & 0 & -\omega_o^2 & -2J\omega_o & 0 & 0 & 0 & 0 & 0 & 0 & 0 & 0 & 0 & 0 \\
\hline
0 & 0 & 0 & 0 & 0 & 0 & 0 & 1 & 0 & 0 & 0 & 0 & 0 & 0 & 0 & 0 \\
0 & F_s\omega_s^2 & 0 & 0 & 0 & 0 & -\omega_s^2 & -2J_s\omega_s & 0 & 0 & 0 & 0 & 0 & 0 & 0 & 0 \\
0 & 0 & 0 & 0 & 0 & 0 & 0 & 0 & 1 & 0 & 0 & 0 & 0 & 0 & 0 & 0 \\
0 & F_r\omega_r^2 & 0 & 0 & 0 & 0 & 0 & 0 & -\omega_r^2 & -2J_r\omega_r & 0 & 0 & 0 & 0 & 0 & 0 \\
0 & 0 & 0 & 0 & 0 & 0 & 0 & 0 & 0 & 0 & 1 & 0 & 0 & 0 & 0 & 0 \\
0 & F_y\omega_y^2 & 0 & 0 & 0 & 0 & 0 & 0 & -\omega_y^2 & -2J_y\omega_y & 0 & 0 & 0 & 0 & 0 & 0 \\
\hline
0 & 0 & 0 & 0 & 0 & 0 & u_{11} & 0 & 0 & 0 & u_{15} & 0 & t_{11} & t_{12} & t_{13} & t_{14} \\
0 & 0 & 0 & 0 & 0 & 0 & u_{21} & u_{22} & 0 & u_{24} & u_{25} & u_{26} & t_{21} & t_{22} & t_{23} & t_{24} \\
0 & 0 & 0 & 0 & 0 & 0 & 0 & 0 & 0 & 0 & 0 & 0 & 0 & 1 & 0 & 0 \\
0 & 0 & 0 & 0 & 0 & 0 & u_{41} & 0 & 0 & 0 & u_{45} & 0 & t_{41} & t_{42} & t_{43} & t_{44}
\end{array}\right]
$$

Table 3.1: Ship Model A_S Matrix

0.	1.	0.	0.	0.	0.	0.	0.
-1.136E+00	-1.507E+00	0.	1.136E+00	0.	0.	0.	0.
0.	0.	0.	1.	0.	0.	0.	0.
0.	0.	-1.136E+00	-1.507E+00	0.	1.136E+00	0.	0.
0.	0.	0.	0.	0.	1.	0.	0.
0.	0.	0.	0.	-1.136E+00	-1.507E+00	0.	0.
0.	0.	0.	0.	0.	0.	0.	1.
0.	5.722E+01	0.	0.	0.	0.	-2.610E-01	-5.202E-01
0.	0.	0.	0.	0.	0.	0.	0.
0.	6.859E+02	0.	0.	0.	0.	0.	0.
0.	0.	0.	0.	0.	0.	0.	0.
0.	6.481E+03	0.	0.	0.	0.	0.	0.
0.	0.	0.	0.	0.	0.	2.423E-03	0.
0.	0.	0.	0.	0.	0.	3.218E-06	1.375E-06
0.	0.	0.	0.	0.	0.	0.	0.
0.	0.	0.	0.	0.	0.	-4.057E-06	0.

Table 3.2: Ship Model A_S Matrix Value, Columns 1 to 8
(H=10ft, ω_m=0.72rad/s)

0.	0.	0.	0.	0.	0.	0.	0.
0.	0.	0.	0.	0.	0.	0.	0.
0.	0.	0.	0.	0.	0.	0.	0.
0.	0.	0.	0.	0.	0.	0.	0.
0.	0.	0.	0.	0.	0.	0.	0.
0.	0.	0.	0.	0.	0.	0.	0.
0.	0.	0.	0.	0.	0.	0.	0.
0.	0.	0.	0.	0.	0.	0.	0.
0.	1.	0.	0.	0.	0.	0.	0.
-4.575E-01	-6.696E-01	0.	0.	0.	0.	0.	0.
0.	0.	0.	1.	0.	0.	0.	0.
0.	0.	-8.111E-01	-4.458E-01	0.	0.	0.	0.
0.	0.	-4.469E-06	0.	-8.343E-03	2.748E-01	1.097E-01	8.041E+00
0.	8.142E-06	-1.999E-08	-1.804E-07	4.343E-05	-1.961E-02	-2.344E-01	1.286E-02
0.	0.	0.	0.	0.	1.	0.	0.
0.	0.	1.299E-07	0.	-4.611E-04	-2.319E-02	4.892E-04	-3.242E-02

Table 3.3: Ship Model A_S Matrix Value, Columns 9 to 16
(H=10ft, ω_m=0.72rad/s)

Ship speed : U=15.5ft/s Wave heading angle : ϕ=45°	
SEA : H=10ft ω_m=0.72rad/s	SEA : H=12ft ω_m=0.4807rad/s
Ship model poles :	
$p_{1,2}$ = -0.754 ± j 0.754	$p_{1,2}$ = -0.470 ± j 0.470
$p_{3,4}$ = -0.754 ± j 0.754	$p_{3,4}$ = -0.470 ± j 0.470
$p_{5,6}$ = -0.754 ± j 0.754	$p_{5,6}$ = -0.470 ± j 0.470
$p_{7,8}$ = -0.223 ± j 0.873	
$p_{9,10}$ = -0.335 ± j 0.588	
$p_{11,12}$ = -0.260 ± j 0.440	SAME
$p_{13,14}$ = -0.00983 ± j 0.484	
$p_{15,16}$ = -0.0204 ± j 0.0597	
Ship model rms motions values :	
σ_{sway} = 0.612ft	σ_{sway} = 1.36ft
σ_{roll} = 4.56°	σ_{roll} = 12.6°
σ_{yaw} = 0.227°	σ_{yaw} = 0.373°

Table 3.4: Ship Model Poles and Rms Motions (at the reference point)

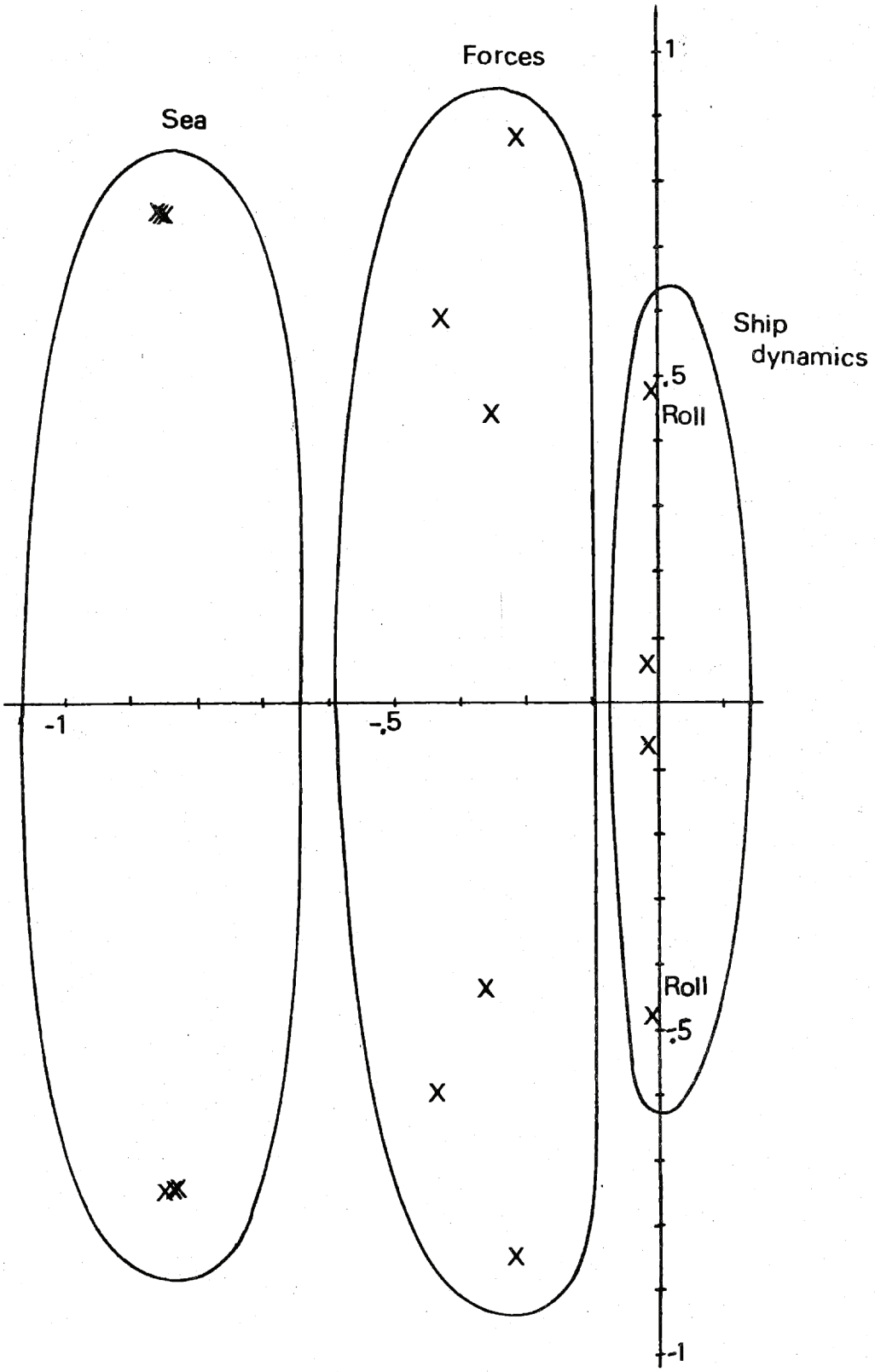

Figure 3.12 : Ship Model Poles (H=10ft, ω_m=0.72rad/s)

Six other poles correspond to the force dynamics (2 for each motion). The four remaining poles correspond to the ship dynamics : there are in fact six poles (two for each motion), but two pure integrators in sway and yaw were eliminated with zeros at the origin. There is a very lightly damped mode with frequency close to 0.5 rad/s, corresponding to the roll oscillation mode. Another lightly damped mode of low frequency appears, but its contribution is small, due to the presence of zeros at the origin.

For the VTOL landing problem, the motions of interest are the motions at the landing pad. The sway motion at the landing area is composed of the sway at the center of the axes, plus contributions from the roll and the yaw angular motions. In the ship coordinates, the landing pad is located at :

$$x_{SLP} = -127 \text{ ft} \tag{3.16}$$

$$z_{SLP} = 34 \text{ ft} \tag{3.17}$$

The sign conventions for the aircraft are also different than those for the ship, so that the output matrix providing the sway, roll and yaw motions of the landing pad in aircraft coordinates is :

$$C_{SLP} = \begin{bmatrix} 0 & 0 & 0 & 0 & 0 & 0 & 0 & 0 & 0 & 0 & 0 & 0 & -1 & 0 & 34 & 127 \\ 0 & 0 & 0 & 0 & 0 & 0 & 0 & 0 & 0 & 0 & 0 & 0 & 0 & 0 & 1 & 0 \\ 0 & 0 & 0 & 0 & 0 & 0 & 0 & 0 & 0 & 0 & 0 & 0 & 0 & 0 & 0 & -1 \end{bmatrix} \tag{3.18}$$

3.7 Summary

In this chapter, a ship model was derived from hydrodynamic data obtained from the geometry of the DD963 ship hull. The ship motion model is divided in a sea model, and a ship model. The sea spectrum appears to be concentrated in a narrow frequency band centered around 1 rad/s, so that all motions have relatively limited power spectra. Roll motion especially appears to be highly concentrated in frequency, as it behaves like a lightly damped second-order system.

Some approximations had to be made in order to obtain a finite dimensional model of reasonable order. It was demonstrated that these approximations were very good in the frequency range of interest. The resulting model, expressed in state-space form, and its salient characteristics were discussed.

CHAPTER 4

SHIP MOTION ESTIMATION AND PREDICTION

4.1 Ship Kalman Filter

The Kalman filter role in an LQG design was indicated in chapter 2. Here the Kalman filter tasks are the following :

- reconstruct the states that are not directly measurable, as for example the sea states (this is essential to the prediction of the ship motions)

- provide optimal estimates of the states, including those that are measurable, but are affected by noise. In this sense, the estimator is really a filter that filters the noise affecting the measurements.

The measurements of ship motions are affected by noise that is not simply the instrument noise, but is also caused by the structural vibrations. These vibrations can be quite significant, and we want these high frequency motions to be filtered by the Kalman filter, and to keep the filter poles within the range of frequencies which is significant of ship motions.

The measurement equation is :

$$\underline{y}_S = C_S \underline{x}_S + \underline{\theta}_S \qquad (4.1)$$

It is assumed that the only measurements available are the sway displacement, the roll angle and the yaw angle, so that :

$$C_S = \begin{bmatrix} 0 & 0 & 0 & 0 & 0 & 0 & 0 & 0 & 0 & 0 & 0 & 0 & 1 & 0 & 0 & 0 \\ 0 & 0 & 0 & 0 & 0 & 0 & 0 & 0 & 0 & 0 & 0 & 0 & 0 & 0 & 1 & 0 \\ 0 & 0 & 0 & 0 & 0 & 0 & 0 & 0 & 0 & 0 & 0 & 0 & 0 & 0 & 0 & 1 \end{bmatrix} \tag{4.2}$$

The filter is designed assuming the measurement noise spectral intensity matrix to be :

$$\Theta_S = \begin{bmatrix} 0.1 & 0 & 0 \\ 0 & 0.0002 & 0 \\ 0 & 0 & 0.0002 \end{bmatrix} \tag{4.3}$$

and the filter poles are within a radius of 1.1 rad/s. The filter poles and the predicted rms estimation errors are indicated in Table 4.1.

The rms estimation errors are the square roots of the diagonal elements of the covariance matrix of the error :

$$P_{ee} = E(\underline{e}_S \cdot \underline{e}_S^T) \tag{4.4}$$

Having :

$$\dot{\underline{x}}_S = A_S \underline{x}_S + \underline{\xi}_S \tag{4.5}$$

$$\underline{y}_S = C_S \underline{x}_S + \underline{\theta}_S \tag{4.6}$$

$$\dot{\hat{\underline{x}}}_S = A_S \hat{\underline{x}}_S + H_S (\underline{y}_S - C_S \hat{\underline{x}}_S) \tag{4.7}$$

The error is defined by :

$$\underline{e}_S = \hat{\underline{x}}_S - \underline{x}_S \tag{4.8}$$

SEA H=10ft ω_m=0.72rad/s	
Kalman filter poles :	Rms estimation errors :
$p_{1,2}$ = -1.067 ± j 1.086	e_{sway} = 0.241 ft
$p_{3,4}$ = -0.457 ± j 1.312	e_{roll} = 0.560°
$p_{5,6}$ = -1.279 ± j 0.477	e_{yaw} = 0.0776°
$p_{7,8}$ = -0.210 ± j 0.934	
$p_{9,10}$ = -0.365 ± j 0.523	
$p_{11,12}$ = -0.087 ± j 0.446	
$p_{13,14}$ = -0.159 ± j 0.165	
$p_{15,16}$ = -0.0203 ± j 0.0595	

Table 4.1: Ship Kalman Filter Poles and Rms Estimation Errors

The error is governed by the differential equation :

$$\dot{\underline{e}}_S = (A_S - H_S C_S)\underline{e}_S - \underline{\xi}_S - H_S\underline{\theta}_S \tag{4.9}$$

so that P_{ee} is the solution of the 16th order Lyapunov equation :

$$(A_S - H_S C_S)P_{ee} + P_{ee}(A_S - H_S C_S)^T + \Xi_S + H_S\Theta_S H_S^T = 0 \tag{4.10}$$

Figures 4.1, 4.2, and 4.3 illustrate time simulations of the ship motions and of the estimated motions by the Kalman filter.

4.2 Sensitivity of the Estimation Error to Parameter Uncertainty

A study of the sensitivity of the estimation error to parameter uncertainty indicates those model parameters that are important in the estimation process.

The error equation of the Kalman filter with incorrect model is given in [16]. Assuming the correct model to be :

$$\dot{\underline{x}}_S = A_S\underline{x}_S + \underline{\xi}_S \tag{4.11}$$

$$\underline{y}_S = C_S\underline{x}_S + \underline{\theta}_S \tag{4.12}$$

and the filter designed with A_S^* and C_S^*, so that :

$$\dot{\underline{\hat{x}}}_S = A_S^*\underline{\hat{x}}_S + H_S(\underline{y}_S - C_S^*\underline{x}_S) \tag{4.13}$$

The error equation is :

$$\dot{\underline{e}}_S = (A_S^* - H_S C_S^*)\underline{e}_S + (A_S^* - A_S - H_S(C_S^* - C_S))\underline{x}_S - \underline{\xi}_S - H_S\underline{\theta}_S \tag{4.14}$$

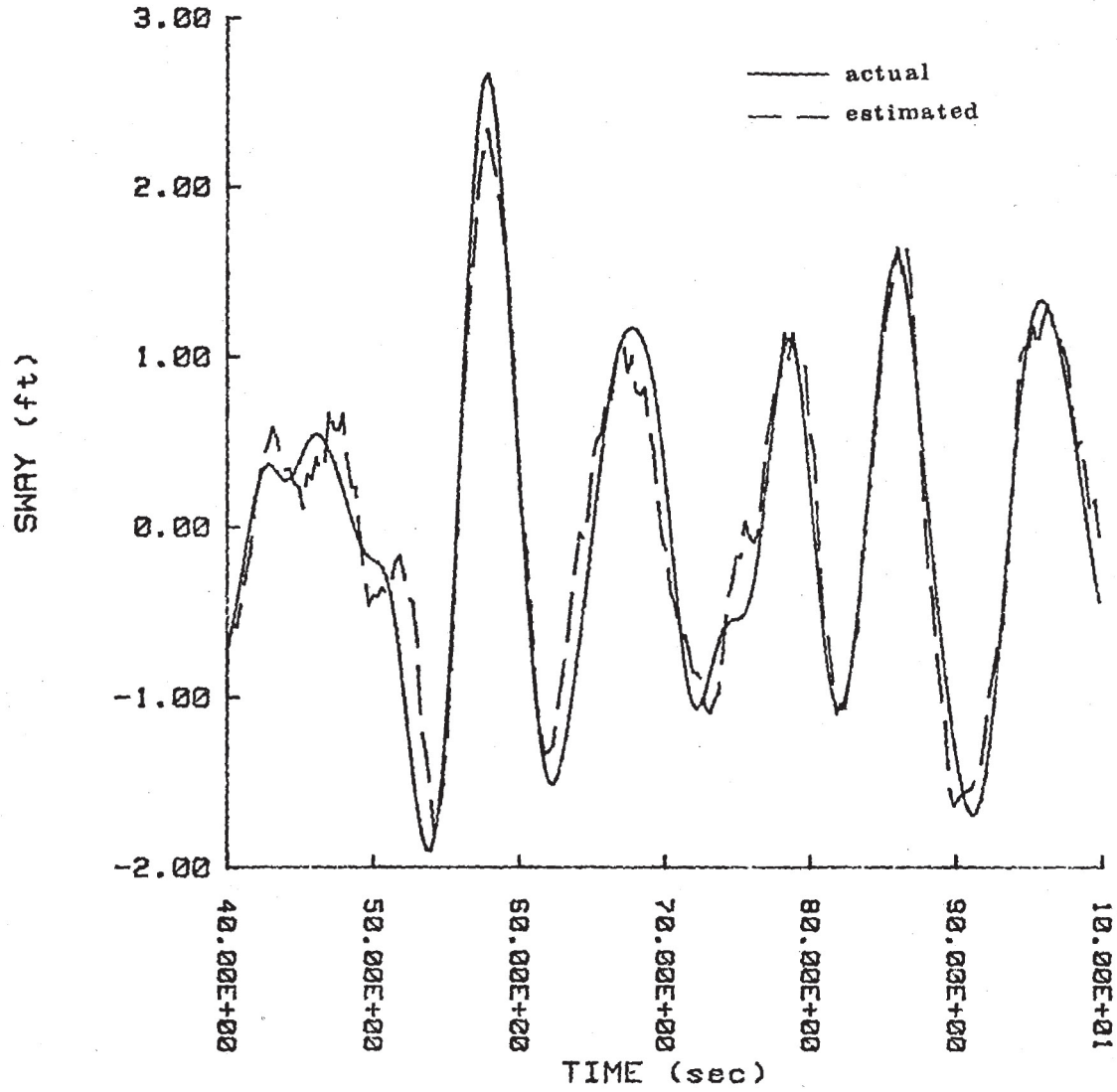

Figure 4.1: Sway Actual and Estimated Motion

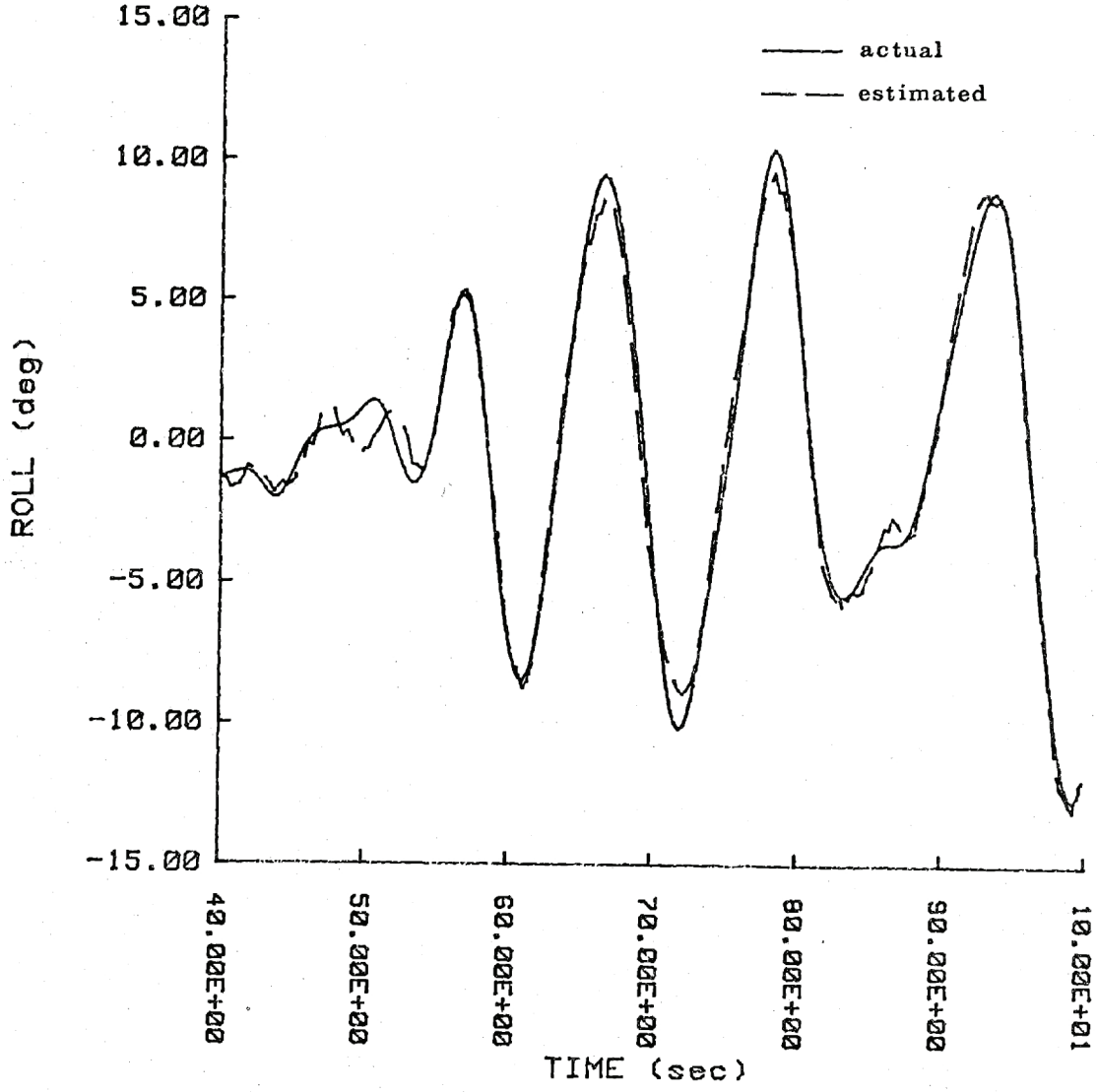

Figure 4.2: Roll Actual and Estimated Motion

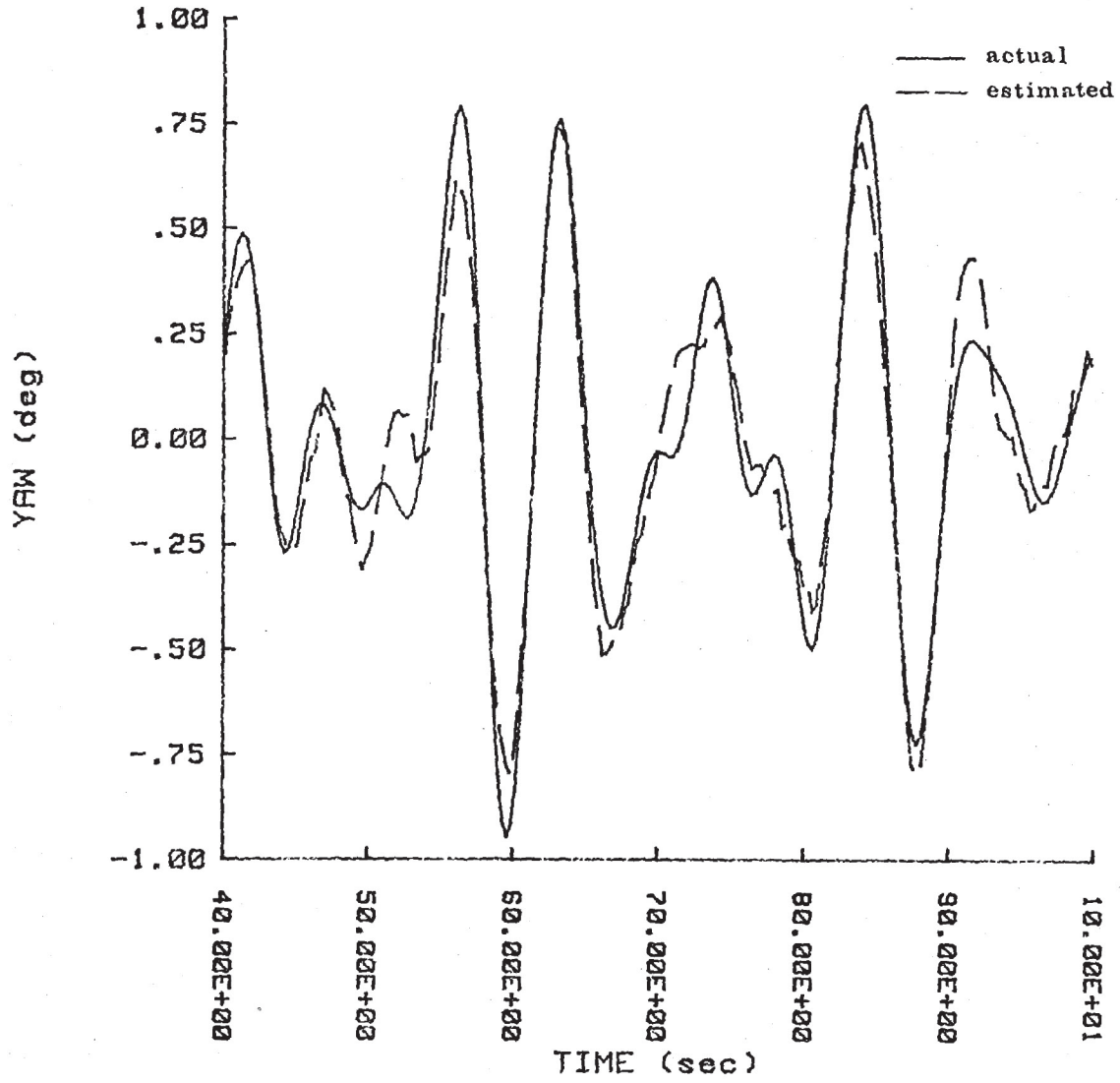

Figure 4.3: Yaw Actual and Estimated Motion

Denoting :

$$P_{ee} = E(\underline{e}_S . \underline{e}_S^T) \tag{4.15}$$

$$P_{xx} = E(\underline{x}_S . \underline{x}_S^T) \tag{4.16}$$

$$P_{xe} = E(\underline{x}_S . \underline{e}_S^T) \tag{4.17}$$

and :

$$P' = \begin{bmatrix} P_{ee} & P_{xe}^T \\ P_{xe} & P_{xx} \end{bmatrix} \tag{4.18}$$

$$A_S' = \begin{bmatrix} A_S^* - H_S C_S^* & (A_S^* - A_S) - H_S (C_S^* - C_S) \\ 0 & A_S \end{bmatrix} \tag{4.19}$$

$$\Xi_S' = \begin{bmatrix} \Xi_S + H_S \Theta_S H_S^T & -\Xi_S \\ -\Xi_S & \Xi_S \end{bmatrix} \tag{4.20}$$

The matrix P' is the solution of the 44th order Lyapunov equation :

$$A_S' P' + P' A_S'^T + \Xi_S' = 0 \tag{4.21}$$

This provides the error covariance matrix and the actual rms estimation errors. Table 4.2 shows the result of the sensitivity study. The most important parameter is the sea modal frequency and this indicates the importance of an accurate estimation of this parameter aboard the ship, in a real-time application.

The influence of systematic measurement errors is studied by using

SEA H=10ft ω_m=0.72rad/s			
	SWAY(ft)	ROLL(°)	YAW(°)
Rms motions	0.612	4.56	0.227
Nominal errors	0.241	0.56	0.0776
Parameter changed:			
U=20ft/s	0.245	0.568	0.0963
ω_m=0.52rad/s	0.314	0.60	0.0858
ϕ=60°	0.296	0.624	0.112
C_s(sway)=0.9	0.255	0.586	0.081
C_s(roll)=0.9	0.247	0.708	0.0808
C_s(yaw) =0.9	0.242	0.56	0.0777
C_s(sway)=0.	0.518	1.21	0.1408
C_s(roll)=0.	0.376	4.08	0.158
C_s(yaw) =0.	0.242	0.563	0.0785

Table 4.2: Sensitivity of the Estimation Errors to Parameter Uncertainty

a calibration factor in the C_S matrix. In the case of a 10% error, the most significant influence is obtained for a roll measurement error. Clearly, the Kalman filter uses mostly the roll measurement in the estimation and improves its estimation of the other motions through the known couplings between the motions. In this regard, the yaw measurement, which for this application is very noisy, has little influence on the filter performance. In the case of a calibration factor 0 (indicating a disconnected measurement), significant errors result, especially for roll.

4.3 Ship Motion Prediction

4.3.1 Introduction

Real-time prediction of ship motions is currently a subject of great interest, with applications not only to aircraft landings (or helicopter, or VTOL landings), but also to many other operations such as ship motion compensation and cargo transfer. Recently, a method has been proposed, that uses time series analysis [17]. Such method does not require any precise ship modelling : it considers the ship as a black box.

In this research, we chose to take advantage of the available knowledge on ship motions, and to derive a better model of the ship a priori, that can be used for estimation and prediction of the ship motions. Note that although the prediction of ship motions is of primary importance, to any piloted landing application, it is useless to an automatic landing using the LQ/LQG methodology, because the knowledge of the predictable part

of future ship motions is in fact completely included in the ship states and is fedforward by the LQ/LQG controller.

4.3.2 Prediction with Correct Model

Given the system :

$$\dot{\underline{x}}_S = A_S \underline{x}_S + \underline{\xi}_S \tag{4.22}$$

The optimal predictor is simply given by :

$$\dot{\hat{\underline{x}}}_S = A_S \hat{\underline{x}}_S \tag{4.23}$$

The error equation is :

$$\underline{e}_S = \hat{\underline{x}}_S - \underline{x}_S \tag{4.24}$$

$$\dot{\underline{e}}_S = A_S \underline{e}_S - \underline{\xi}_S \tag{4.25}$$

The covariance matrix of the error is time-varying, and is the solution of the linear differential matrix equation :

$$P_{ee} = A_S P_{ee} + P_{ee} A_S^T + \Xi_S \tag{4.26}$$

In a first approach, we assume that the state at t=0 is perfectly known, i.e. :

$$\hat{\underline{x}}_S(0) = \underline{x}_S(0) \tag{4.27}$$

For $t \to \infty$, since A_S is stable, the estimate $\hat{\underline{x}}_S$ goes to 0. This reflects the fact that the ship motion is stochastic and that the knowledge of the state

at any time does not imply any knowledge about the state at a distant time in the future. Consequently, the error eventually reaches the rms value of the motion.

The evolution of the rms error, normalized by the rms motion is shown in Fig. 4.4. Roll appears to be the easiest motion to predict. Under perfect conditions, good prediction could be obtained for up to 10 seconds. This reflects the highly-tuned shape of the roll power spectrum, which is mostly a second-order very lightly damped oscillator.

The above is a significant result for landing purposes, because roll motion is really one of the most important motions to predict. From the lateral motions, the yaw motion is very small, while the sway motion consists mostly, at the landing pad, of a roll induced motion.

Sway and yaw are much harder to predict, as shown in Fig.4.4, which reflects the much broader power spectrum of these motions.

The oscillations in the prediction covariance can be explained by a simple derivation for a second-order system.

Assuming a second-order system :

$$\dot{\underline{x}} = A\underline{x} + \underline{\xi} \tag{4.28}$$

where :

$$A = \begin{bmatrix} 0 & 1 \\ -b & -a \end{bmatrix} \tag{4.29}$$

$$\Xi = \begin{bmatrix} 0 & 0 \\ 0 & 1 \end{bmatrix} \tag{4.30}$$

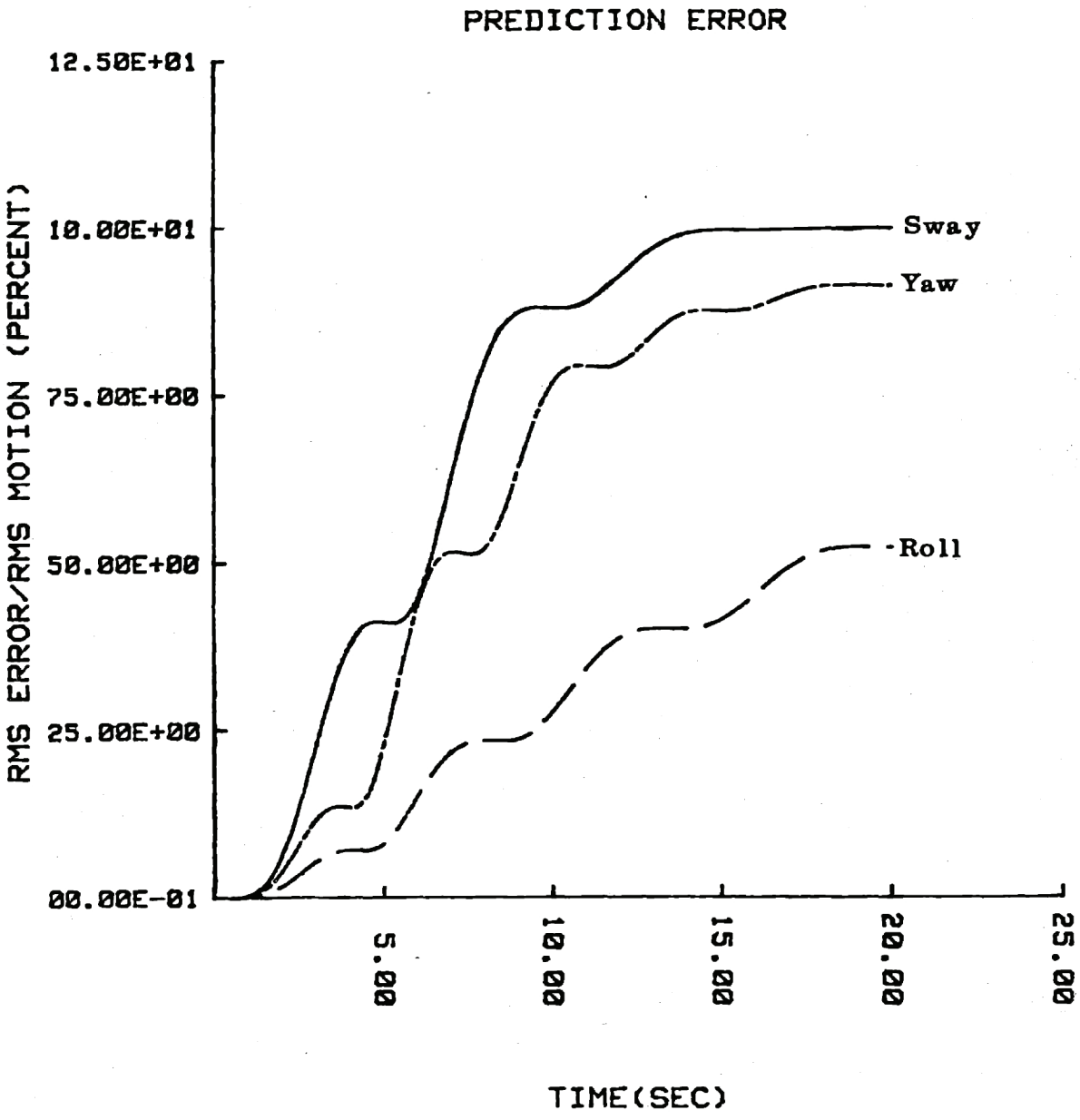

Figure 4.4: Rms Prediction Errors (H=10ft, ω_m=0.72rad/s)

The covariance matrix propagation equation is :

$$\dot{P} = A\,P + P\,A^{T} + \Xi \tag{4.31}$$

with :

$$P = \begin{bmatrix} P_{11} & P_{12} \\ P_{12} & P_{22} \end{bmatrix} \tag{4.32}$$

The equation (4.31) can be rewritten :

$$\begin{bmatrix} \dot{P}_{11} \\ \dot{P}_{12} \\ \dot{P}_{22} \end{bmatrix} = \begin{bmatrix} 0 & 2 & 0 \\ -b & -a & 1 \\ 0 & -2b & -2a \end{bmatrix} \cdot \begin{bmatrix} P_{11} \\ P_{12} \\ P_{22} \end{bmatrix} + \begin{bmatrix} 0 \\ 0 \\ 1 \end{bmatrix} \tag{4.33}$$

This is a linear differential matrix equation. The eigenvalues of the above 3x3 matrix are :

$$\lambda = -a \tag{4.34}$$

$$\lambda = -a \pm \sqrt{a^2 - 4b} \tag{4.35}$$

The eigenvalues of the original system are :

$$\lambda = (-a \pm \sqrt{a^2 - 4b})/2 \tag{4.36}$$

In other words, the linear system modelling the covariance matrix propagation has eigenvalues which are equal to twice the original system eigenvalues. This explains the oscillations of the prediction errors which are at a frequency double that of the ship motion peak frequency.

Time simulations of the ship motions and of the prediction estimates are reproduced in Figs. 4.5, 4.6, and 4.7. The prediction starts at t=40sec. The previous remarks on the predictability of the motions are easily seen in these plots.

In an actual realization, the ship states are not directly available and must be estimated. Fig. 4.8 shows the structure of the estimator/predictor. Prediction can be seen as an extension of filtering, with the measurement branch broken. In an actual application, the Kalman filter would be running in real-time, continuously, while the predictor would compute the predicted motions for a specific time Δt ahead, in parallel. This is indicated schematically in Fig. 4.9.

Some simulations are shown in Figs 4.10, 4.11, 4.12 and 4.13. The Kalman filter provides estimates at t=40s that are used to predict the ship motion. Good prediction is still obtained for roll, while yaw becomes almost unpredictable.

4.3.3 Implementation Issues

The actual implementation of the estimator/predictor described above will require the use of a digital computer and, hence, the discretization of the differential equation. Although the Kalman filter requires a large number of computations at relatively small time steps (with measurement update), the particular structure of the predictor makes the additional computational load very small. Given the optimal estimate of the Kalman filter at time t, $\hat{\underline{x}}_S(t)$, the optimal estimate of the predictor at

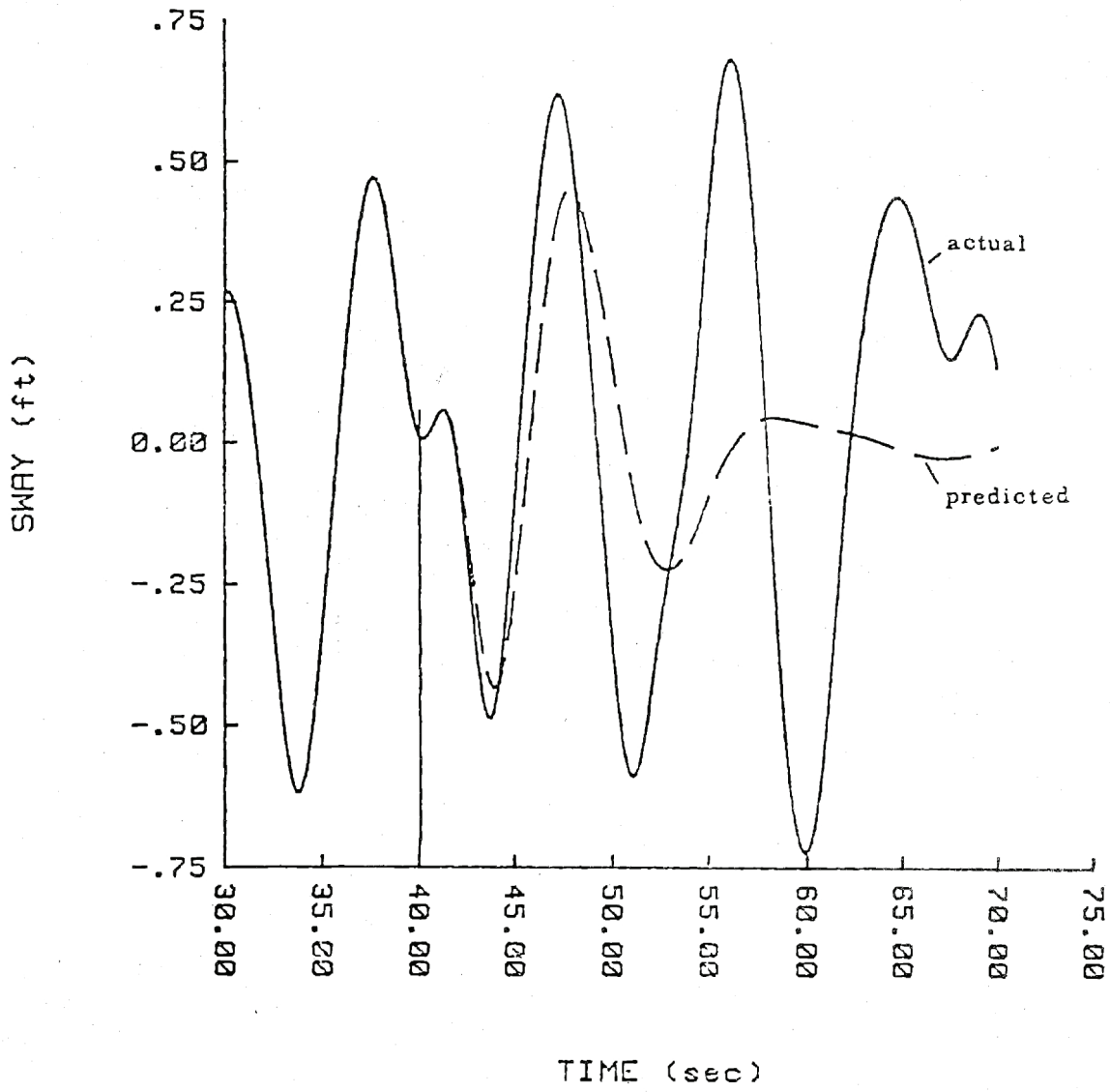

Figure 4.5: Sway Actual and Predicted Motion

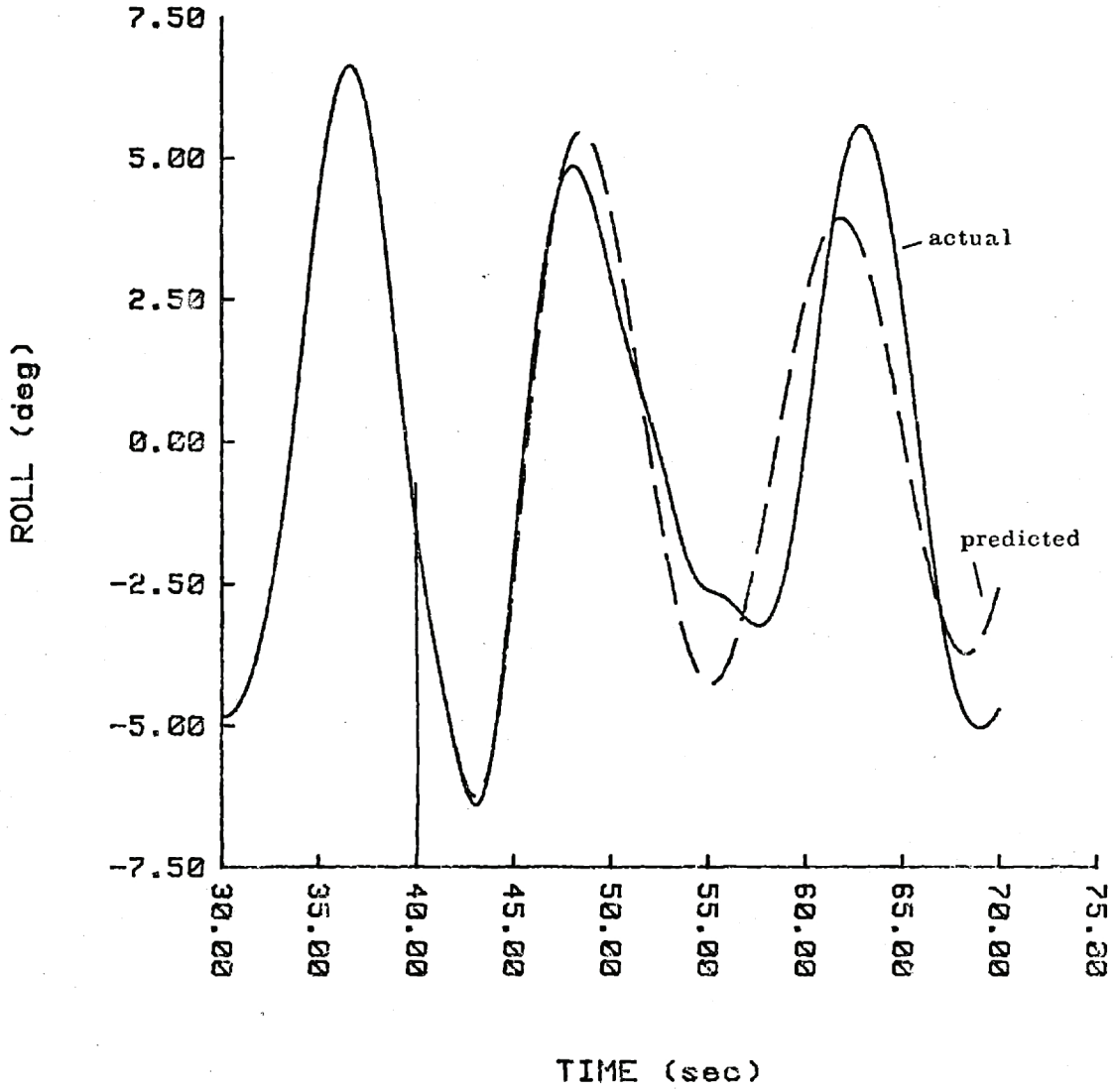

Figure 4.6: Roll Actual and Predicted Motion

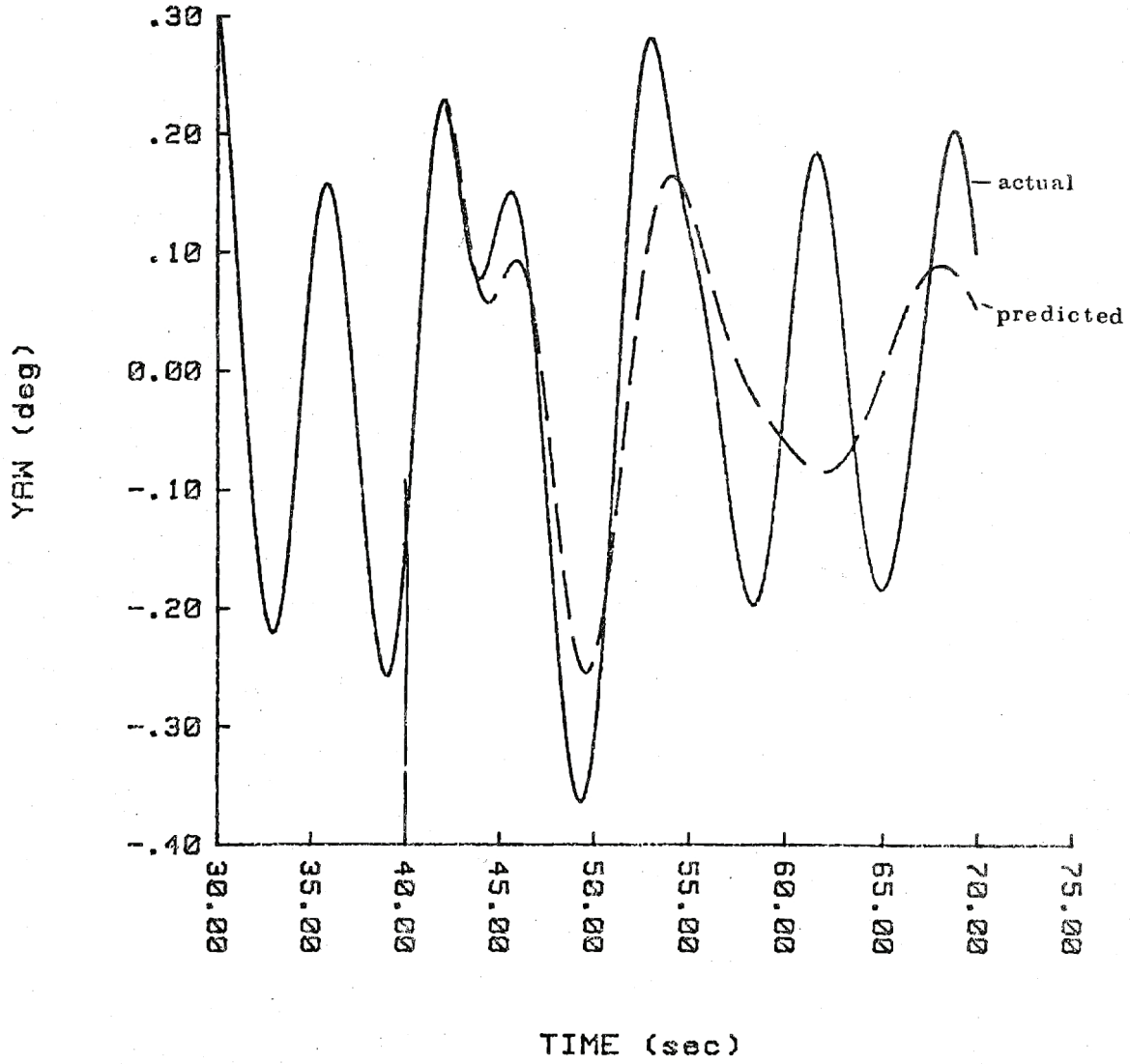

Figure 4.7: Yaw Actual and Predicted Motion

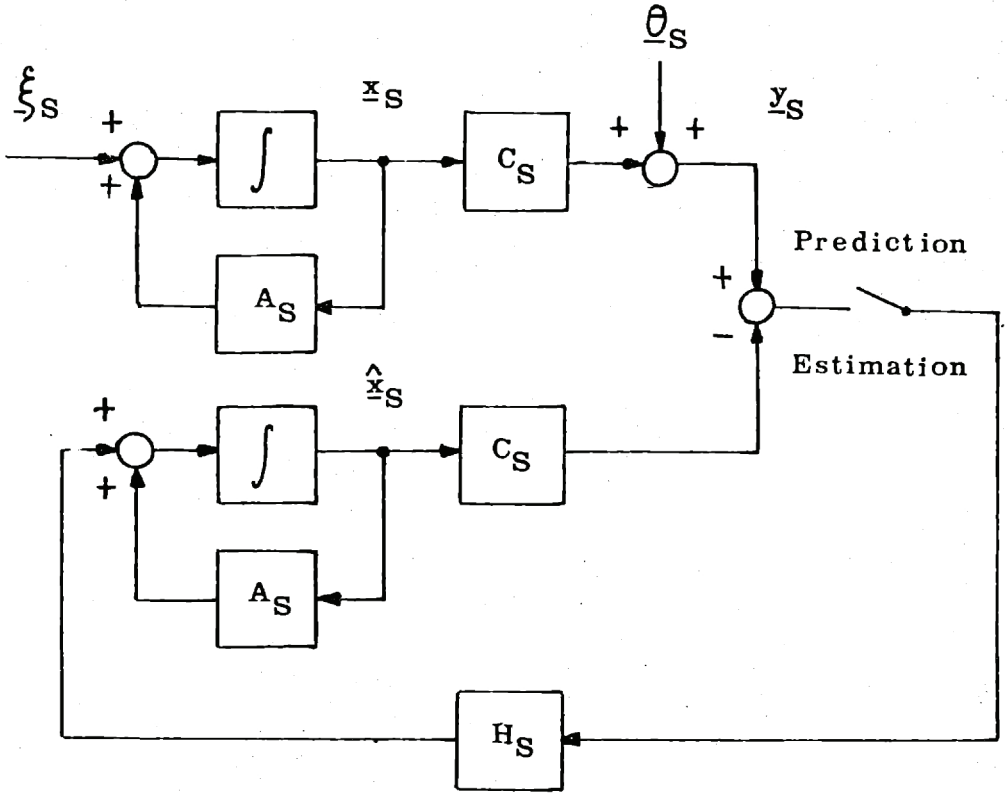

Figure 4.8: Estimator/Predictor Structure

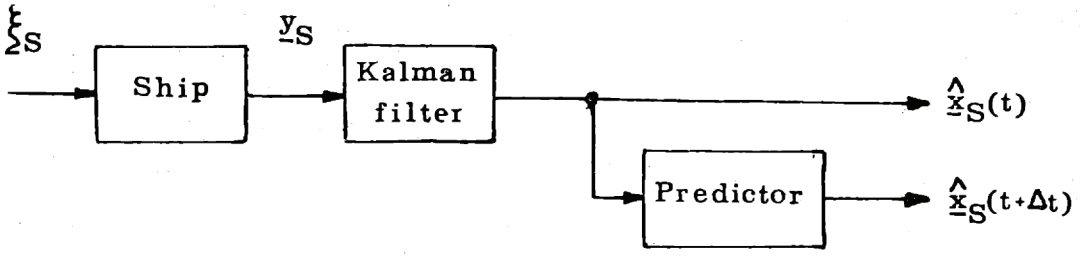

Figure 4.9: Estimator/Predictor Practical Structure

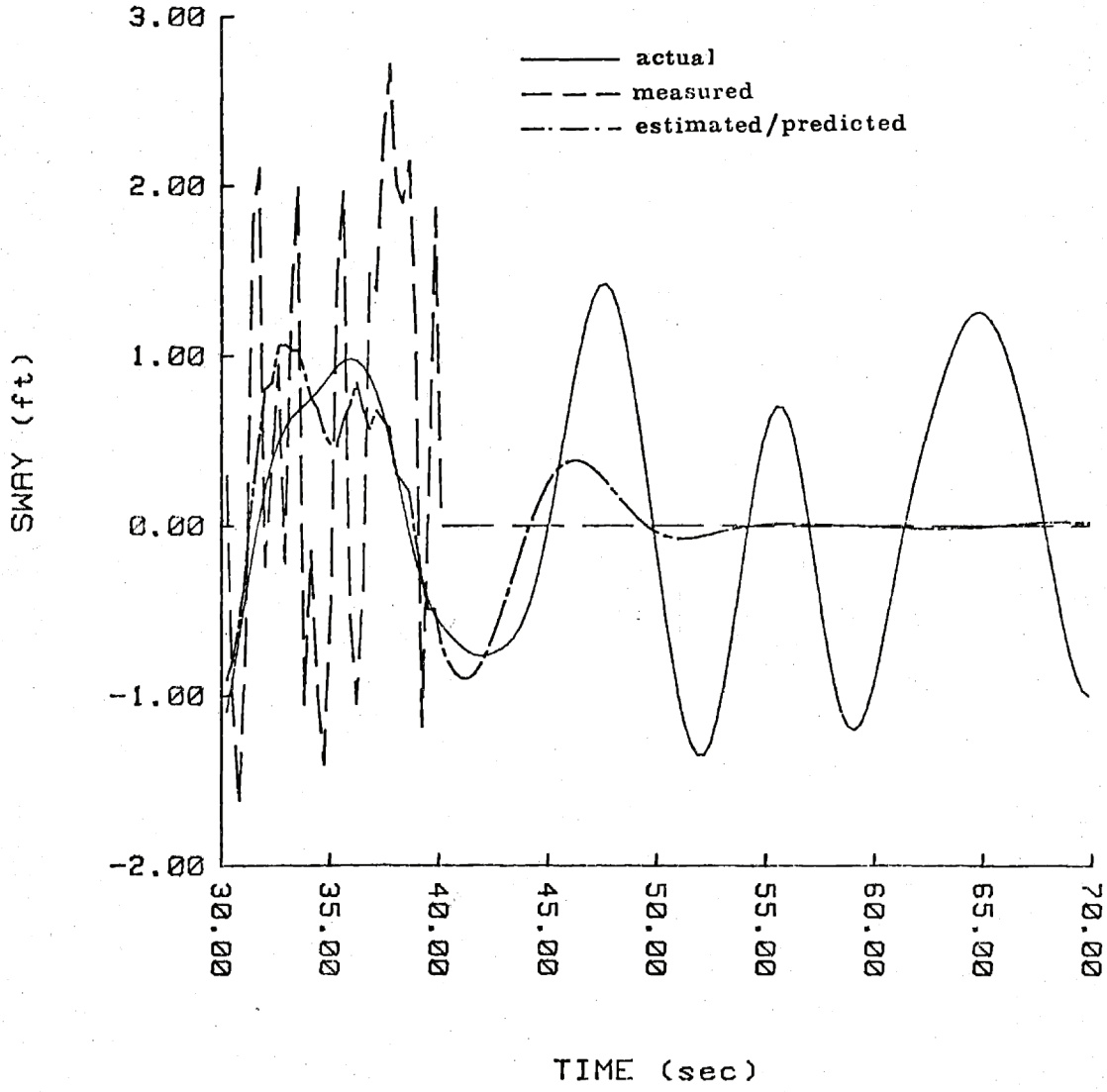

Figure 4.10: Sway Prediction with Noisy Measurements

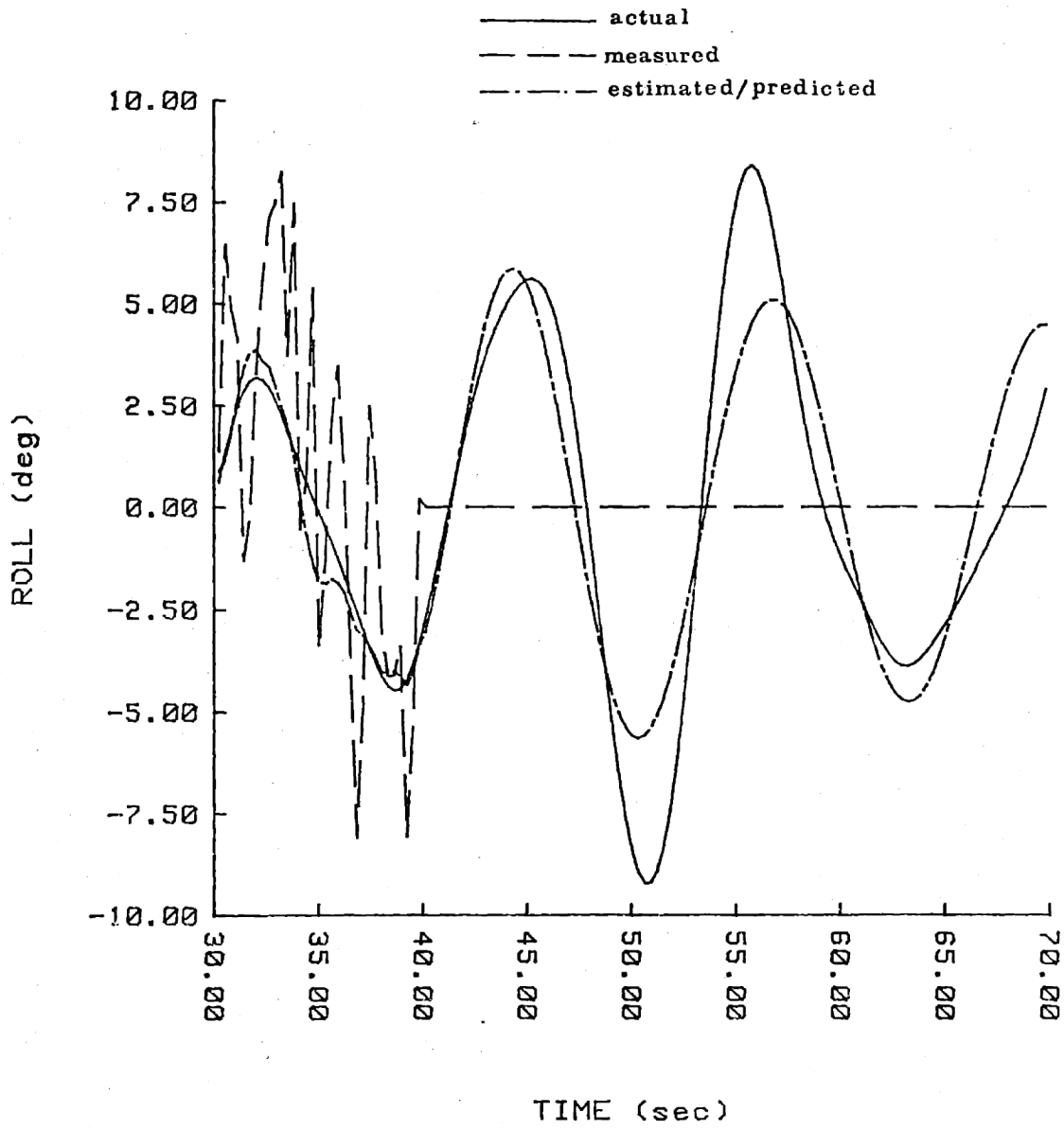

Figure 4.11: Roll Prediction with Noisy Measurements

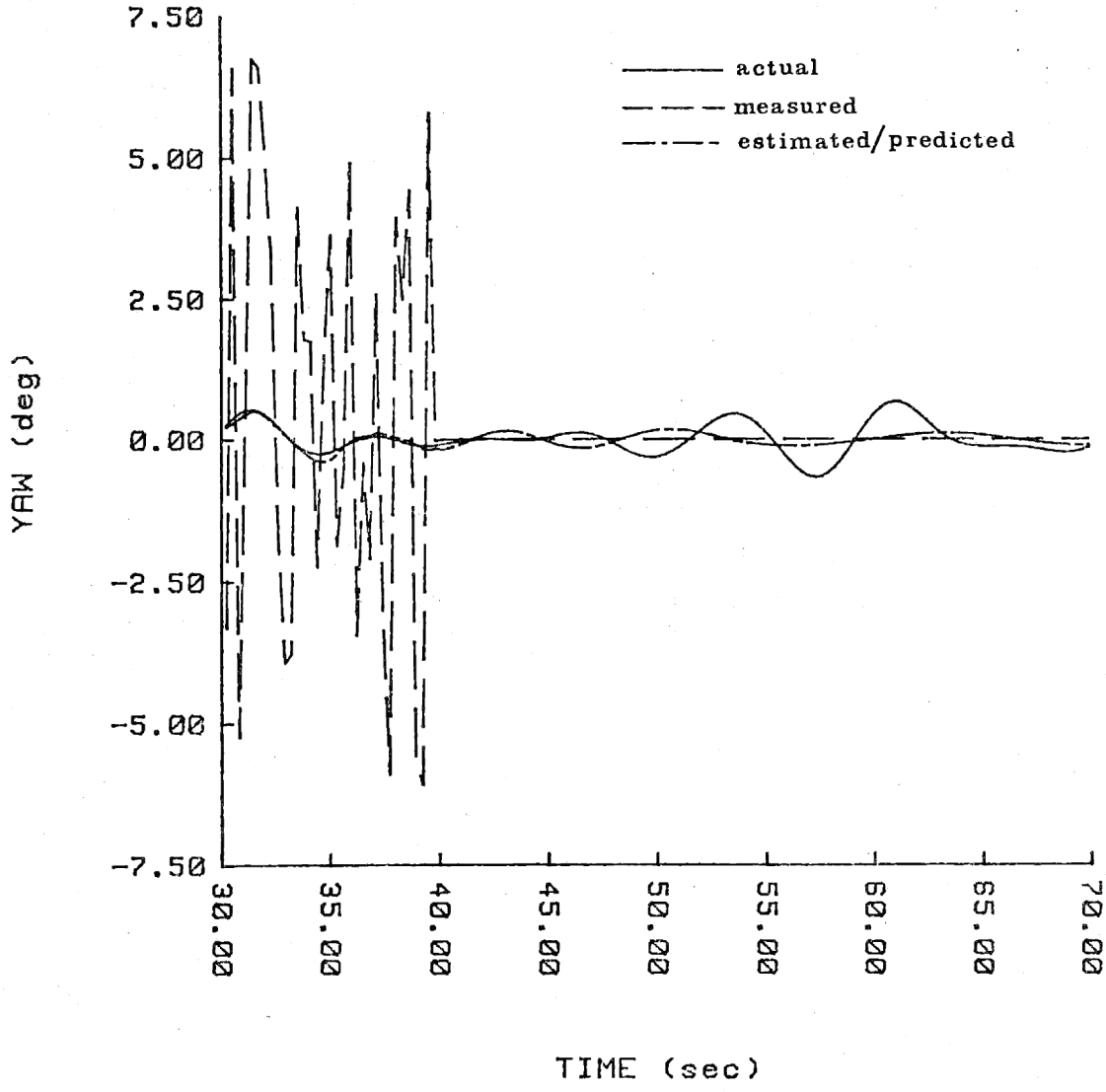

Figure 4.12: Yaw Prediction with Noisy Measurements

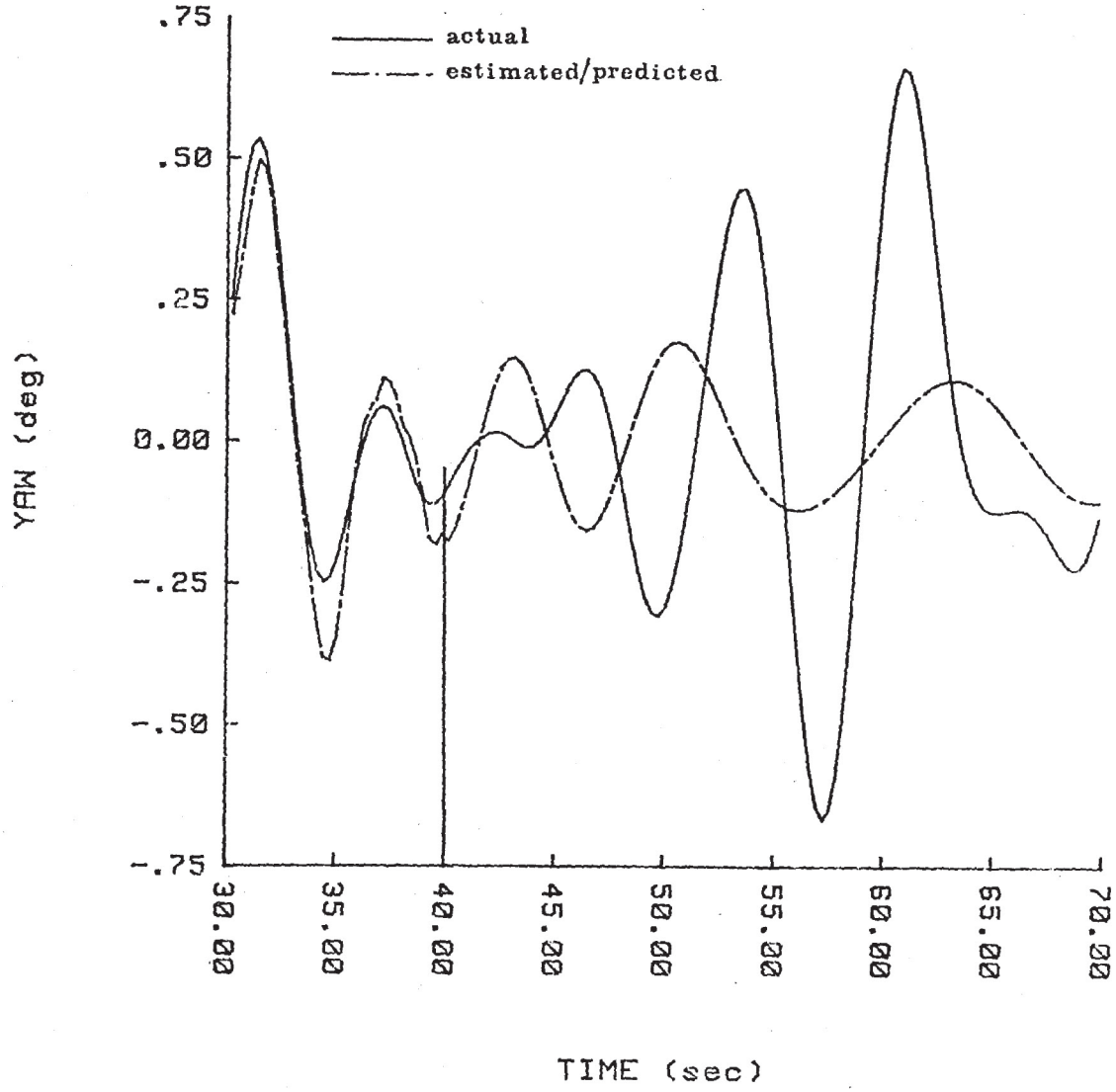

Figure 4.13: Yaw Prediction with Noisy Measurements (detail)

time $t+\Delta t$ is simply :

$$\underline{\hat{x}}_S(t+\Delta t) = e^{A_S \Delta t}\, \underline{\hat{x}}_S(t) \tag{4.37}$$

Having computed $e^{A_S \Delta t}$, and considering that we are only interested in predicting the motions (and not the other states), this operation results in multiplying a matrix (3x16) by a vector (16x1). These are the only computations required if we are only interested in predicting the motions Δt seconds ahead (and not their evolution in between). In this case, there is no need to integrate the differential equation, as for the Kalman filter.

In the case when the complete time evolution is desired, and that the differential equation has to be integrated numerically, the same equation (4.37) provides the discretized equation corresponding to the differential equation :

$$\dot{\underline{\hat{x}}}_S = A_S\, \underline{\hat{x}}_S \tag{4.38}$$

It is very tempting to approximate this equation by the simple difference equation :

$$\underline{\hat{x}}_S(t+\Delta t) = \underline{\hat{x}}_S(t) + \Delta t(A_S \underline{\hat{x}}_S(t)) \tag{4.39}$$

which is the same as approximating :

$$e^{A_S \Delta t} \simeq I + A_S \Delta t \tag{4.40}$$

for a small Δt.

However, due to the presence of the very lightly damped roll mode, large errors can occur even for small Δt, compared to the time constants of the system. In fact, if Δt is not very small, the mode becomes even less damped, as indicated in Appendix B. More precise approximations to $e^{A_S \Delta t}$ are advisable for the implementation of the predictor (see for example [18]). Such problems do not appear for the Kalman filter which does not have this very lightly damped mode.

4.3.4 Prediction with Wrong Model

In a previous subsection, the important influence of the sea modal frequency on the performance of the Kalman filter was assessed. This paragraph addresses the same question for the predictor. The calculation of the errors is a little more complex in this case.

Given the system :

$$\dot{\underline{x}}_S = A_S \underline{x}_S + \underline{\xi}_S \tag{4.41}$$

and the predictor with wrong model :

$$\dot{\hat{\underline{x}}}_S = A_S^* \hat{\underline{x}}_S \tag{4.42}$$

The error is given by :

$$\dot{\underline{e}}_S = (A_S^* - A_S)\underline{x}_S + A_S^* \underline{e}_S - \underline{\xi}_S \tag{4.43}$$

The global system is :

$$\begin{bmatrix} \dot{\underline{e}}_S \\ \dot{\underline{x}}_S \end{bmatrix} = \begin{bmatrix} A_S^* & A_S^*-A_S \\ 0 & A_S \end{bmatrix} \cdot \begin{bmatrix} \underline{e}_S \\ \underline{x}_S \end{bmatrix} + \begin{bmatrix} -\underline{\xi}_S \\ \underline{\xi}_S \end{bmatrix} \tag{4.44}$$

Denoting :

$$P' = \begin{bmatrix} P_{ee} & P_{xe}^T \\ P_{xe} & P_{xx} \end{bmatrix} \tag{4.45}$$

$$A_S' = \begin{bmatrix} A_S^* & A_S^*-A_S \\ 0 & A_S \end{bmatrix} \tag{4.46}$$

$$\Xi_S' = \begin{bmatrix} \Xi_S & -\Xi_S \\ -\Xi_S & \Xi_S \end{bmatrix} \tag{4.47}$$

P' is the solution of the linear differential equation :

$$\dot{P}' = A_S' P' + P' A_S'^T + \Xi_S' \tag{4.48}$$

which can be separated in :

$$\dot{P}_{xx} = A_s P_{xx} + P_{xx} A_S^T + \Xi_S \tag{4.49}$$

$$\dot{P}_{xe} = A_S P_{xe} + P_{xx}(A_S^*-A_S)^T + P_{xe} A_S^{*T} - \Xi_s \tag{4.50}$$

$$\dot{P}_{ee} = A_S^* P_{ee} + (A_S^*-A_S) P_{xe} + P_{ee} A_S^{*T} + P_{xe}^T (A_S^*-A_S)^T + \Xi_S \tag{4.51}$$

The original system (the ship) is assumed to be in steady-state, so that $\dot{P}_{xx} = 0$, and P_{xx} is the solution of the Lyapunov equation :

$$A_S P_{xx} + P_{xx} A_S^T + \Xi_S = 0 \qquad (4.52)$$

Replacing P_{xx} by its steady-state value (given by (4.52)) in equations (4.50) and (4.51), we obtain a 32nd order linear differential matrix equation in P_{xe} and P_{ee}, with initial conditions $P_{xe}(0) = P_{ee}(0) = 0$ (the initial state is assumed to be perfectly known).

Figures 4.14, 4.15 and 4.16 show the results of the integration of this equation, in the case of an error in the sea modal frequency. The filter was designed with ω_m=0.72 rad/s, while the actual value was assumed to be 0.52 rad/s. The degradation in performance is again significant and the roll prediction time is about divided by two. This indicates (again) the importance of the estimation of the sea modal frequency in real-time applications.

4.4 Summary

In this chapter, we addressed the important questions of ship motion estimation and prediction. First, a Kalman filter was designed, whose task is to filter the noise in the measurements (mostly due to the ship structural noise), and to provide estimates of the states that are not available for measurement. These estimates can then be used for optimal prediction of the ship motion, and in the feedforward path of the LQG controller for the VTOL landing.

A sensitivity analysis showed the relative importance of the model parameters, and the sea modal frequency appeared to be a significant

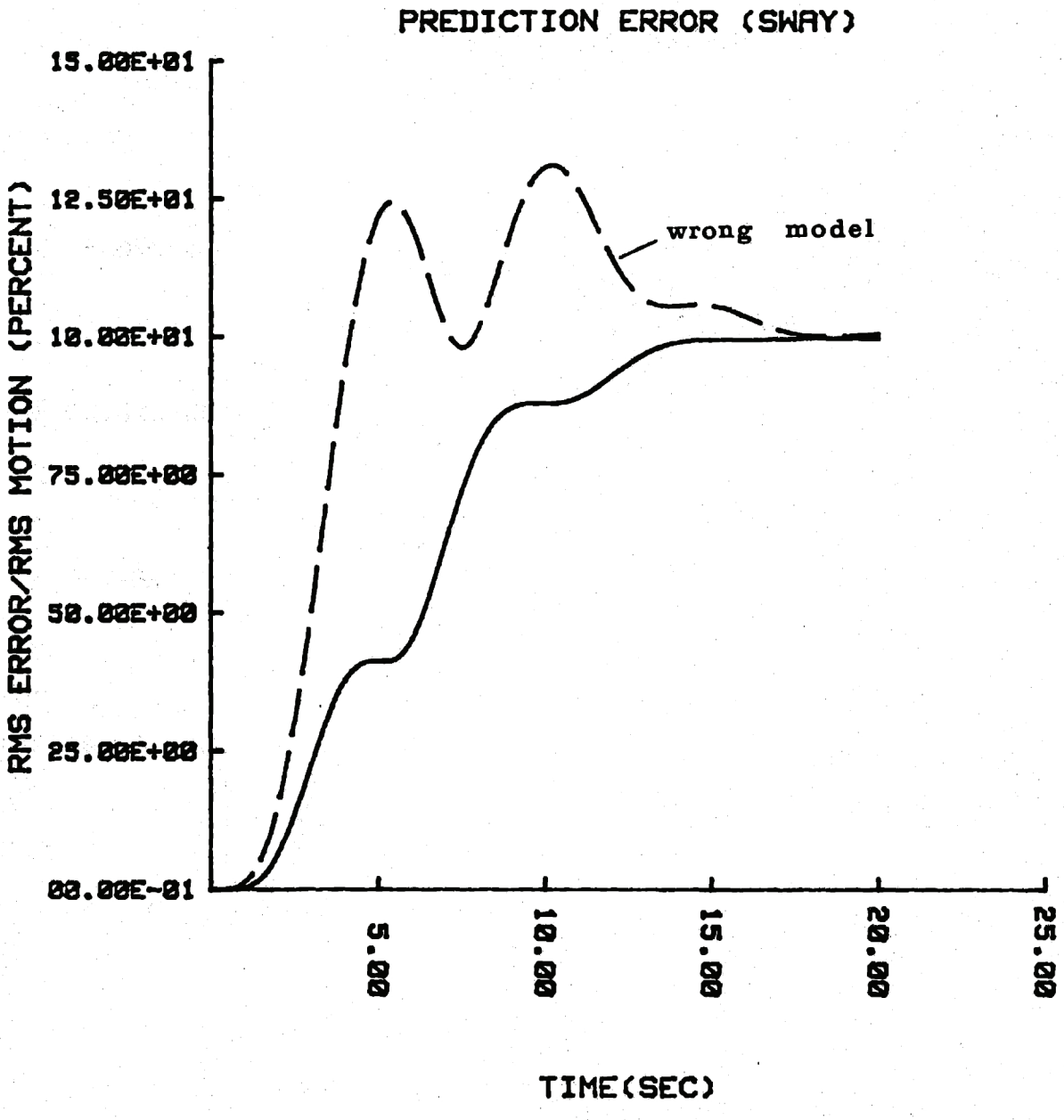

Figure 4.14: Sway Rms Prediction Error with Wrong Model

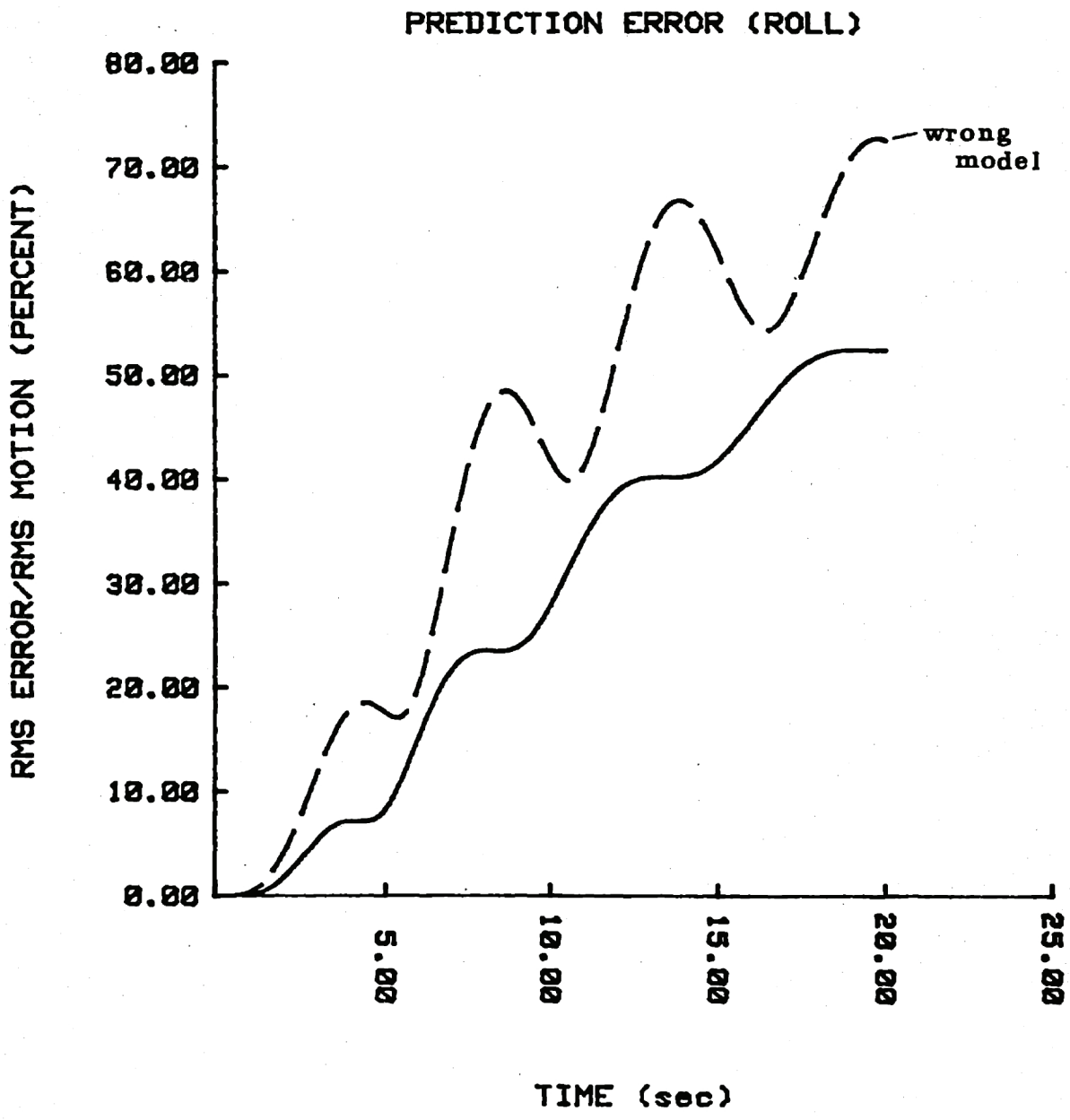

Figure 4.15: Roll Rms Prediction Error with Wrong Model

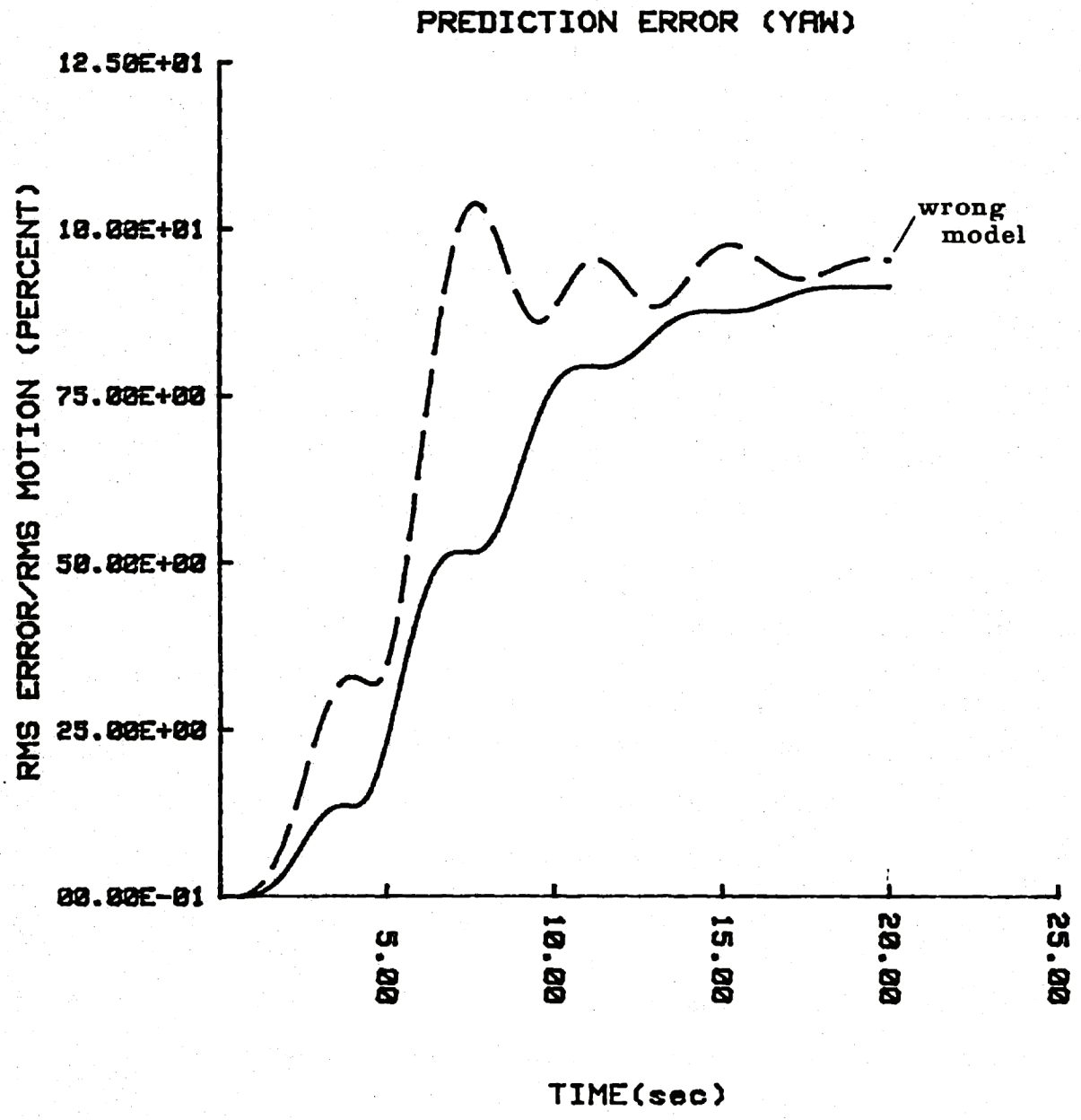

Figure 4.16: Yaw Rms Prediction Error with Wrong Model

parameter.

The prediction of ship motions, assuming perfect knowledge of the initial state, was studied, so that lower bounds on the prediction errors were obtained. Due to its concentrated power spectrum, the roll motion turned out to be the easiest to predict (optimally 5 to 10 sec. prediction time). The sea modal frequency was shown to be an important parameter for all motions, which indicated the need for an accurate estimation of this parameter in a real-time application.

CHAPTER 5

AIRCRAFT MODEL

5.1 Introduction

Since the beginning of VTOL aircraft technology development, a large number of configurations were conceived, and sometimes built and tested. The most studied and extensively tested VTOL is probably the AV-8A Harrier. Another VTOL aircraft which has been extensively studied is the Lift/Cruise Fan V/STOL Research Technology Aircraft (RTA). For this aircraft, complete simulator programming data is available in [19]. In the former study of the longitudinal controls required for VTOL landings on destroyers [1], a linearized model, written in state-space form, was derived from the data. It includes both longitudinal and lateral motions. In addition to the rigid body equations of motion and the contributions of the fan forces and moments, this model also accounts for ram drag forces and moments, and internal momentum effects (gyroscopic terms) due to the rotating engines and fans. Neglected are the aerodynamic effects, the ship airwake turbulence, and the ground effects. The actuators are modelled by first order dynamics, whose time constants are to be selected by the control system designer.

5.2 Lateral Motions Model

To a first approximation, the longitudinal and lateral motions of the aircraft can be decoupled. This corresponds to neglecting the cross-coupling terms between roll, yaw, and pitch due to gyroscopic effects from the

engines and fans. The effect of this approximation on the overall system performance and stability margins is an interesting issue which is not addressed in this thesis, but is probably worth a subsequent study.

The general ship-aircraft configuration is shown in Fig. 5.1. The lateral motions, and the sign conventions used, are indicated: they are sway (lateral translation), roll and yaw (angular motions). The definition of the controls requires some care. Strictly speaking, there are 9 variables on which the controller can act: the 3 values of the thrusts at the fans, the 3 values of the longitudinal deflections of these thrusts, and the 3 values of the lateral deflections. However, these controls are not independent: for example, deflecting the thrusts T_1 and T_2 laterally and in opposite directions would result in counteracting forces, and, consequently, in an inefficient use of the controls available. Considering reasonable use of the controls, we find three independent controls for the lateral motions (corresponding to the three degrees of freedom):

1) an equal lateral deflection of the aft louvers, denoted by $\delta\alpha_{1,2}$

2) an exchange of thrust from T_2 to T_1, denoted by $\delta T_{1,2}$ (this can easily be done, as the engines 1 and 2 are mechanically coupled)

3) a lateral deflection of the front louver, denoted by $\delta\alpha_3$.

These control variables are grouped in a vector denoted by $\underline{c}$.

In the original work by McMuldroch [1], the vector input was chosen in a slightly different manner. It is denoted by $\underline{u}$ in this thesis.

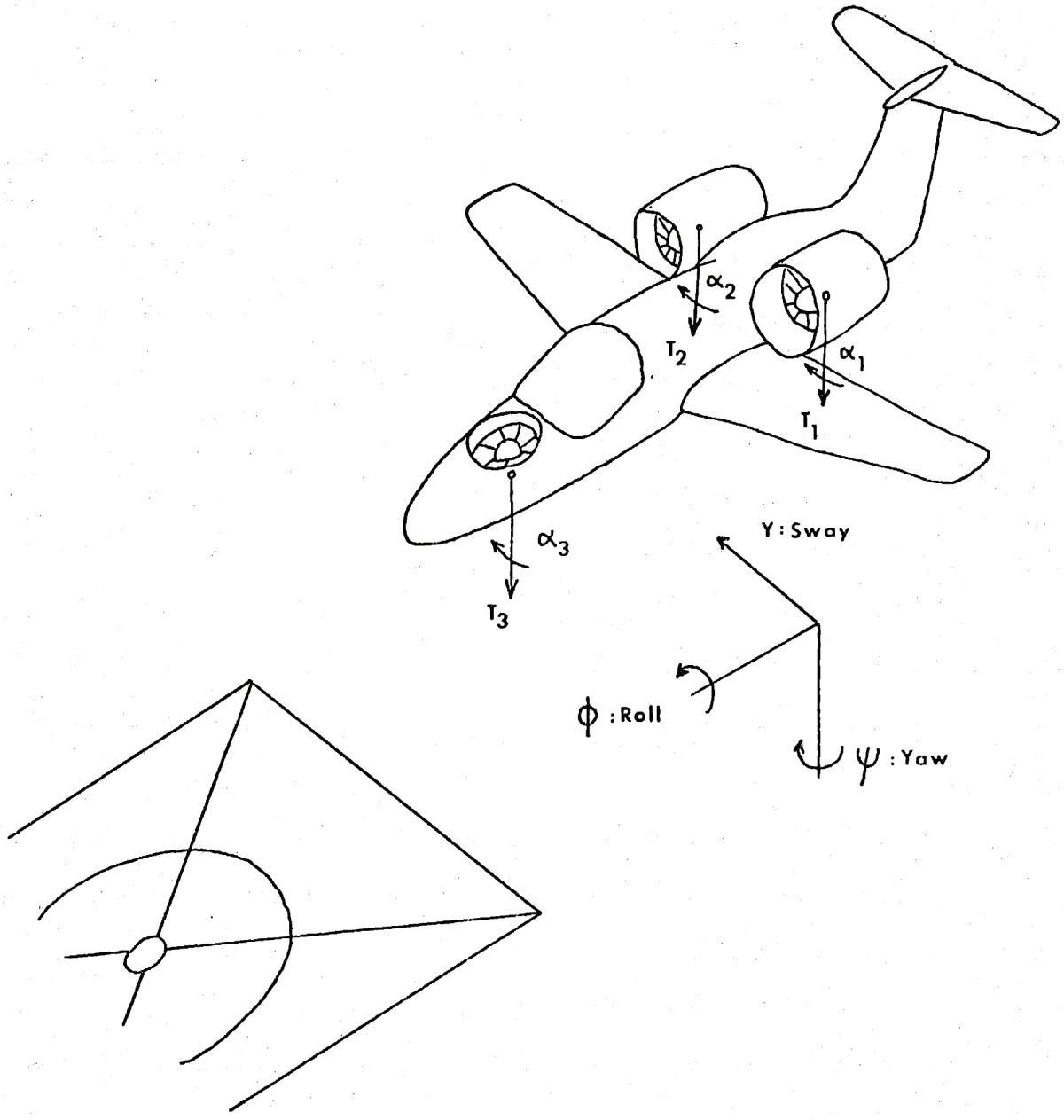

Figure 5.1: VTOL Aircraft Lateral Motions and Controls

Its components are:

1) δy_c: an equal lateral deflection of all the louvers, to produce (mostly) a sway acceleration

2) $\delta\phi_c$: an exchange of thrust from T_2 to T_1, to produce a roll acceleration

3) $\delta\psi_c$: an opposite lateral deflection of the front and aft louvers, to produce a yaw acceleration.

In this thesis, we keep the McMuldroch formulation, but the control weights in the quadratic cost and the robustness criterions will be expressed in terms of the vector $\underline{c}$, which is the actual physical control input. The transformation from $\underline{c}$ to $\underline{u}$ and $\underline{u}$ to $\underline{c}$ is straightforward. Figure 5.2 indicates the structure of the aircraft model.

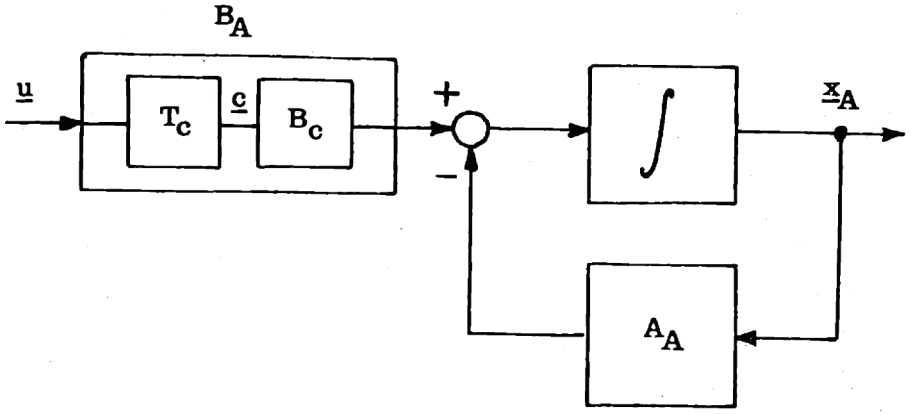

Figure 5.2: Aircraft Model Structure

The numerical values of the matrices are given in Table 5.1. The units of the model are:

- ft for y_A
- ft/s for $\dot{y}_A$
- rad for ϕ_A, ψ_A, $\delta\alpha_{1,2}$, $\delta\alpha_3$, δy_c, $\delta\psi_c$
- rad/s for $\dot{\phi}_A$, $\dot{\psi}_A$
- fraction of the nominal thrust for $\delta T_{1,2}$ (the nominal thrust of $T_{1,2}$ is 9057.5 lb) and for $\delta\phi_c$

The only difference between the model indicated here and the model given in [1], is the absence of actuators dynamics which, in[1], were selected as integrator dynamics. For the lateral case, the actuators dynamics are well beyond the significant ship motion frequencies (0.5 to 1.5 rad/s): the thrust deflection can be done almost instantenuously, while the exchange of thrust - which does not require any overall increase of power - has a time constant of about 0.1 s (a shaft-coupled configuration is considered here). For these reasons, and for simplicity, the actuators dynamics are neglected here.

The resulting model is very simple: it contains only 6 states, specifically the aircraft motions and velocities. As indicated earlier, a simple model is desirable on the control system point of view, although it necessarily implies some crude approximations and, therefore, increases the need for good robustness properties. On the other hand, the interpretation of the elements of the model is easier from a simple model, as will be seen in the next section.

$$\underline{u} = \begin{bmatrix} \delta y_c \\ \delta \phi_c \\ \delta \psi_c \end{bmatrix} \qquad \underline{c} = \begin{bmatrix} \delta\alpha_{1,2} \\ \delta T_{1,2} \\ \delta\alpha_3 \end{bmatrix} \qquad \underline{x}_A = \begin{bmatrix} y_A \\ \phi_A \\ \psi_A \\ \dot{y}_A \\ \dot{\phi}_A \\ \dot{\psi}_A \end{bmatrix}$$

$$A_A = \begin{bmatrix} 0 & 0 & 0 & 1 & 0 & 0 \\ 0 & 0 & 0 & 0 & 1 & 0 \\ 0 & 0 & 0 & 0 & 0 & 1 \\ 0 & 32.2 & 0 & -.085922 & -.052023 & -.39174 \\ 0 & 0 & 0 & -.00271 & -.1025 & -.04206 \\ 0 & 0 & 0 & -.005087 & -.0117 & -.1471 \end{bmatrix} \qquad B_A = \begin{bmatrix} 0 & 0 & 0 \\ 0 & 0 & 0 \\ 0 & 0 & 0 \\ 32.2 & 0 & 0 \\ -4.2411 & 4.5953 & 0.5346 \\ -.17896 & .1939 & 8.0464 \end{bmatrix}$$

$$T_c = \begin{bmatrix} -1 & 0 & 1 \\ 0 & 1 & 0 \\ -1 & 0 & -1.9302 \end{bmatrix} \qquad B_c = \begin{bmatrix} 0 & 0 & 0 \\ 0 & 0 & 0 \\ 0 & 0 & 0 \\ -21.211 & & -10.989 \\ 2.976 & 4.5953 & 1.265 \\ 2.864 & .1939 & -2.685 \end{bmatrix}$$

Table 5.1: Aircraft Model Values

5.3 Model Interpretation

The important couplings inherent to a VTOL aircraft are represented in the model, and it is worth taking some time analyzing them.

A first important coupling is a dynamic coupling between roll and sway. As the aircraft is banked, a lateral component of the thrust appears, which results in an important side force. This is represented by the $A_A(4,2)$ element (cf table 5.1). It is equal to g (32.2 ft/s^2) because, under the small angle approximation, the side force is equal to the weight times the roll angle.

The other elements coupling the velocities in the A_A matrix are due to the ram drag forces and moments, and are responsible for most of the aircraft dynamics in this model (especially its instability).

An important coupling appearing in the B_A matrix is the $B_A(5,1)$ term. It indicates that a lateral deflection of the thrusts produces an important roll moment. Note that if this effect is not compensated for, the roll moment will produce a roll angle which, by the effect described above, will in turn produce a sway force opposite to the sway force originally produced by the louvers deflections. The origin of the roll moment is in the difference between the center of gravity and the center of thrust of the fans (the center of gravity is 3.12 ft higher).

Finally, an interesting, although apparently not very significant term, is the $B_A(6,2)$ term. It tells us that an exchange of thrust in the aft fans produces a yaw acceleration. Although no yaw moment is produced by this control, a small yaw acceleration results from the roll moment, due to the

angular difference between the principal axes and the body axes (in other words, due to the presence of a cross-term I_{xz} in the inertia tensor).

The above summarizes the important couplings present in the VTOL aircraft. These couplings are dynamic (reflected in the A_A matrix), as well as control couplings (reflected in the B_A matrix), and are captured in the simplified, linearized model given here.

In fact, not only is the system strongly coupled, but it is also open-loop unstable. The open-loop poles are shown in Fig. 5.3. Two of the six poles are at the origin and correspond to the pure integrators in sway and yaw motions.

5.4 Summary

In this chapter, we described the aircraft model for the lateral motions. We showed that three independent controls can be used to track the lateral deck motions, but that some important couplings are present amongst the controls and motions (especially between sway and roll).

The aircraft model is written in state-space form, and the state vector contains 6 states, namely the aircraft motions and velocities. The important couplings of the VTOL are represented in the model, and it was shown to be open-loop unstable.

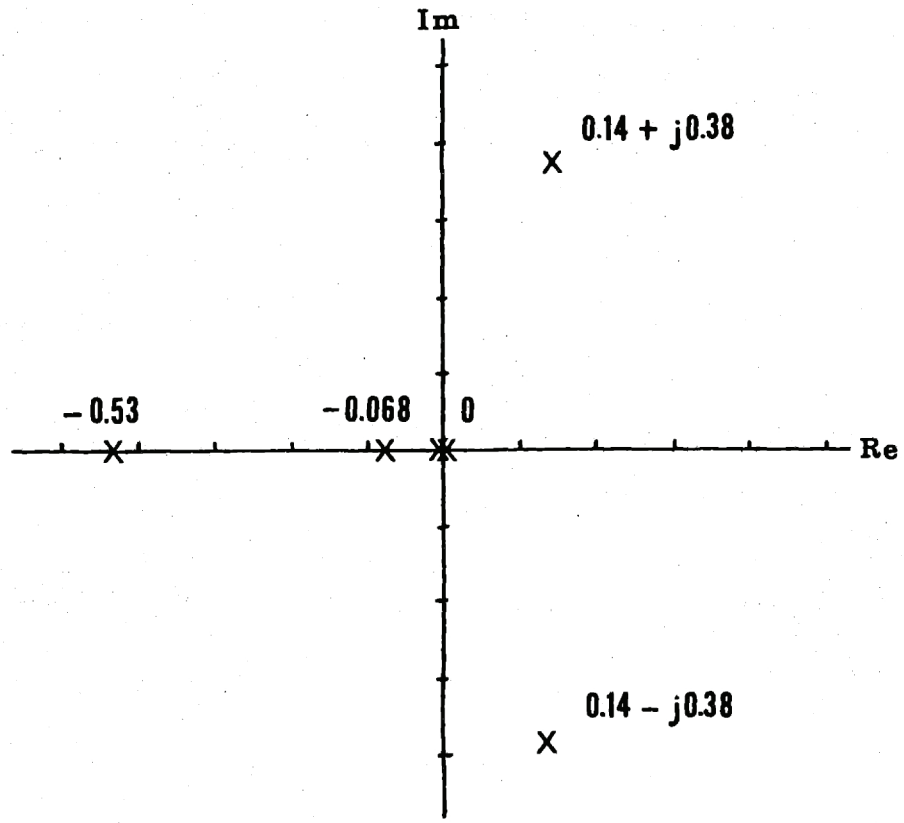

Figure 5.3: Aircraft Open-Loop Poles, Plotted in the s-plane

CHAPTER 6

LINEAR QUADRATIC REGULATOR DESIGN

6.1 Introduction

The LQ/LQG design methodology was introduced in chapter 2. As a first step, it is assumed that all states of the system are available (output matrix C = I), so that full state feedback can be used. Note that while this assumption is generally a rather unrealistic assumption, it is not the case for the simplified aircraft model that was obtained in chapter 5. Angular motions as well as angular rates are available through gyros and rate gyros. Similarly, estimates of position as well as velocity can be obtained from accelerometer measurements combined with MLS/DME measurements, with a high quality. In a sense, a Kalman filter is not strictly necessary for the aircraft. For these reasons, significant attention has been given to this part of the design.

6.2 Choice of the Quadratic Weights

Under the assumption of full state feedback, the only parameters left to the designer are the Q and R weighting matrices in the quadratic cost. A very natural way to select these matrices is the diagonal inverse-square weighting [20]. Some other methods have been proposed, as for example the method proposed in [21] and [22] to achieve desirable asymptotic regulator properties. In any case, it is interesting to note that the robustness properties of LQ regulators can be seriously deteriorated if a non-diagonal

matrix R is chosen [23][24]. For this reason, it is wise to select a diagonal R matrix, or equivalently, to pick $R = \rho I$, after some scaling of the inputs.

In this thesis, we decided to start with a simple diagonal inverse square weighting, leaving some parameters to acheive a desirable eigenstructure, with a careful study of their influence on the optimal root-locus. The quadratic cost that we want to minimize is given by (2.25). As a first step, we want to weight all the state variables (motions and velocities), so that:

$$\underline{w}_A = W_A \underline{x}_A = \underline{x}_A \tag{6.1}$$

$$W_A = I \tag{6.2}$$

$$Q = Q_w \tag{6.3}$$

The Q matrix is chosen diagonal:

$$Q = \begin{bmatrix} \left(\frac{1}{y_{max}}\right)^2 & 0 & 0 & 0 & 0 & 0 \\ 0 & \left(\frac{1}{\phi_{max}}\right)^2 & 0 & 0 & 0 & 0 \\ 0 & 0 & \left(\frac{1}{\psi_{max}}\right)^2 & 0 & 0 & 0 \\ 0 & 0 & 0 & \left(\frac{T_z}{y_{max}}\right)^2 & 0 & 0 \\ 0 & 0 & 0 & 0 & \left(\frac{T_z}{\phi_{max}}\right)^2 & 0 \\ 0 & 0 & 0 & 0 & 0 & \left(\frac{T_z}{\psi_{max}}\right)^2 \end{bmatrix} \tag{6.4}$$

where y_{max}, ϕ_{max}, ψ_{max} are arbitrarily chosen maximal deviations of the states:

$$y_{max} = 4 \text{ ft} \tag{6.5}$$

$$\phi_{max} = \psi_{max} = 10 \text{ degrees} = 0.1745 \text{ rad} \tag{6.6}$$

A parameter T_z is left in the Q matrix. For $T_z = 0$, only the motions are weighted. For $T_z \neq 0$, the motions and the velocities are weighted. They are weighted equally if $T_z = 1$. In the VTOL landing problem, the velocity tracking errors can be as important as the position tracking errors (they determine the shock at the landing), which justifies the weighting of both in the quadratic cost. Also, it is known that, sometimes, the weighting of outputs only may lead to underdamped second-order type systems, and that this can be improved by weighting derivatives as well as outputs. At this stage, the variable T_z is then left as a design parameter.

The control weighting R matrix is chosen diagonal at the point of the actual controls:

$$R_c = \rho \begin{bmatrix} \left(\frac{1}{\delta\alpha_{1,2_{max}}}\right)^2 & 0 & 0 \\ 0 & \left(\frac{1}{\delta T_{1,2_{max}}}\right)^2 & 0 \\ 0 & 0 & \left(\frac{1}{\delta\alpha_{3_{max}}}\right)^2 \end{bmatrix} \tag{6.7}$$

and:

$$R = T_c^T \, R_c \, T_c \tag{6.8}$$

with $\delta\alpha_{1,2_{max}}$, $\delta T_{1,2_{max}}$, and $\delta\alpha_{3_{max}}$ are arbitrarily chosen maximal values of the control authority.

$$\delta\alpha_{1,2_{max}} = \delta\alpha_{3_{max}} = 10 \text{ degrees} = 0.1745 \text{ rad} \tag{6.9}$$

$$\delta T_{1,2_{max}} = 0.3 \quad (30\% \text{ of the nominal thrust value}) \tag{6.10}$$

Another parameter of the design, ρ, is left here, and indicates the relative importance of the control versus state deviations.

6.3 Optimal Root-Locus

An optimal root-locus is defined as the locus of the closed-loop poles of the system with optimal LQ feedback, when the parameter ρ in the R matrix is varied from ∞ to 0.

It is interesting to note that this problem in itself does not require the solution of the associated Riccatti equation. The closed-loop poles are the left half plane eigenvalues of the Hamiltonian system [9] and[25]:

$$\dot{z} = Z \, z \tag{6.11}$$

with:

$$Z = \begin{bmatrix} A & -\frac{1}{\rho} B \, R^{-1} \, B^T \\ -Q & -A^T \end{bmatrix} \tag{6.12}$$

This replaces the problem of solving a n^{th} order Riccatti equation (n being the order of the system) and a n^{th} order eigenvalue problem, by a $2n^{th}$ order eigenvalue problem.

The points of departure of the optimal root-locus are the stable open-loop poles, combined with the mirror images of the unstable open-loop poles (symmetric position about the imaginary axis). In our case, two poles are at the origin, two are on the negative real axis, and two are oscillatory unstable, and are then reflected in the left-half plane.

The points of arrival define the asymptotic behavior of the system as $\rho \to 0$, and are somewhat harder to obtain. Some poles go to infinity along specific asymptotic patterns (Butterworth patterns) depending on the rank of $Q^{\frac{1}{2}}B$. The other poles go to the zeroes of transmission of the system $Q^{\frac{1}{2}}(sI-A)^{-1}B$ (with the same remarks for right-half plane zeroes as for unstable poles when $\rho \to \infty$). The zeroes of transmission z_i are the solution of the generalized eigenvalue problem:

$$\begin{bmatrix} (A-z_i I) & B \\ -Q^{\frac{1}{2}} & 0 \end{bmatrix} \cdot \begin{bmatrix} x_i \\ u_i \end{bmatrix} = A' \cdot \begin{bmatrix} x_i \\ u_i \end{bmatrix} = 0 \qquad (6.13)$$

The system has as many inputs as outputs, so that the zeroes of transmission are the z_i's that make the matrix A' (defined by (6.13)) rank degenerate (the full rank is m+n, where m is the number of inputs, and n the number of states).

The matrix Q is diagonal, so that we can take:

$$Q^{\frac{1}{2}} = \text{diag}\left(\frac{1}{y_{max}}, \frac{1}{\phi_{max}}, \frac{1}{\psi_{max}}, \frac{T_z}{y_{max}}, \frac{T_z}{\phi_{max}}, \frac{T_z}{\psi_{max}} \right) \qquad (6.14)$$

and A' is given in Table 6.1.

The matrix is three times rank degenerate at $z_i = -1/T_z$. Then the row 1 is a linear combination of the rows 7 and 10 (similarly for 2, 8, 11 and 3, 9, 12). In other words, the inclusion of the velocities in the quadratic cost results in the introduction of three transmission zeroes in the optimal root-locus. It turns out that the three remaining zeroes of transmission are at the infinity. The case when $T_z=0$ can be seen as a limiting case when the weights on the derivatives go to zero. All the transmission zeroes are then at infinity.

Figures 6.1, 6.2, and 6.3 show the optimal root-loci for $T_z=0$, $T_z=1$, and $T_z=0.5$ and are labelled for different values of ρ. The structure of the root-locus for high values of ρ is the same for different values of T_z and is not repeated in the last two plots.

The previous comments concerning the points of departure and of arrival are easily checked. For non-zero T_z, the poles eventually reach the negative real axis, and three go to infinity, while the others reach the zeroes at $-1/T_z$. As T_z goes to zero, the zeroes move to infinity, and the case of zero velocity weights appears clearly as a limiting case from the three figures. Then, the asymptotic structure consists of three second-order Butterworth patterns.

As expected, the root-loci reach faster higher damping regions when

$$
A' = \begin{bmatrix}
-z_i & 0 & 0 & 1 & 0 & 0 & 0 & 0 & 0 \\
0 & -z_i & 0 & 0 & 1 & 0 & 0 & 0 & 0 \\
0 & 0 & -z_i & 0 & 0 & 1 & 0 & 0 & 0 \\
0 & A_A(4,2) & 0 & A_A(4,4)-z_i & A_A(4,5) & A_A(4,6) & B_A(4,1) & 0 & 0 \\
0 & 0 & 0 & A_A(5,4) & A_A(5,5)-z_i & A_A(5,6) & B_A(5,1) & B_A(5,2) & B_A(5,3) \\
0 & 0 & 0 & A_A(6,4) & A_A(6,5) & A_A(6,6)-z_i & B_A(6,1) & B_A(6,2) & B_A(6,3) \\
\frac{-1}{y_{max}} & 0 & 0 & 0 & 0 & 0 & 0 & 0 & 0 \\
0 & \frac{-1}{\phi_{max}} & 0 & 0 & 0 & 0 & 0 & 0 & 0 \\
0 & 0 & \frac{-1}{\psi_{max}} & 0 & 0 & 0 & 0 & 0 & 0 \\
0 & 0 & 0 & \frac{-T_z}{y_{max}} & 0 & 0 & 0 & 0 & 0 \\
0 & 0 & 0 & 0 & \frac{-T_z}{\phi_{max}} & 0 & 0 & 0 & 0 \\
0 & 0 & 0 & 0 & 0 & \frac{-T_z}{\psi_{max}} & 0 & 0 & 0
\end{bmatrix}
$$

Table 6.1: A' Matrix Structure

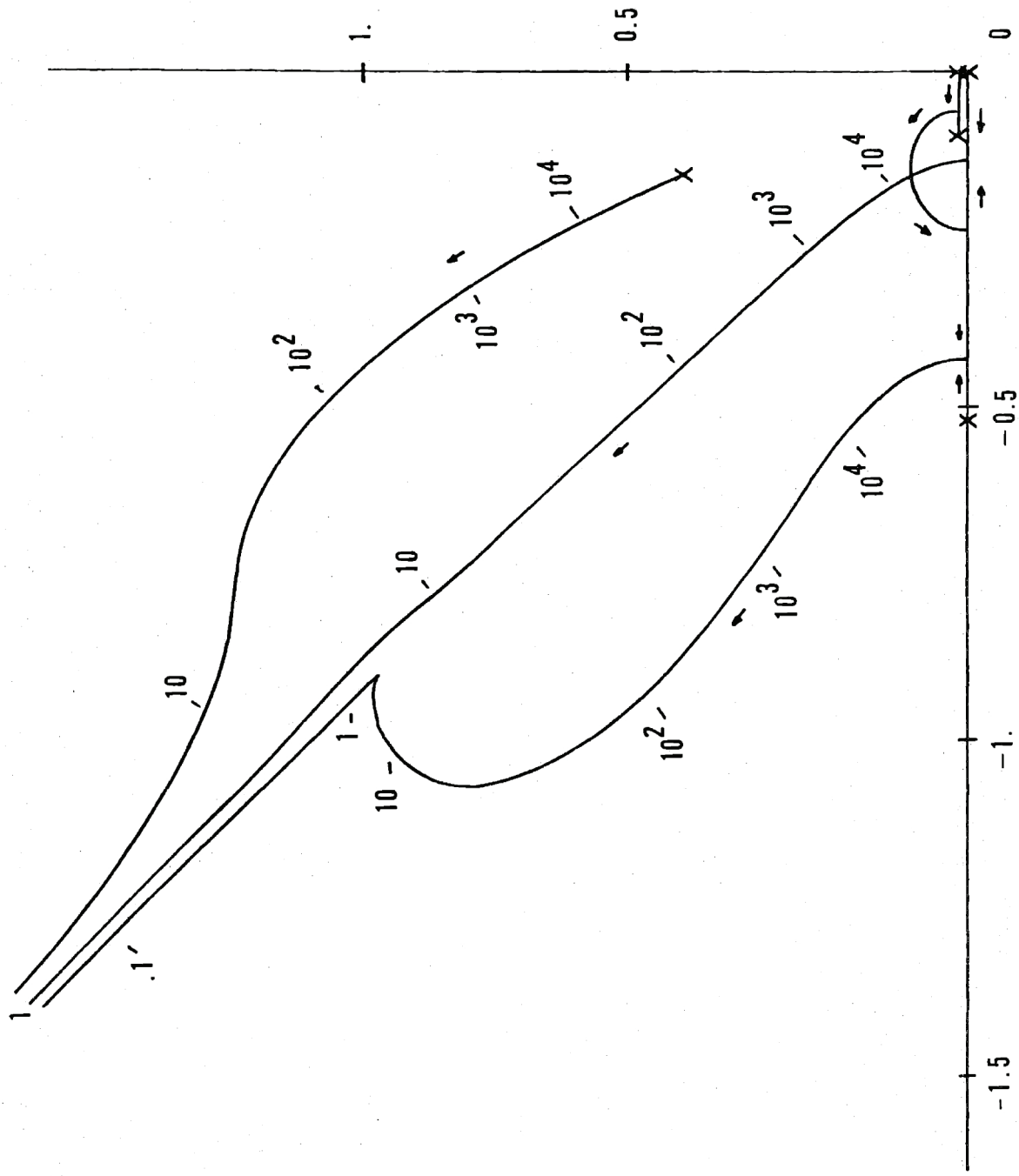

Figure 6.1: Optimal Root-Locus (T_z=0)

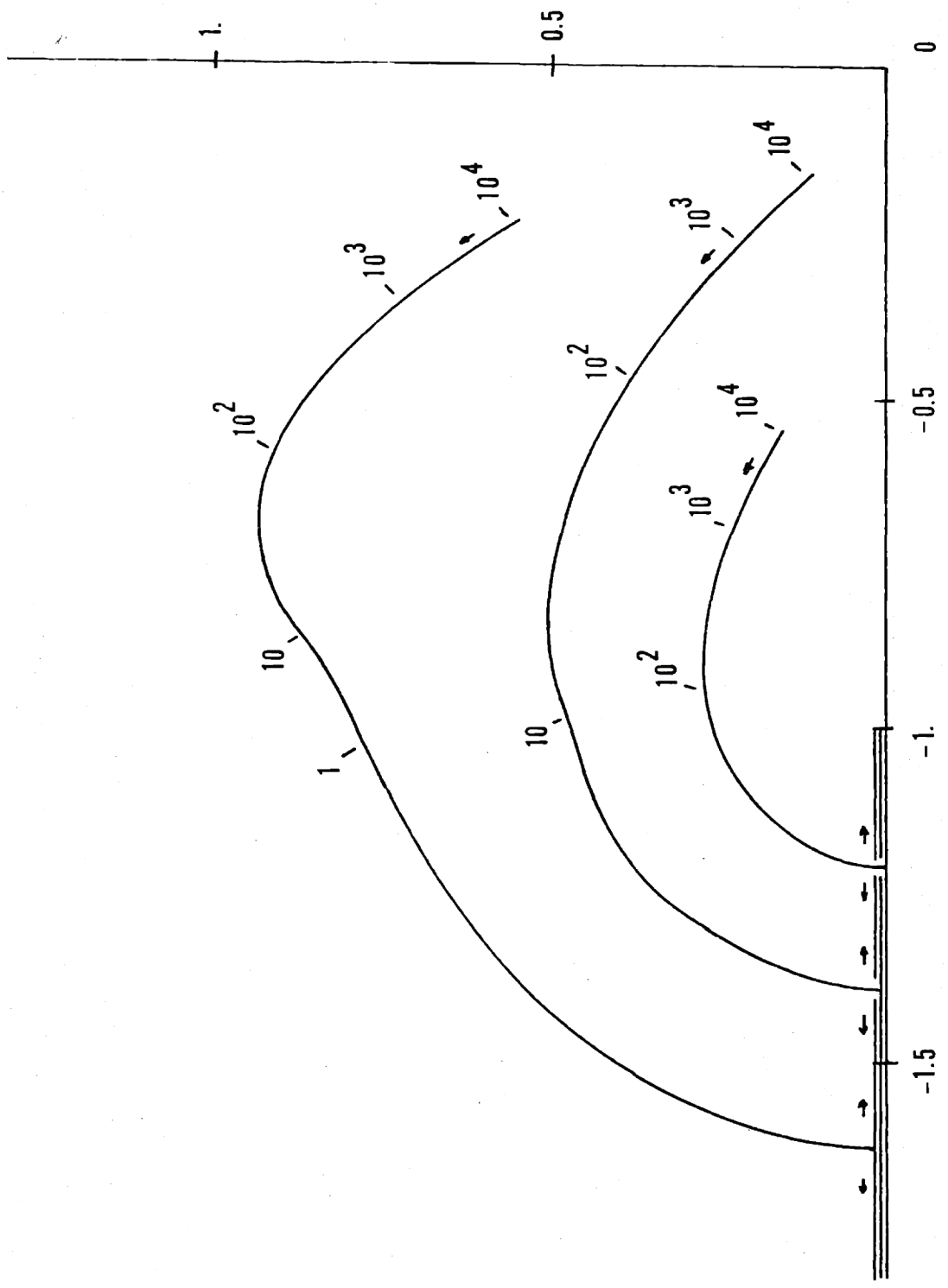

Figure 6.2: Optimal Root-Locus (T_z=1)

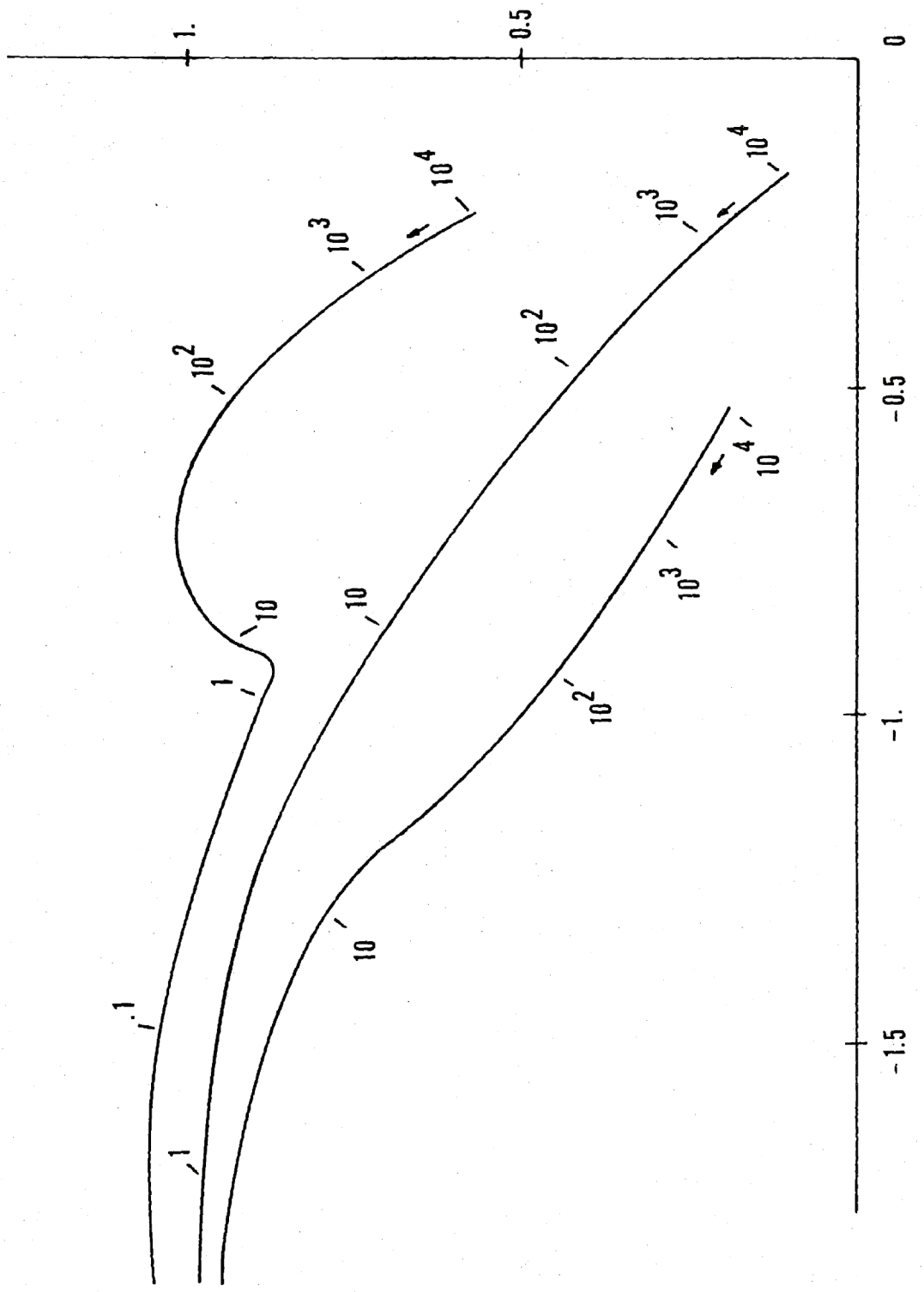

Figure 6.3: Optimal Root-Locus (T_z=0.5)

derivative weights are included. However, the asymptotic behavior with no velocity weights is a desirable one. At this point, no decision is made about which case is better (T_z=0 or T_z=1). This depends on which value of ρ corresponds to a realistic design (acceptable tracking errors and control authority). If high values of ρ are reasonable, choosing T_z=1 will probably improve the design. If small values of ρ are reasonable, choosing T_z=0 may be better, as it leads to desirable closed-loop poles locations.

It turns out that the range of ρ between $\rho = 0.3$ and $\rho = 30$ is a realistic one, as will be elaborated in the sequel. The corresponding pole locations are satisfactory for $T_z = 0$, and this case will be considered as the nominal one from now on.

Finally, an interesting characteristic of the root-loci presented here is their rather peculiar behavior around the 1 rad/s region. This appears in all three cases. For $T_z = 0$, the behavior is quite surprising, as one pole (one complex pair) seems to come back before going to infinity along the 45 degrees line. At some point, this point "slows" down as if it was reaching a zero. This point is found to be approximately at $0.91 \pm j\ 0.87$ and $\rho \simeq 3$. No attempt is made to justify this behavior mathematically, but some physical connection can be found, and will be explained below.

It can be expected that the important couplings between sway and roll previously mentionned have some importance in this strange behavior. Actually, while a small relative change of ρ produces only a very small

movement of the pole near $\rho = 3$, a comparatively small change of the weight on $\delta T_{1,2}$ ($\delta T_{1,2_{max}}$) produces a much larger movement of this pole. It is clear then that the roll control variable is crucial in the optimal lateral control system design, as it is probably in any VTOL lateral control system design.

6.4 Step Responses

As a first step in the evaluation of the control system design, responses to deviations from equilibrium are computed and plotted. The aircraft is assumed to be left with a zero velocity and some position error at t=0. Figures 6.4, 6.5, 6.6, 6.7, show the response to a 4 ft sway initial error, and Figures 6.8, 6.9, 6.10, and 6.11 the responses to a 10 degrees roll initial error. The responses to a yaw initial error are not significant (they require comparatively very small control authority), and are not reproduced here. Similarly, the deflections $\delta\alpha_{1,2}$ and $\delta\alpha_3$ are about the same, and only $\delta\alpha_{1,2}$ is shown.

The sway error response is particularly interesting: for high values of ρ (high control cost), the roll response is important, while the fan deflection (which mainly produces a sway force) is small. In fact, the controller flies the VTOL as a helicopter: as the weight on the state is small, and the weight on the controls is high, the controller slowly banks the aircraft and uses the lateral component of the thrust to obtain a sway acceleration; then, after some time, it banks the aircraft in opposite direction to reduce the sway speed to zero, together with the sway deviation.

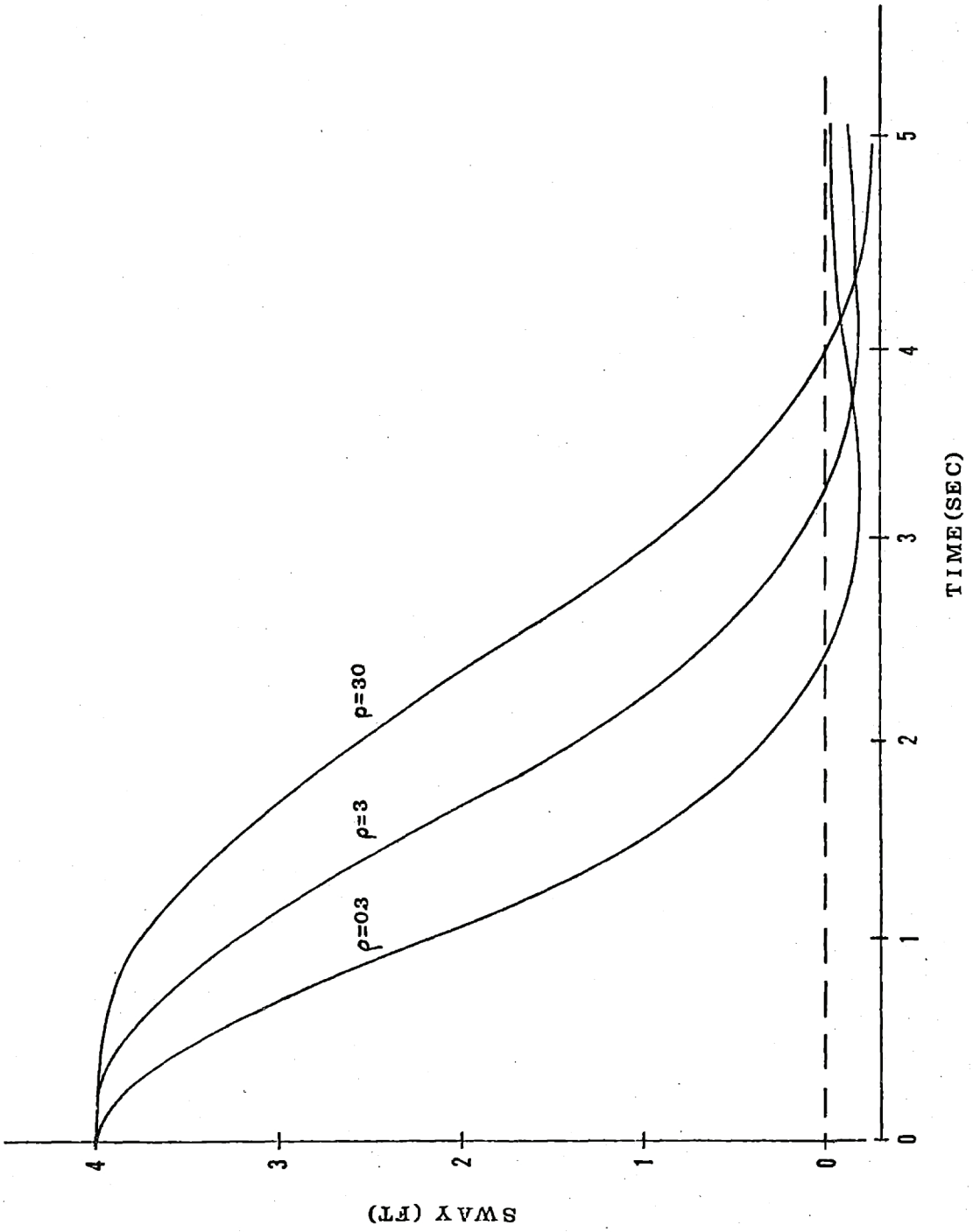

Figure 6.4: Sway Response to a Sway Initial Error

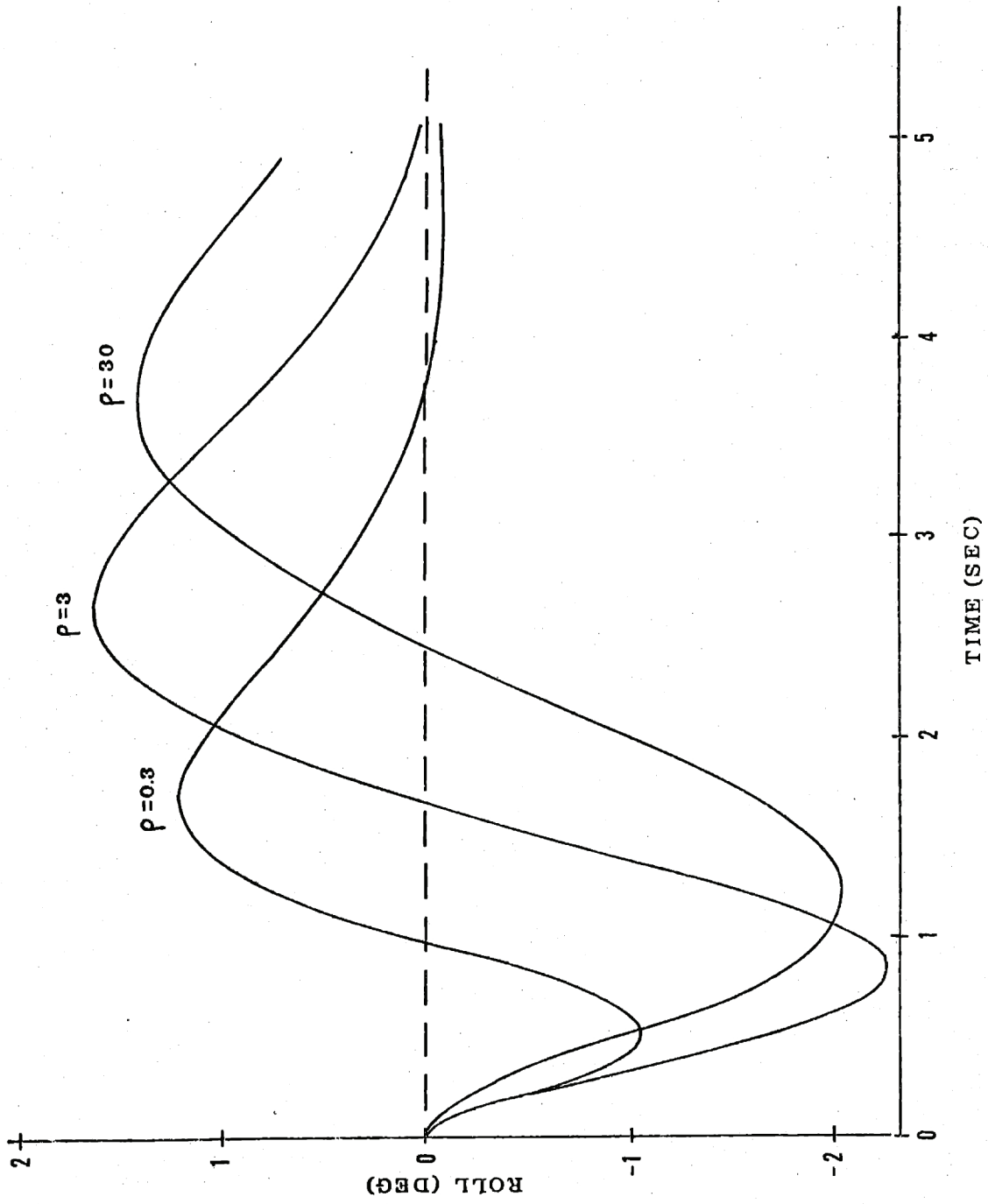

Figure 6.5: Roll Response to a Sway Initial Error

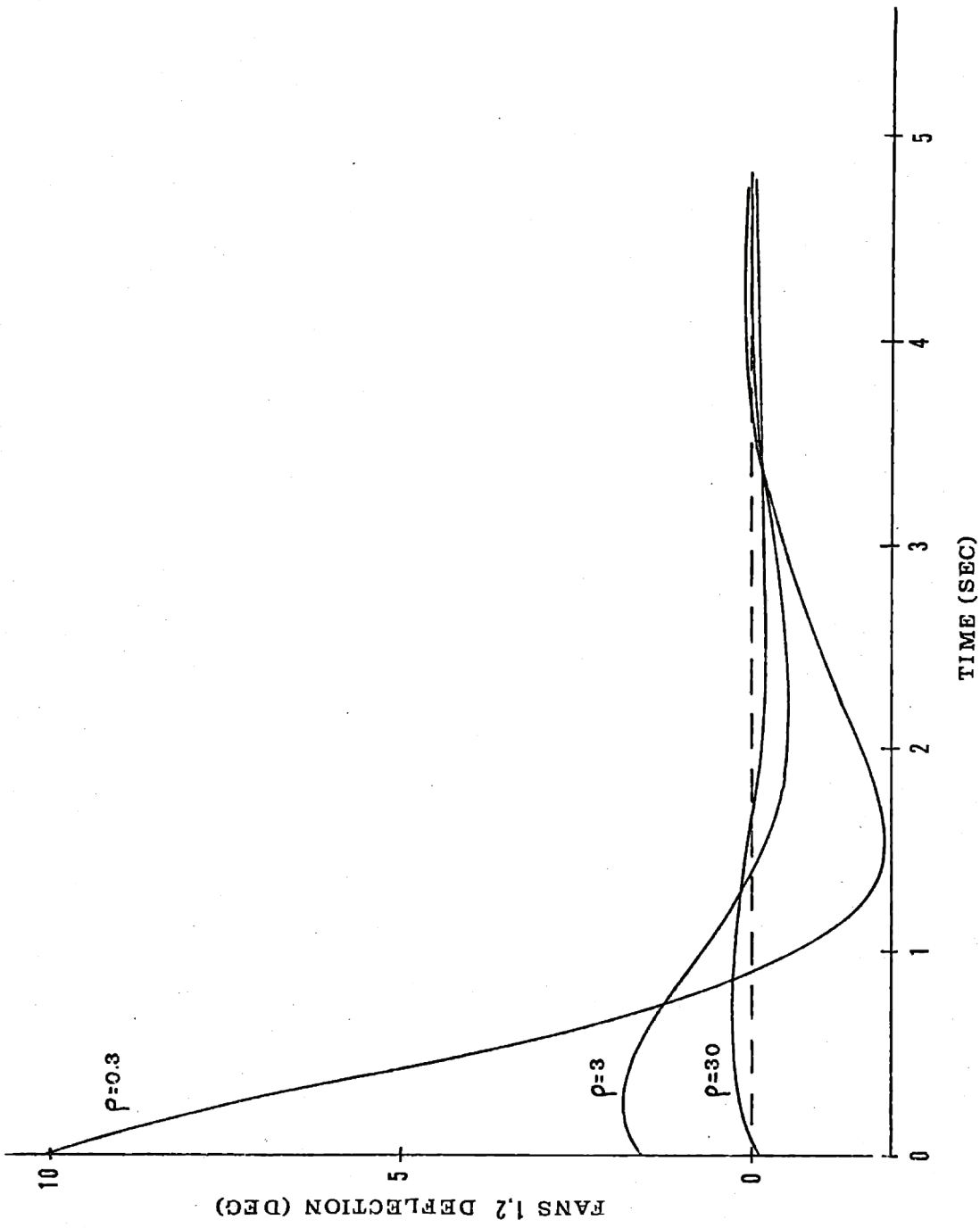

Figure 6.6: Fans Deflection Response to a Sway Initial Error

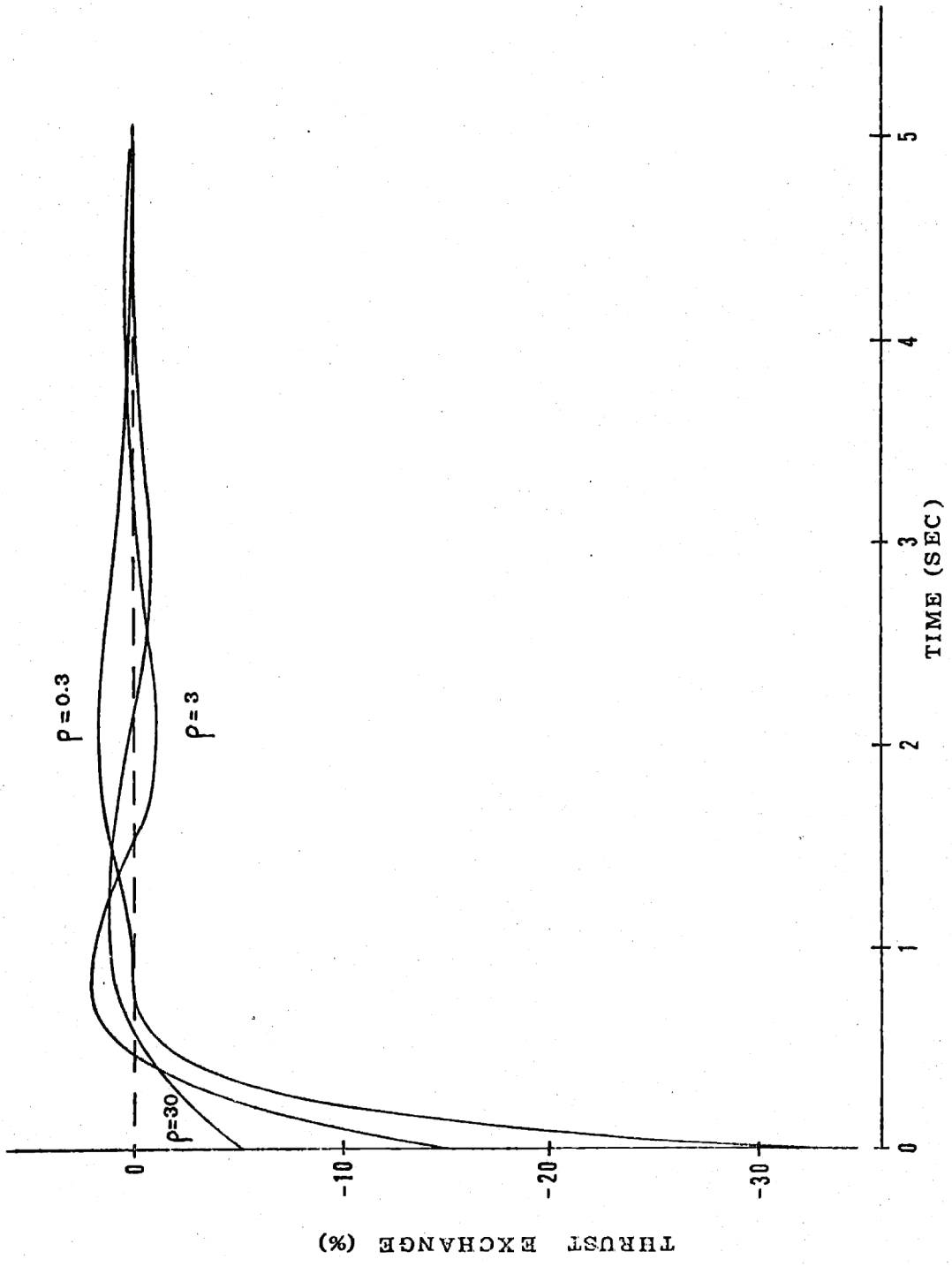

Figure 6.7: Thrust Exchange Response to a Sway Initial Error

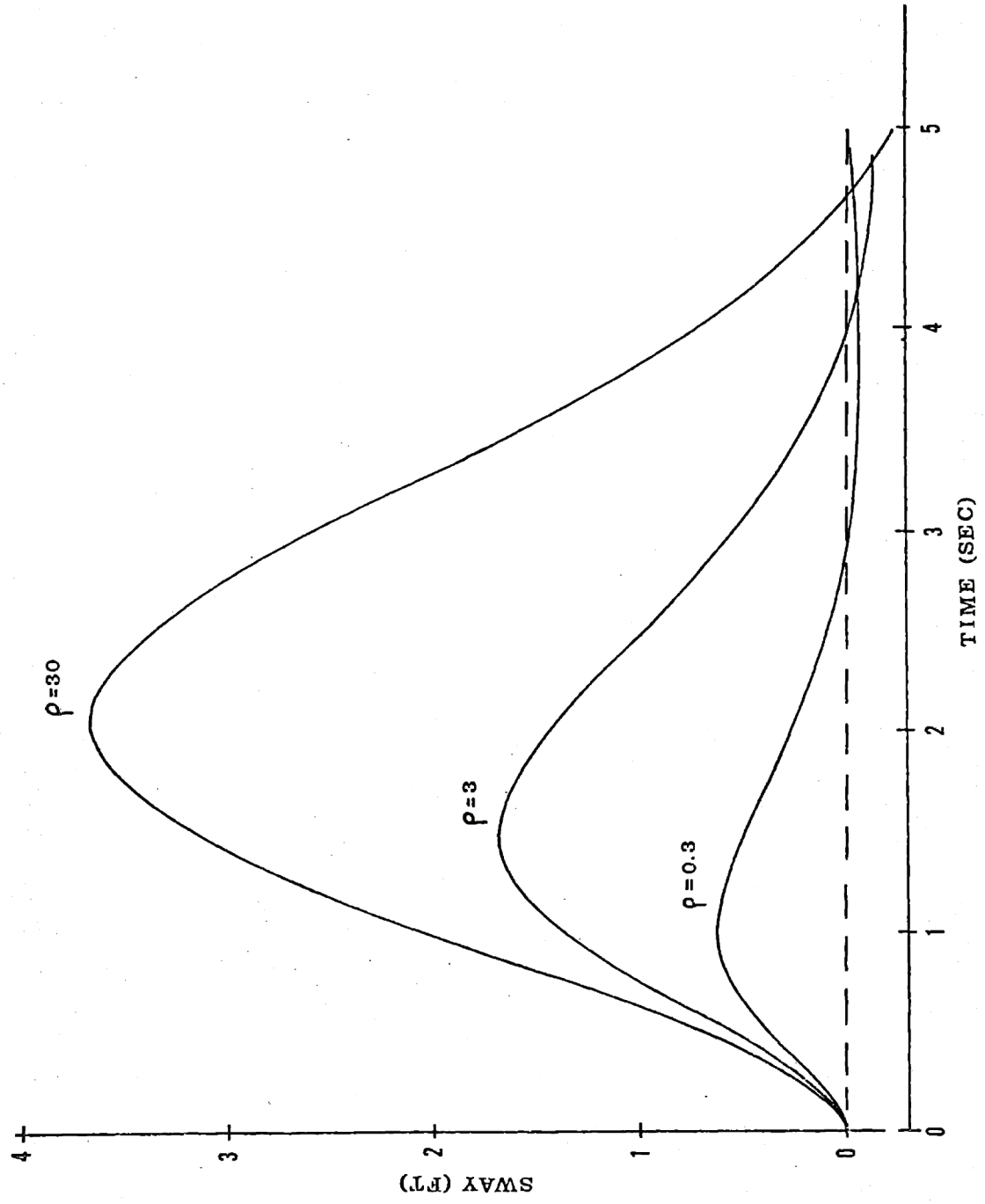

Figure 6.8: Sway Response to a Roll Initial Error

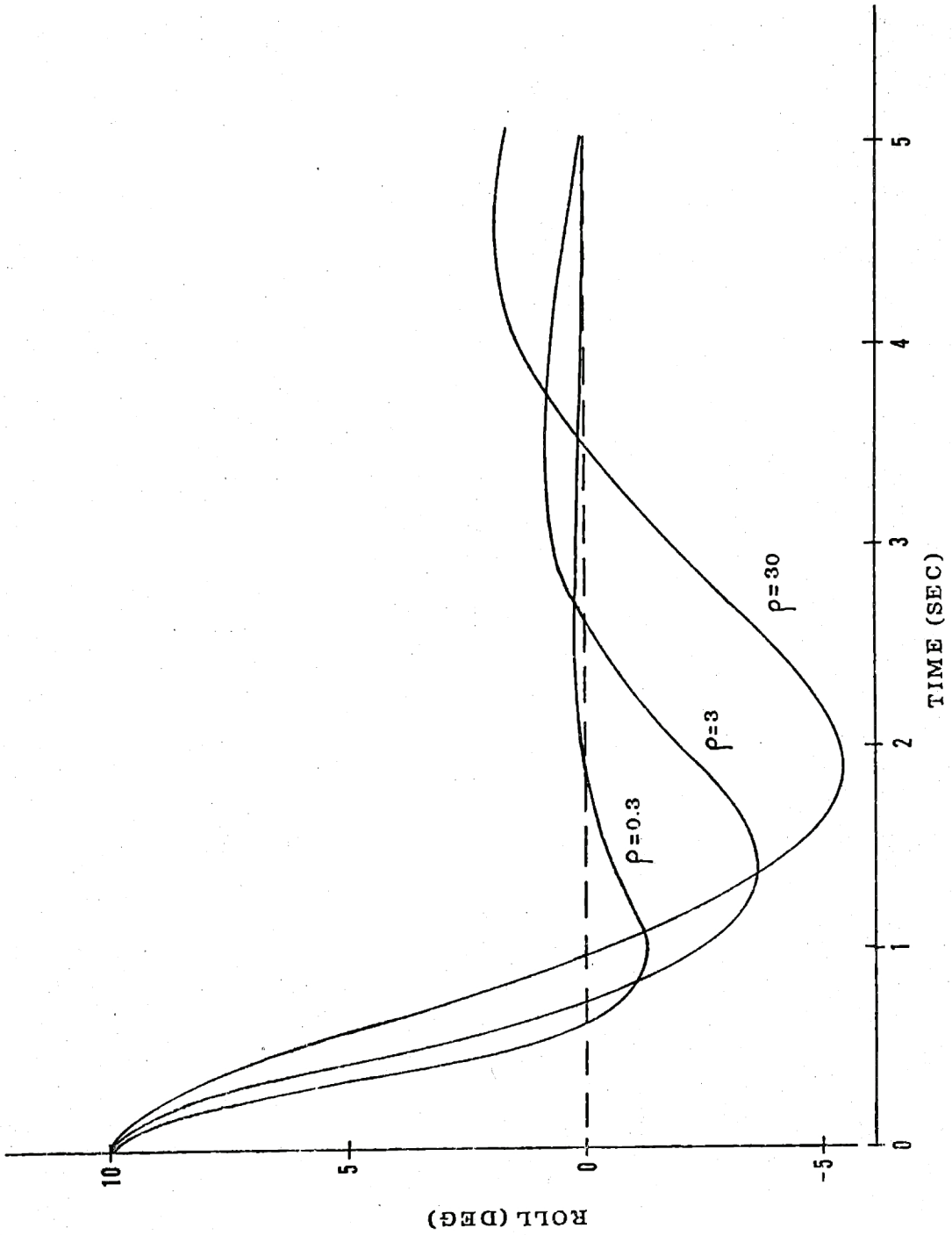

Figure 6.9: Roll Response to a Roll Initial Error

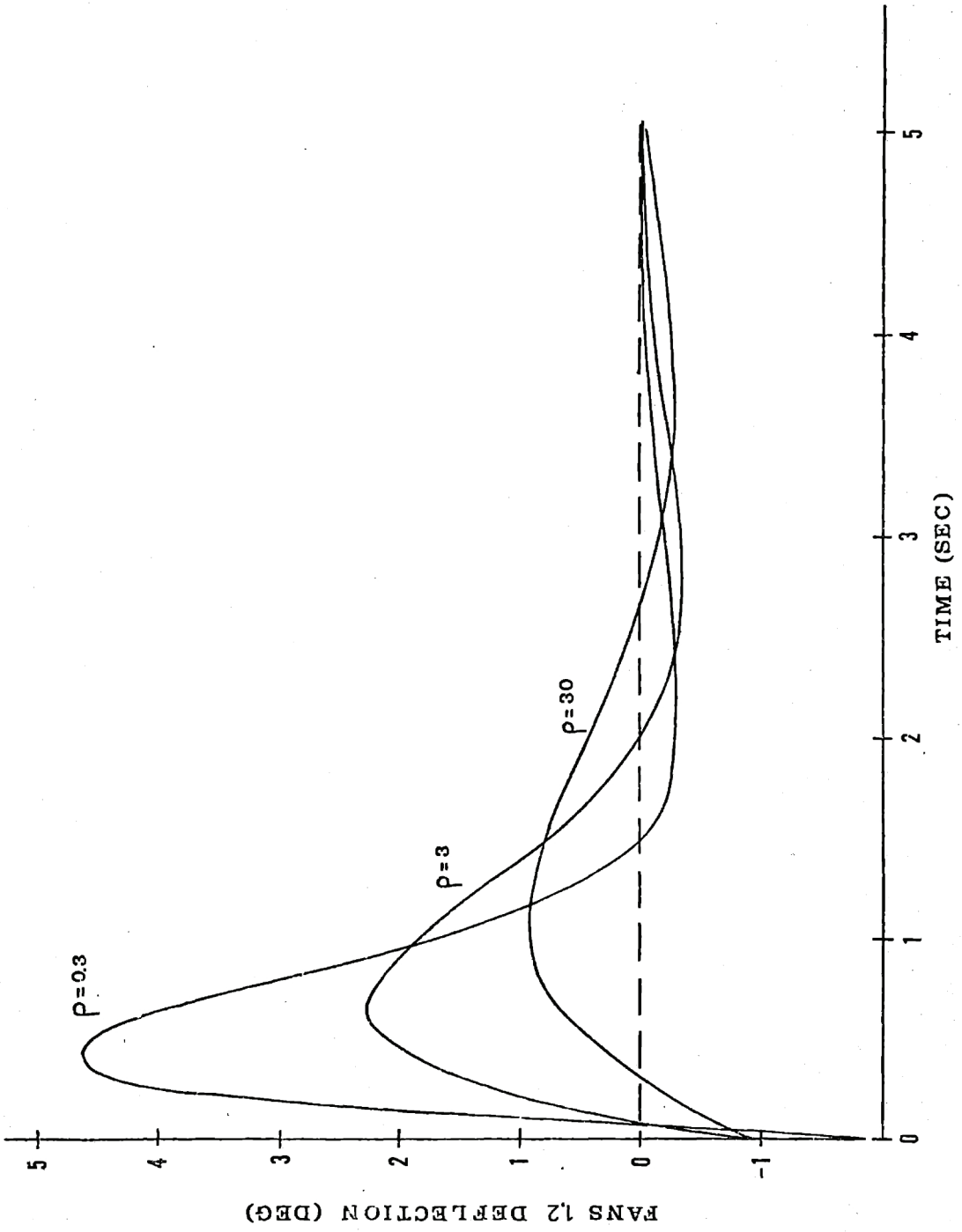

Figure 6.10: Fans Deflection Response to a Roll Initial Error

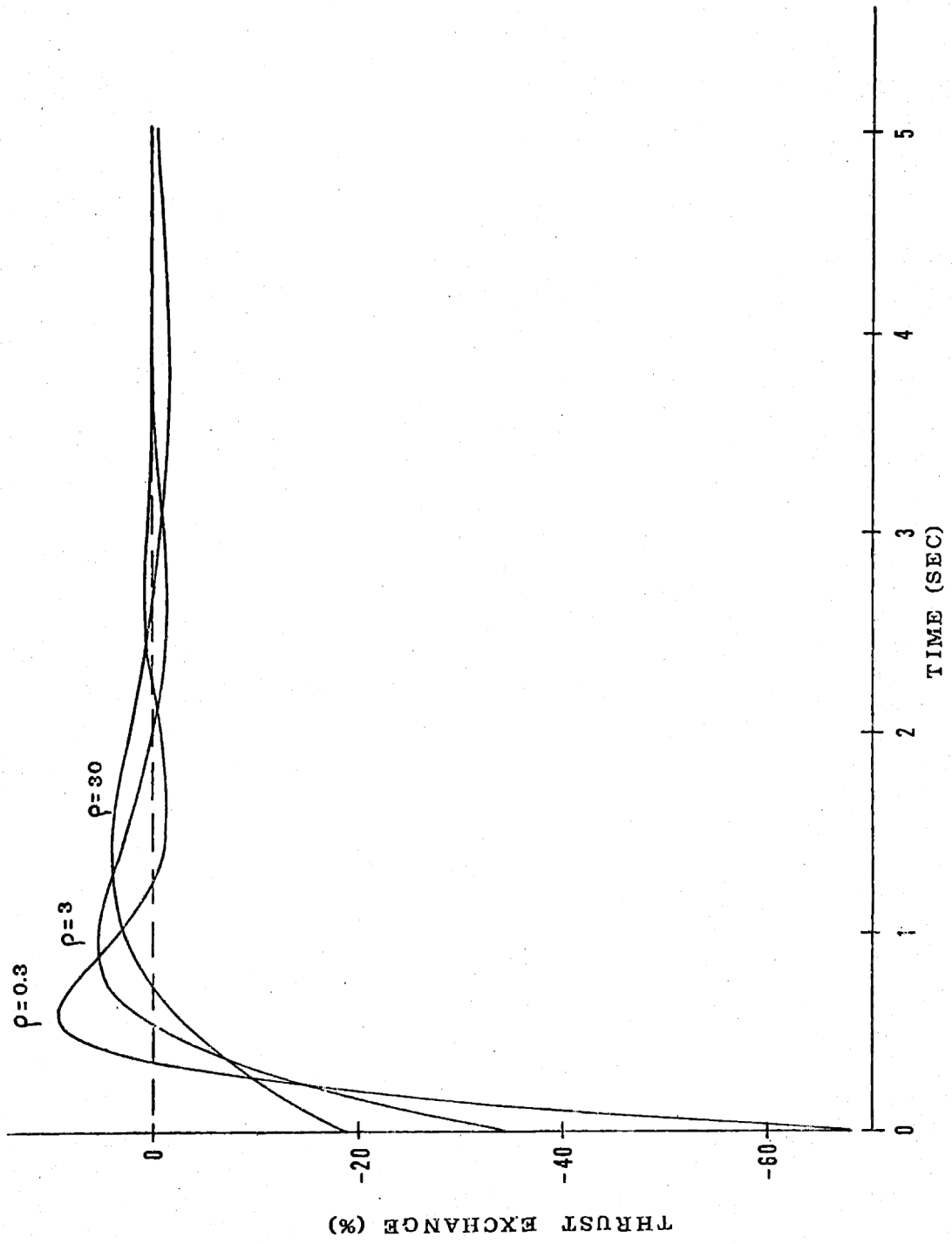

Figure 6.11: Thrust Exchange Response to a Roll Initial Error

For small ρ (high state deviation cost), the situation is very different, and a dramatic increase in fan deflection response can be observed on Fig. 6.6, while the roll response on Fig. 6.5 is much smaller. This shows that the turning point observed in the root-locus of Fig. 6.1 corresponds also to a change in strategy of the controller.

A similar conclusion can be obtained from the responses to a roll initial error. For a high value of ρ (ρ=30), the sway induced by the initial roll angle is important, and it is then compensated by an important opposite roll (about half of the initial roll angle).

We conclude from this discussion that the quadratic optimization problem leads to solutions which, when understood, are very logical, and simply express specific characteristics of the system, which, at first, may be obscured by its multiple-input multiple-output structure. One advantage of the LQ methodology is that it leads to coupled controller designs that exploit the dynamic coupling phenomena.

6.5 A Special Example

To illustrate the above remarks, a limiting case is presented; it corresponds to $\rho = 10$, $T_z = 0$, but with the penalty on the sway error multiplied by 10^6. The resultant closed-loop matrix:

$$A_{A,CL} = A_A - B_A G_A \tag{6.15}$$

and the gain matrix G_A are given in Table 6.2.

The most interesting terms are the $A_{A,CL}(4,2)$ and the $G_A(2,1)$ terms.

$$A_{CL,A} = \begin{bmatrix} 0. & 0. & 0. & 1. & 0. & 0. \\ 0. & 0. & 0. & 0. & 1. & 0. \\ 0. & 0. & 0. & 0. & 0. & 1. \\ -32.96 & -0.11 & 0.0155 & -25.55 & -0.3263 & 0.0021 \\ 44.77 & -12.04 & -0.4046 & 2.634 & -5.656 & -0.4832 \\ 17.93 & -0.2405 & -1.175 & 1.279 & -0.3219 & -1.539 \end{bmatrix}$$

$$G_A = \begin{bmatrix} 10.2360 & 1.0034 & -0.00005 & 0.7914 & 0.0009 & -0.0012 \\ -0.0637 & 3.5568 & 0.0071 & 0.1737 & 1.2153 & 0.0065 \\ -1.9995 & -0.0093 & 0.1443 & -0.1462 & 0.0009 & 0.1711 \end{bmatrix}$$

Table 6.2: Closed-Loop Matrix and Feedback Gains for a High Sway Error Penalty

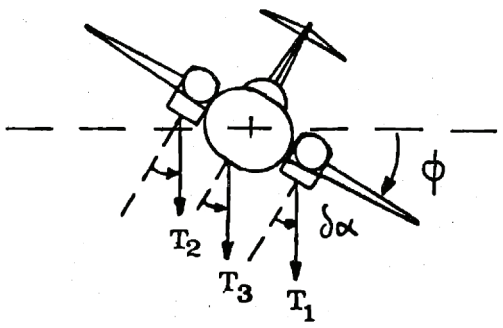

Figure 6.12: Exact Compensation of the Lateral Force Due to a Roll Angle with a Thrust Deflection

Compared to the original $A_A(4,2) = 32.2$, the term $A_{A,CL}(4,2)=-0.11$ is reduced almost to zero; we recall that this term expressed the lateral force due to a roll angle of the aircraft. The weight on a sway error being very large, the controller compensates this effect very logically with a deflection of the thrusts in opposite direction than the roll angle. This is accomplished by the $G_A(1,2)$ term, which, in the limit, would be equal to 1 (see Fig. 6.12).

6.6 Ship Motion Tracking

Up to now, the VTOL controller was designed as a stabilizer, or zero state tracking controller. As indicated earlier, the feedback structure of the controller is independent of the specific reference signal to follow, i.e. the ship motion at the landing pad. The ship model is required in the definition of the forward gain matrix value (G_S). The importance of the ship model is mostly in the computation of the rms tracking errors and controls, which define the performance of the controller.

In chapter 2, we denoted by $\underline{w}_A$ and $\underline{w}_S$ the vectors of the aircraft and ship variables that we want to track. They are the aircraft and ship motions (at the landing pad), so that:

$$\underline{w}_A = W_A \underline{x}_A \tag{6.16}$$

$$\underline{w}_S = W_S \underline{x}_S \tag{6.17}$$

with:

$$W_A = \begin{bmatrix} 1 & 0 & 0 & 0 & 0 & 0 \\ 0 & 1 & 0 & 0 & 0 & 0 \\ 0 & 0 & 1 & 0 & 0 & 0 \end{bmatrix} \tag{6.18}$$

$$W_S = C_{SLP} \tag{6.19}$$

The tracking errors are denoted $\underline{w}_{A-S}$, so that:

$$\underline{w}_{A-S} = \underline{w}_A - \underline{w}_S = W_{A-S}\,\underline{x} \tag{6.20}$$

where:

$$W_{A-S} = (-W_S \ , \ W_A) \tag{6.21}$$

$$\underline{x} = \begin{bmatrix} \underline{x}_S \\ \underline{x}_A \end{bmatrix} \tag{6.22}$$

The overall system equations are:

$$\dot{\underline{x}} = A\underline{x} + B\underline{u} + \underline{\xi} \tag{6.23}$$

$$\underline{c} = T_c\,\underline{u} \tag{6.24}$$

where:

$$A = \begin{bmatrix} A_S & 0 \\ 0 & A_A \end{bmatrix} \tag{6.25}$$

$$B = \begin{bmatrix} 0 \\ B_A \end{bmatrix} \tag{6.26}$$

$$\underline{\xi} = \begin{bmatrix} \underline{\xi}_S \\ \underline{\xi}_A \end{bmatrix} \tag{6.27}$$

The spectral intensity of $\underline{\xi}$ is:

$$\Xi = \begin{bmatrix} \Xi_S & 0 \\ 0 & \Xi_A \end{bmatrix} \tag{6.28}$$

The LQ controller is designed, using a Q matrix:

$$Q = W_{A-S}^T \, Q_w \, W_{A-S} = \begin{bmatrix} W_S^T \, Q_w \, W_S & -W_S^T \, Q_w \, W_A \\ -W_A^T \, Q_w \, W_S & W_A^T \, Q_w \, W_S \end{bmatrix} \tag{6.29}$$

where Q_w is the same matrix as the one used in 6.2 and defined by (6.4). Similarly, the matrix R is chosen as defined by equations (6.7) and (6.8). The control law is :

$$\underline{u} = -G\underline{x} = -G_S \underline{x}_S - G_A \underline{x}_A \tag{6.30}$$

In this state-space framework, the rms values of the tracking errors $\underline{w}_{A-S}$ and of the controls $\underline{c}$ are very easily obtained. The covariance of the states deviations is obtained by solving the Lyapunov equation:

$$(A-BG)^T P + P(A-BG) + \Xi = 0 \tag{6.31}$$

where:

$$P = E(\underline{x}\ \underline{x}^T) \tag{6.32}$$

The rms tracking errors and rms controls are the square roots of the diagonal elements of the covariance matrices:

$$E(\underline{w}_{A-S}\ \underline{w}_{A-S}^T) = W_{A-S}\ P\ W_{A-S}^T \tag{6.33}$$

$$E(\underline{c}\ \underline{c}^T) = T_c\ G\ P\ G^T\ T_c^T \tag{6.34}$$

Tables 6.3 and 6.4 contain the results obtained for the two sea conditions discussed in chapter 3. Table 6.5 contains the closed-loop poles locations corresponding to the different values of ρ.

SEA H=12ft ω_m=0.4807 rad/s							
		Sway (ft)	Roll (deg)	Yaw (deg)	Controls		
Ship motion at landing pad		7.155	12.64	0.373	$\delta\alpha_{1,2}$ (deg)	$\delta T_{1,2}$ (%)	$\delta\alpha_3$ (deg)
Tracking errors	ρ=30	1.124	14.98	0.414	0.26	2.04	0.28
	ρ=3	0.971	13.35	0.203	1.93	3.06	1.96
	ρ=0.3	0.465	6.36	0.099	9.15	15.35	9.16
A/C driving noise incl.	ρ=0.3	0.801	6.41	0.329	9.72	16.74	9.37

Table 6.3: LQ Controller Performance (decaying sea)

SEA H=10ft ω_m=0.72 rad/s							
		Sway (ft)	Roll (deg)	Yaw (deg)	Controls		
Ship motion at landing pad		2.551	4.556	0.227	$\delta\alpha_{1,2}$ (deg)	$\delta T_{1,2}$ (%)	$\delta\alpha_3$ (deg)
Tracking errors	ρ=30	0.517	5.405	0.172	0.10	0.12	0.10
	ρ=3	0.444	4.830	0.082	0.70	1.10	0.71
	ρ=0.3	0.227	2.322	0.044	3.34	5.61	3.34
A/C driving noise incl.	ρ=0.3	0.691	2.480	0.317	4.72	8.78	3.92

Table 6.4: LQ Controller Performance (fully developed sea)

Closed-loop poles locations			
ρ=30	-0.598 ± j 0.585	-1.038 ± j 0.611	-0.642 ± j 1.054
ρ=3	-0.906 ± j 0.87	-1.054 ± j 1.039	-1.528 ± j 1.552
ρ=0.3	-1.064 ± j 1.036	-1.869 ± j 1.863	-2.792 ± j 2.803

Table 6.5: LQ Controller Closed-Loop Poles Locations

For ρ = 0.3, good tracking is obtained, with reasonable control authority (for H =12 ft, ω_m = 0.4807 rad/s, some higher value of ρ may however be appropriate). The value of ρ = 0.3 was chosen as a nominal value for the control system. The closed-loop poles are also at desirable locations for a VTOL control system.

For this nominal design, the effect of wind turbulence is also indicated. The results are obtained by introducing an aircraft driving noise matrix Ξ_A, and are also indicated in Tables 6.3 and 6.4. Values for wind disturbances are found in the form of Dryden spectra in [19]. The derivation of the Ξ_A matrix from this data is included in Appendix C.

As for the aircraft controller step responses, the values of the rms tracking errors and controls give us some interesting indications about the physical aspects of the problem. The yaw tracking errors are very small, compared to the maximal values given in the quadratic cost. Similarly, the rms deflections $\delta\alpha_{1,2}$ and $\delta\alpha_3$ are very close. This indicates that yaw tracking is not at all a problem for the aircraft. The control authority is clearly more than sufficient to track the ship motion (which is very small anyway), or to reject wind disturbances.

On the other hand, roll tracking errors are much higher than the sway and yaw errors (compared proportionnally to the maximal values given in the quadratic cost). For ρ = 30, the rms error is even larger than the rms ship motion. This probably indicates that roll is the "least easily controllable" state of the VTOL aircraft, but it also reflects two

basic contradictions faced by the controller in the tracking of the sway and roll motions. The first comes from the ship motion at the landing pad. From the sway at the landing pad, a large part is coming from the roll motion, due to the difference in altitude between the landing pad and the center of rotation of the ship. It has been seen earlier that an easy way for the aircraft to track a sway reference is to roll the aircraft as a helicopter would do. However, the roll angle required to follow the ship sway motion by this mean is precisely opposite to the ship roll angle that has produced the sway motion of the landing pad. This is illustrated schematically on Fig. 6.13.

The second adverse effect has been mentioned previously and is illustrated on Fig. 6.14. It is shown that a roll moment is induced by a lateral deflection of the thrusts (term $B_A(5,1)$). It is opposite to the ship roll motion.

It is possible to improve the roll tracking by increasing its penalty in the Q matrix. Considering the physical problems mentioned here above, this will probably result in a large increase in control authority. Moreover, precise roll tracking is not necessary, and not even desirable. For the same reasons as the ones mentioned here above, precise roll tracking would result in large lateral accelerations at the pilot location and this would probably be unacceptable.

Finally, it can be noted that only the influence of wind gusts was considered here, while the mean wind was neglected (together with the aerodynamic effects, as in [1]). The influence of the mean wind will be

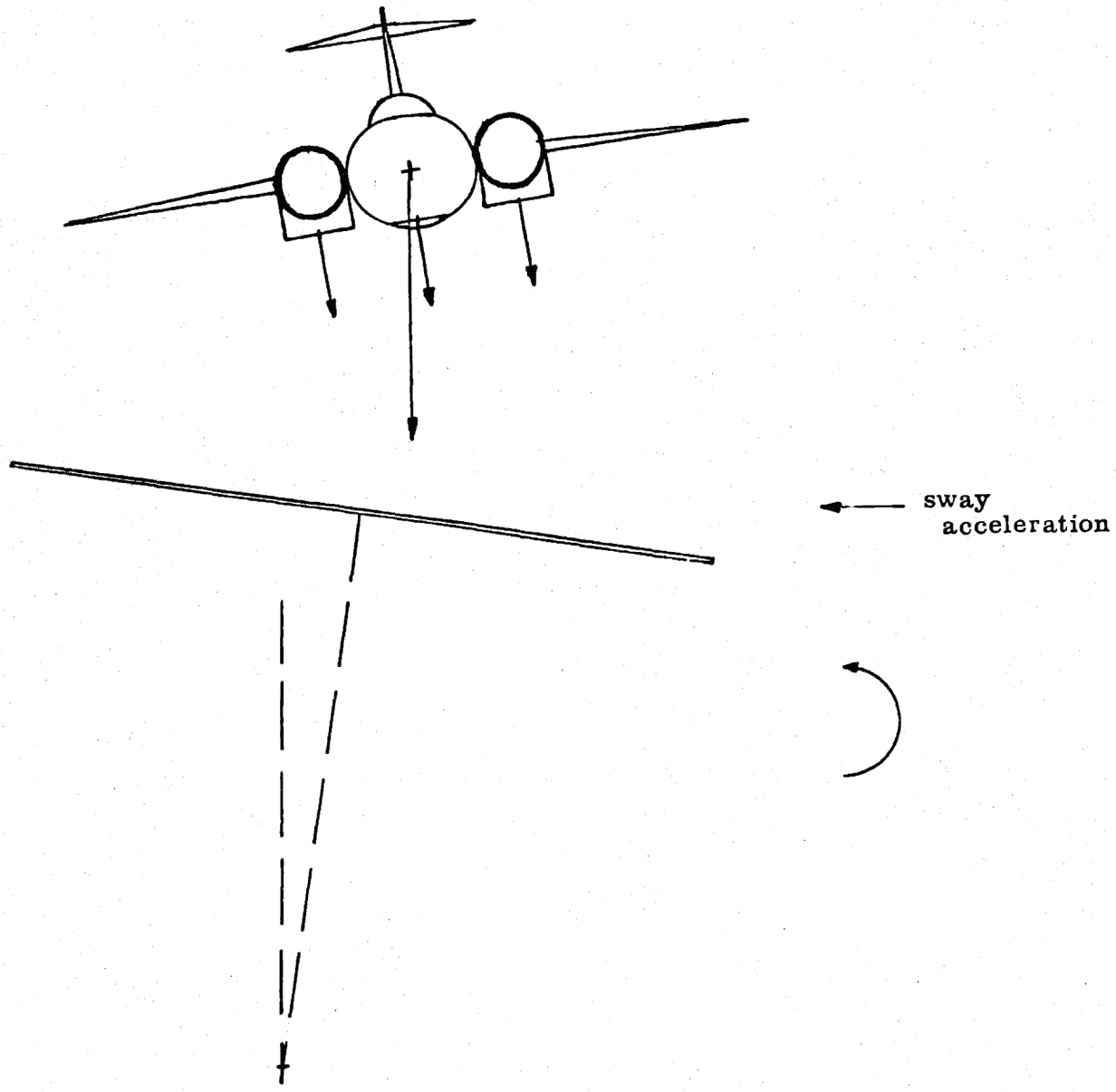

Figure 6.13: Adverse Sway/Roll Coupling in the Ship Motion

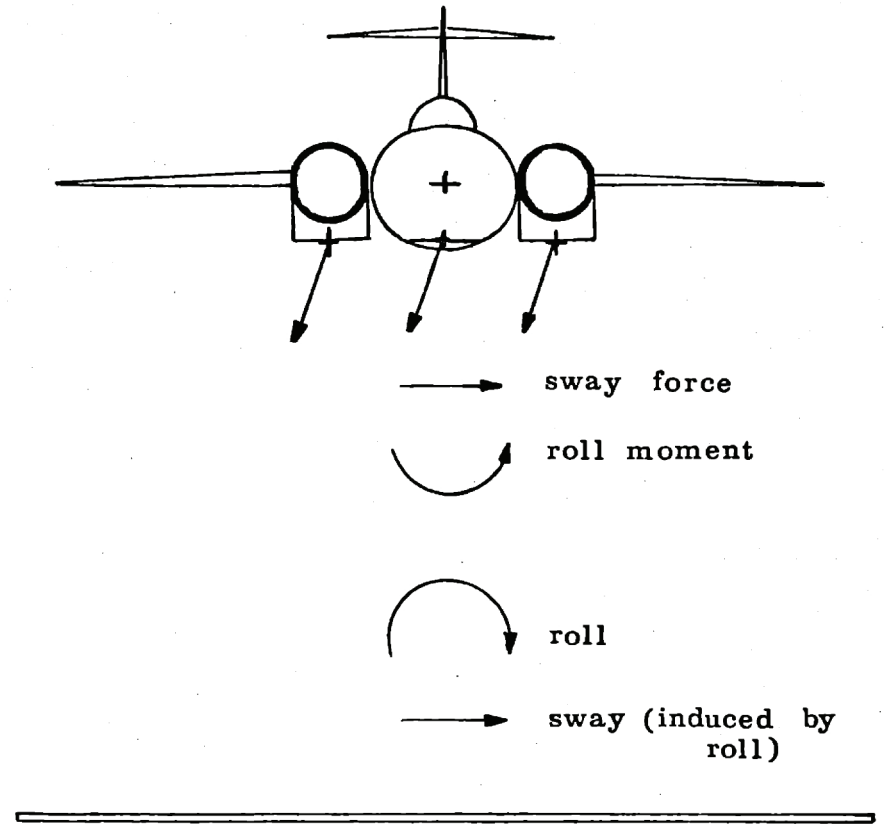

Figure 6.14: Adverse Sway/Roll Coupling in the Aircraft Motion

to produce a steady-state tracking error whose amplitude depends on the amplitude of the mean wind and on the feedback gains. This can easily be compensated for, if necessary, by introducing some integral compensation (for example, by augmenting the system and recomputing the feedback gains).

6.7 Time Domain Simulations

Some time domain simulations are illustrated in Figures 6.15 to 6.27. Figs 6.15 to 6.19 correspond to the case $\rho = 0.3$, without aircraft driving noise (wind gusts). As expected roll tracking is the worst of all, and the aircraft roll motion is systematically smaller than the ship motion.

Figures 6.20 to 6.22 illustrate the tracking in the presence of wind disturbances. As expected, the yaw tracking is the most severely affected, but the aircraft motion remains small.

Figures 6.23 to 6.27 show the case $\rho = 30$, without wind disturbances. While sway tracking remains good, the roll tracking is simply out of phase most of the time. This demonstrates again the "helicopter" behavior of the controlled aircraft for high values of ρ.

6.8 Summary

In this chapter, we described the design of a linear quadratic (LQ) regulator. This design assumes perfect knowledge of the states at any moment. For the aircraft part, the assumption is not unrealistic (especially if a good navigation system is used aboard the aircraft), as all the states are available for measurement, and the only role of an optimal estimator is to filter the noise, and provide optimal estimates on the

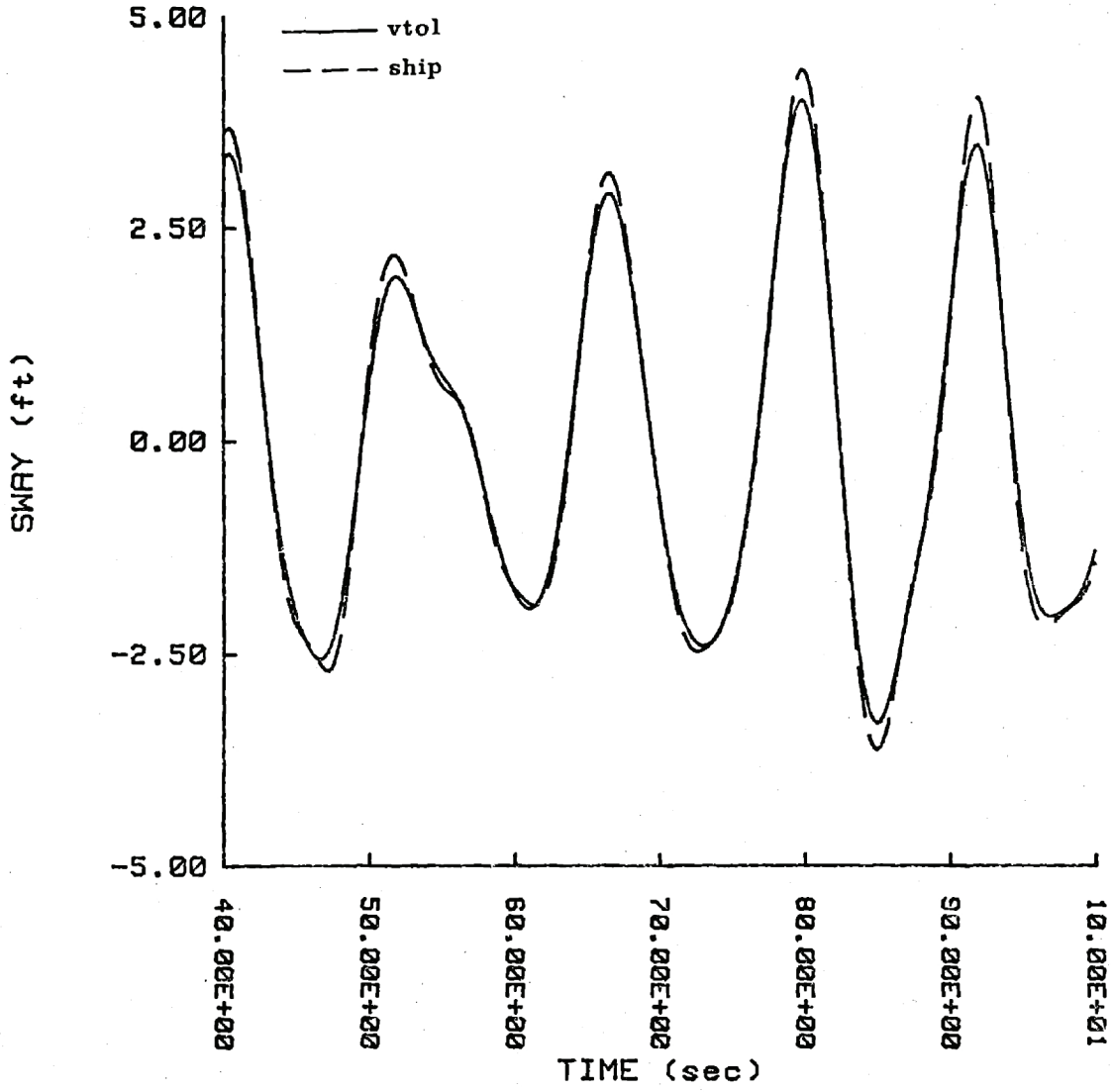

Figure 6.15: Sway Tracking (ρ=0.3)

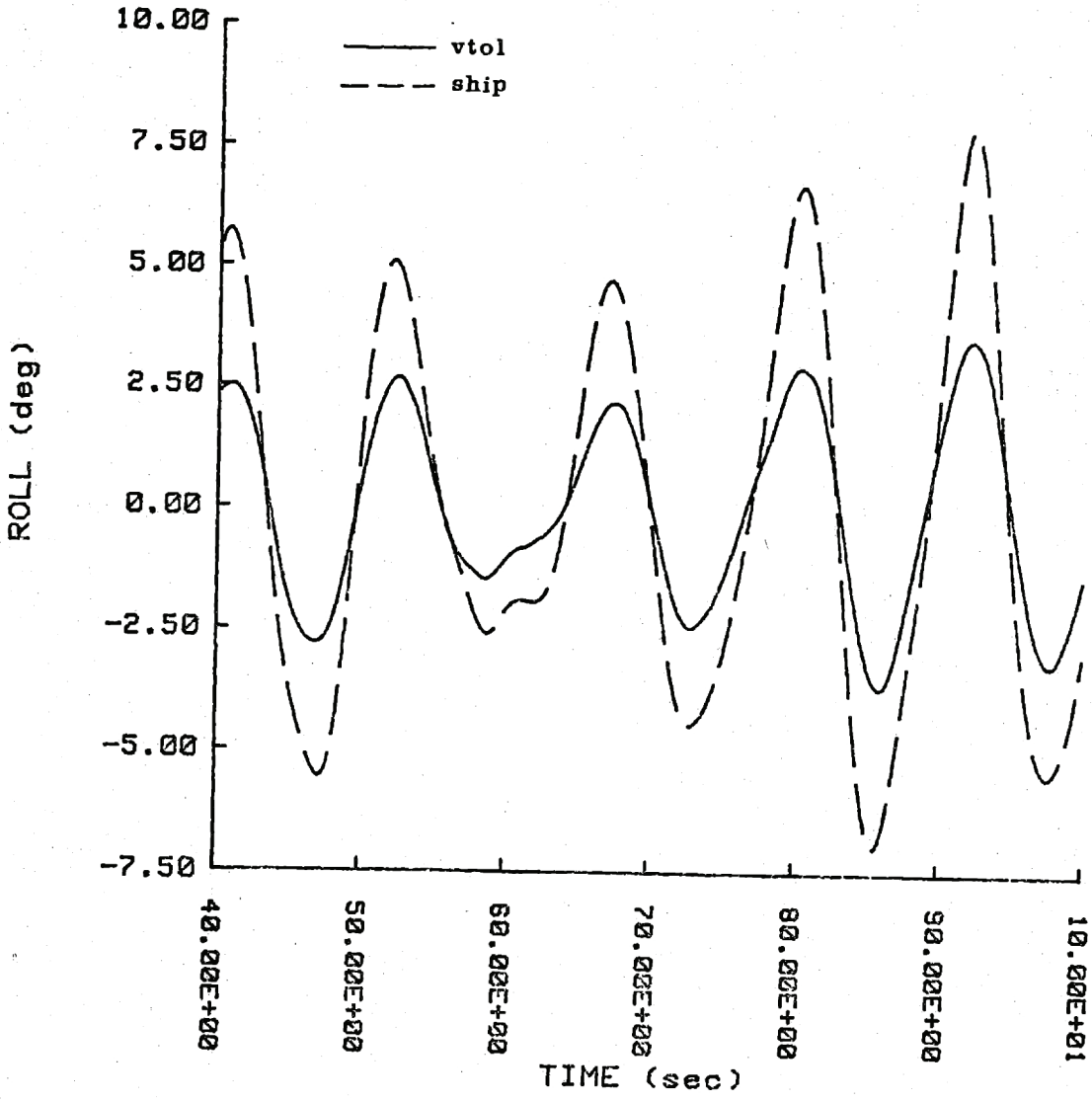

Figure 6.16: Roll Tracking (ρ=0.3)

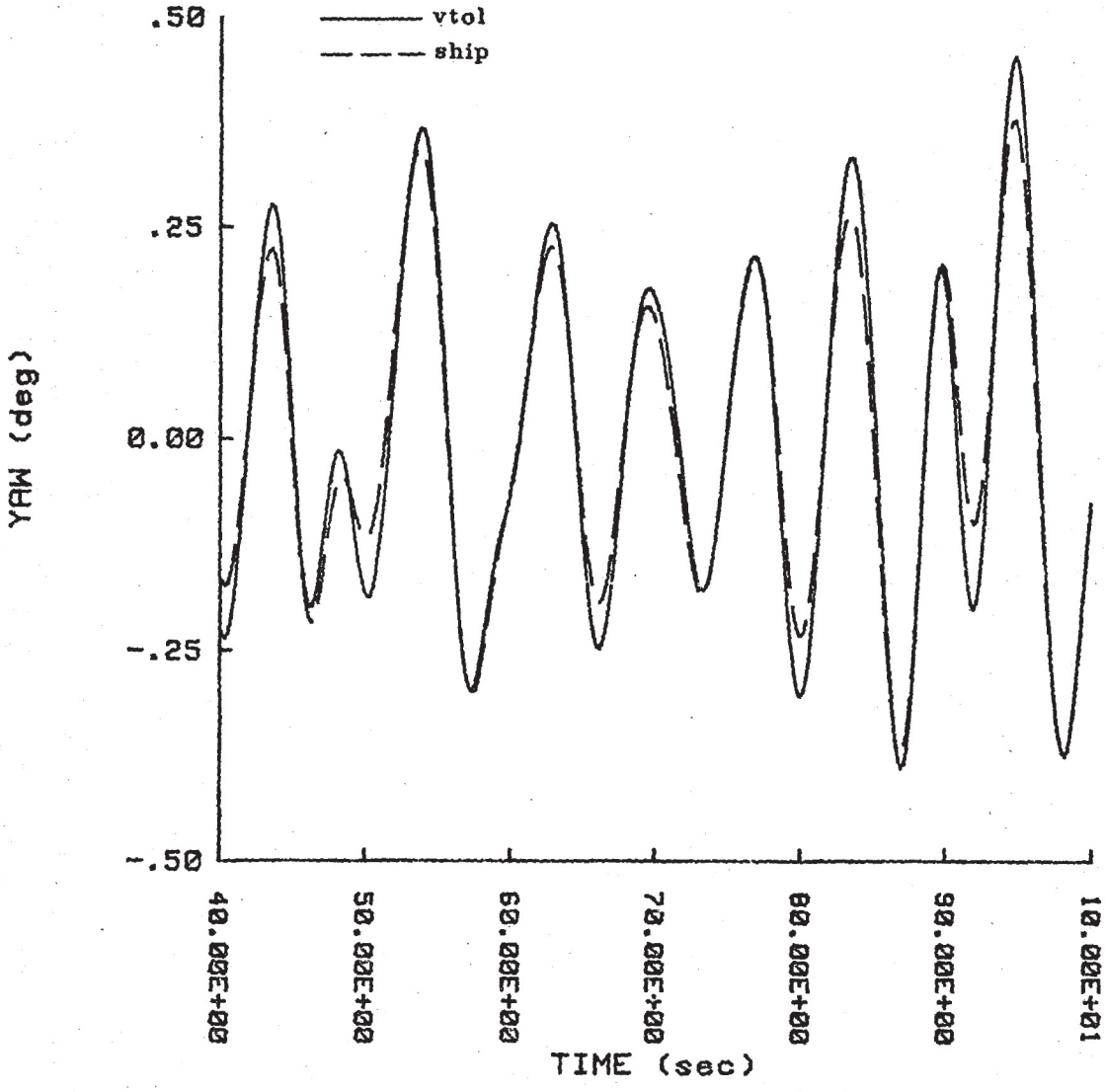

Figure 6.17: Yaw Tracking (ρ=0.3)

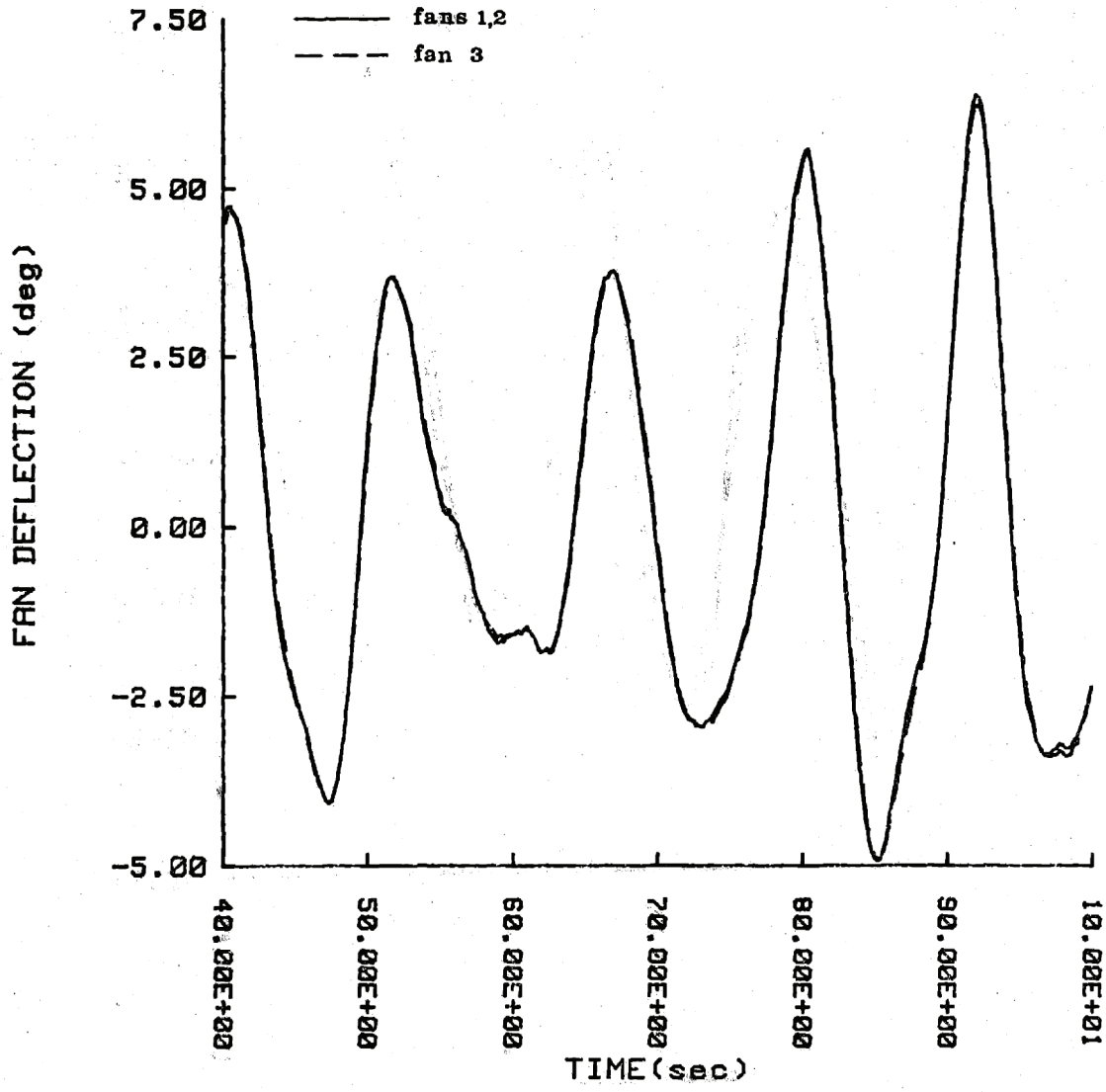

Figure 6.18: Fans Deflection (ρ=0.3)

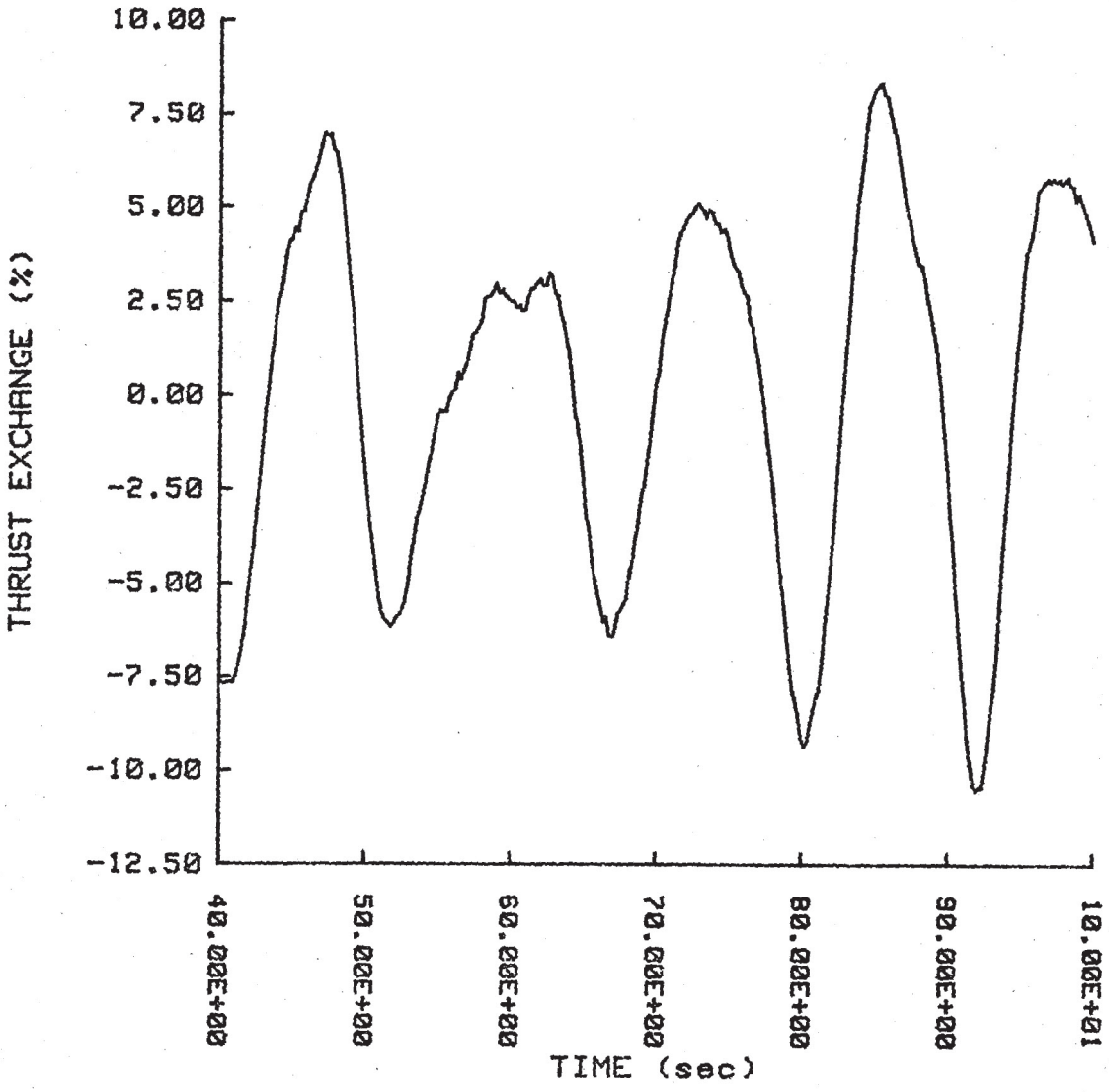

Figure 6.19: Thrust Exchange (ρ=0.3)

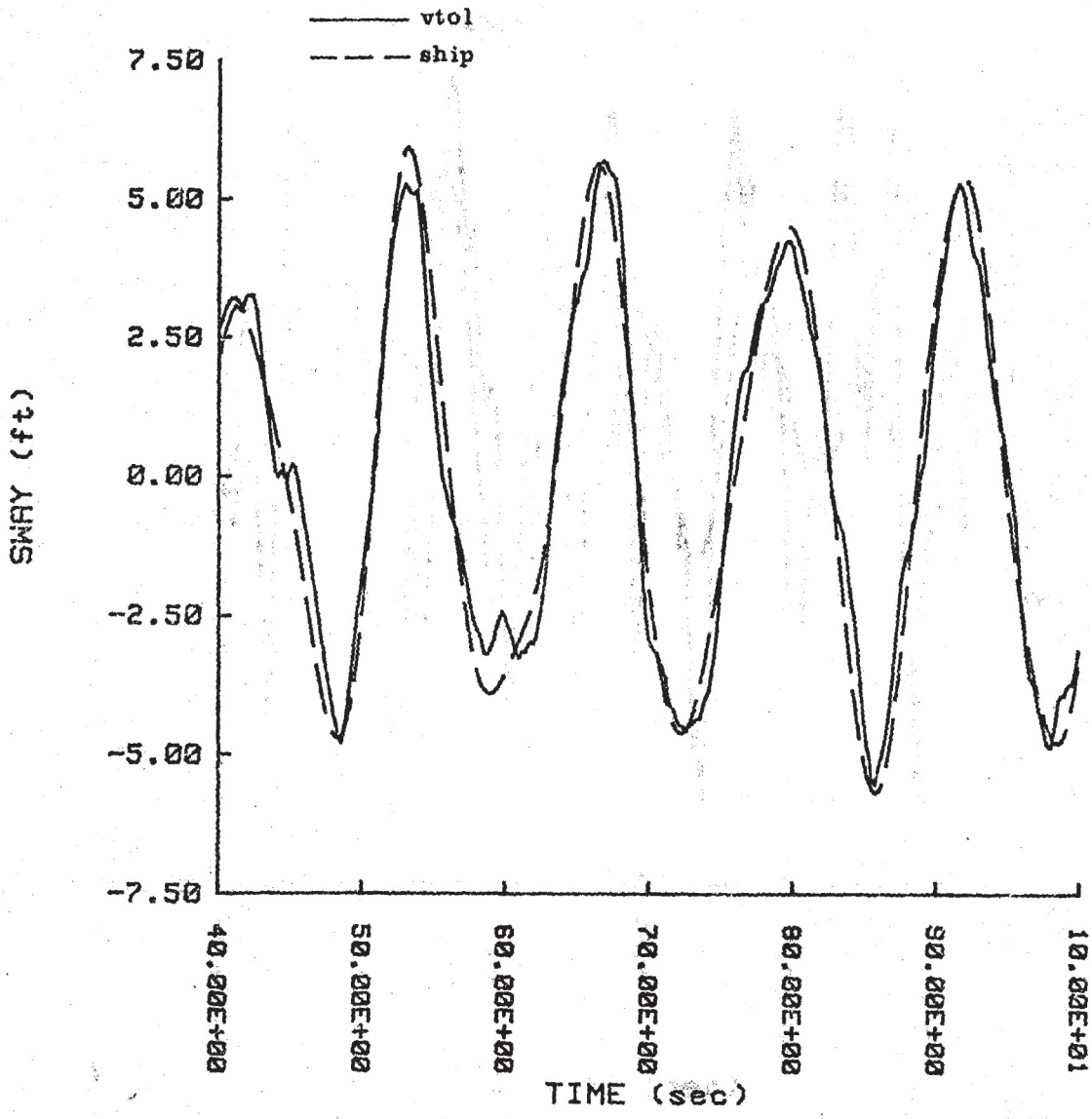

Figure 6.20: Sway Tracking with Wind Disturbances (ρ=0.3)

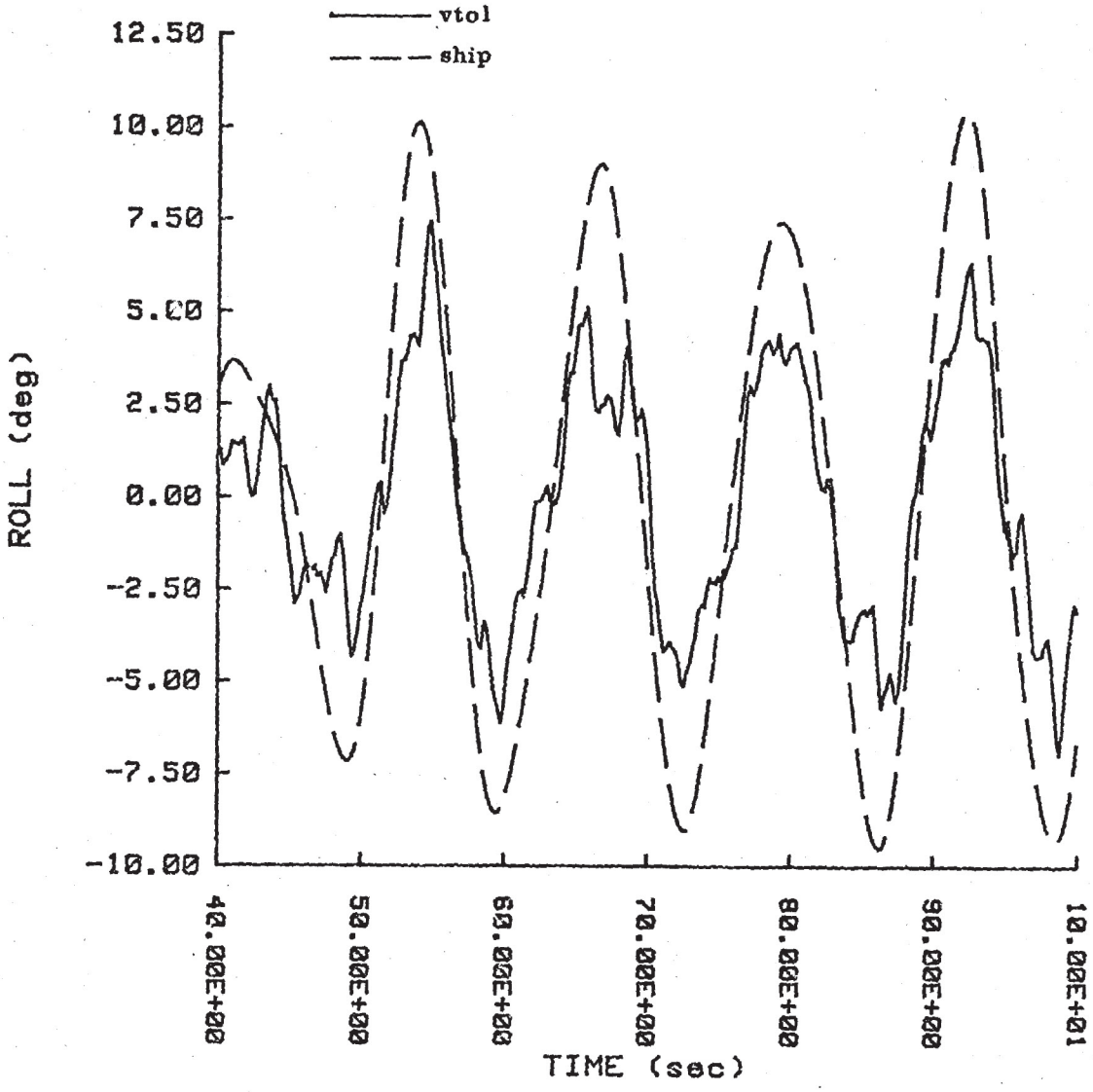

Figure 6.21: Roll Tracking with Wind Disturbances (ρ=0.3)

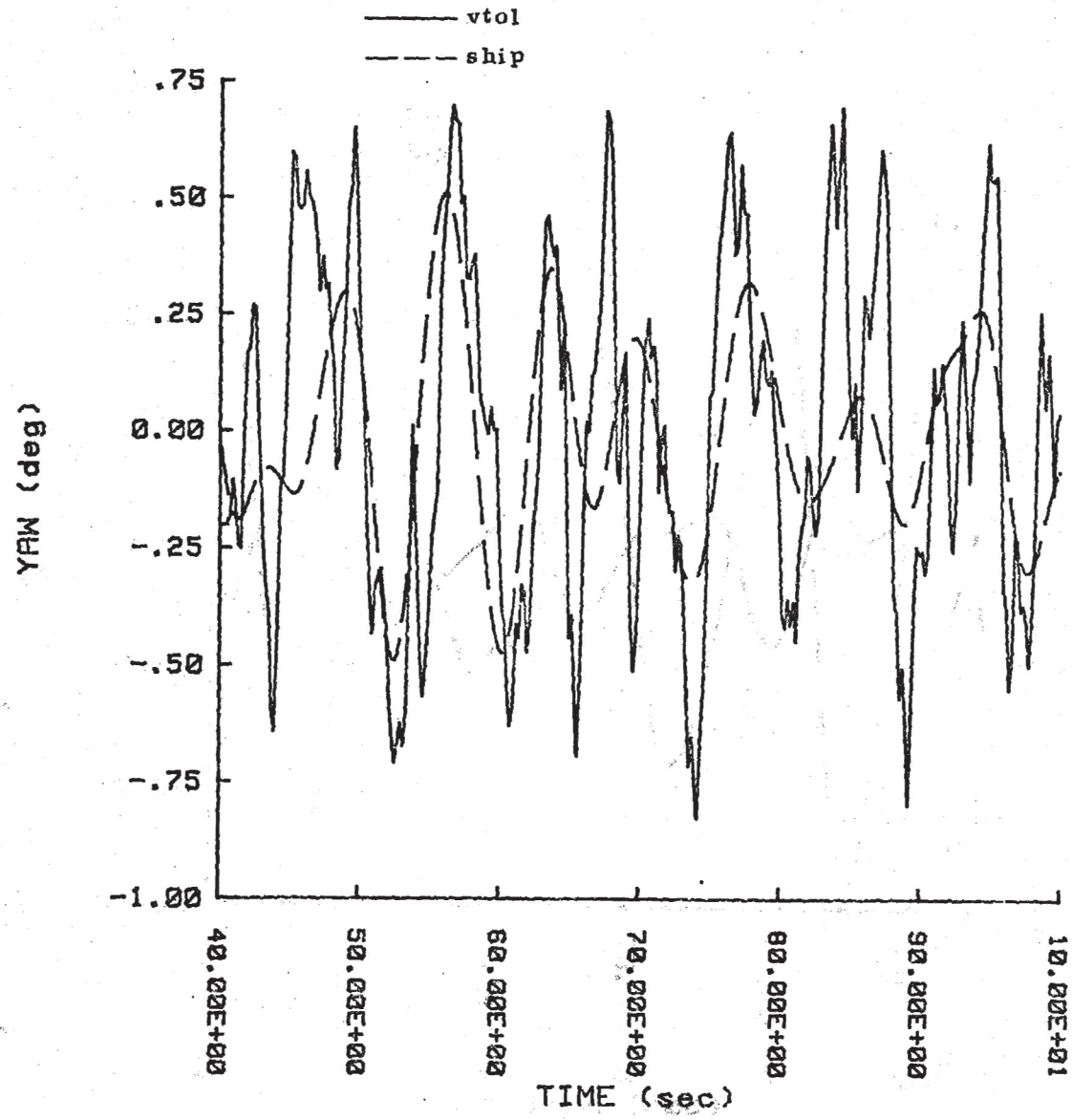

Figure 6.22: Yaw Tracking with Wind Disturbances (ρ=0.3)

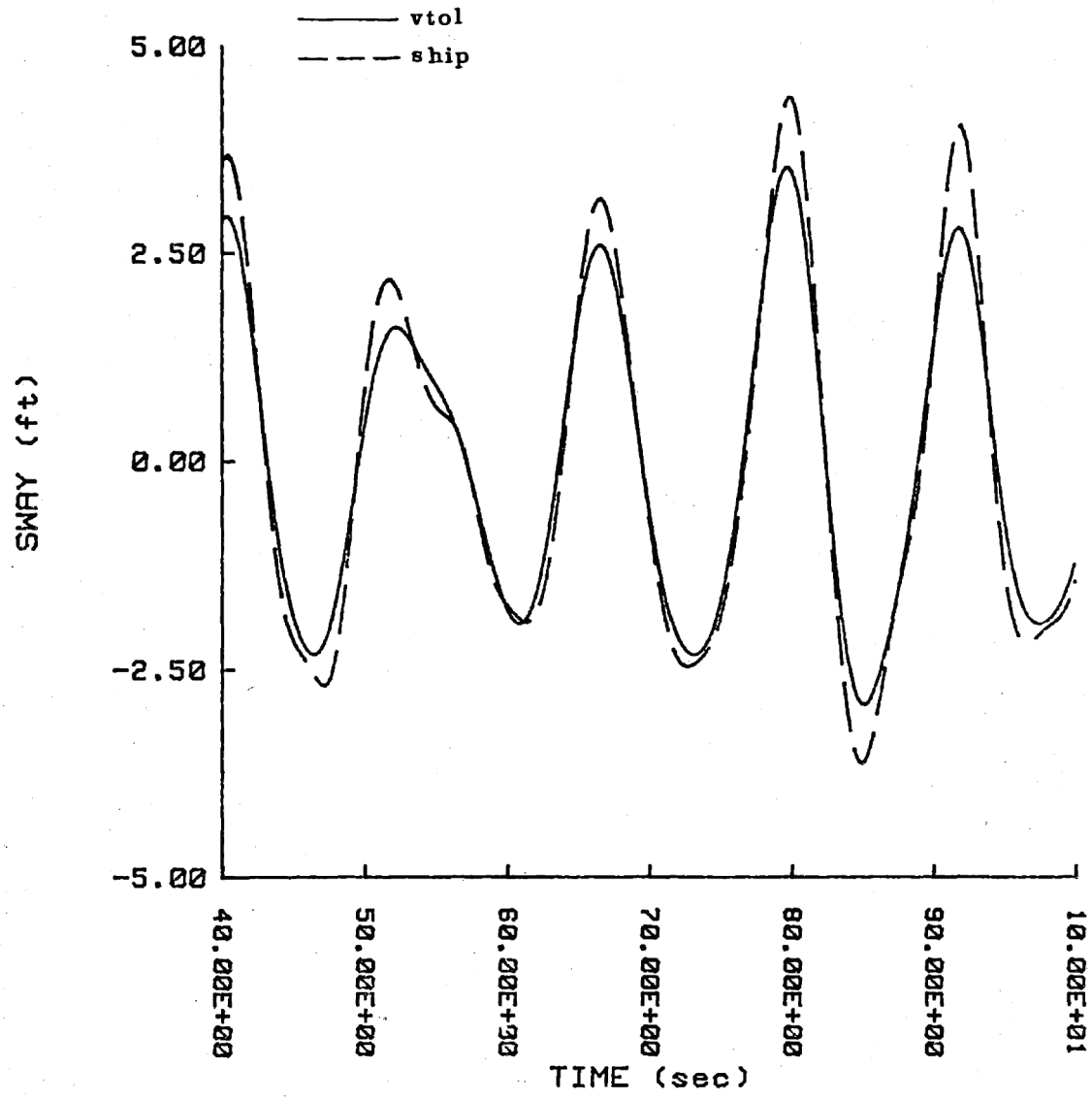

Figure 6.23: Sway Tracking (ρ=30)

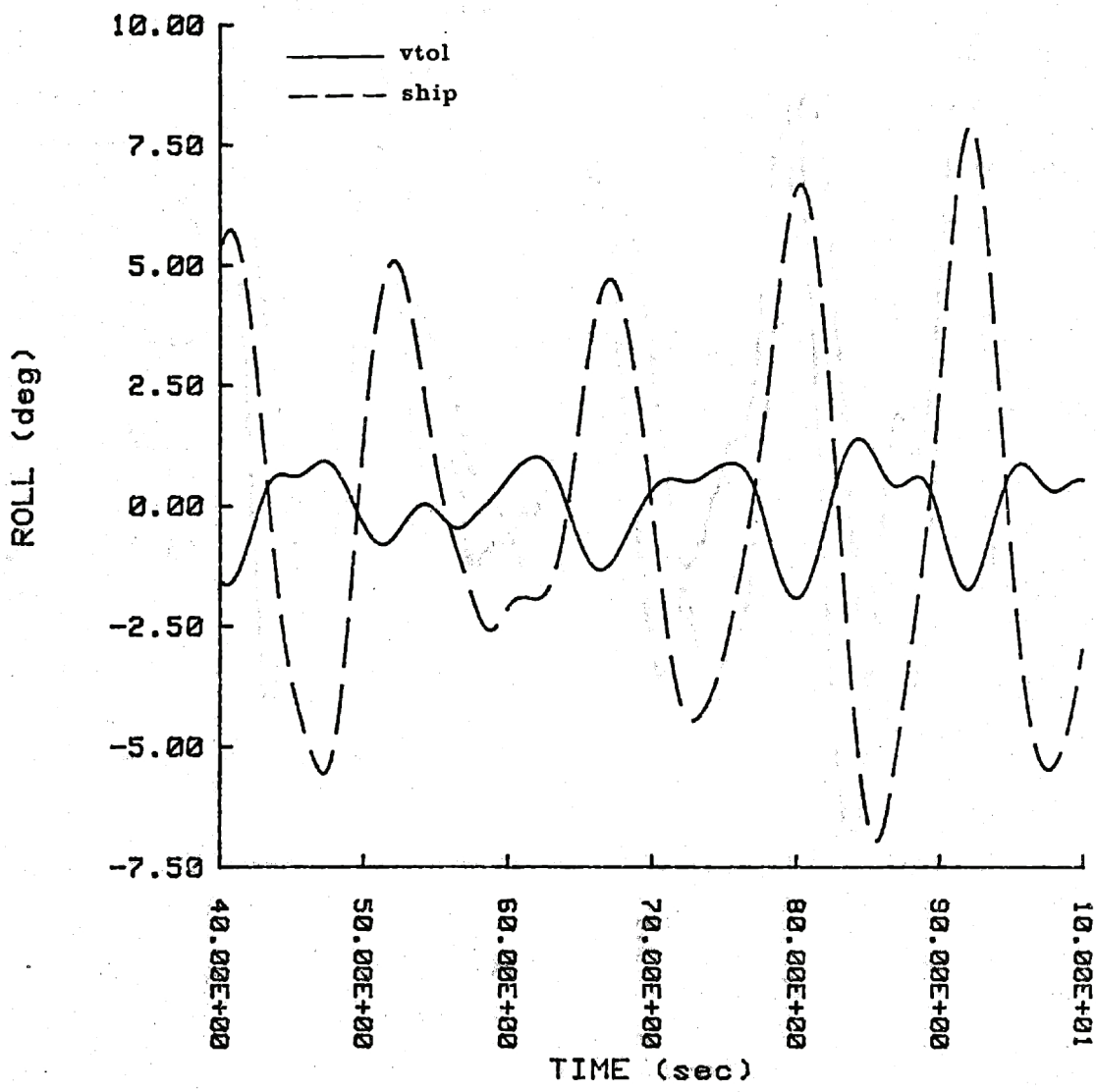

Figure 6.24: Roll Tracking (ρ=30)

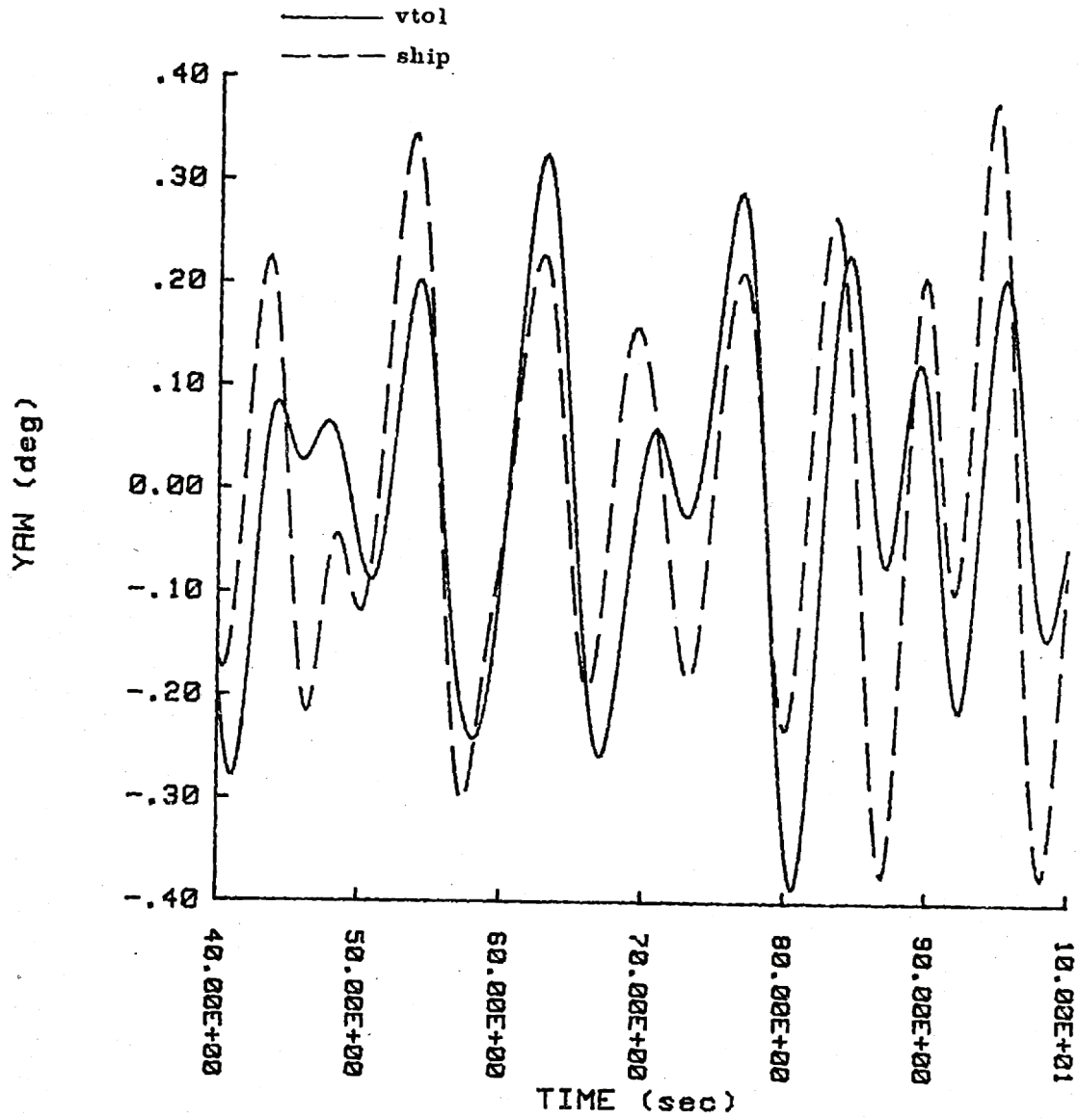

Figure 6.25: Yaw Tracking (ρ=30)

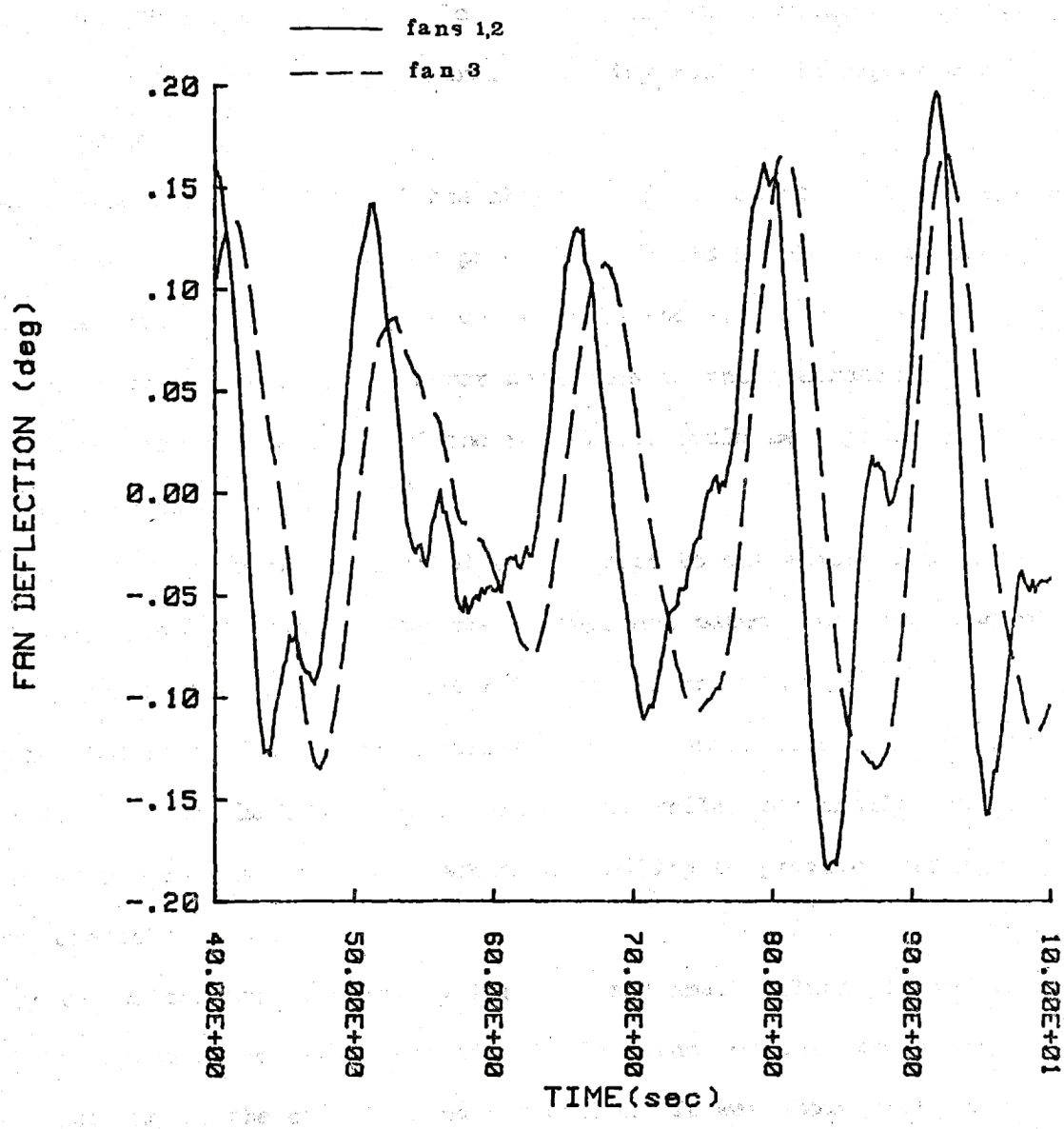

Figure 6.26: Fans Deflection (ρ=30)

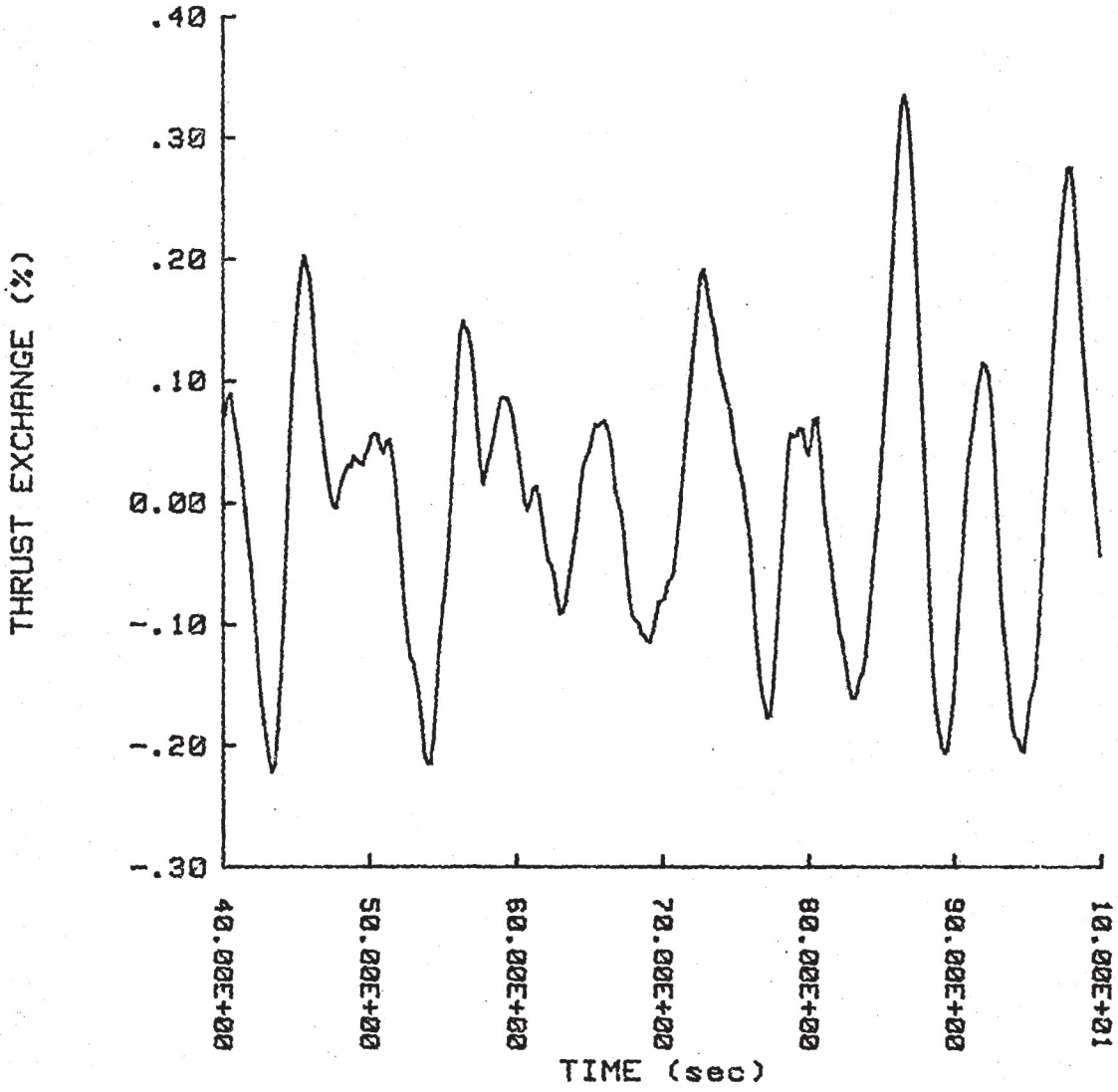

Figure 6.27: Thrust Exchange (ρ=30)

basis of the known dynamics of the aircraft.

For the ship however, a Kalman filter is necessary to reconstruct the states that are not available, and the results indicating the rms tracking errors for a given control authority must be interpreted as lower bounds.

Due to the decoupling of the ship and of the aircraft in the LQG design, the optimal closed-loop poles locus could be plotted independently from the ship motion. It was shown that the root-locus can be shaped by the introduction of velocity error penalties in the quadratic cost, and that some peculiar behavior of the root-locus could be explained on the basis of physical arguments.

The responses of the controlled aircraft to deviations from equilibrium were plotted, and the important couplings between the sway and roll were shown to have a significant influence on the behavior of the controlled aircraft. For high values of the control penalty, the controller appeared to fly the VTOL like a helicopter, while, for smaller values, it used much more the thrust deflection capability to provide lateral accelerations.

The difference in strategy for high and small values of the control penalty appeared to have a significant influence on the errors achieved in the tracking of the ship landing pad motion. It was shown that the controller faced two important contradictory phenemena in the tracking of the roll motion, especially due to the sway motion induced at the landing pad by the roll motion. Although precise roll tracking is not necessary,

the high values that the roll motion can reach in high sea states make imperative the limitation of the tracking errors (to avoid a contact of the wing tip at the landing for example),and the constraints present in the simultaneous tracking of the sway and roll motion are basic limitations in the tracking of the lateral motions.

CHAPTER 7

LINEAR QUADRATIC GAUSSIAN REGULATOR DESIGN

7.1 Introduction

Having designed the linear quadratic regulator, the next step to the final control system is the optimal estimation of the system states. As all the states are not available for feedback, and as those which are measurable are affected by measurement noise, a state estimator is necessary and, in the general assumptions of the LQG methodology, this state estimator is a Kalman filter. The overall control system is then composed of a Kalman filter whose state estimates are multiplied by constant gains, determined as in the LQ problem.

It has been previously indicated that the estimation problem can be reasonably decoupled. The ship motion estimation problem has been addressed in chapter 4, so that this chapter will concentrate on the aircraft motion estimation problem, and on the overall system performance.

7.2 Navigation Systems

The accuracy of the navigation systems used aboard the ship and aboard the aircraft will be a determining factor in the performance obtained in the tracking of the ship motions.

Some previous studies [26], [27], have addressed the navigation problem of VTOL landings on destroyers. An inertial measurement unit aboard the ship provides measurements of the ship motions that are data-linked to the

aircraft (in our configuration, the full ship state, estimated by the ship Kalman filter described in chapter 4, is data-linked to the aircraft). Aboard the aircraft, the combined use of an inertial measurement unit, microwave (scanning beam) landing system, and distance measuring equipment (MLS/DME), leads to estimates of the aircraft position and attitude. The aircraft navigation system considered in [26], [27] is a low to medium quality navigation system, so that even if the whole aircraft state is available for measurement, some improvement can be gained by an aircraft Kalman filter that estimates the aircraft total state using the model for the aircraft dynamics and control effectiveness. This is the subject of section 7.3.

However, it should be noted that with the use of a good quality aircraft inertial measurement unit, much better estimation accuracy can be achieved. The appropriate Kalman filter formulation in this case uses an error state formulation, where the state variables are the very low frequency errors in the indicated position , velocity, and attitude of the inertial system. The radio measurements (MLS/DME) are used to estimate these low frequency errors. The precise structure of such a navigation system is not studied in this thesis, which concentrates on the control aspects of the VTOL landing problem. If the accuracy and response time of the navigation system is such that the aircraft navigation errors and the time lags are negligible, an aircraft Kalman filter, using the known dynamics of the aircraft, is not necessary, and the control loop around the aircraft is equivalent to the LQ control loop. The robustness of the

control system is then the same as the robustness of the LQ system (cf chapter 8), and the degradation in performance, as compared to the LQ controller performance indicated in chapter 6, is due to the ship Kalman filter, and the estimation of the ship states that are not available for measurement. The reduction in performance is small, however, as will be indicated in section 7.4.

7.3 Aircraft Kalman Filter

First, we assume that the aircraft controller has available noisy absolute position and attitude measurements that are used as input of the aircraft Kalman filter. The measurement (output) matrix is then:

$$C_A = \begin{bmatrix} 1 & 0 & 0 & 0 & 0 & 0 \\ 0 & 1 & 0 & 0 & 0 & 0 \\ 0 & 0 & 1 & 0 & 0 & 0 \end{bmatrix} \tag{7.1}$$

From data available in [26] and [27], the intensity matrix of the measurements noise is selected to be:

$$\Theta_A = \begin{bmatrix} 0.286 & 0 & 0 \\ 0 & 0.001 & 0 \\ 0 & 0 & 0.001 \end{bmatrix} \tag{7.2}$$

With this choice of measurement noise, and with the driving noise resulting from the wind turbulence model, the Kalman filter poles are located at: $-0.5743 \pm j\ 0.5593$, $-1.317 \pm j\ 1.104$ and $-1.107 \pm j\ 1.318$.

If measurements of the angular rates and velocities, as well as angles and displacements, are available from the navigation system, a Kalman filter can be designed, assuming the measurement of all the 6 states. The measurement matrix is then the identity matrix:

$$C_A = I \tag{7.3}$$

The measurement noise intensity matrix is selected, using the same references as before, and is equal to:

$$\Theta_A = \begin{bmatrix} 0.286 & 0 & 0 & 0 & 0 & 0 \\ 0 & 0.001 & 0 & 0 & 0 & 0 \\ 0 & 0 & 0.001 & 0 & 0 & 0 \\ 0 & 0 & 0 & 0.286 & 0 & 0 \\ 0 & 0 & 0 & 0 & 0.00024 & 0 \\ 0 & 0 & 0 & 0 & 0 & 0.00024 \end{bmatrix} \tag{7.4}$$

In this case, the closed-loop poles turn out to be at: -0.4981, $-0.5662 \pm j\ 0.5804$, -0.91, -3.92, -4.819.

The first design is referred in the next sections as the 3 measurements case, and the second as the 6 measurements case.

Note that in the situation when the 6 measurements are available, we are very close to the full state feedback. The role of the Kalman filter is not to reconstruct the unavailable states, as it was the case for the ship Kalman filter for example. In this case, its role is to provide optimal estimates of the states from noisy measurements, using the known

dynamics of the aircraft: it is actually nothing else than a filter. In the closed-loop system, its role is to filter the noise and so, it decreases the bandwidth of the system. The consequence is, theoretically (i.e. in the assumption of white measurement noise), an increased performance compared to the full (noisy) state feedback, at the expenses however of robustness, as will be seen in the next chapter.

7.4 LQG Controller Performance

The evaluation of the controller performance can be done as for the LQ controller in chapter 6, by computing the rms values of the tracking errors and of the controls.

To determine the rms values of the states (ship, aircraft, and Kalman filter states), we write the overall system equations:

$$\begin{bmatrix} \dot{\underline{x}} \\ \dot{\hat{\underline{x}}} \end{bmatrix} = A' \cdot \begin{bmatrix} \underline{x} \\ \hat{\underline{x}} \end{bmatrix} + \begin{bmatrix} \underline{\xi} \\ H\underline{\theta} \end{bmatrix} \tag{7.5}$$

where:

$$A' = \begin{bmatrix} A & -BG \\ HC & A-BG-HC \end{bmatrix} \tag{7.6}$$

The overall state covariance matrix is obtained by solving the Lyapunov equation:

$$A'^{T}P + PA' + \Xi' = 0 \tag{7.7}$$

with:

$$\Xi' = \begin{bmatrix} \Xi & 0 \\ 0 & H\Theta H^T \end{bmatrix} \tag{7.8}$$

and:

$$P = \begin{bmatrix} E(\underline{x}\underline{x}^T) & E(\underline{x}\underline{\hat{x}}^T) \\ E(\underline{\hat{x}}\underline{x}^T) & E(\underline{\hat{x}}\underline{\hat{x}}^T) \end{bmatrix} \tag{7.9}$$

The rms values of the tracking errors and controls are the square roots of the diagonal elements of:

$$E(\underline{w}_{A-S}\underline{w}_{A-S}^T) = W_{A-S}\ E(\underline{x}\underline{x}^T)\ W_{A-S}^T \tag{7.10}$$

and:

$$E(\underline{c}\underline{c}^T) = T_c\ G\ E(\underline{\hat{x}}\underline{\hat{x}}^T)\ G^T\ T_c^T \tag{7.11}$$

respectively.

Tables 7.1 and 7.2 show the results obtained for the rms tracking errors and controls. In the case when the aircraft navigation system is of quality such that the navigation errors are negligible, the aircraft total state Kalman filter is not necessary. The ship Kalman filter is still required as a state reconstructor. The degradation in the tracking errors (compared with the unrealizable full ship and aircraft state feedback case) is then very small, while the rms controls required are

SEA H=12ft ω_m=0.4807rad/s						
Rms Tracking Errors and Controls	Sway (ft)	Roll (deg)	Yaw (deg)	$\delta\alpha_{1,2}$ (deg)	$\delta T_{1,2}$ (%)	$\delta\alpha_3$ (deg)
LQ (1)	0.801	6.410	0.329	9.72	16.70	9.37
LQG (2)	0.913	6.432	0.341	9.71	16.73	9.36
LQG (3)	2.312	7.249	2.547	11.39	23.61	10.42
LQG (4)	1.401	6.567	1.499	10.10	18.13	9.61

(1), (2), (3), and (4) see below

Table 7.1: LQG Controller Performance (decaying sea)

SEA H=10ft ω_m=0.72rad/s						
Rms Tracking Errors and Controls	Sway (ft)	Roll (deg)	Yaw (deg)	$\delta\alpha_{1,2}$ (deg)	$\delta T_{1,2}$ (%)	$\delta\alpha_3$ (deg)
LQ (1)	0.691	2.480	0.317	4.72	8.78	3.92
LQG (2)	0.812	2.529	0.328	4.70	8.76	3.89
LQG (3)	2.274	4.193	2.545	7.60	18.82	6.01
LQG (4)	1.338	2.856	1.496	5.45	11.19	4.47

(1) : LQ Controller, with wind disturbances
(2) : LQG Controller, with only the ship Kalman filter
(3) : LQG Controller, 3 measurements case
(4) : LQG Controller, 6 measurements case

Table 7.2: LQG Controller Performance (fully developed sea)

sometimes smaller, due to the decrease in bandwidth caused by the ship Kalman filter.

When the aircraft navigation system is of lower quality, and an aircraft total state Kalman filter is used, along with the ship Kalman filter, the degradation in performance is more serious, but still reasonable in the 6 measurements case.

7.5 Summary

In this chapter, we considered the optimal estimation of the aircraft states from noisy measurements. Two cases were considered: the first corresponded to measurements of position and attitude only, the second to measurements of position, attitude, and their derivatives (full state measurement). The second case is considered the nominal one.

The degradation in performance due to the estimation of the ship states and of the aircraft states from noisy measurements was indicated. It was shown to be very small if only the ship states had to be estimated, and reasonable in the case of the noisy measurement of the full aircraft state vector.

CHAPTER 8

ROBUSTNESS ANALYSIS

8.1 Introduction

The robustness of a feedback system to modelling errors (parameter uncertainty, unmodelled dynamics, neglected couplings ...) is certainly as important as the stability of the nominal closed-loop system. It is fundamental for aerospace applications in which, very often, the nominal open-loop system is unstable. While the open-loop system is an optimally robust system when it is stable, the existence of an optimally robust closed-loop system can be conceived in the case when the open-loop system is unstable.

Although the issues of robustness are well understood, and easily expressed for single-input single-output systems, they are much more complex for multiple-input multiple-output systems. Much research has been done recently in this area, showing mainly the usefulness of singular values to quantify robustness properties of multiple-input multiple-output feedback systems. In this thesis, we will mainly refer to the results found in [23], [24], [28].

8.2 Robustness Measures

8.2.1 Single-Input Single-Output (SISO) Case

The stability of SISO feedback systems can be determined by the use of the Nyquist diagram. The Nyquist contour D_R is defined as two segments

of the positive and negative imaginary axis, connected by a half circle whose radius R is, to the limit, taken to be infinite, so that the whole right half plane is then included in the contour. The Nyquist contour transformed by the complex function g(s) (the open-loop transfer function) is then plotted in the complex plane. The closed-loop system is guaranteed to be stable if the number of counterclockwise encirclements of the (-1,0) point is equal to the number of open-loop unstable poles.

Robustness is easily measured by the distance from the transformed contour to the (-1,0) point. It is usually expressed in gain and phase margins. They indicate what minimal multiplicative perturbation (constant gain or phase shift) would make the Nyquist diagram pass through the (-1,0) point. This would be at the limit to change the number of encirclements, and, consequently, the stability of the closed-loop system.

8.2.2 Multiple-Input Multiple-Output (MIMO) Case

The stability of MIMO feedback systems can be determined in a very similar manner by a Nyquist diagram. The transfer function to be plotted on the Nyquist diagram is now (-1 + det(I+G(s))) where G(s) is the open-loop transfer matrix. The same criterion can then be used.

We note immediately however that det(I + kG(s)) is different from 1+kdet(G(s)). This indicates already that no stability margins can be found from the MIMO Nyquist diagram, as in the SISO case.

Very often, separate loop-by-loop stability margins, similar to the ones used in SISO systems, are considered indicative of the overall system

robustness. They are however clearly insufficient. Perturbations are not likely to occur separately, and simultaneous perturbations in different channels may be much more dangerous for the stability than separate perturbations. The importance of possible cross-channel disturbances has also to be evaluated, and is not reflected by a single loop-by-loop robustness analysis. Consequently, going back to the SISO case, with a single loop-by-loop analysis is not a satisfactory way to study the robustness of MIMO feedback systems.

Unfortunately, the distance from the (-1,0) point to the Nyquist contour transformed by (-1+det(I+G(s))) - which is the same as the distance from det(I+G(s)) to 0 - is not a reliable measure of robustness. In fact, numerical analysts have long recognized that the specific value of the determinant of a matrix is a poor measure of the nearness of this matrix to singularity (or rank deficiency). In other words, det(I+G(s)) can be large, although a small additive perturbation E can make det(I+G(s)+E) equal to zero.

8.2.3 Singular Values

These shortcomings can be avoided by the use of singular values. The singular values of a complex matrix A are defined as the square roots of the eigenvalues of the matrix $A^H A$ (A^H is the complex conjugate transpose of A), i.e.:

$$\sigma_i(A) = \lambda_i^{\frac{1}{2}}(A^H A) \tag{8.1}$$

The maximum singular value of a matrix A is indicative of its "size", as it is equal to the spectral norm of the matrix A:

$$\sigma_{max}(A) = \| A \|_2 = \max_{\underline{x} \neq 0} \frac{\| A\underline{x} \|_2}{\| \underline{x} \|_2} \tag{8.2}$$

where:

$$\| \underline{x} \|_2 = \sqrt{\Sigma x_i^2} \tag{8.3}$$

The minimum singular value of a matrix A is indicative of its nearness to singularity. If $\sigma_{min}=\alpha$, there exists a perturbation E such that $\sigma_{max}(E)=\alpha$ and $\det(A+E)=0$. Moreover, no matrix E such that $\sigma_{max}(E)<\alpha$ will make A+E singular. The minimum singular value is then an indication of the minimal "size" of the additive perturbation required to bring the matrix A to singularity.

An advantage of the use of singular values is that it also allows to compute the minimal perturbation E through the singular values decomposition. If U and V are matrices containing the unit eigenvectors of AA^H and A^HA (known as left and right singular vectors of the matrix A), and if Σ is a diagonal matrix containing the singular values of A, then A can be decomposed as:

$$A = U \Sigma V^H \tag{8.4}$$

And the matrix E can be decomposed as:

$$E = U \cdot \begin{bmatrix} P_S & 0 \\ 0 & -\sigma_n \end{bmatrix} \cdot V^H \qquad (8.5)$$

where P_S is any n-1 x n-1 matrix such that $\| P_S \|_2 \leq \sigma_n$ and where it is assumed that the singular values have been ordered so that $\sigma_n = \sigma_{min}(A)$. Without loss of generality, one can select $P_S=0$, so that:

$$E = -\sigma_n u_n v_n^H \qquad (8.6)$$

8.2.4 Robustness of MIMO Systems

The robustness of MIMO systems is defined by the size of the minimal perturbation E that brings the closed-loop system at the limit of instability. Then, the return difference matrix $I+\tilde{G}(s)$ (where $\tilde{G}(s)$ is the perturbed open-loop transfer matrix) is singular for some s on the Nyquist contour.

Different structures of perturbation can be imagined, for example, an additive perturbation:

$$\tilde{G} = G + E \qquad (8.7)$$

or a multiplicative perturbation:

$$\tilde{G} = G\,(1+E) = G.L \qquad (8.8)$$

In the first case, the closed-loop system stability is guaranteed if:

$$\sigma_{min}(I+G(s)) > \sigma_{max}(E) \tag{8.9}$$

In the second case, if:

$$\sigma_{min}(I+G^{-1}(s)) > \sigma_{max}(E) \tag{8.10}$$

Other structure of errors have been analyzed in [23] and showed the use of $\sigma_{min}((I+G)(I-G)^{-1})$ for some type of perturbations.

As in the SISO case, the transfer matrices go to zero as $s \to \infty$, so that the only important of the Nyquist contour is the imaginary axis, and s can be replaced by $j\omega$ in the previous formulas.

8.2.5 Guaranteed Gain and Phase Margins

Guaranteed gain and phase margins can also be obtained from the minimum singular values. Although only diagonal perturbations are considered here, they are not limited to the case when only one channel is perturbed at a time. At the contrary, simultaneous gain or phase changes in all channels together are considered. The results presented here can be found in [23]. The gain and phase margins obtained are guaranteed (or conservative) margins. In other words, the gains (or phases) in all channels can be changed simultaneously within the limits indicated by the gain (phase) margins without causing instability, but it is not necessarily possible to find some perturbation of this amplitude that will cause instability (at the contrary of the previous case where a general type of perturbation was considered).

For the different type of errors considered in [23], the guaranteed gain and phase margins are:

$$\sigma_{min}(I+G) > \alpha \rightarrow GM \supset \left(\frac{1}{1-\alpha}, \frac{1}{1+\alpha}\right) \tag{8.11}$$

$$PM \supset \left(-2\sin^{-1}\frac{\alpha}{2}, 2\sin^{-1}\frac{\alpha}{2}\right) \tag{8.12}$$

$$\sigma_{min}(I+G^{-1}) > \alpha \rightarrow GM \supset (1-\alpha, 1+\alpha) \tag{8.13}$$

$$PM \supset \left(-2\sin^{-1}\frac{\alpha}{2}, 2\sin^{-1}\frac{\alpha}{2}\right) \tag{8.14}$$

$$\sigma_{min}((I+G)(I-G)^{-1}) > \alpha \rightarrow GM \supset \left(\frac{1-\alpha}{1+\alpha}, \frac{1+\alpha}{1-\alpha}\right) \tag{8.15}$$

$$PM \supset (-2\tan^{-1}\alpha, 2\tan^{-1}\alpha) \tag{8.16}$$

8.3 VTOL Control System Robustness

8.3.1 Introduction

The robustness results summarized above are applied to the LQ and LQG control system designs of chapter 6 and chapter 7. Note that the computation of singular values of transfer matrices can be done quite rapidly, by the use of efficient algorithms [29], [30], [31].

For the LQ design, we have:

$$\dot{\underline{x}} = A\underline{x} + B\underline{u} \tag{8.17}$$

$$\underline{u} = -G\underline{x} \tag{8.18}$$

The open-loop transfer matrix is:

$$G(j\omega) = G\ (j\omega I - A)^{-1}\ B \tag{8.19}$$

We can also consider the transfer matrix:

$$G'(j\omega) = R^{\frac{1}{2}}\ G(j\omega)\ R^{-\frac{1}{2}} \tag{8.20}$$

which is equivalent to consider a normalized transfer matrix (normalized by the weights attributed to each control in the R matrix).

The Kalman inequality is:

$$(I+G'(j\omega)^{H}\ (I+G'(j\omega)) \geq I \tag{8.21}$$

This guarantees that:

$$\sigma_{min}(I+G'(j\omega)) \geq 1 \tag{8.22}$$

and then:

$$GM \supset (1/2,\ \infty) \tag{8.23}$$

$$PM \supset (-60deg, 60deg) \tag{8.24}$$

As:

$$\sigma_{min}(I+G') + 1 \geq \sigma_{min}(I+G'^{-1}) \tag{8.25}$$

This also implies that:

$$\sigma_{min}(I+G'^{-1}(j\omega)) \geq 1/2 \tag{8.26}$$

For the LQG design, we have:

$$\dot{\underline{x}} = A\underline{x} + B\underline{u} \tag{8.27}$$

$$\underline{u} = -G\hat{\underline{x}} \tag{8.28}$$

$$\dot{\hat{\underline{x}}} = (A-BG)\hat{\underline{x}} + H(\underline{y}-C\underline{x}) \tag{8.29}$$

$$\underline{y} = C\underline{x} \tag{8.30}$$

so that:

$$G(j\omega) = (0 \quad G)\cdot\left[j\omega I - \begin{bmatrix} A & 0 \\ HC & A-BG-HC \end{bmatrix}\right]^{-1} \cdot \begin{bmatrix} B \\ 0 \end{bmatrix} \tag{8.31}$$

Again, to have some normalization of the transfer matrix, the matrix:

$$G'(j\omega) = R^{\frac{1}{2}}\, G(j\omega)\, R^{-\frac{1}{2}} \tag{8.32}$$

can be used. In the LQG case, there is no inequality as (8.22), (8.26), and, consequently, no guarantee on the robustness of the closed-loop system.

In the next subsections, the minimum singular values of the loop transfer matrices for the LQ and LQG designs are indicated. To provide some normalization, the loop transfer matrices considered are those given by (8.20),(8.32) (note that the parameter ρ has no influence in this normalization).

8.3.2 LQ Minimum Singular Values

The minimum singular values of the LQ design are shown in Figures 8.1, 8.2, and 8.3. It is easily checked that $\sigma_{min}(I+G^{-1}) \geq 1/2$ and $\sigma_{min}(I+G) \geq 1$.

It is interesting to note that the minimum over ω of the minimum singular value (for any perturbation criterion) is smaller for $\rho = 30$ than for $\rho = 0.3$. In other words, the closed-loop system with higher loop gains is more robust than the others. This is probably due to the instability of the open-loop system.

8.3.3 LQG Minimum Singular Values

The minimum singular values of the LQG design with 3 measurements (aircraft position and attitude) are illustrated in Figures 8.4, 8.5, and 8.6. For the 6 measurements case (motions and derivatives), the values are shown in Figures 8.7, 8.8, and 8.9.

The first conclusion is that the robustness is seriously degraded when only position measurements are available. The estimation of positions and velocities from noisy measurements of positions only does not only result in degraded performance, as indicated previously (tables 7.1 and 7.2), but also in reduced stability margins.

The robustness is improved when the 6 measurements are used in the Kalman filter. However, the minimum singular values drop significantly for very low frequency in the nominal case $\rho=0.3$.

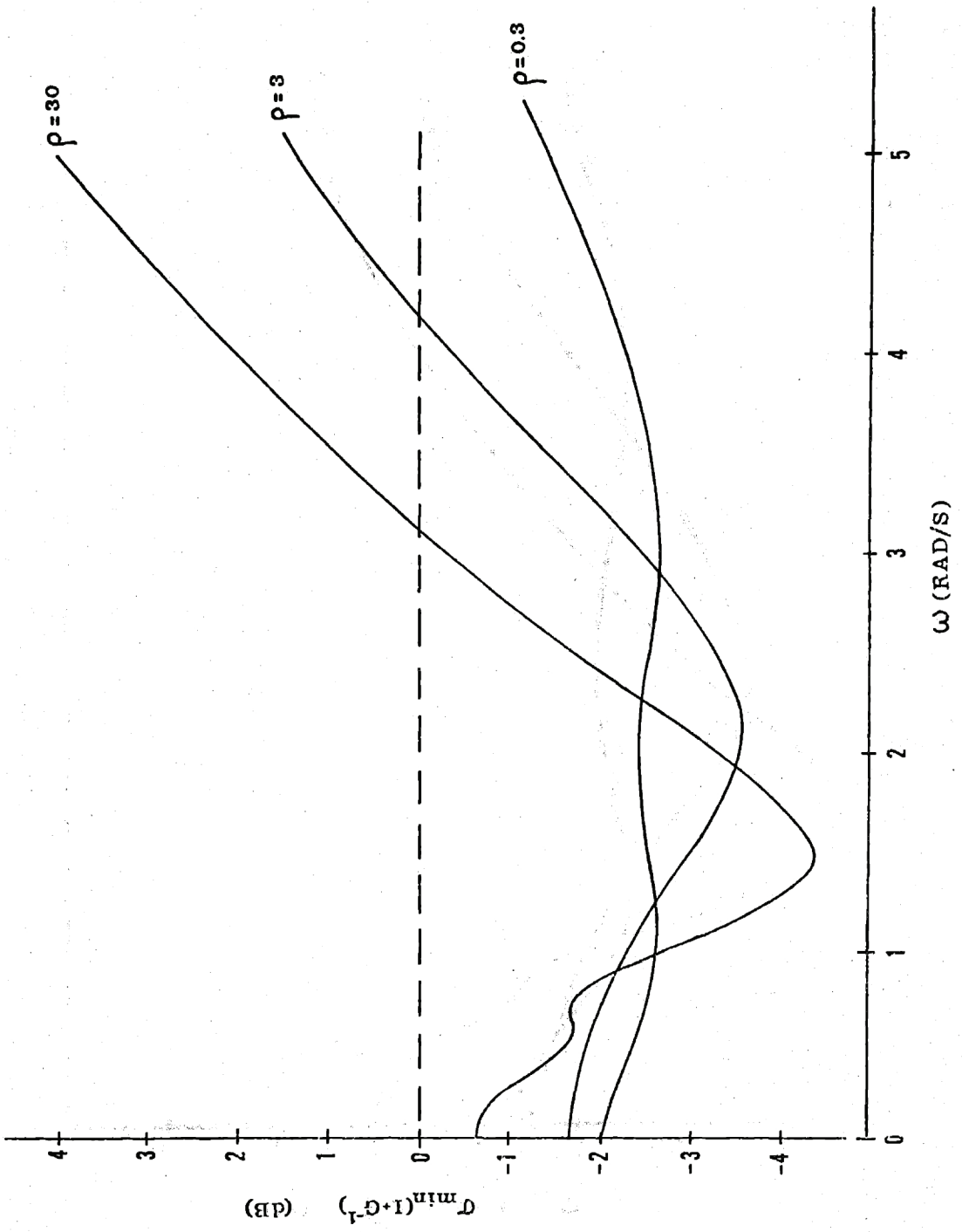

Figure 8.1: LQ Minimum Singular Values

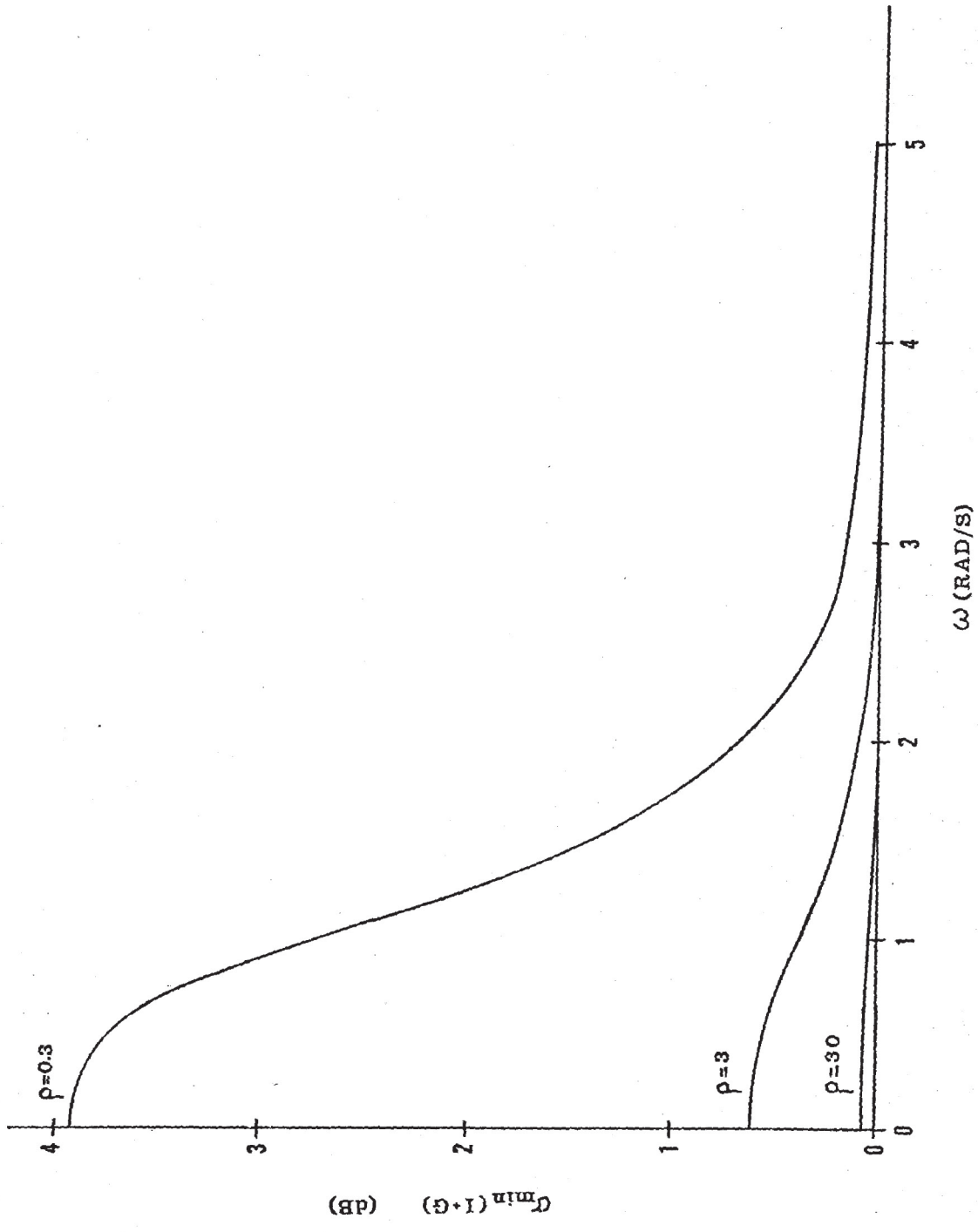

Figure 8.2: LQ Minimum Singular Values

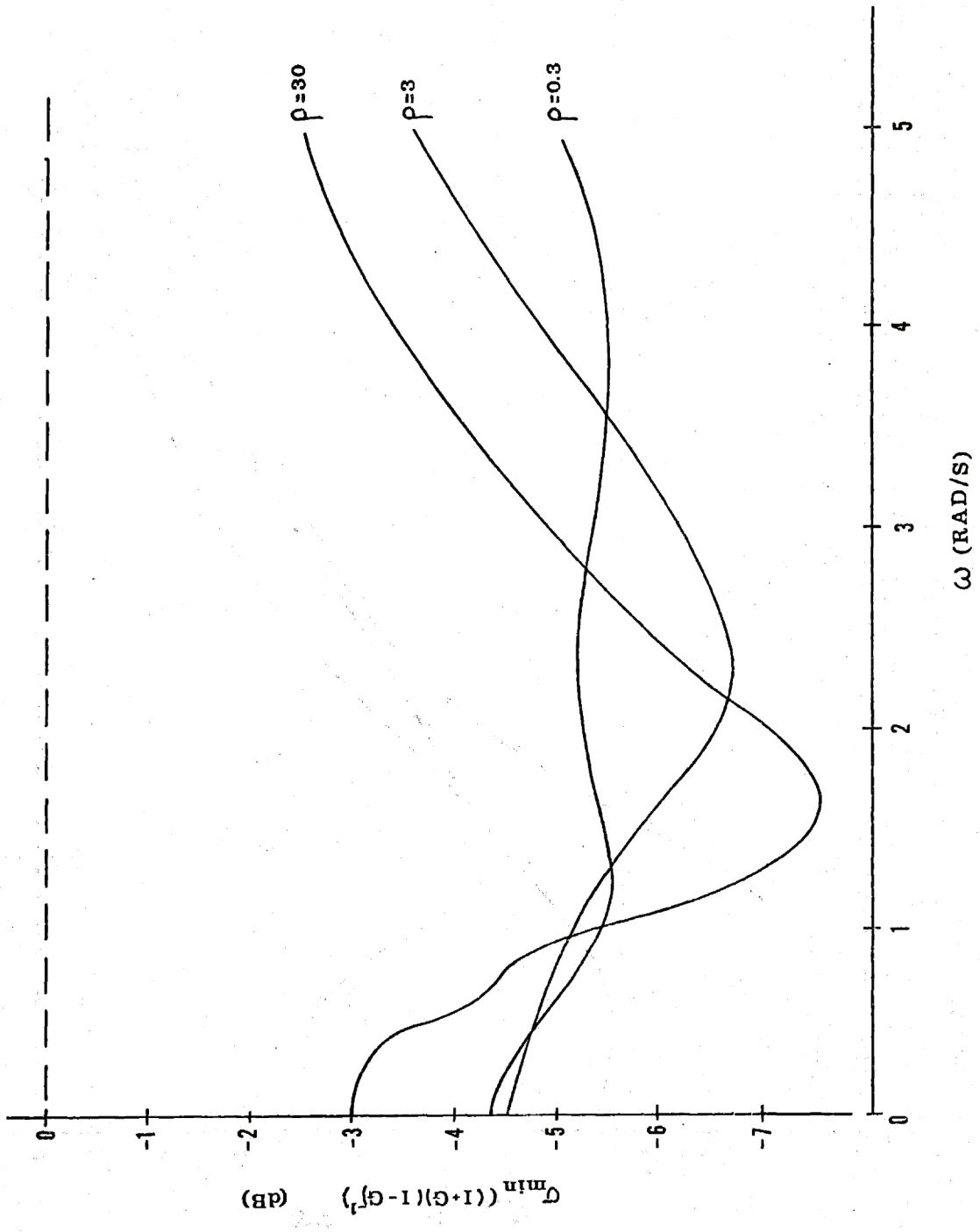

Figure 8.3: LQ Minimum Singular Values

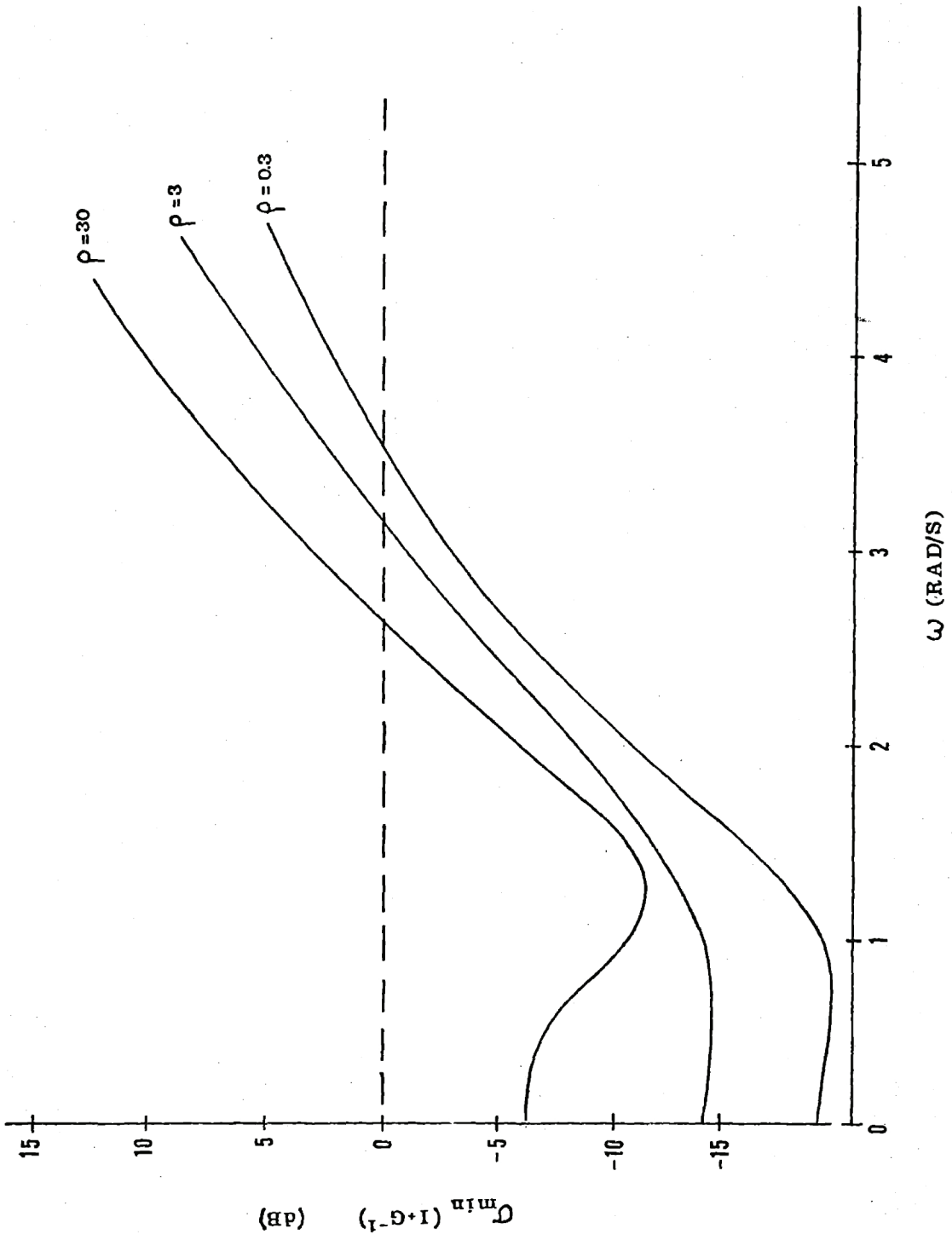

Figure 8.4: LQG Minimum Singular Values (3 measurements case)

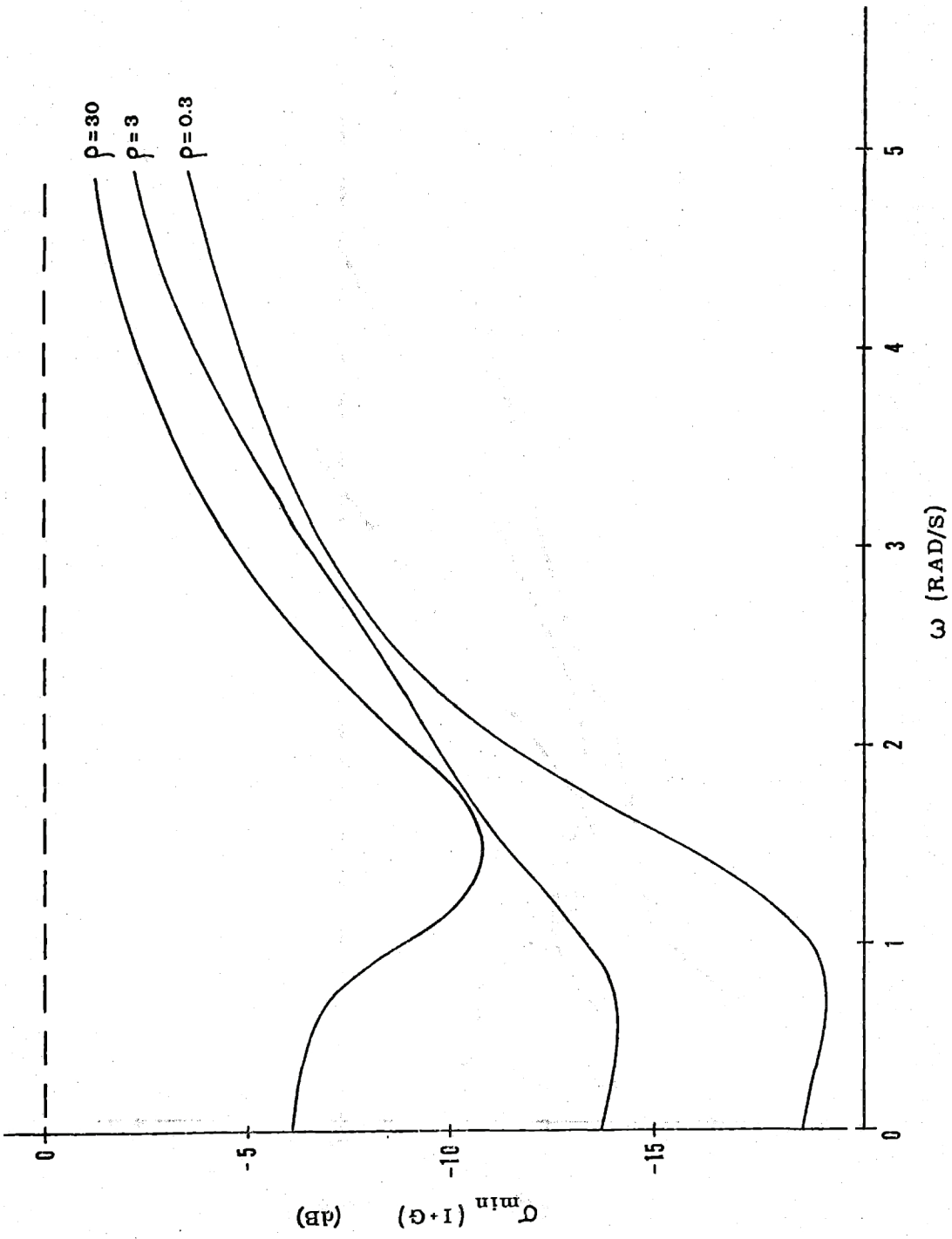

Figure 8.5: LQG Minimum Singular Values (3 measurements case)

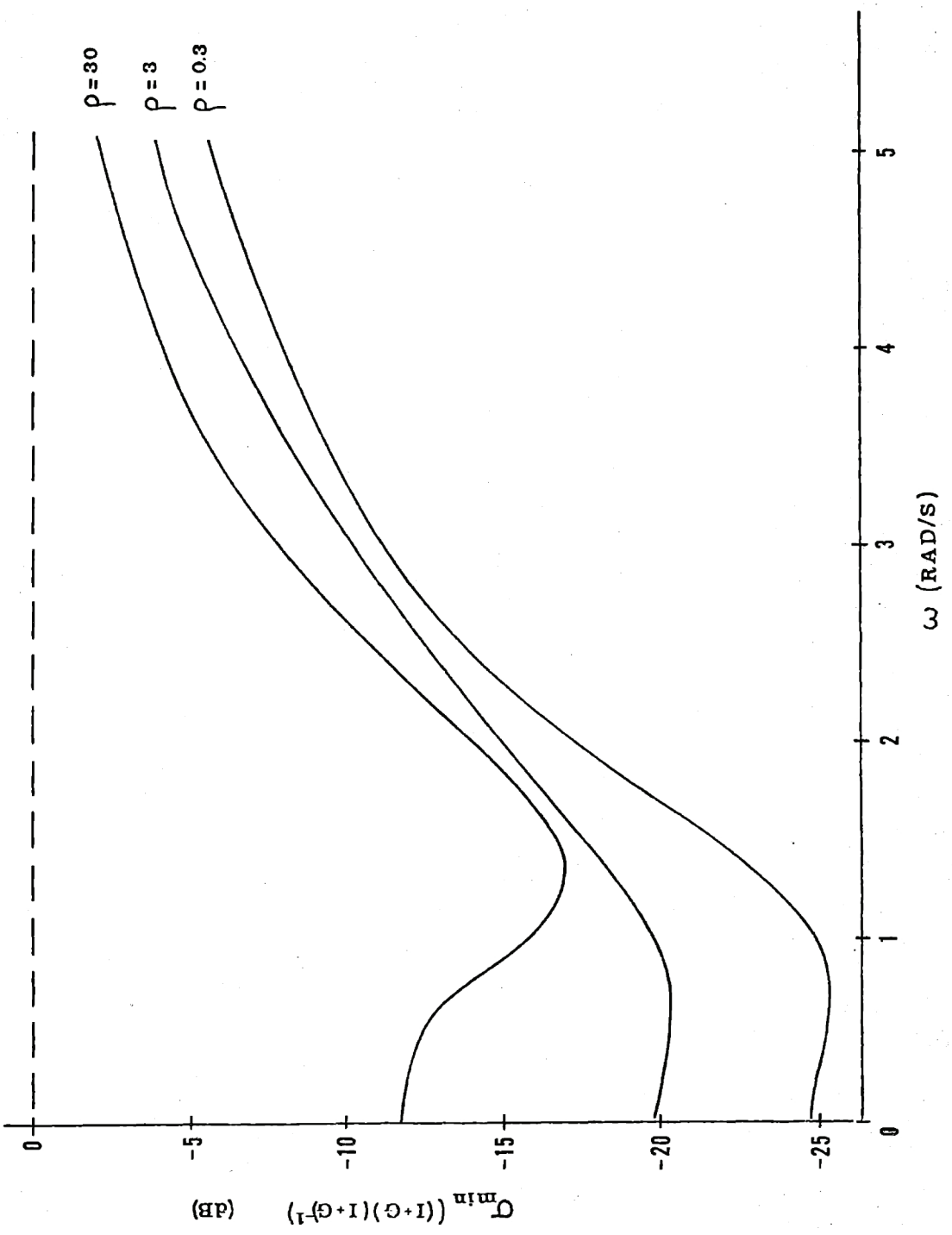

Figure 8.6: LQG Minimum Singular Values (3 measurements case)

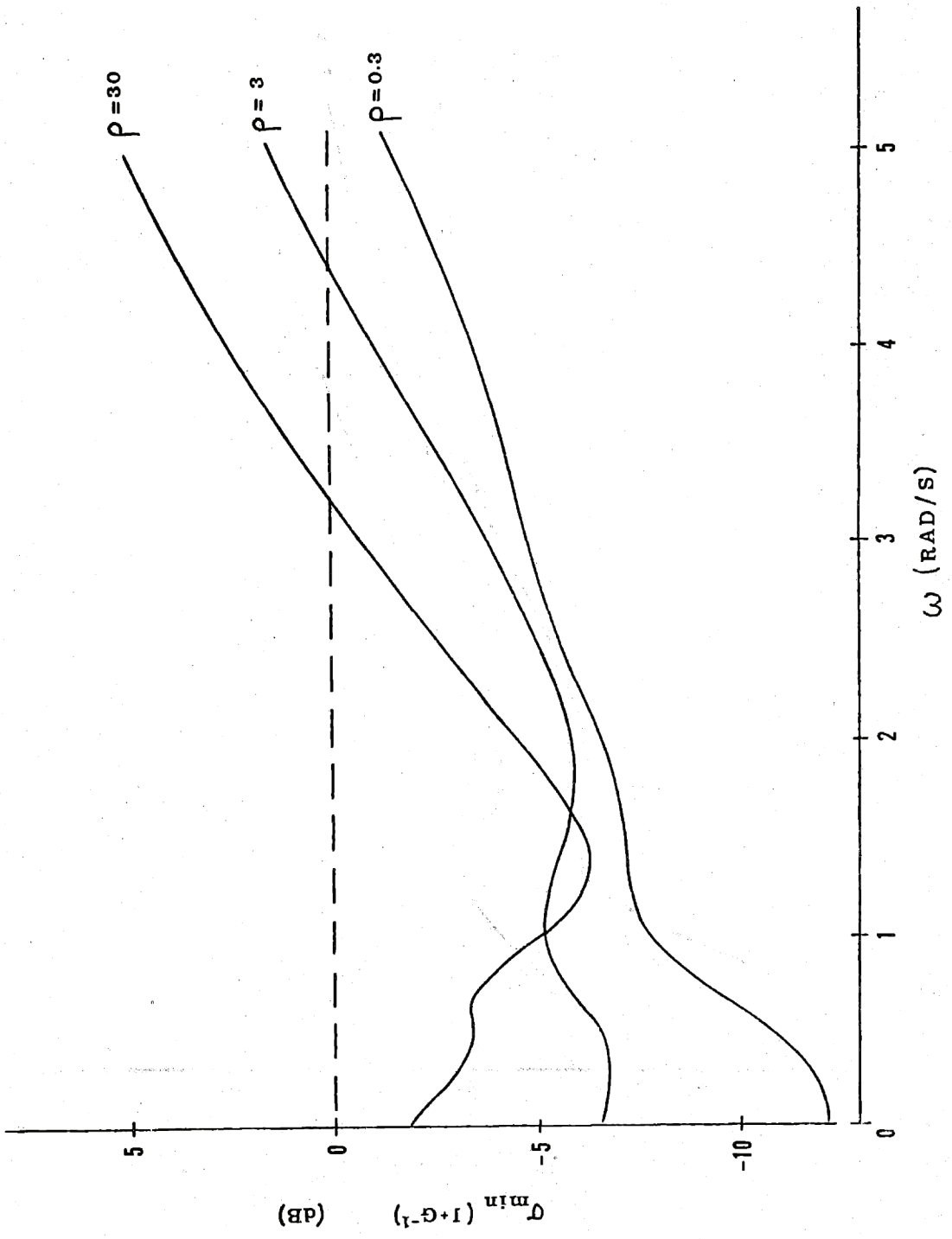

Figure 8.7: LQG Minimum Singular Values (6 measurements case)

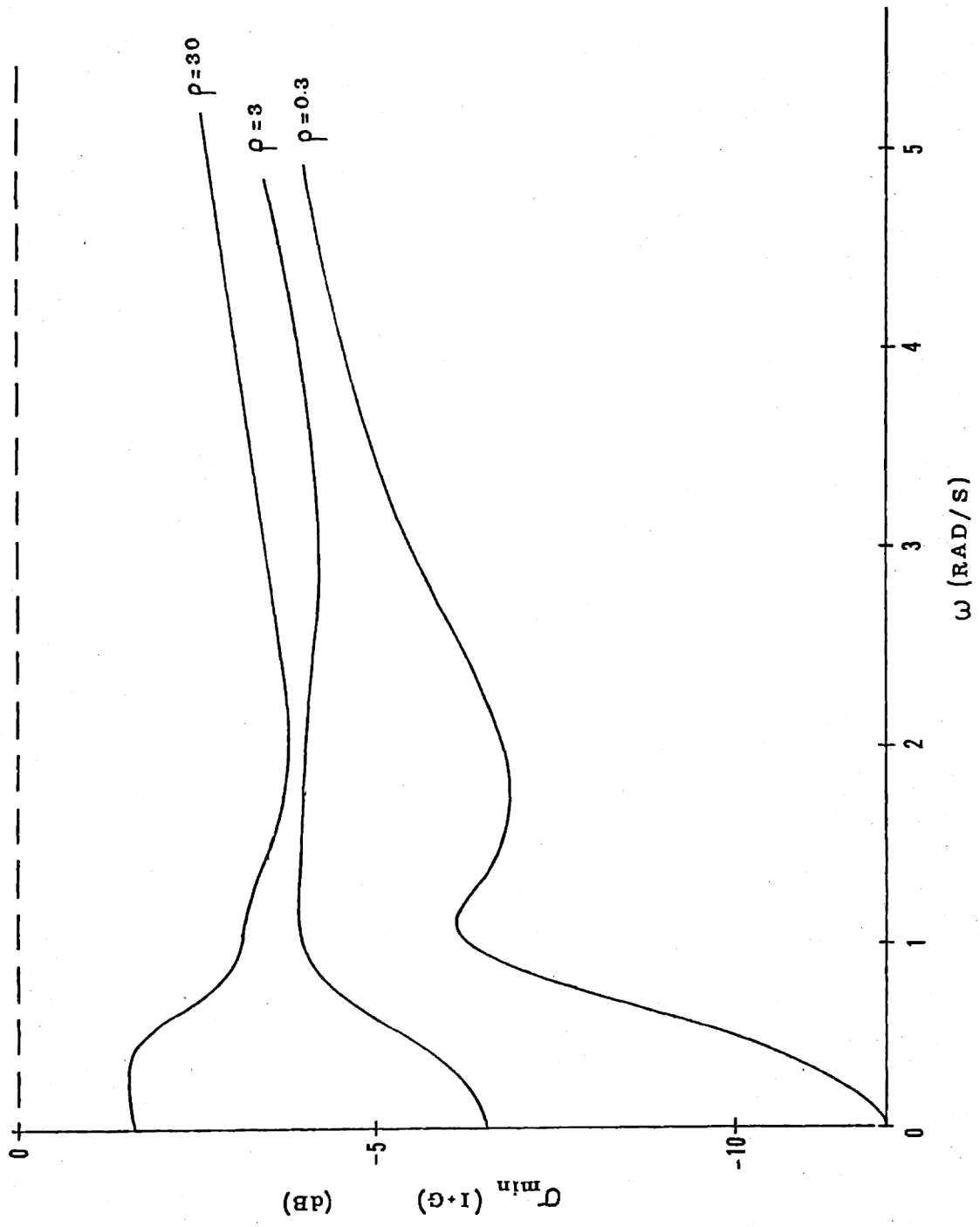

Figure 8.8: LQG Minimum Singular Values (6 measurements case)

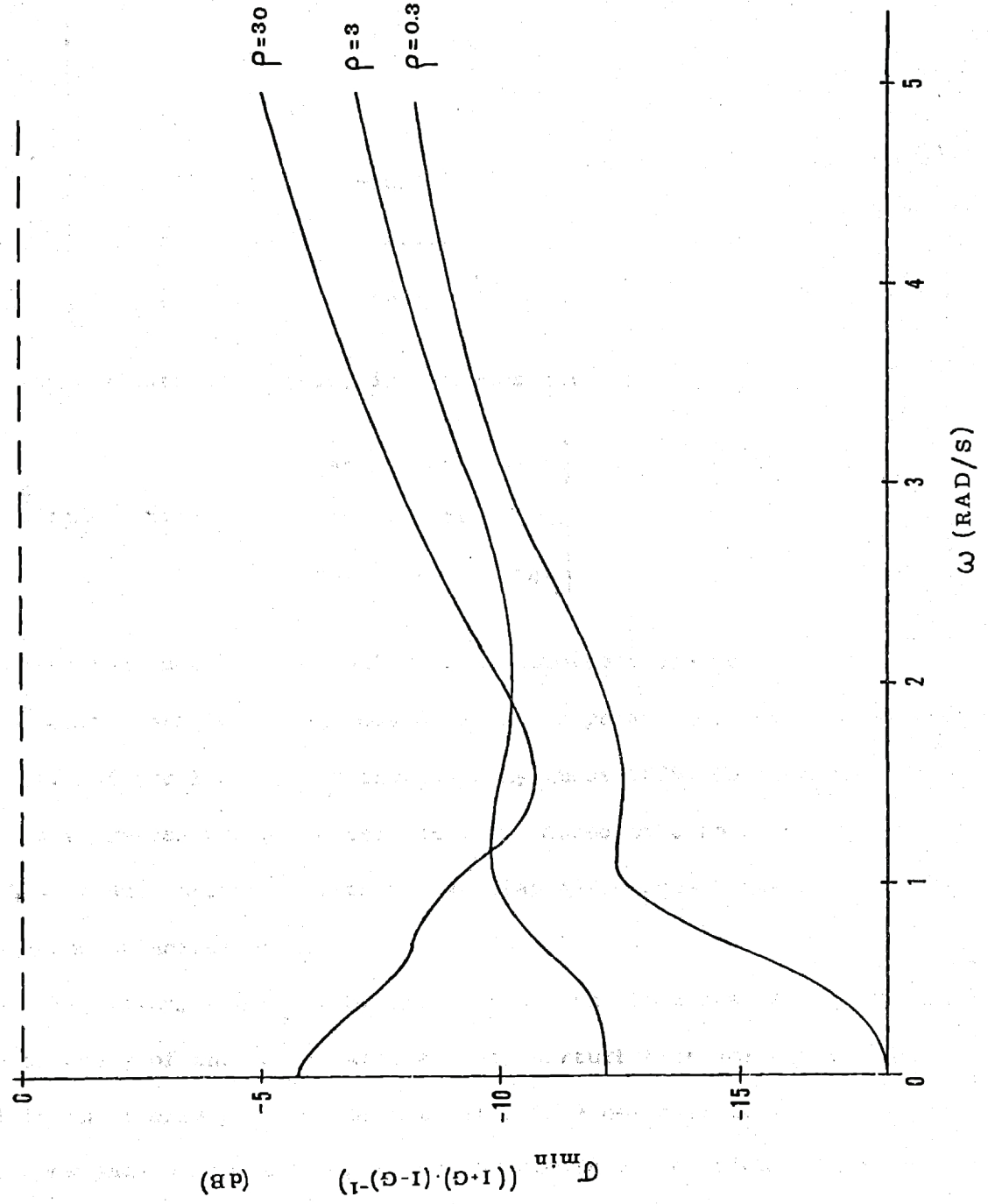

Figure 8.9: LQG Minimum Singular Values (6 measurements case)

The singular value decomposition can be used to obtain the minimal destabilizing perturbation, and get some insight about what physical effects are implied by this perturbation. The minimal destabilizing perturbation, computed for $\rho=0.3$ and $\omega=0$, depends on the error criterion selected, but it turns out that the different results are very similar. The minimal multiplicative perturbation, indicated by $\sigma_{min}(I+G^{-1})$, is:

$$L = \begin{bmatrix} 0.889 & 0.063 & -0.065 \\ 0.0785 & 0.955 & 0.046 \\ 0.133 & -0.076 & 1.079 \end{bmatrix} \tag{8.33}$$

This can be interpreted in many different ways. For example, we can assume that this perturbation is due to modelling errors in the B matrix (force generation part, or control effectiveness). This would mean a change from B_c to $\tilde{B}_c=B_cL$. The nominal B_c was given in Table 5.1:

$$B_c = \begin{bmatrix} 0 & 0 & 0 \\ 0 & 0 & 0 \\ 0 & 0 & 0 \\ -21.211 & 0 & -10.989 \\ 2.976 & 4.595 & 1.265 \\ 2.864 & 0.194 & -2.685 \end{bmatrix} \tag{8.34}$$

The matrix $\tilde{B}_c$ is then:

$$\tilde{B}_c = \begin{bmatrix} 0 & 0 & 0 \\ 0 & 0 & 0 \\ 0 & 0 & 0 \\ -20.334 & -0.290 & -10.468 \\ 3.438 & 4.443 & 1.536 \\ 2.217 & 0.410 & -3.071 \end{bmatrix} \tag{8.35}$$

which, for the last three rows, is a change of:

$$\left(\frac{\tilde{B}_{c,ij} - B_{c,ij}}{B_{c,ij}} \right) = \begin{bmatrix} -4\% & \infty & -5\% \\ 16\% & -3\% & 21\% \\ -23\% & 111\% & 14\% \end{bmatrix} \tag{8.36}$$

We see that the "destabilization" requires important changes in terms that were quite small originally, and could be called parasitic. For example, the second term of the last row is increased by about 100%. We remember that this term expresses the yaw acceleration produced by a roll command, and that this is due, originally, to the angular difference between the body axes and the principal axes.

At this point, the designer will decide, on the basis of the knowledge of the accuracy of the model, whether such perturbation (or error in the model) is physically possible or not. This is a delicate task that requires a good knowledge of the system, and of the precision to which the model is known. In our case, no data could be found in [1], and in the original

model [19] about the precision of the model, so that this question could not be answered with certitude. However, small singular values over some frequency range are indicative of decreased stability margins of the closed-loop system, and the best solution is, if possible, to change this characteristic: it is the subject of the next section.

8.4 Robustness Recovery

The robustness recovery for LQG designs refers to the recovery of the LQ transfer matrix - and consequently stability margins - from the LQG design. The robustness recovery technique was proposed in [28], following a procedure very similar to the one proposed in[32].

The idea is simply to modify the Kalman filter in order to approach the LQ design. The filter is redesigned with a new value of the driving noise spectral intensity matrix:

$$\Xi = \Xi_o + q\, BB^T \tag{8.37}$$

This corresponds to assume that some white noise is present at the input, and, consequently, tells to the mathematical expression of the problem that there are uncertainties at this point. It can be shown[28] that, as $q \to \infty$, the LQ loop transfer matrix is asymptotically approached by the LQG loop transfer matrix.

The robustification procedure is applied to the LQG design described in chapter 8 (6 measurements case), and is illustrated in Figures 8.10, 8.11, and 8.12. For q=0.01, the robustness properties are seriously

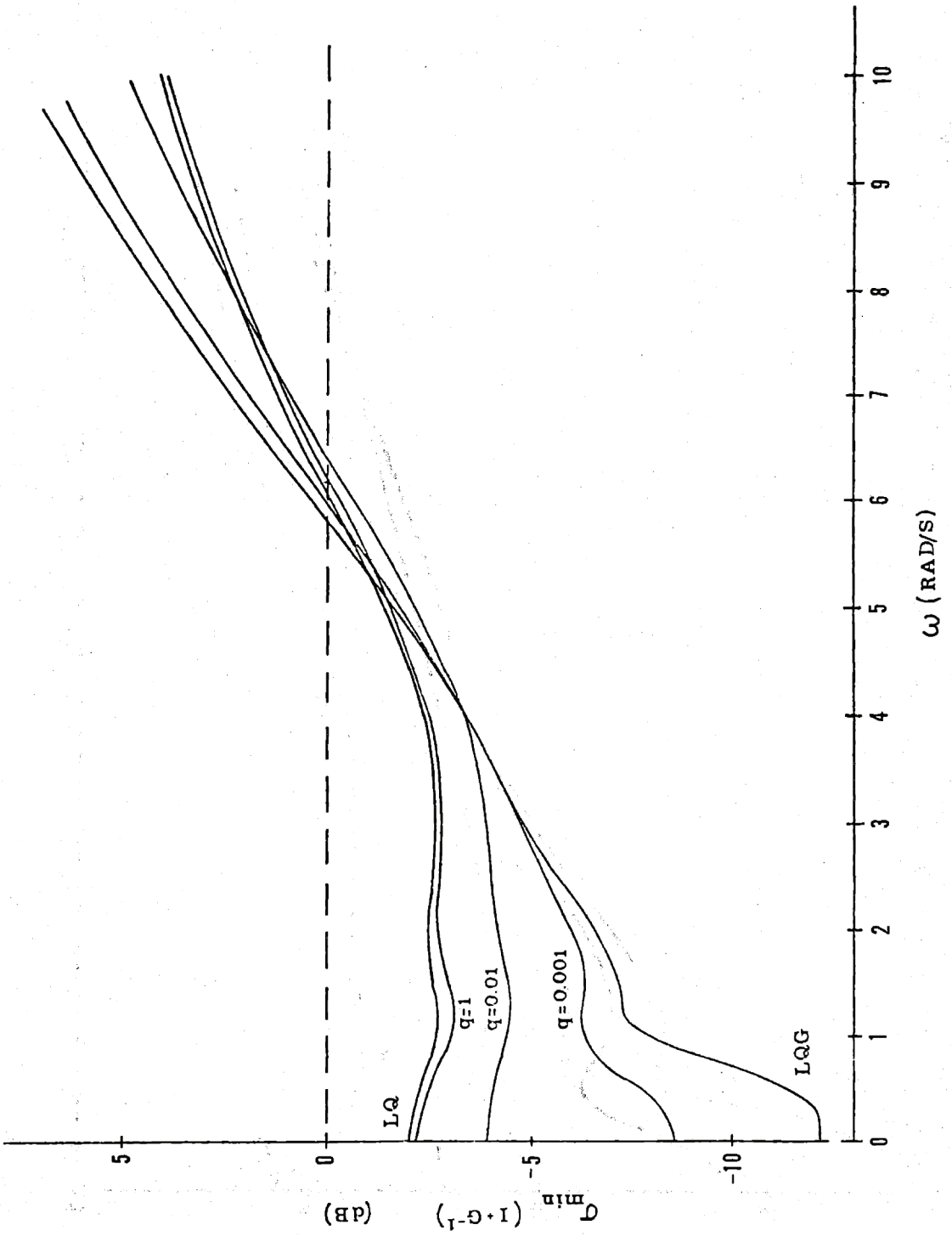

Figure 8.10: LQG Minimum Singular Values (6 meas., with robustification)

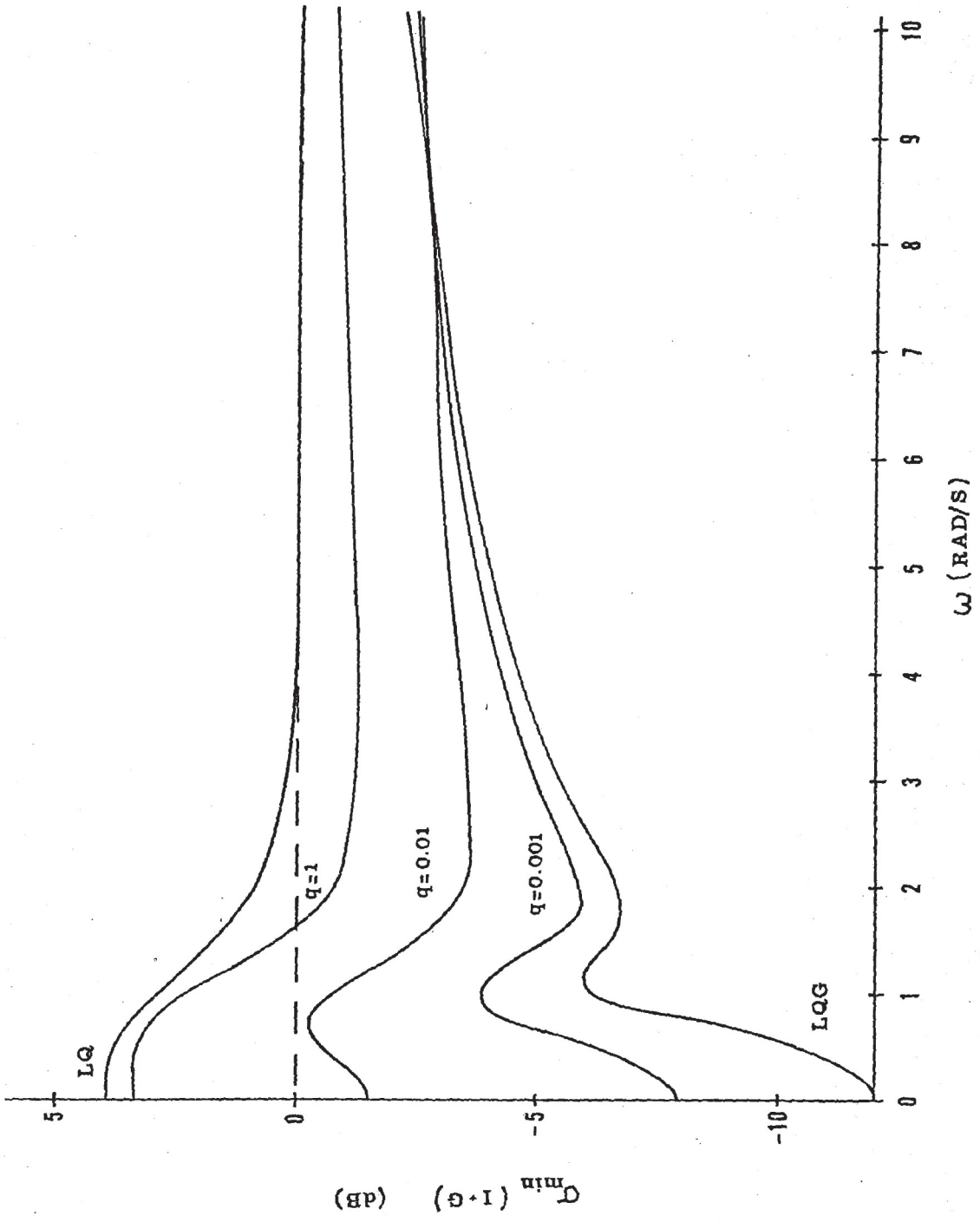

Figure 8.11: LQG Minimum Singular Values (6 meas., with robustification)

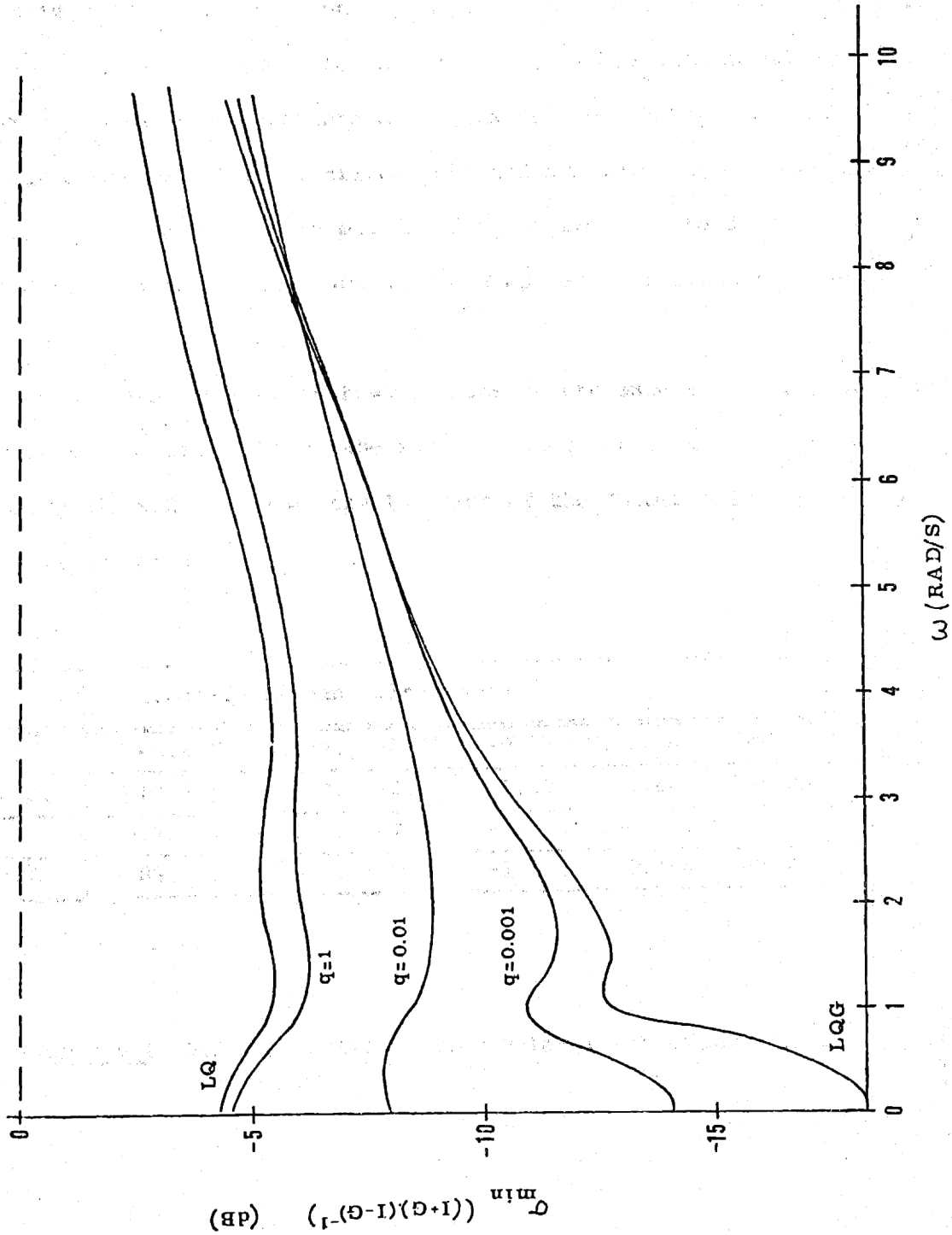

Figure 8.12: LQG Minimum Singular Values (6 meas., with robustification)

	$I+G^{-1}$			$I+G$			$(I+G).(I-G)^{-1}$		
q	σ_{min}(dB)	GM	PM	σ_{min}(dB)	GM	PM	σ_{min}(dB)	GM	PM
0. (LQG)	-12.17	<u>0.754</u> <u>1.246</u>	±14.2	-12.02	0.799 <u>1.334</u>	<u>±14.4</u>	-17.98	0.776 1.289	±14.4
0.001	-8.53	<u>0.626</u> <u>1.374</u>	±21.6	-7.97	0.714 <u>1.666</u>	<u>±23.1</u>	-13.95	0.666 1.502	±22.7
0.01	-4.57	<u>0.409</u> <u>1.591</u>	±34.4	-3.57	0.601 <u>2.967</u>	±38.7	-8.85	0.469 2.131	<u>±39.7</u>
1.	-3.04	<u>0.295</u> <u>1.705</u>	±41.3	-1.35	0.539 <u>6.961</u>	±50.7	-6.25	0.345 2.898	<u>±51.9</u>
∞ (LQ)	-2.70	<u>0.267</u> <u>1.733</u>	±43.0	0.	0.5 <u>∞</u>	<u>±60.0</u>	-5.50	0.307 3.261	±55.9

<u>Table 8.1</u>: LQG Guaranteed Gain and Phase Margins (6 meas., with robustification)

The indicated gain and phase margins are conservative, so that the overall guaranteed gain and phase margins are those underligned.

improved, and for q=1 the LQ singular values are almost recovered.

The minimal values of the minimum singular values over the whole range of frequencies, and the gain and phase margins obtained from equations (8.11) to (8.16) are shown in Table 8.1. As these margins are guaranteed, or conservative, the overall guaranteed margins are the union of the margins corresponding to the different criterions, and are underligned in Table 8.1. For q=0.01, the guaranteed gain margin is about from 0.4 to 3, and the guaranteed phase margin about ±40deg. These appear sufficient for our application.

The robustness recovery is however made at the expense of the performance. In fact, the bandwidth of the Kalman filter increases quickly as q increases. Table 8.2 indicates the location of the Kalman filter poles for different values of q.

q	Aircraft Kalman filter poles
0	-4.82, -3.92, -0.91, -0.57 ± j 0.58, -0.5
0.01	-10.81, -5.37, -2.23, -1.12, -0.60, -0.49
1	-97. , -43. , -7.49, -1. , -0.5 , -0.49
100	-989. , -429. , -69. , -1. , -0.49, -0.49

Table 8.2: Aircraft Kalman Filter Poles (with robustification)

The size of the loop transfer matrix G is represented by its maximal singular value, so that the bandwidth of the control system can be defined by the crossover frequency of the transfer function $\sigma_{max}(G(j\omega))$. The evolution of this transfer function with the parameter q is shown in Figure 8.13. The increase in bandwidth resulting from the robustification procedure can be directly observed from this figure.

The increase in bandwidth may result in improved or degraded tracking performance, but almost certainly in increased control authority, as more noise is passed through the filter. Table 8.3 illustrates the changes in the rms tracking errors and control authority for different values of q.

SEA H=10ft ω_m=0.72 rad/s						
Rms Errors and Controls	Sway (ft)	Roll (deg)	Yaw (deg)	$\delta\alpha_{1,2}$ (deg)	$\delta T_{1,2}$ (%)	$\delta\alpha_3$ (deg)
LQ w.A/C noise	0.691	2.480	0.317	4.719	8.78	3.917
LQG q=0	1.338	2.856	1.491	5.448	11.19	4.467
q=0.01	1.350	2.869	1.482	5.456	11.83	4.653
q=1	1.239	2.851	1.445	6.394	18.70	5.825

Table 8.3: LQG Controller Performance (6 meas., with robustification)

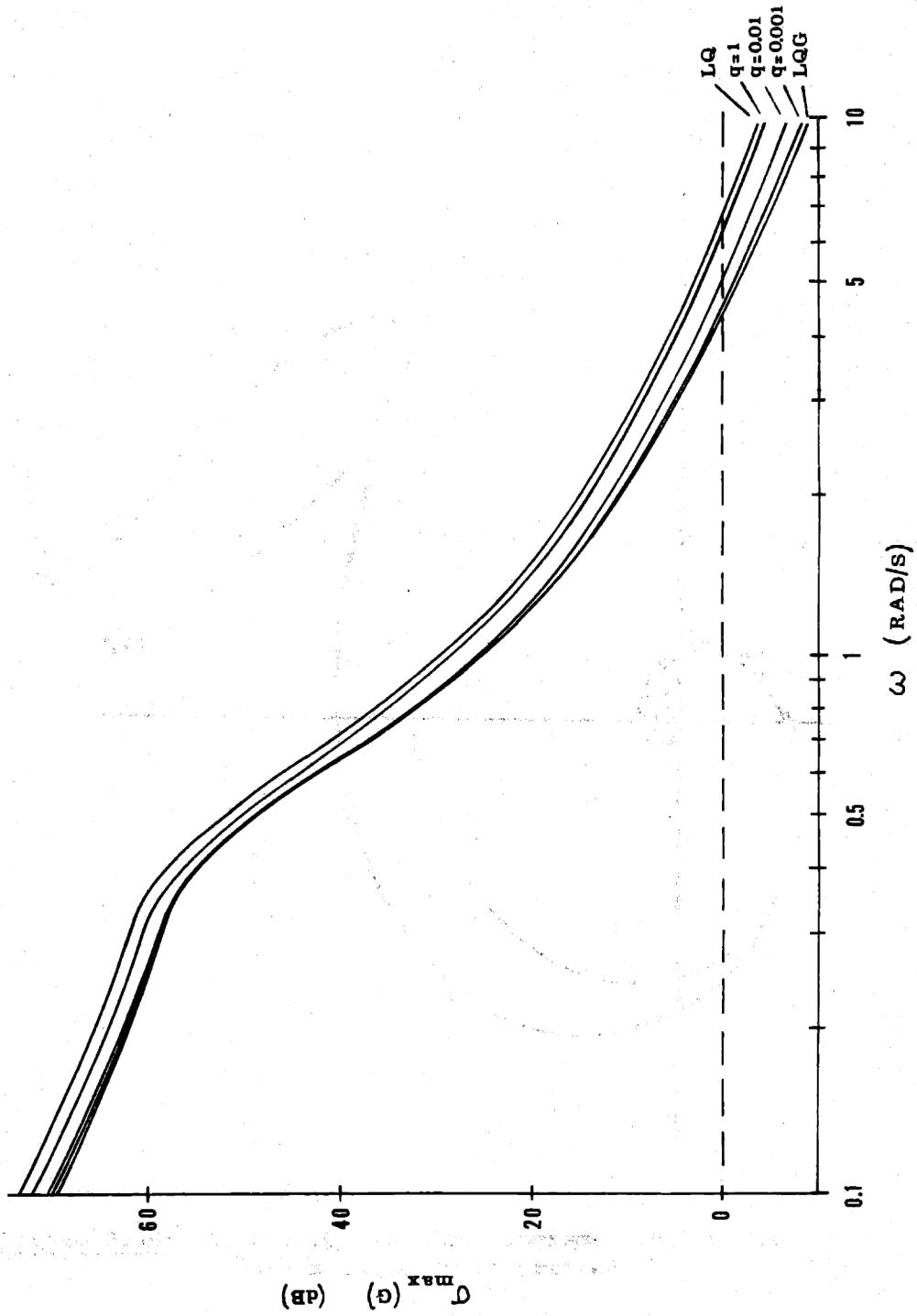

Figure 8.13: LQG Loop Transfer Matrix Maximum Singular Values (6 meas., with robustification)

For q=0.01, the decrease in performance is very small, while for q=1 it becomes significant. The design corresponding to q=0.01 appears to be a very satisfactory one, both for the performance and the robustness. Note however that in this performance evaluation, white measurement noise has been assumed. In reality, the noise will be bandlimited, and the degradation will probably be less than indicated. In fact,as all the states are available (but noisy), an LQ controller, without Kalman filter (using the known dynamics of the aircraft), is not an unrealistic possibility: its performance would be less than the performance of an LQG design, but the robustness would be increased, and the computational load would be dramatically reduced (this would be the case if a good navigation system is available aboard the aircraft, cf. chapter 7).

8.5 Nyquist Diagrams

Some Nyquist diagrams will illustrate the facts indicated at the beginning of this chapter. Figure 8.14 shows the function $-1+\det(I+G(j\omega))$, $\omega \geq 0$. To plot it, it is convenient to compress the distances radially by a logarithmic transformation which is chosen to be:

$$r = \frac{\log(1+\sqrt{x^2+y^2})}{\sqrt{x^2+y^2}} \tag{8.38}$$

$$x' = x.r \tag{8.39}$$

$$y' = y.r \tag{8.40}$$

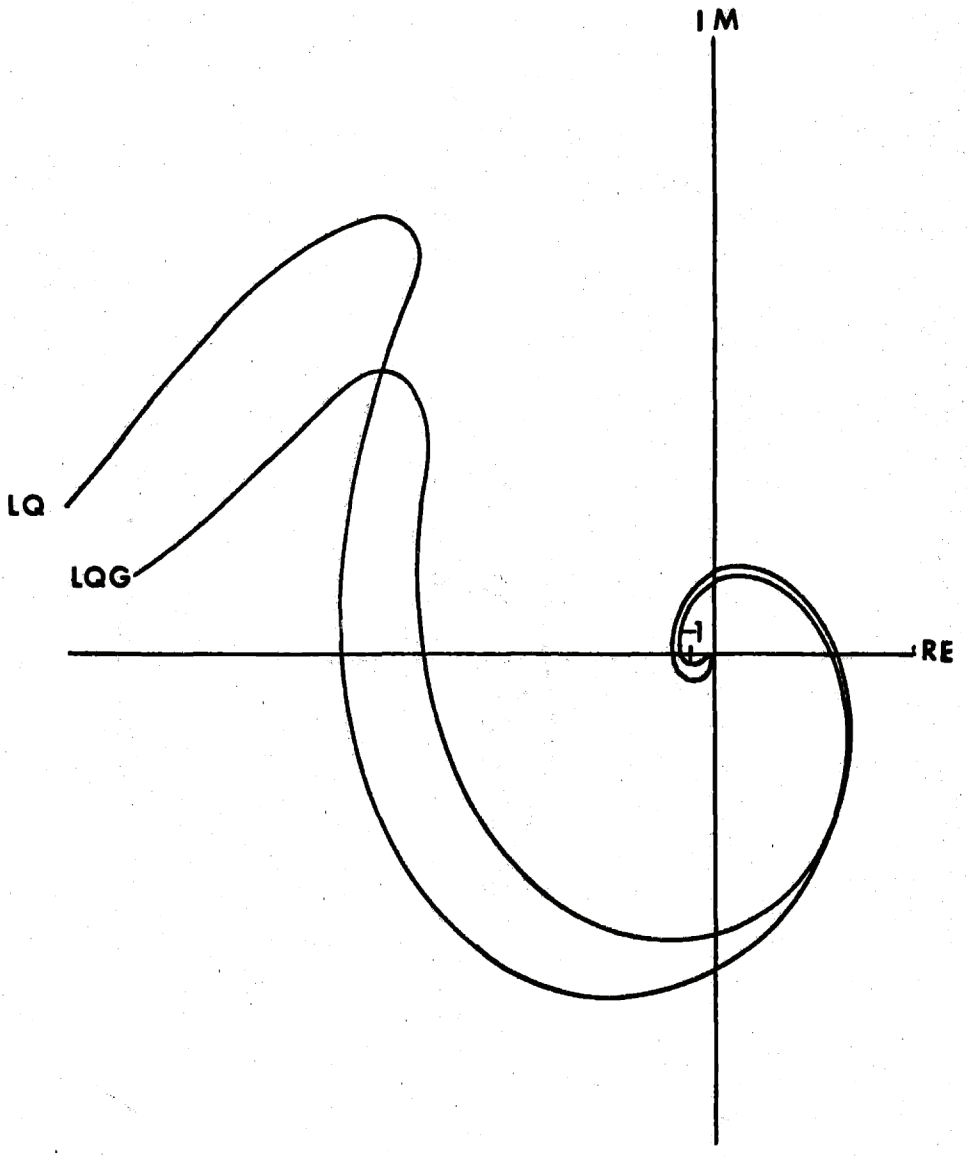

Figure 8.14: LQ and LQG Nyquist Diagrams, for Positive ω Only (diagram radially compressed)

For MIMO systems, such compression of the distances is almost unavoidable, as the transfer function det(I+G(s)) is of an order equal to the order of the system (equal to 6 here).

Figure 8.15 shows the complete contour, and the number of encirclements for the LQ design. There are 3 counterclockwise encirclements, and 1 clockwise encirclement. Remembering that there are two unstable open-loop poles, this confirms the closed-loop stability of the LQ controller. As in the SISO case, some attention has to be given to the two poles at the origin, and to the encirclement at the infinity.

Figure 8.16 shows (in normal cartesian coordinates) the Nyquist diagrams for the LQ and LQG design (6 meas.,q=0) near the critical point. It is checked that the Nyquist diagram for the LQ design never enters the unit circle centered at -1. This is a consequence of the Kalman inequality (8.21) [33].

The minimum singular values shown in the previous subsection indicate the size of the minimal perturbation that destabilizes the closed-loop system. It is also possible to compute the value of the multiplicative (or additive) perturbation L, such that the perturbed transfer matrix G.L is at the limit of instability. In terms of Nyquist diagrams, the minimal perturbation L is the perturbation that,at the specific frequency ω where it is computed, brings the point of the Nyquist diagram $-1+\det(I+G(j\omega))$ to the -1 point (then $\det(I+G(j\omega))=0$). At <u>any</u> frequency, the minimum singular value indicates the size of the minimal perturbation that will make the Nyquist diagram pass through the -1 point, and bring the system

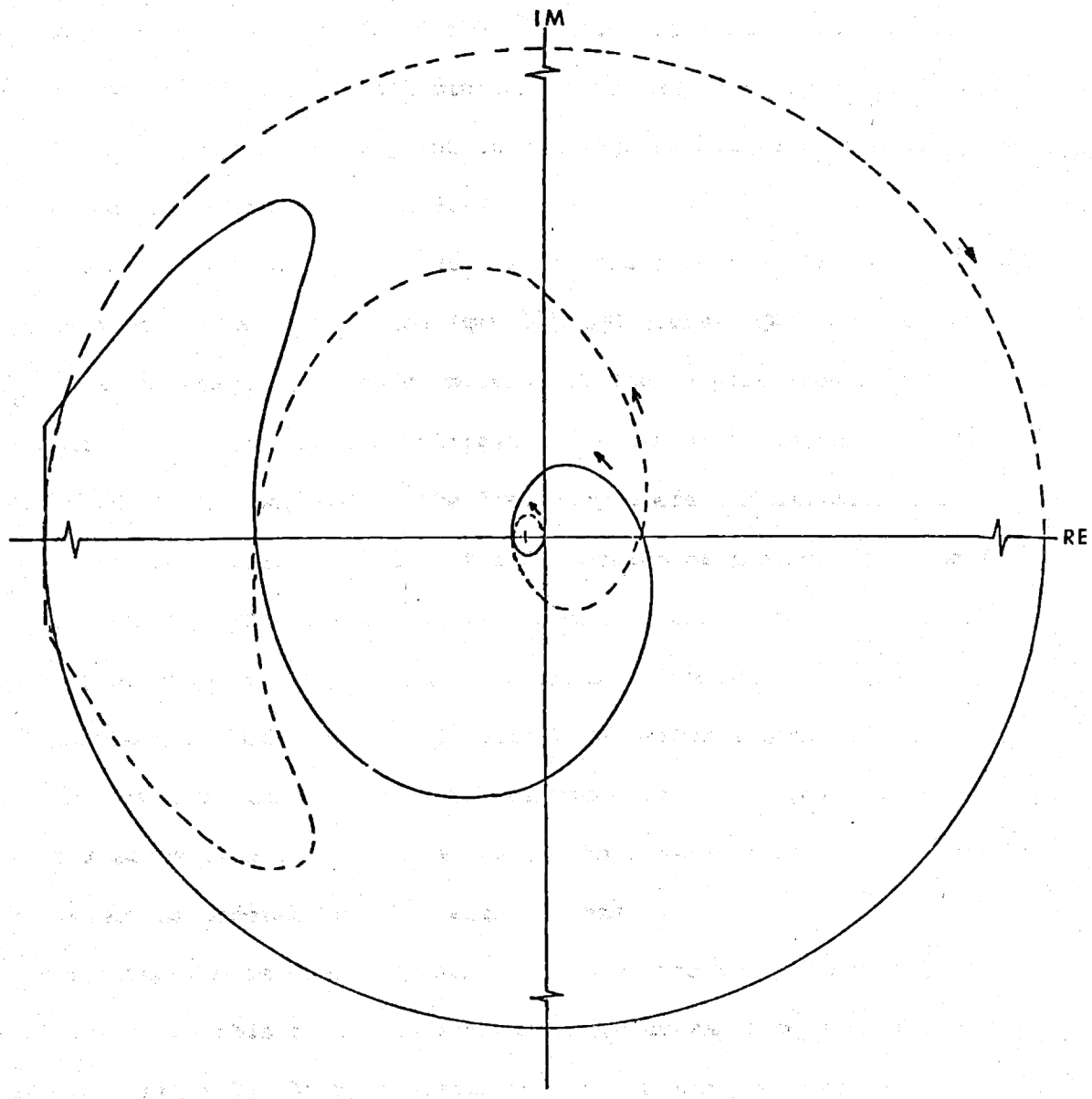

Figure 8.15: LQ Complete Nyquist Diagram

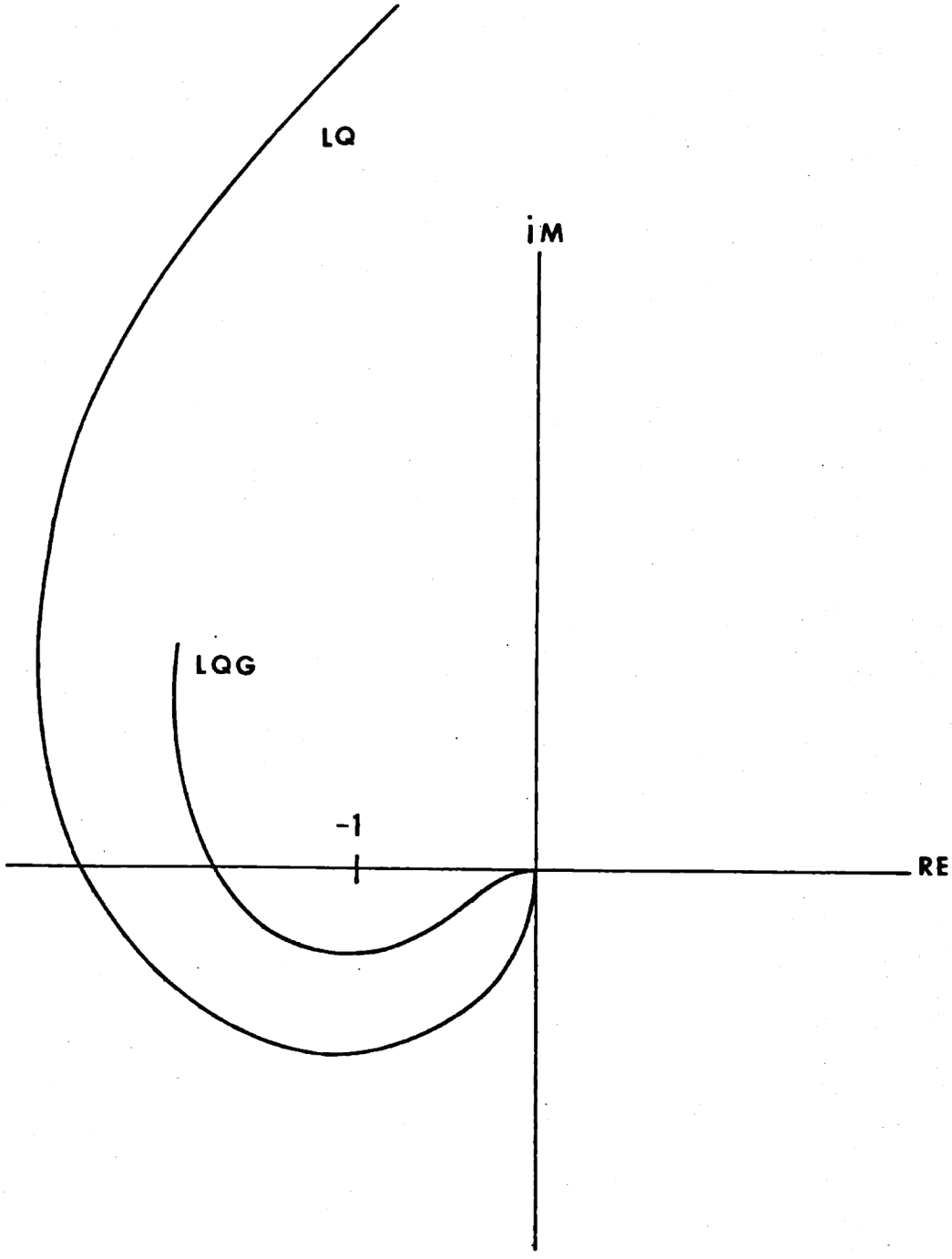

Figure 8.16: LQ and LQG Nyquist Diagrams near the Origin

at the limit of instability. Over the whole range of frequencies, the minimal value of the minimum singular value gives, from all the minimal perturbations found at each frequency, the constant perturbation that has the minimal size. The meaning of the previous discussion, is that the frequency at which this overall minimum occurs may correspond to a point located very far from the -1 point on the Nyquist diagram. This is illustrated in Figures 8.17 and 8.18.

Fig. 8.17 show the Nyquist diagram of the loop transfer matrix G corresponding to the robustified (q=0.01) LQG (curve LQG) together with the diagram of the loop transfer matrix G.L (curve perturbed LQG). The perturbation L is the minimal multiplicative perturbation that corresponds to Fig.8.10. It is computed at the frequency where the minimum singular value is minimal, i.e. 1.15rad/s. The distortion of the Nyquist diagram is quite peculiar. The point that is brought to the -1 point is not at all the closest point of the Nyquist diagram, although it is the closest point on the basis of minimal multiplicative perturbation. This is a practical proof of the fact that the distance to the -1 point in the Nyquist diagram is not representative of the closeness to instability, with respect to general type of perturbations.

The situation is even more surprising for the non-robustified LQG design (q=0). In this case, the minimum singular value goes to its minimum at $\omega=0$ (cf. Fig.8.7). At this frequency, due to the presence of the two poles at the origin, the determinant of $I+G(j\omega)$ is infinite. This means that the closest point (closest in the sense of minimal norm additive or

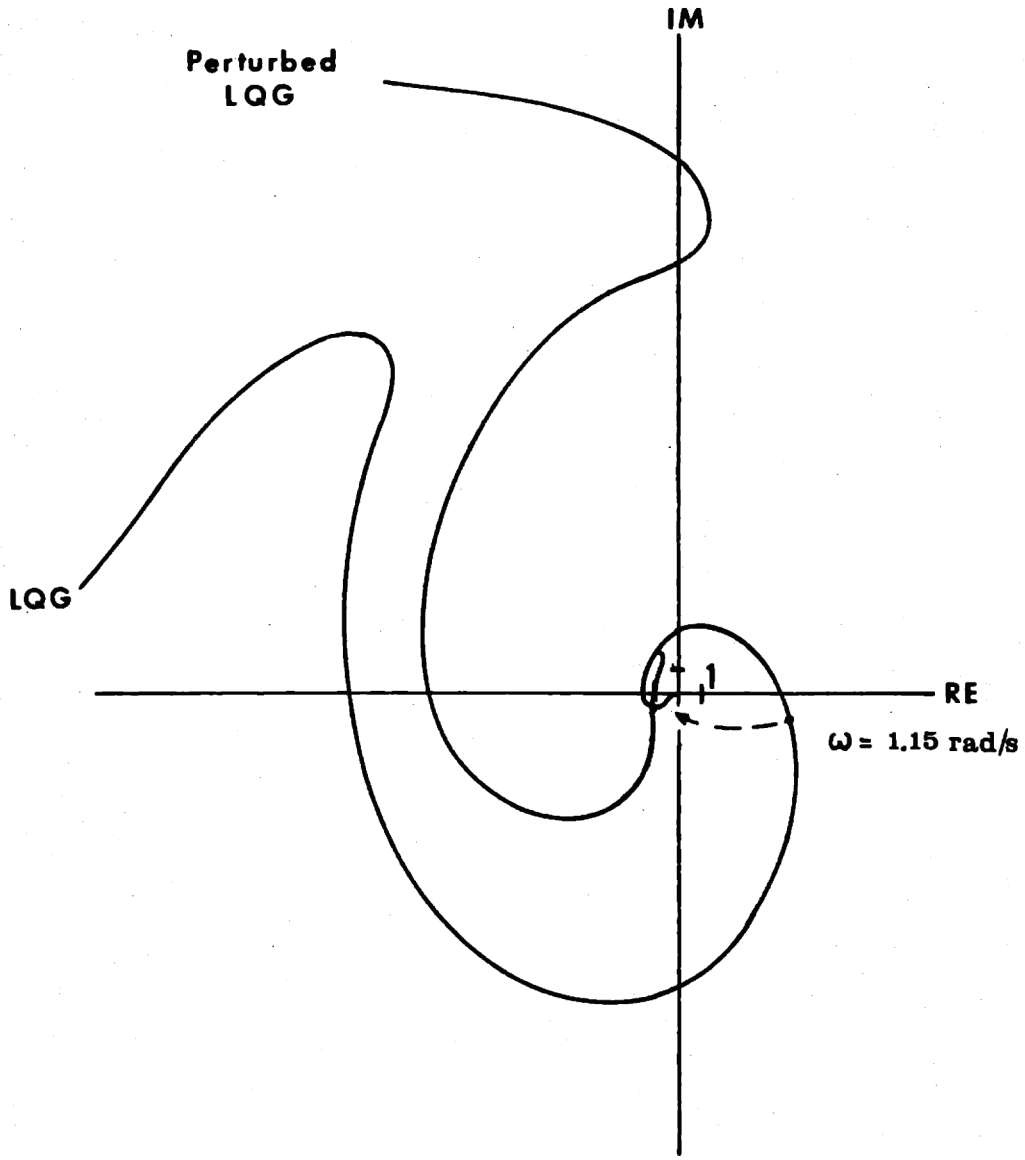

Figure 8.17: LQG and Perturbed LQG Nyquist Diagrams, Robustified Case with q=0.01 (diagram radially compressed)

multiplicative perturbation of $G(j\omega)$) from the Nyquist diagram to the -1 point is the point at infinity! This is illustrated in Fig.8.18. As this case is numerically perfectly ill-conditioned, the minimal multiplicative perturbation is computed at ω=0.1 rad/s, where the minimum singular value is very close to the minimum value reached at ω=0rad/s.

8.6 Summary

In this chapter, we addressed the important issues of the control system robustness to modelling errors and parameter uncertainty. Due to the decoupling between the ship and the aircraft, this problem only involved the aircraft model and the feedback from the aircraft states.

The importance of the singular values analysis in the definition of multivariable robustness measures was first introduced, and some recent results concerning the stability margins of multivariable systems were summarized.

The singular values analysis was used for the different transfer matrices of interest, and for different designs considered previously. For the nominal design, it was shown that reduced stability margins were obtained at very low frequency, and some physical interpretations were indicated for the minimal multiplicative destabilizing error given by the singular value decomposition. A robustification procedure was used, and appeared successful in retrieving the favorable robustness properties of the LQ design, with a limited degradation in performance.

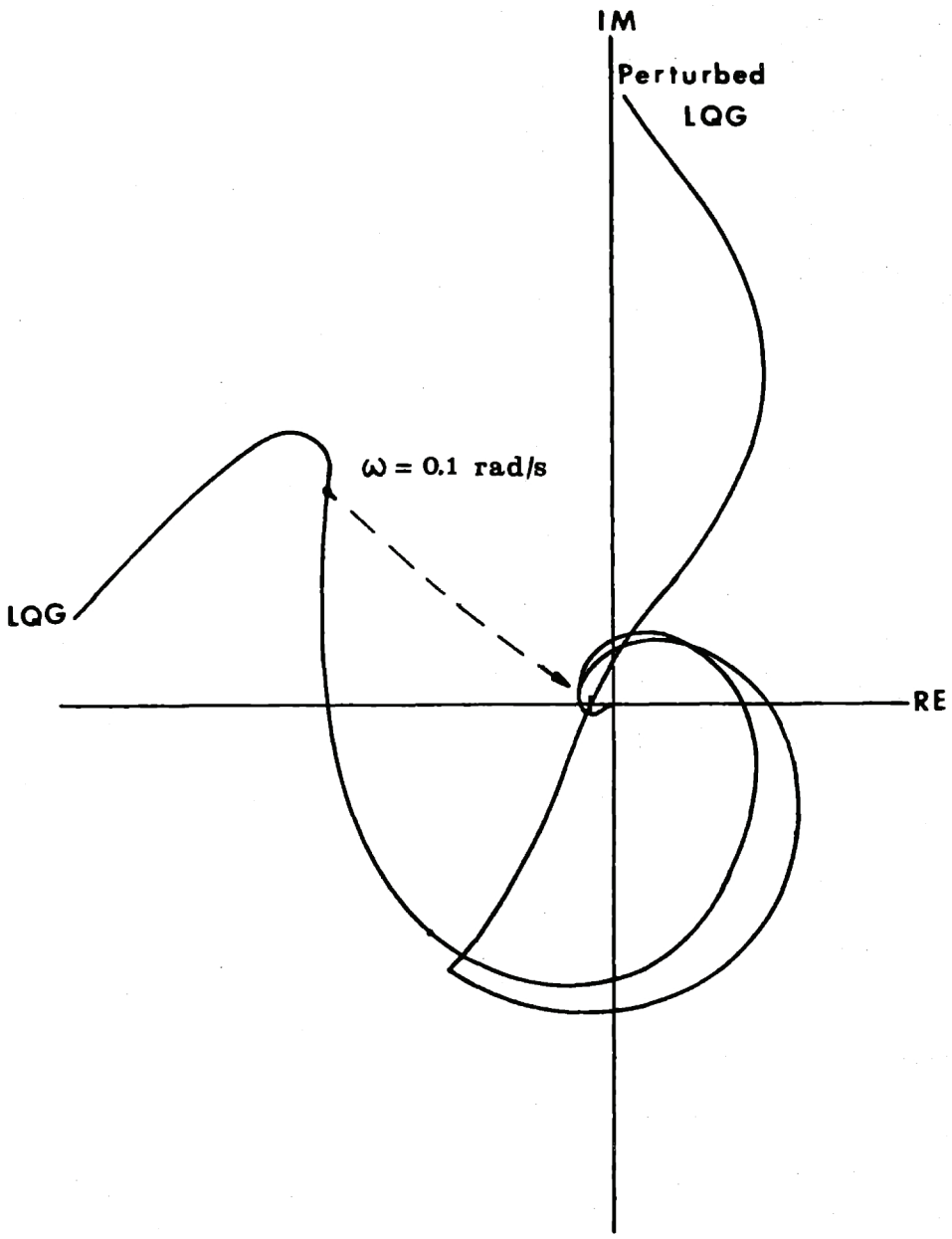

Figure 8.18: LQG and Perturbed LQG Nyquist Diagrams
(diagram radially compressed)

Finally, some Nyquist diagrams illustrated the theoretical results mentioned previously, especially the impossibility of defining stability margins from the Nyquist diagram in the MIMO case, in contradistinction to the SISO case.

CHAPTER 9

CONCLUSIONS

9.1 General Conclusions

Two major aspects of the problem of landing VTOL aircrafts on small ships were addressed in this thesis. The first is the estimation and prediction of ship motions, mostly for applications in piloted landings, and the second is the design and evaluation of an automatic controller, for use in fully or partially automatic landing schemes.

An accurate ship model was first derived, using hydrodynamic data for the DD963 destroyer. It was shown that the ship motions have power spectra that are concentrated in a narrow frequency band, especially the roll motion. Consequently, good prediction time could be obtained, and the roll motion could be predicted for as far as 5 to 10 seconds ahead. This was a significant result, as the roll motion turns out to be the most important lateral motion in the VTOL landing problem. In particular, the lateral translation of the landing pad is due to a large extent to the roll motion, as the location of the landing pad is significantly higher than the ship center of rotation.

The sea modal frequency is a significant parameter of the ship model, and its large influence on the estimation and prediction errors justifies a precise estimation of this parameter in a real-time application.

The aircraft model was briefly described, and the important couplings amongst the motions were mentioned. Two of them appeared significant, and

contradictory: the first is the lateral acceleration due to a roll angle of the aircraft, and the second is the roll moment due to a lateral deflection of the thrusts.

The design of an automatic controller, defined as a tracker of the ship motions, made clear some other of the constraints related to the tracking of the ship motions. The relations between the lateral translation of the ship landing pad induced by the roll motion at the center of rotation, and the roll motion itself, appeared to be contradictory with the two important couplings of these motions in the aircraft itself. These constraints are specific to the landing problem, and are independent of the control system design methodology. Although the roll motion may often be neglected, its possibly large amplitude in high sea states makes imperative to take these limitations into account in an engineering design.

The design of the automatic controller also illustrated some results and recent advances in the design of an optimal controller, using the LQG methodology. The relations between the choice of the state and control weighting matrices in the quadratic cost, and the resulting root-loci were explained, and justified the careful selection of these matrices.

The usefulness of the singular values analysis in the definition of realistic stability margins was indicated, and some Nyquist diagrams illustrated related theoretical results, and the important differences between the MIMO and the SISO case.

The robustification procedure appeared to be very successful in the design of robust LQG control systems, and led to increased stability

margins, with moderate degradation in the performance.

9.2 Suggestions for Future Research

Among the possible topics for future research, we note:

- the evaluation of the performance and of the stability margins of an automatic controller including the longitudinal and the lateral motions, and the study of the influence of the cross-coupling terms (gyroscopic terms)

- the inclusion of the aerodynamic effects in the aircraft model, and of the ship airwake turbulence and ground effects; the aerodynamic effects being nonlinear, some nonlinear theories may then be useful

- although this research concentrated on the landing problem, some interesting results may be obtained from the design of a control system for the transition flight, and from the use of modern control theories for this time-varying problem.

APPENDIX A

SHIP MODEL COMPLEMENTS

A.1 Ship Model Values

A.1.1 Sea

$J = 0.707$

$$\alpha = \frac{U}{g}\omega_m \cos\phi$$

$$B(\alpha) = \frac{1.9339}{1+2\alpha}$$

$$S_o = 0.3125 \frac{H^2}{\omega_m} B(\alpha)$$

$$\omega_o = \frac{\omega_m(1+\alpha)}{0.8409}$$

A.1.2 Force Dynamics

U=0, ϕ=90 degrees:

$F_{s,o} = 310$ $\quad J_{s,o} = 0.72$ $\quad \omega_{s,o} = 0.6$

$F_{r,o} = 2120$ $\quad J_{r,0} = 0.7$ $\quad \omega_{r,o} = 0.76$

$F_{y,o} = 11300$ $\quad J_{y,o} = 0.35$ $\quad \omega_{y,o} = 0.96$

Any U, ϕ:

$$F_s = F_{s,o}\sin\phi, \quad J_s = J_{s,o}\sin\phi, \quad \omega_s = \left(\omega_{s,o} + \omega_{s,o}^2 \frac{U}{g}\cos\phi\right)\sin\phi$$

$$F_r = F_{r,o}\sin\phi, \quad J_r = J_{r,o}\sin\phi, \quad \omega_r = \left(\omega_{r,o} + \omega_{r,o}^2 \frac{U}{g}\cos\phi\right)\sin\phi$$

$$F_y = F_{y,o}\sin\phi, \quad J_y = J_{y,o}\sin\phi, \quad \omega_y = \left(\omega_{y,o} + \omega_{y,o}^2 \frac{U}{g}\cos\phi\right)\sin\phi$$

A.3.1 Ship Dynamics

U=0, ϕ=90 degrees:

$$M = \begin{bmatrix} 215 & 988 & -230 \\ 988 & 104000 & 0 \\ -230 & 0 & 3.76\ 10^6 \end{bmatrix}$$

$$A_{h,o} = \begin{bmatrix} 223 & -759 & 14600 \\ -759 & 22900 & 182000 \\ 14600 & 182000 & 4.18\ 10^6 \end{bmatrix}$$

$$B_{h,o} = \begin{bmatrix} 10.6 & -55.4 & 423 \\ -55.4 & 887\text{xRDF} & 6270 \\ 423 & 6270 & 144000 \end{bmatrix}$$

$$C_h = \begin{bmatrix} 0 & 0 & 0 \\ 0 & 28800 & 0 \\ 0 & 0 & 0 \end{bmatrix}$$

RDF=3 (the roll damping factor takes the nonlinear damping into account)

Any U, ϕ:

$$A_h = A_{h,o} + \frac{U}{\omega_p^2} \cdot \begin{bmatrix} 0 & 0 & B_{h,o_{1,1}} \\ 0 & 0 & B_{h,o_{1,2}} \\ -B_{h,o_{1,1}} & -B_{h,o_{1,2}} & U.A_{h,o_{1,1}} \end{bmatrix}$$

$$B_h = B_{h,o} + U \cdot \begin{bmatrix} 0 & 0 & -A_{h,o_{1,1}} \\ 0 & 0 & -A_{h,o_{1,2}} \\ A_{h,o_{1,1}} & A_{h,o_{1,2}} & \frac{U}{\omega_p^2} B_{h,o_{1,1}} \end{bmatrix}$$

where:

$$\omega_p = 0.425 + \frac{U \cos\phi}{178.27}$$

A.2 Ship Dynamics: State-Space Model

We have the equation of motion:

$$(M+A_h)\ddot{\underline{x}}_h + B_h\dot{\underline{x}}_h + C_h\underline{x}_h = \underline{F}$$

where:

$$\underline{x}_h = \begin{bmatrix} x_1 \\ x_2 \\ x_3 \end{bmatrix} = \begin{bmatrix} \text{sway} \\ \text{roll} \\ \text{yaw} \end{bmatrix}$$

$$\underline{F} = \begin{bmatrix} F_1 \\ F_2 \\ F_3 \end{bmatrix} = \begin{bmatrix} \text{sway force} \\ \text{roll moment} \\ \text{yaw moment} \end{bmatrix}$$

We call:

$$R = (M+A_h)^{-1} = \{r_{ij}\}$$

$$P = (M+A_h)^{-1}B_h = \{p_{ij}\}$$

$$Q = (M+A_h)^{-1}C_h = R.C_h$$

Roll is the only motion having a spring constant so that:

$$C_h = \begin{bmatrix} 0 & 0 & 0 \\ 0 & C_{rr} & 0 \\ 0 & 0 & 0 \end{bmatrix}$$

and:

$$Q = \begin{bmatrix} 0 & r_{12}C_{rr} & 0 \\ 0 & r_{22}C_{rr} & 0 \\ 0 & r_{32}C_{rr} & 0 \end{bmatrix}$$

Using Laplace transforms, we write:

$$s^2\underline{x} = -Ps\underline{x} - Q\underline{x} + R\underline{F}$$

or:

$$s(x_1) = (sx_1)$$

$$s(x_2) = (sx_2)$$

$$s(x_3) = (sx_3)$$

$$s(sx_1) = -p_{11}(sx_1) - p_{12}(sx_2) - r_{12}C_{rr}(x_2) - p_{13}(sx_3) + r_{11}F_1 + r_{12}F_2 + r_{13}F_3 \qquad (A.1)$$

$$s(sx_2) = - p_{21}(sx_1) - p_{22}(sx_2) - r_{22}C_{rr}(x_2) - p_{23}(sx_3) + r_{21}F_1 + r_{22}F_2 + r_{23}F_3 \quad (A.2)$$

$$s(sx_3) = - p_{31}(sx_1) - p_{32}(sx_2) - r_{32}C_{rr}(x_2) - p_{33}(sx_3) + r_{31}F_1 + r_{32}F_2 + r_{33}F_3 \quad (A.3)$$

which is equivalent to a state-space representation having 6 states. There is an implicit pole-zero cancellation at the origin, between the the poles of the sway and the yaw motions and the zeroes of the corresponding force and moment.

To avoid this, we rewrite eq.(A.2):

$$C_{rr}\frac{x_2}{s} = -\frac{1}{r_{22}}sx_2 - \frac{p_{21}}{r_{22}}x_1 - \frac{p_{22}}{r_{22}}x_2 - \frac{p_{23}}{r_{22}}x_3 + \frac{r_{21}}{r_{22}}\frac{F_1}{s} + \frac{F_2}{s} + \frac{r_{23}}{r_{22}}\frac{F_3}{s} \quad (A.4)$$

and use (A.4) with (A.1) to obtain:

$$s(x_1) = t_{11}(x_1) + t_{12}(sx_2) + t_{13}(x_2) + t_{14}(x_3) + u_{11}(\frac{F_1}{s}) + u_{15}(\frac{F_3}{s}) \quad (A.5)$$

where:

$$t_{11} = \frac{r_{12}}{r_{22}}p_{21} - p_{11}$$

$$t_{12} = \frac{r_{12}}{r_{22}}$$

$$t_{13} = \frac{r_{12}}{r_{22}}p_{22} - p_{12}$$

$$t_{14} = \frac{r_{12}}{r_{22}} p_{23} - p_{13}$$

$$u_{11} = r_{11} - \frac{r_{12}}{r_{22}} r_{21}$$

$$u_{15} = r_{13} - \frac{r_{12}}{r_{22}} r_{23}$$

Similarly, (A.4)and (A.3) give:

$$s(x_3) = t_{41}(x_1) + t_{42}(sx_2) \quad t_{43}(x_2) \quad + t_{44}(x_3) + u_{41}(\frac{F_1}{s}) + u_{45}(\frac{3}{s}) \tag{A.6}$$

where:

$$t_{41} = \frac{r_{32}}{r_{22}} p_{21} - p_{31}$$

$$t_{42} = \frac{r_{32}}{r_{22}}$$

$$t_{43} = \frac{r_{32}}{r_{22}} p_{22} - p_{32}$$

$$t_{44} = \frac{r_{32}}{r_{22}} p_{23} - p_{33}$$

$$u_{41} = r_{31} - \frac{r_{32}}{r_{22}} r_{21}$$

$$u_{45} = r_{33} - \frac{r_{32}}{r_{22}} r_{23}$$

And, of course:

$$s(x_2) = (sx_2) \tag{A.7}$$

Finally, (A.4), (A.5), (A.6), and (A.2) lead to:

$$s(sx_2) = t_{21}(x_1) + t_{22}(sx_2) + t_{23}(x_2) + t_{24}(x_3) + u_{21}\left(\frac{F_1}{s}\right) + u_{22}(F_1) + u_{24}(F_2) + u_{25}\left(\frac{F_3}{s}\right) + u_{26}(F_3) \qquad \text{(A.8)}$$

where:

$$t_{21} = - p_{21}t_{11} - p_{23}t_{41}$$

$$t_{22} = - p_{21}t_{12} - p_{23}t_{42} - p_{22}$$

$$t_{23} = - p_{21}t_{13} - p_{23}t_{43} - r_{22}C_{rr}$$

$$t_{24} = - p_{21}t_{14} - p_{23}t_{44}$$

$$u_{21} = - p_{21}u_{11} - p_{23}u_{41}$$

$$u_{22} = r_{21}$$

$$u_{24} = r_{22}$$

$$u_{25} = - p_{21}u_{15} - p_{23}u_{45}$$

$$u_{26} = r_{23}$$

Equations (A.4), (A.5), (A.6), (A.7), and (A.8) constitute the new state-space representation, with only 4 states:

$$s\begin{bmatrix} x_1 \\ sx_2 \\ x_2 \\ x_3 \end{bmatrix} = T \cdot \begin{bmatrix} x_1 \\ sx_2 \\ x_2 \\ x_3 \end{bmatrix} + U \cdot \begin{bmatrix} F_1/s \\ F_1 \\ F_2 \\ F_3/s \\ F_3 \end{bmatrix}$$

and:

$$T = \{t_{ij}\}$$

$$U = \{u_{ij}\}$$

are given above.

The pole-zero cancellations are eliminated by the introduction of the integrals of the sway force and yaw moment, which, instead of being computed (implicitely) in the ship dynamics model, can directly be obtained "drift-free" from the transfer functions between the sea height and the generated forces.

APPENDIX B

DISCRETIZATION PROBLEMS

A simple derivation is presented here that explains some difficulties that can be encountered in discretizing systems containing lightly damped second-order modes.

Assuming the system:

$$\dot{\underline{x}} = A\,\underline{x}$$

having a second-order mode $\lambda(A) = -\sigma \pm j\omega$. The exact discretization of the system is:

$$\underline{x}(t+\Delta t) = A_d\,\underline{x}(t)$$

where:

$$A_d = e^{A\Delta t}$$

It would lead to the equivalent mode in the z-plane:

$$\lambda(A_d) = e^{(-\sigma \pm j\omega)\Delta t}$$

If we use an approximate representation:

$$\underline{x}(t+\Delta t) = (I+A\Delta t)\underline{x}(t)$$

the modes will, instead, be at:

$$\lambda(I+A\Delta t) = (1-\sigma\Delta t) \pm j\omega\Delta t$$

Let us consider consider a system A', having modes at $-a \pm jb$ in the continuous time domain which, discretized, would have the same modes as $I+A\Delta t$.

The following equations can then be obtained:

$$e^{-a\Delta t} \cdot e^{jb\Delta t} = \sqrt{(1-\sigma\Delta t)^2+(\omega\Delta t)^2}\, e^{j\tan^{-1}(\frac{\omega\Delta t}{1-\sigma\Delta t})}$$

and:

$$a = -\frac{1}{\Delta t} \ln \sqrt{(1-\sigma\Delta t)^2+(\omega\Delta t)^2}$$

$$b = \frac{1}{\Delta t} \tan^{-1}(\frac{\omega\Delta t}{1-\sigma\Delta t})$$

It is easily checked that for Δt vanishingly small, a approaches σ, and b approaches ω so that the discretization is valid.

The question is to determine how small Δt actually has to be. For b to approach ω, we need:

$$\omega\Delta t << 1 \qquad \text{and} \qquad \sigma\Delta t << 1$$

or:

$$\Delta t << 1/\omega \qquad \text{and} \qquad \Delta t << 1/\sigma$$

which is the expected condition that Δt must be small compared to the time

constants of the system.

The condition for a is a little different. We need:

$$\sqrt{1-2\sigma\Delta t+(\sigma\Delta t)^2+(\omega\Delta t)^2} \simeq \sqrt{1-2\sigma\Delta t} \simeq 1-\sigma\Delta t$$

so that the conditions are:

$$2\sigma\Delta t << 1 \ , \quad (\sigma\Delta t)^2 << 2\sigma\Delta t \ , \text{ and } \quad (\omega\Delta t)^2 << 2\sigma\Delta t$$

or:

$$\Delta t << 1/2\sigma$$

$$\Delta t << 2/\omega.(\sigma/\omega)$$

The first condition is similar to the previous one, while the second is similar only if σ/ω is close to one. If σ/ω is much less than one (lightly damped mode), the required time step is much smaller than the one indicated by the time constants of the system. If this is not taken into account, the term $(\omega\Delta t)^2$ will influence the $2\sigma\Delta t$ term, which is equivalent to reducing the value of σ. This implies a reduced value of the real part, while the imaginary part remains constant. In conclusion, the discretization of very lightly damped second-order modes with approximate discretization may lead to even less damped equivalent discrete modes, even if small time steps - compared to the time constants of the system - are used.

APPENDIX C

TURBULENCE MODEL

A wind disturbance model is available in [19] and is summarized here. The mean wind component has been neglected (only the turbulence is considered), and the air turbulence considered does not include the ship airwake and the ground effects.

The turbulence is modelled as the outputs of Dryden filters driven by white noises of intensity 1. The outputs are additional turbulent velocities of the aircraft v_{BN} (sway), p_{BN} (roll), and r_{BN} (yaw). The expressions given in [19]are:

$$\rho_2 \rightarrow \sigma_v \sqrt{\frac{L_v}{V}} \quad \frac{1 + \sqrt{3}\,\frac{L_v}{V}\,s}{\left(1 + \frac{L_v}{V}\,s\right)^2} \rightarrow \quad v_{BN}$$

$$\rho_4 \rightarrow \sigma_w \sqrt{\frac{8}{L_w V}} \quad \left(\frac{\pi L_w}{4b}\right)^{1/6} \frac{1}{1 + \frac{4b}{\pi V}\,s} \rightarrow p_{BN}$$

$$v_{BN} \rightarrow -\frac{1}{V} \quad \frac{s}{1 + \frac{3b}{\pi V}\,s} \quad \rightarrow \quad r_{BN}$$

where ρ_2 and ρ_4 are white noises of intensity 1.

In the condition considered in this thesis:

h=40ft (altitude of the stationkeeping point)

V=15.5ft/s (≃10kts)

V_{WIND}=30ft/s (≃20kts)

And the parameters of the filters given in [19] are:

L_v=600ft

σ_v=6ft/s

b=44.43ft

σ_w=3.058ft/s

L_w=69.1ft

To bring this wind turbulence model to a standard state-space formulation, the outputs of the Dryden filters are first multiplied by s, and entered in the acceleration equation of the aircraft model, instead of the velocity equation. Next, the time constants of the shaping filters being large compared to the time constants of interest, they are neglected, so that the Dryden filters become simple gains:

$$\rho_2 \rightarrow \sigma_v \sqrt{3\frac{V}{L_v}} \rightarrow \dot{v}_{BN}$$

$$\rho_4 \rightarrow \sigma_w \sqrt{\frac{8}{L_w V}} \left(\frac{\pi L_w}{4b}\right)^{1/6} \frac{\pi V}{4b} \rightarrow \dot{p}_{BN}$$

$$\dot{v}_{BN} \rightarrow -\frac{\pi}{3b} \rightarrow \dot{r}_{BN}$$

And the driving noise spectral intensity for the aircraft model is then:

$$\Theta_A = \begin{bmatrix} 0 & 0 & 0 & 0 & 0 & 0 \\ 0 & 0 & 0 & 0 & 0 & 0 \\ 0 & 0 & 0 & 0 & 0 & 0 \\ 0 & 0 & 0 & 2.79 & 0 & -.0657 \\ 0 & 0 & 0 & 0 & -.00561 & 0 \\ 0 & 0 & 0 & -.0657 & 0 & .00155 \end{bmatrix}$$

APPENDIX D

GAIN MATRICES AND AIRCRAFT POLES

D.1 Ship Gain Matrices

The matrices are given for the nominal case: H=10ft, ω_m=0.72rad/s, U=15.5ft/s, ϕ=45deg, ρ=0.3, T_z=0, q=0.01 (6 meas. case)

Kalman Filter Gain Matrix H_S

ROW \ COL	1	2	3
1	-4.6134D-01	1.4458D+01	2.7702D+00
2	-2.8914D+00	-5.5774D+01	-8.3641D+00
3	1.0408D+00	3.9739D+01	6.4446D+00
4	-3.8338D+00	-6.5996D+01	-9.1990D+00
5	3.7748D+00	6.5939D+01	8.4311D+00
6	-3.3059D+00	-5.0290D+01	-6.2364D+00
7	8.1117D+01	3.2181D+03	5.3151D+02
8	-1.3968D+02	-1.7453D+03	-2.3981D+02
9	3.6723D+02	2.6746D+04	4.8504D+03
10	-1.7817D+03	-2.8682D+04	-4.3007D+03
11	-1.5594D+03	1.7822D+05	4.0871D+04
12	-2.1862D+04	-4.1617D+05	-7.1668D+04
13	5.8324D-01	6.4656D+00	7.9196D-01
14	-1.0493D-03	1.5716D-01	3.1149D-02
15	1.2931D-02	4.7797D-01	4.7370D-02
16	1.5839D-03	4.7370D-02	9.1689D-03

Feedforward Gain Matrix G_S

ROW \ COL	1	2	3	4	5	6
1	5.1087D-04	-7.3047D-04	1.6527D-04	-2.7353D-04	5.1166D-05	-9.9003D-05
2	1.7439D-03	-1.9028D-03	6.0739D-04	-7.2401D-04	2.0720D-04	-2.7717D-04
3	3.4578D-05	-1.2955D-05	1.3776D-05	-1.1610D-05	4.9162D-06	-6.1738D-06

7	8	9	10	11	12
1.1108D-04	4.7791D-05	1.1348D-06	-4.7337D-06	-7.5781D-07	-2.4962D-07
3.0083D-04	1.6679D-04	4.3843D-06	-1.4924D-05	-1.8849D-06	-8.0059D-07
1.0475D-07	1.6906D-06	6.9925D-08	-1.6319D-07	4.8016D-08	5.3488D-09

13	14	15	16
4.5487D-02	-1.0492D+00	-6.3963D-01	-5.4086D+00
9.2824D-02	-3.7542D+00	-4.1785D+00	-9.9567D+00
-1.0912D-03	-2.6243D-02	-1.4186D-03	9.8906D-01

D.2 Aircraft Gain Matrices

Kalman Filter Gain Matrix H_A

ROW \ COL	1	2	3	4	5	6
1	9.1151D-01	1.8097D+00	-6.8603D-01	6.7683D-01	-4.5774D-01	-7.8292D+00
2	6.3276D-03	3.3360D-01	5.6023D-02	1.6645D-02	8.9397D-01	3.6619D-01
3	-2.3987D-03	5.6023D-02	4.5755D-01	-2.6443D-03	-1.1862D-02	6.8487D-01
4	6.7683D-01	4.7604D+00	-7.5627D-01	2.6779D+00	2.4863D+00	-5.7722D+01
5	-3.8412D-04	2.1455D-01	-2.8469D-03	2.0864D-03	4.7115D+00	7.4267D-03
6	-6.5700D-03	8.7886D-02	1.6437D-01	-4.8438D-02	7.4267D-03	1.8715D+00

Feedback Gain Matrix G_A

ROW \ COL	1	2	3	4	5	6
1	4.3613D-02	-1.0417D-01	-3.3551D-01	3.7792D-02	-8.1850D-02	-1.3893D-01
2	8.7849D-02	4.0469D+00	-9.7677D-02	1.0427D-01	1.2890D+00	-4.6082D-02
3	-9.1154D-04	6.9076D-02	8.7931D-01	1.3588D-04	3.2002D-03	4.5089D-01

D.3 Aircraft Poles

Open-loop poles: $\lambda(A_A)$

	REAL PART	IMAG PART	NAT FREQ(HZ)	ZETA	FREQ(HZ)
1	-5.324D-01	0.0	8.473D-02	1.000000	0.0
2	1.425D-01	3.788D-01	6.441D-02	-0.352163	6.029D-02
3	1.425D-01	-3.788D-01	6.441D-02	-0.352163	6.029D-02
4	-6.820D-02	0.0	1.085D-02	1.000000	0.0
5	0.0	0.0	0.0	0.0	0.0
6	0.0	0.0	0.0	0.0	0.0

LQ Closed-loop poles: $\lambda(A_A-B_AG_A)$

	REAL PART	IMAG PART	NAT FREQ(HZ)	ZETA	FREQ(HZ)
1	-2.792D+00	2.803D+00	6.296D-01	0.705716	4.460D-01
2	-2.792D+00	-2.803D+00	6.296D-01	0.705716	4.460D-01
3	-1.869D+00	1.863D+00	4.200D-01	0.708310	2.965D-01
4	-1.869D+00	-1.863D+00	4.200D-01	0.708310	2.965D-01
5	-1.064D+00	1.036D+00	2.363D-01	0.716447	1.649D-01
6	-1.064D+00	-1.036D+00	2.363D-01	0.716447	1.649D-01

Kalman Filter poles $\lambda(A_A - H_A C_A)$

	REAL PART	IMAG PART	NAT FREQ(HZ)	ZETA	FREQ(HZ)
1	-1.081D+01	0.0	1.720D+00	1.000000	0.0
2	-5.368D+00	0.0	8.544D-01	1.000000	0.0
3	-2.231D+00	0.0	3.550D-01	1.000000	0.0
4	-1.118D+00	0.0	1.780D-01	1.000000	0.0
5	-6.010D-01	0.0	9.566D-02	1.000000	0.0
6	-4.920D-01	0.0	7.830D-02	1.000000	0.0

Compensator poles $\lambda(A_A - B_A G_A - H_A C_A)$

	REAL PART	IMAG PART	NAT FREQ(HZ)	ZETA	FREQ(HZ)
1	-1.679D+01	0.0	2.672D+00	1.000000	0.0
2	-8.875D+00	0.0	1.413D+00	1.000000	0.0
3	-3.744D+00	0.0	5.959D-01	1.000000	0.0
4	-1.165D+00	0.0	1.854D-01	1.000000	0.0
5	-6.061D-01	0.0	9.646D-02	1.000000	0.0
6	-5.707D-01	0.0	9.083D-02	1.000000	0.0

the compensator is stable.

REFERENCES

1. C.G. McMuldroch, "VTOL Controls for Shipboard Landings", S.M. Thesis, Laboratory for Information and Decision Systems, M.I.T., Cambridge, MA, June 1979.

2. L. Corliss, R.K. Greif, R.M. Gerdes, "Comparison of Ground-Based and In-Flight Simulation of VTOL Hover Control Concepts", Journal of Guidance and Control, Vol 1, No 3, May June 1978.

3. S.T. Donley, "Evaluation of Several Control/Display Concepts for V/STOL Shipboard Landing", SAE, Technical Paper 801205, October 1980.

4. R.L. Stapleford, "Velocity Command/Position Hold: A New Flight Control Concept for Hovering VTOL Aircraft", SAE, Technical Paper 801206, October 1980.

5. J.W. Smolka, "An Automatic Shipboard Landing System for the AV-8A Harrier", S.M. Thesis, Department of Aeronautics and Astronautics, M.I.T., Cambridge, MA, December 1979.

6. R.C. Radford, D. Andrisani, J.L. Beilman, "An Experimental Investigation of VTOL Flying Qualities Requirements for Shipboard Landings", Calspan Corporation, Buffalo, NY, August 1981.

7. D.L. Kohlman, V/STOL Airplanes, Iowa State University Press/Ames Iowa, 1981.

8. M. Athans, "The Role and Use of the Stochastic Linear-Quadratic-Gaussian Problem in Control System Design", IEEE Trans. on Automatic Control, Vol AC-16, December 1971.

9. H. Kwakernaak, R. Sivan, Linear Optimal Control Systems, Wiley, 1972.

10. T. Potsbergh, "Dynamic Control Systems Software - User's Manual", Laboratory for Information and Decision Systems, M.I.T., Cambridge,MA, 1980.

11. R.L. Fortenbaugh, "Mathematical Models for the Aircraft Operational Environment of DD963 Class Ships", Vought Corporation, Report 2-55800/8R-3500, September 1978.

12. M. Triantafyllou, M. Athans, "Real Time Estimation of the Heaving and Pitching Motions of a Ship Using a Kalman Filter", Proc. Oceans '81, Boston, MA, September 1981.

13. M. Triantafyllou, M. Bodson, M. Athans, "Real Time Estimation of Ship Motions Using Kalman Filtering Techniques", Laboratory for Information and Decision Systems, M.I.T., Cambridge, MA, 1982.

14. M. Triantafyllou, M. Bodson, "Real Time Prediction of Marine Vessel Motions, Using Kalman Filtering Techniques", Proc OTC '82, Houston, May 1982.

15. "5-Degrees of Freedom Seakeeping Program Manual", Design Laboratory, Ocean Engineering Department, M.I.T., Cambridge, MA, 1980.

16. A. Gelb, Applied Optimal Estimation, M.I.T. Press, 1974.

17. I.R. Yumori, "Real Time Prediction of Ship Response to Ocean Waves Using Time Series Analysis", Proc. Oceans '81, Boston, MA, Sept.1981.

18. C.F. Van Loan, "Computing Integrals Involving the Matrix Exponential", IEEE Trans. on Automatic Control, Vol AC-23, June 1978.

19. M.P. Bland, B. Fajar, R.K. Konsewicz, "Mathematical Model for Lift/Cruise Fan V/STOL Aircraft Simulator Programming Data" NASA CR-151916, 1976.

20. A. Bryson, Y.C. Ho, Applied Optimal Control, Hemisphere Publishing Corporation, 1975.

21. C. Harvey, G. Stein, "Quadratic Weights for Asymptotic Regulator Properties", IEEE Trans. on Automatic Control, Vol AC-23, June 1978.

22. G. Stein, "Generalized Quadratic Weights for Asymptotic Regulator Properties", IEEE Trans. on Automatic Control, Vol AC-24, Aug 1979.

23. N. Lehtomaki, "Practical Robustness Measures in Multivariable Control System Analysis", PhD Dissertation, Laboratory for Information and Decision Systems, M.I.T., Cambridge, MA, May 1981.

24. N.A. Lehtomaki, N.R. Sandel, M. Athans, "Robustness Results in Linear-Quadratic-Gaussian Based Multivariable Control Designs", IEEE Trans. on Automatic Control, Vol AC-26, Feb 1981.

25. P.M. Thompson, "Linear State Feedback, Quadratic Weights, and Closed-Loop Eigenstructures", S.M. Thesis, Laboratory for Information and Decision Systems, Cambridge, MA, June 1979.

26. J.A. Sorensen, T. Goka, A.V. Phatak, S.F. Schmidt, "An Investigation of Automatic Guidance Concepts to Steer a VTOL Aircraft to a Small Aviation Facility Ship", NASA CR-152407, July 1980.

27. L.A. McGee, C.H. Paulk, S.A. Steck, S.F. Schmidt, A.W. Merz, "Evaluation of the Navigation Performance of Shipboard VTOL Landing Guidance Systems", AIAA Guidance and Control Conference, Boulder, CO, August 1979.

28. J.C. Doyle, G. Stein, "Robustness with Observers", IEEE Trans. on Automatic Control, Vol AC-24, August 1979.

29. N. Lehtomaki, "A Functional Description of Computer Programs for the Robustness Analysis of Multivariable Control Systems", Laboratory for Information and Decision Systems, Cambridge, MA, June 1981.

30. A.J. Laub, "Efficient Multivariable Frequency Response Computations", IEEE Trans. on Automatic Control, Vol AC-26, April 1981.

31. J.J. Dongarra, et al. "LINPACK User's Guide", SIAM, Philadelphia, PA, 1979.

32. H. Kwakernaak, "Optimal Low-Sensitivity Linear Feedback Systems", Automatica, Vol 5, May 1969.

33. W.R. Perkins, J.B. Cruz, "Feedback Properties of Linear Regulators", IEEE Trans. on Automatic Control, Vol AC-16, December 1971.